

BULLETIN OF RUSSIAN STATE MEDICAL UNIVERSITY

BIOMEDICAL JOURNAL OF PIROGOV RUSSIAN NATIONAL RESEARCH MEDICAL UNIVERSITY

EDITOR-IN-CHIEF Denis Rebrikov, DSc, professor

DEPUTY EDITOR-IN-CHIEF Alexander Oettinger, DSc, professor

EDITORS Valentina Geidebrekht, PhD; Nadezda Tikhomirova

TECHNICAL EDITOR Evgeny Lukyanov

TRANSLATORS Nadezda Tikhomirova, Vyacheslav Vityuk

DESIGN AND LAYOUT Marina Doronina

EDITORIAL BOARD

Averin VI, DSc, professor (Minsk, Belarus)
Alipov NN, DSc, professor (Moscow, Russia)
Belousov VV, DSc, professor (Moscow, Russia)
Bogomilskiy MR, corr. member of RAS, DSc, professor (Moscow, Russia)
Bozhenko VK, DSc, CSc, professor (Moscow, Russia)
Bylova NA, CSc, docent (Moscow, Russia)
Gainetdinov RR, CSc (Saint-Petersburg, Russia)
Gendlin GYe, DSc, professor (Moscow, Russia)
Ginter EK, member of RAS, DSc (Moscow, Russia)
Gorbacheva LR, DSc, professor (Moscow, Russia)
Gordeev IG, DSc, professor (Moscow, Russia)
Gudkov AV, PhD, DSc (Buffalo, USA)
Gulyaeva NV, DSc, professor (Moscow, Russia)
Gusev EI, member of RAS, DSc, professor (Moscow, Russia)
Danilenko VN, DSc, professor (Moscow, Russia)
Zarubina TV, DSc, professor (Moscow, Russia)
Zatevakhin II, member of RAS, DSc, professor (Moscow, Russia)
Kagan VE, professor (Pittsburgh, USA)
Kzyzhkowska YuG, DSc, professor (Heidelberg, Germany)
Kobriniskii BA, DSc, professor (Moscow, Russia)
Kozlov AV, MD PhD (Vienna, Austria)
Kotelevtsev YuV, CSc (Moscow, Russia)
Lebedev MA, PhD (Darem, USA)
Manturova NE, DSc (Moscow, Russia)
Milushkina OYu, DSc, professor (Moscow, Russia)
Mitupov ZB, DSc, professor (Moscow, Russia)
Moshkovskii SA, DSc, professor (Moscow, Russia)
Munblit DB, MSc, PhD (London, Great Britain)

Negrebetsky VV, DSc, professor (Moscow, Russia)
Novikov AA, DSc (Moscow, Russia)
Pivovarov YuP, member of RAS, DSc, professor (Moscow, Russia)
Polunina NV, corr. member of RAS, DSc, professor (Moscow, Russia)
Poryadin GV, corr. member of RAS, DSc, professor (Moscow, Russia)
Razumovskii AYU, corr. member of RAS, DSc, professor (Moscow, Russia)
Rebrova OYu, DSc (Moscow, Russia)
Rudoy AS, DSc, professor (Minsk, Belarus)
Rylova AK, DSc, professor (Moscow, Russia)
Savelieva GM, member of RAS, DSc, professor (Moscow, Russia)
Semiglazov VF, corr. member of RAS, DSc, professor (Saint-Petersburg, Russia)
Skoblina NA, DSc, professor (Moscow, Russia)
Slavyanskaya TA, DSc, professor (Moscow, Russia)
Smirnov VM, DSc, professor (Moscow, Russia)
Spallone A, DSc, professor (Rome, Italy)
Starodubov VI, member of RAS, DSc, professor (Moscow, Russia)
Stepanov VA, corr. member of RAS, DSc, professor (Tomsk, Russia)
Suchkov SV, DSc, professor (Moscow, Russia)
Takhchidi KhP, member of RAS, DSc, professor (Moscow, Russia)
Trufanov GE, DSc, professor (Saint-Petersburg, Russia)
Favorova OO, DSc, professor (Moscow, Russia)
Filipenko ML, CSc, leading researcher (Novosibirsk, Russia)
Khazipov RN, DSc (Marsel, France)
Chundukova MA, DSc, professor (Moscow, Russia)
Shimanovskii NL, corr. member of RAS, DSc, professor (Moscow, Russia)
Shishkina LN, DSc, senior researcher (Novosibirsk, Russia)
Yakubovskaya RI, DSc, professor (Moscow, Russia)

SUBMISSION <http://vestnikrgmu.ru/login?lang=en>

CORRESPONDENCE editor@vestnikrgmu.ru

COLLABORATION manager@vestnikrgmu.ru

ADDRESS ul. Ostrovityanova, d. 1, Moscow, Russia, 117997

Indexed in Scopus. CiteScore 2022: 0.6

Scopus[®]

SCImago Journal & Country Rank 2020: 0.14

SJR

Scimago Journal & Country Rank

Indexed in WoS. JCR 2021: 0.5

WEB OF SCIENCE[™]

Listed in HAC 31.01.2020 (№ 507)



**ВЫСШАЯ
АТТЕСТАЦИОННАЯ
КОМИССИЯ (ВАК)**

Five-year h-index is 8

Google
scholar

Open access to archive

CYBERLENINKA

Issue DOI: 10.24075/brsmu.2024-01

The mass media registration certificate № 012769 issued on July 29, 1994

Founder and publisher is Pirogov Russian National Research Medical University (Moscow, Russia)

The journal is distributed under the terms of Creative Commons Attribution 4.0 International License www.creativecommons.org



Approved for print 29.02.2024
Circulation: 100 copies. Printed by Print.Formula
www.print-formula.ru

ВЕСТНИК РОССИЙСКОГО ГОСУДАРСТВЕННОГО МЕДИЦИНСКОГО УНИВЕРСИТЕТА

НАУЧНЫЙ МЕДИЦИНСКИЙ ЖУРНАЛ РНИМУ ИМ. Н. И. ПИРОГОВА

ГЛАВНЫЙ РЕДАКТОР Денис Ребриков, д. б. н., профессор

ЗАМЕСТИТЕЛЬ ГЛАВНОГО РЕДАКТОРА Александр Эттингер, д. м. н., профессор

РЕДАКТОРЫ Валентина Гейдебрехт, к. б. н.; Надежда Тихомирова

ТЕХНИЧЕСКИЙ РЕДАКТОР Евгений Лукьянов

ПЕРЕВОДЧИКИ Надежда Тихомирова, Вячеслав Витюк

ДИЗАЙН И ВЕРСТКА Марины Дорониной

РЕДАКЦИОННАЯ КОЛЛЕГИЯ

В. И. Аверин, д. м. н., профессор (Минск, Белоруссия)
Н. Н. Алипов, д. м. н., профессор (Москва, Россия)
В. В. Белоусов, д. б. н., профессор (Москва, Россия)
М. Р. Богомилский, член-корр. РАН, д. м. н., профессор (Москва, Россия)
В. К. Боженко, д. м. н., к. б. н., профессор (Москва, Россия)
Н. А. Былова, к. м. н., доцент (Москва, Россия)
Р. Р. Гайнетдинов, к. м. н. (Санкт-Петербург, Россия)
Г. Е. Гендлин, д. м. н., профессор (Москва, Россия)
Е. К. Гинтер, академик РАН, д. б. н. (Москва, Россия)
Л. Р. Горбачева, д. б. н., профессор (Москва, Россия)
И. Г. Гордеев, д. м. н., профессор (Москва, Россия)
А. В. Гудков, PhD, DSc (Буффало, США)
Н. В. Гуляева, д. б. н., профессор (Москва, Россия)
Е. И. Гусев, академик РАН, д. м. н., профессор (Москва, Россия)
В. Н. Даниленко, д. б. н., профессор (Москва, Россия)
Т. В. Зарубина, д. м. н., профессор (Москва, Россия)
И. И. Затевахин, академик РАН, д. м. н., профессор (Москва, Россия)
В. Е. Каган, профессор (Питтсбург, США)
Ю. Г. Кжышковска, д. б. н., профессор (Гейдельберг, Германия)
Б. А. Кобринский, д. м. н., профессор (Москва, Россия)
А. В. Козлов, MD PhD (Вена, Австрия)
Ю. В. Котелевцев, к. х. н. (Москва, Россия)
М. А. Лебедев, PhD (Дарем, США)
Н. Е. Мантурова, д. м. н. (Москва, Россия)
О. Ю. Милушкина, д. м. н., доцент (Москва, Россия)
З. Б. Митупов, д. м. н., профессор (Москва, Россия)
С. А. Мошковский, д. б. н., профессор (Москва, Россия)
Д. Б. Мунблит, MSc, PhD (Лондон, Великобритания)

В. В. Негребцкий, д. х. н., профессор (Москва, Россия)
А. А. Новиков, д. б. н. (Москва, Россия)
Ю. П. Пивоваров, д. м. н., академик РАН, профессор (Москва, Россия)
Н. В. Полунина, член-корр. РАН, д. м. н., профессор (Москва, Россия)
Г. В. Порядин, член-корр. РАН, д. м. н., профессор (Москва, Россия)
А. Ю. Разумовский, член-корр., профессор (Москва, Россия)
О. Ю. Реброва, д. м. н. (Москва, Россия)
А. С. Рудой, д. м. н., профессор (Минск, Белоруссия)
А. К. Рылова, д. м. н., профессор (Москва, Россия)
Г. М. Савельева, академик РАН, д. м. н., профессор (Москва, Россия)
В. Ф. Семглазов, член-корр. РАН, д. м. н., профессор (Санкт-Петербург, Россия)
Н. А. Скоблина, д. м. н., профессор (Москва, Россия)
Т. А. Славянская, д. м. н., профессор (Москва, Россия)
В. М. Смирнов, д. б. н., профессор (Москва, Россия)
А. Спаллоне, д. м. н., профессор (Рим, Италия)
В. И. Стародубов, академик РАН, д. м. н., профессор (Москва, Россия)
В. А. Степанов, член-корр. РАН, д. б. н., профессор (Томск, Россия)
С. В. Сучков, д. м. н., профессор (Москва, Россия)
Х. П. Тахчиди, академик РАН, д. м. н., профессор (Москва, Россия)
Г. Е. Труфанов, д. м. н., профессор (Санкт-Петербург, Россия)
О. О. Фаворова, д. б. н., профессор (Москва, Россия)
М. Л. Филипенко, к. б. н. (Новосибирск, Россия)
Р. Н. Хазипов, д. м. н. (Марсель, Франция)
М. А. Чундокова, д. м. н., профессор (Москва, Россия)
Н. Л. Шимановский, член-корр. РАН, д. м. н., профессор (Москва, Россия)
Л. Н. Шишкина, д. б. н. (Новосибирск, Россия)
Р. И. Якубовская, д. б. н., профессор (Москва, Россия)

ПОДАЧА РУКОПИСЕЙ <http://vestnikrgmu.ru/login>

ПЕРЕПИСКА С РЕДАКЦИЕЙ editor@vestnikrgmu.ru

СОТРУДНИЧЕСТВО manager@vestnikrgmu.ru

АДРЕС РЕДАКЦИИ ул. Островитянова, д. 1, г. Москва, 117997

Журнал включен в Scopus. CiteScore 2022: 0,6

Журнал включен в WoS. JCR 2021: 0,5

Индекс Хирша (h²) журнала по оценке Google Scholar: 8

Scopus[®]

SCImago Journal & Country Rank 2020: 0,14

SJR
Scimago Journal & Country Rank

WEB OF SCIENCE[™]

Журнал включен в Перечень 31.01.2020 (№ 507)



**ВЫСШАЯ
АТТЕСТАЦИОННАЯ
КОМИССИЯ (ВАК)**

Google
scholar

Здесь находится открытый архив журнала

CYBERLENINKA

DOI выпуска: 10.24075/vrgmu.2024-01

Свидетельство о регистрации средства массовой информации № 012769 от 29 июля 1994 г.

Учредитель и издатель — Российский национальный исследовательский медицинский университет имени Н. И. Пирогова (Москва, Россия)

Журнал распространяется по лицензии Creative Commons Attribution 4.0 International www.creativecommons.org



Подписано в печать 29.02.2024

Тираж 100 экз. Отпечатано в типографии Print.Formula
www.print-formula.ru

ORIGINAL RESEARCH

4

Molecular cytogenetic characteristics of small supernumerary marker chromosomes 15 and 22 in asymptomatic carriers

Yurchenko DA, Markova ZhG, Minzhenkova ME, Vorontsova EO, Shilova NV

Молекулярно-цитогенетическая характеристика малых сверхчисленных маркерных хромосом 15 и 22 у асимптотических носителей

Д. А. Юрченко, Ж. Г. Маркова, М. Е. Миньженкова, Е. О. Воронцова, Н. В. Шилова

ORIGINAL RESEARCH

11

Filaggrin loss-of-function mutations 2282del4, R501X, R2447X and S3247X in atopic dermatitis

Verbenko DA, Karamova AE, Chikin VV, Kozlova IV, Aulova KM, Kubanov AA, Gorodnichev PV

Мутации 2282del4, R501X, R2447X, S3247X филаггрина при атопическом дерматите

Д. А. Вербенко, А. Э. Карамова, В. В. Чикин, И. В. Козлова, К. М. Аулова, А. А. Кубанов, П. В. Гордничев

ORIGINAL RESEARCH

19

Determining the diagnostic value of the markers of congenital metabolic disorders by chromatography–mass spectrometry

Mamedov IS, Zolkina IV, Sukhorukov VS, Krapivkin AI

Определение диагностической значимости маркеров наследственных болезней обмена с применением метода хромато-масс-спектрометрии

И. С. Мамедов, И. В. Золкина, В. С. Сухоруков, А. И. Крапивкин

ORIGINAL RESEARCH

27

Information capacity of the NF- κ B and AP-1 signaling activation sensors in *in vitro* assessment of dermatotoxic effects

Tolstova TV, Purezcky VK, Kozhin PM, Luzgina NG, Rusanov AL

Информативность сенсоров активации сигнальных путей NF- κ B и AP-1 при оценке дерматотоксических эффектов *in vitro*

Т. В. Толстова, В. К. Пурецкий, П. М. Кожин, Н. Г. Лузгина, А. Л. Русанов

ORIGINAL RESEARCH

35

Comparison of lipid alterations in astrocytomas with increasing grade

Pekov SI, Bocharov KV, Bormotov DS, Eliferov VA, Parochkina EV, Sorokin AA, Nikolaev EN, Popov IA

Сравнение липидных изменений в астроцитомах по мере роста их злокачественности

С. И. Пеков, К. В. Бочаров, Д. С. Бормотов, В. А. Елиферов, Е. В. Парочкина, А. А. Сорокин, Е. Н. Николаев, И. А. Попов

ORIGINAL RESEARCH

40

Effect of probenecid on astrocyte activation *in vitro*

Babkina II, Mazeeva VV, Morozova MP, Gorbacheva LR

Влияние пробенецида на активацию астроцитов *in vitro*

И. И. Бабкина, В. В. Мазеева, М. П. Морозова, Л. Р. Горбачева

OPINION

49

Deep learning in modelling the protein–ligand interaction: new pathways in drug development

Barykin AD, Chepurnykh TV, Osipova ZM

Глубокое обучение в моделировании белок–лигандного взаимодействия: новые пути в разработке лекарственных препаратов

А. Д. Барыкин, Т. В. Чепурных, З. М. Осипова

ORIGINAL RESEARCH

54

Emerging prediction of preeclampsia based on the expression of exosomal SUMO proteins

Gusar VA, Timofeeva AV, Fedorov IS, Tarasova AM, Sukhova YuV, Ivanets TYU

Новые возможности прогнозирования преэклампсии на основе экспрессии экзосомных белков SUMO

В. А. Гусар, А. В. Тимофеева, И. С. Федоров, А. М. Тарасова, Ю. В. Сухова, Т. Ю. Иванец

ORIGINAL RESEARCH

66

Specifics of gut microbiota in women with idiopathic recurrent miscarriage

Gumenyuk LN, Borydugov MD, Sarchuk EV, Knyazeva SV, Zastavskii VA, Krickaya DV, Saitibragimova SE, Kurtvelieva AI

Особенности микробиоты кишечника у женщин с идиопатическим привычным выкидышем

Л. Н. Гуменюк, М. Д. Бордюгов, Е. В. Сарчук, С. В. Князева, В. А. Заставский, Д. В. Крицкая, Ш. Э. Сайтибрагимова, А. И. Куртвелиева

ORIGINAL RESEARCH

74

Assessing clinical efficacy of new method for adaptive infusion control in phacoemulsification

Aznabaev BM, Mukhamadeev TR, Ismagilov TN, Dibaev TI

Оценка клинической эффективности нового способа адаптивного управления инфузией при фактоэмульсификации

Б. М. Азнабаев, Т. Р. Мухамадеев, Т. Н. Исмагилов, Т. И. Дибаяв

MOLECULAR CYTOGENETIC CHARACTERISTICS OF SMALL SUPERNUMERARY MARKER CHROMOSOMES 15 AND 22 IN ASYMPTOMATIC CARRIERS

Yurchenko DA ✉, Markova ZhG, Minzhenkova ME, Vorontsova EO, Shilova NV

Research Centre for Medical Genetics, Moscow, Russia

Small supernumerary marker chromosomes (sSMC) are structurally abnormal chromosomes that cannot be identified unambiguously by standard cytogenetic methods. A comprehensive approach involving the use of molecular cytogenetic methods is required for the more thorough morphological assessment of such chromosomes, as well as for the development of strategy for genetic counseling of the patients being the sSMC carriers. It is widely accepted that the development of abnormal phenotype by the patients having sSMC in their karyotype is associated with the presence of euchromatic region material in the marker chromosome. Therefore, it results from the presence of relatively large DNA copy number variations (CNVs) in the form of duplication, triplication, and more increased copy numbers; which are localized in the pericentromeric region of the appropriate chromosome. Pericentromeric CNVs can be involved in the chromosome imbalance in asymptomatic carriers of sSMC as well, however, the boundaries of such imbalance have not been clearly identified. The study was aimed to acquire additional information about the genomic topology of the DNA regions insensitive to the genes copy number increase. FISH analysis with commercial and homemade DNA probes was performed in 18 carriers of sSMC 15 and 22 having no clinically significant phenotypic abnormalities. The molecular cytogenetic testing showed that pericentromeric euchromatic regions sized 1.2 Mb and 714 kb, respectively, were found in 33% of cases (6 out of 18). We assume that these regions comprise no potentially dosage-sensitive genes.

Keywords: sSMC, CNV, pericentromeric euchromatin, FISH, homemade DNA probe

Funding: this work was carried out at the expense of budgetary funds within the framework of research topic № 122032300370-1, "Study of Structural and Functional Features and Mechanisms of the Formation of Chromosomal Abnormalities and Genomic Imbalance."

Author contribution: Yurchenko DA — study design, development of homemade DNA probes, FISH diagnosis and data interpretation, manuscript writing; Markova ZhG and Minzhenkova ME — FISH analysis with commercial DNA probes; Vorontsova EO — implementation of the protocol of FISH with homemade DNA probes; Shilova NV — study concept and design, discussion, scientific editing of manuscript.

Compliance with ethical standards: the study was approved by the Ethics Committee of the Research Centre for Medical Genetics (protocol No. 4/2 dated 19 April 2021). The patients submitted the informed consent to participation in scientific research.

✉ **Correspondence should be addressed:** Darya A. Yurchenko
Moskvorechye, 1, Moscow, 115522, Russia; dashalbv@mail.ru

Received: 23.10.2023 **Accepted:** 06.01.2024 **Published online:** 31.01.2024

DOI: 10.24075/brsmu.2024.001

МОЛЕКУЛЯРНО-ЦИТОГЕНЕТИЧЕСКАЯ ХАРАКТЕРИСТИКА МАЛЫХ СВЕРХЧИСЛЕННЫХ МАРКЕРНЫХ ХРОМОСОМ 15 И 22 У АСИМПТОМАТИЧЕСКИХ НОСИТЕЛЕЙ

Д. А. Юрченко ✉, Ж. Г. Маркова, М. Е. Миньженкова, Е. О. Воронцова, Н. В. Шилова

Медико-генетический научный центр имени Н. П. Бочкова, Москва, Россия

Малые сверхчисленные маркерные хромосомы (мСМХ) — структурно аномальные хромосомы, которые невозможно однозначно идентифицировать с использованием методов стандартной цитогенетики. Для более детального анализа морфологии таких хромосом и разработки стратегии медико-генетического консультирования пациентов-носителей мСМХ необходим комплексный подход, включающий молекулярно-цитогенетические методы. Общепринят тот факт, что формирование аномального фенотипа у пациентов с мСМХ в кариотипе связано с наличием материала эухроматиновых районов, вовлеченных в состав маркерной хромосомы. И, как следствие, обусловлено присутствием в геноме протяженных вариаций числа копий участков ДНК (copy number variations, CNV) в виде дупликации, трипликации и большей копийности, которые локализованы в прицентромерном районе соответствующей хромосомы. Прицентромерные CNV могут быть вовлечены в хромосомный дисбаланс и у асимптотических носителей мСМХ, однако границы такого дисбаланса окончательно не установлены. Целью исследования было получить дополнительные сведения о геномной топографии участков ДНК, не чувствительных к увеличению копийности генов. Был проведен FISH-анализ с коммерческими и несерийными ДНК-зондами у 18 носителей мСМХ 15 и 22 без клинически значимых аномалий фенотипа. Установлено, что в 33% (6 из 18) случаев присутствуют участки прицентромерного эухроматина размером 1,2 м.п.н. и 714 т.п.н. соответственно. Мы предполагаем, что эти регионы не содержат потенциально чувствительных к дозе генов.

Ключевые слова: мСМХ, CNV, прицентромерный эухроматин, FISH, несерийный ДНК-зонд

Финансирование: исследование проведено в рамках темы НИР №122032300370-1 «Изучение структурно-функциональных особенностей и механизмов формирования хромосомных аномалий и геномного дисбаланса».

Вклад авторов: Д. А. Юрченко — дизайн исследования, разработка несерийных ДНК-зондов, проведение FISH-диагностики и интерпретация полученных данных, подготовка рукописи; Ж. Г. Маркова и М. Е. Миньженкова — проведение FISH-исследования с коммерческими ДНК-зондами; Е. О. Воронцова — отработка протокола FISH-исследования с несерийными ДНК-зондами; Н. В. Шилова — концепция и дизайн исследования, обсуждение результатов, научное редактирование рукописи.

Соблюдение этических стандартов: исследование одобрено этическим комитетом ФГБНУ «МГНЦ» (протокол № 4/2 от 19 апреля 2021 г.). Получено добровольное информированное согласие на участие пациентов в научном исследовании.

✉ **Для корреспонденции:** Дарья Александровна Юрченко
ул. Москворечье, д. 1, г. Москва, 115522, Россия; dashalbv@mail.ru

Статья получена: 23.10.2023 **Статья принята к печати:** 06.01.2024 **Опубликована онлайн:** 31.01.2024

DOI: 10.24075/vrgmu.2024.001

Small supernumerary marker chromosomes (sSMC) represent a heterogeneous group of structurally abnormal chromosomes that cannot be identified unambiguously by standard cytogenetic testing due to their small size and the features of genetic makeup, specifically due to the submicroscopic copy number variation of DNA (Copy Number Variations, CNV) [1]. The share of sSMC carriers among newborns in the population is 0.044%, among them 70% have no apparent clinical manifestations [2, 3]. This sSMCs can originate from any one of the 24 human chromosomes and can have different shapes, such as inverted duplication (inv dup), ring (r), and minute (min) shapes [4, 5]. In people having the 47,XN,+mar karyotype, sSMC most often originate from chromosomes 15 (about 30%) and 22 (about 20%) [1]. Clinical manifestations associated with the presence of sSMC in the karyotype can vary considerably, from normal phenotype to significant disturbances of physical and psychomotor development. These manifestations depend on the chromosomes involved in their development, the presence of euchromatic regions, gene content, degree of mosaicism and uniparental disomy.

Phenotypically normal carriers of sSMC can have CNVs in the form of duplication/triplication located in the pericentromeric euchromatic regions [6]. This suggests that such CNVs comprise no dosage sensitive genes, so the increase in the number of copies do not results in major phenotype alterations. Over the past decade, there is growing evidence of the fact that the presence of CNVs involving rather long euchromatic regions, sized up to several million base pairs (Mb), does not cause phenotypic alterations in the carriers [7].

Thus, euchromatic sSMC in the karyotype of asymptomatic carriers can represent a perfect model for analysis of the length of human genome regions insensitive to the changes in the copy number of genes located in the pericentromeric regions. This will make it possible to more accurately define the boundaries, where the dosage-insensitive regions end and the genome regions, the changes in the copy number of which can result in abnormal phenotype and psychomotor development delay, begin [8]. Thorough assessment of each sSMC case and accumulation of additional data contribute to the expansion of knowledge about the mechanisms of formation and pathogenetic significance of CNVs associated with the presence of such supernumerary marker chromosomes in the genome. The study was aimed to acquire additional data on the genome topology of the DNA regions insensitive to the genes copy number increase.

METHODS

The study involved 18 peripheral blood samples collected from asymptomatic carriers of sSMC 15 ($n = 9$: 3 males, 6 females) and sSMC 22 ($n = 9$: 5 males, 4 females). Inclusion criteria: all individuals taking part in the assisted reproductive technology program.

Cytogenetic assessment of the GTG-banding chromosomes was carried out in accordance with the standard protocol [9]. The marker chromosomes were identified by FISH with the commercial DNA probes for the centromeric (pericentromeric) regions of chromosomes 15 (SE 15, Kreatech; Netherlands) and 22 (CCP22-Pericentromeric, CytoTest Inc.; USA), as well as for the regions 15q11.2 (LSI SNRPN, Kreatech; Netherlands) and 22q11.2 (LSI TBX1, Kreatech; Netherlands), in order to rule out the clinically significant euchromatic regions comprised in the marker chromosome. FISH analysis involving the use of commercial DNA probes was performed in accordance with the manufacturers' protocols (Kreatech, CytoTest Inc.; USA).

Denaturation and hybridization were performed using the ThermoBrite hybridization system (StatSpin; USA). The analysis involved the use of the Axiolmager M.1 epifluorescence microscope (Carl Zeiss; Germany) and the Isis software tool for digital image processing (MetaSystems; Germany)

A fundamental phase of the study involved the development of our own (homemade) DNA probes for the pericentromeric euchromatin of chromosomes 15 and 22 and FISH analysis aimed to identify CNVs potentially insensitive to the increase in the DNA region copy number. Primers were selected using the Primer-BLAST NCBI software [10] and the UCSC Genome Browser database [11]. The OligoAnalyzer™ Tool was used to test specificity of the selected primers [12]. Primers were synthesized by Evrogen (Russia). The nucleotide sequences of the DNA primers selected are provided in Table 1.

The sequences of the selected DNA primers were used to conduct Long-range PCR using the BioMaster LR HS-PCR (2x) kit (Biolabmix; Russia) in the GeneAmp PCR System 9700 (Applied Biosystems; USA) in accordance with the manufacturer's protocol [13]. The resulting amplicons were purified on the columns using the diaGene kit for the reaction mixture DNA purification (Dia-M; Russia) in accordance with the manufacturer's instructions, then the purified DNA products were combined in one tube in order to obtain a DNA probe with the size of 10–30 thousand base pairs (kb). Nick translation was used to introduce a fluorescent label into the DNA probe [14–16].

To perform FISH with homemade DNA probes, we denatured DNA of the chromosome preparation and DNA probe separately [14, 15, 17].

DAPI I (Abbott Molecular; USA) dissolved in the Vectashield solution (Vector Labs; USA) to a ratio of 1:20 was used for counterstaining of chromosomes. The images of metaphase chromosomes were analyzed using the Isis software tool for digital image processing (MetaSystems; Germany) and the Axiolmager M.1 epifluorescence microscope (Carl Zeiss; Germany).

RESULTS

Conventional cytogenetics analysis revealed the karyotype with a supernumerary marker chromosome (47,XN,+mar) in all patients ($n = 18$). Mosaicism with high levels of abnormal clone (above 40%) was observed in all cases. FISH with commercial DNA probes for the centromeric regions of acrocentric chromosomes made it possible to identify sSMC as the one originating from chromosome 15 in 9 cases and as the one originating from chromosome 22 in 9 cases (Fig. 1A). Furthermore, the molecular cytogenetic analysis results confirmed the lack of clinically significant CNVs in the small supernumerary marker chromosomes in all the cases (Fig. 1B).

FISH analysis aimed to detect CNVs in the proximal euchromatic regions involved the chromosome preparations derived from cultured lymphocytes of all 18 asymptomatic carriers of the sSMC derived from chromosomes 15 and 22. The homemade locus specific DNA probes (hm) were developed for this purpose. When selecting localization of these DNA probes, we were guided by knowledge about the pericentromeric euchromatic regions of chromosomes 15 and 22 which are insensitive to changes gene dosage. It was 3 Mb for chromosome and about 100 kb for chromosome 22 [7, 18]. Thus, two hm with the size of about 10–30 kb were designed for chromosome 15. The proximal DNA probe that was most close to the centromere (hm-15-prox) was located at a distance of 1.2 Mb from the pericentromeric heterochromatin, while the

Table 1. Nucleotide sequences of primers used in the study

Chromosome region	DNA probe location relative to centromere	Sequences of DNA primers	PCR product size (bp)
15q11.2	Proximal	F 5'-TACATCTTACACCCACCCACCCAAACC-3' R 5'-TTTGCGGAAGGCATTAGTCCCCTTTGTT-3'	9882
	Distal	F 5'-TTAAAACGTGGGCTCTTCATTATCGCCT-3' R 5'-TGGACACCAGACAAAACAAGGAGTCAA-3'	9323
		F 5'-TGACTCCTTTGTTTTGTCTGGTGTCAA-3' R 5'-CTTATCCTTCCACACTCGCTGAGAACAG-3'	9140
		F 5'-CATGGTAATGTTGCGGTGTGCTTTGTT-3' R 5'-CTATCTTAGGCTGCTTGTCTGGTGCTT-3'	9676
22q11.2	Proximal	F 5'-CCCATCCTTTCCCAAACCAACACGA-3' R 5'-TTTTTCCCTCTGAACCTGGTTTCTGCACT-3'	9441
		F 5'-AGTGCAGAAACCAGTTCAGAGGGAAAA-3' R 5'-GAACCATCCACGAGGGAGAGTAGTTTTG-3'	9842
		F 5'-TCGCCATGTACTTCACTTTGTTCTGGTT-3' R 5'-GACTGGTCAAGGATGAGGATTTGTCAGG-3'	9600
	Median	F 5'-TCTTCTTGCCTGGAGGTGGGATCTAGT-3' R 5'-GAGGAGGGAGGGTGTCTGACAAAACGAA-3'	9531
		F 5'-CAATGTCTAGGGGCAACAGAGGGCAGAT-3' R 5'-AGGGCAGGAAATGTGTTCTGCTCGCTTA-3'	9316
	Distal	F 5'-AGAGAGAGGAAGGGGTGGCTCAAAC-3' R 5'-TGTGGGGTGTGGTGACATGGAGTATGG-3'	9718
		F 5'-CAATCCATGCCACAACATACCAGCCAC-3' R 5'-TATCACTGCCACCCCATCCCAATTCTG-3'	9862
		F 5'-CAGAAATGGGGATGGGGTGGCAGTGATA-3' R 5'-CAAGAGGCTGGGGCTTCTCTGGTCTTAG-3'	9761

distal DNA probe (hm-15-dist) was located at a distance of 2.2 Mb from the pericentromeric heterochromatin of chromosome 15 (Fig. 2A). The interval between two DNA probes was 1 Mb. Three homemade locus specific DNA probes (hm) with the size of about 30 kb were designed in order to assess the pericentromeric euchromatic region of chromosome 22. The proximal DNA probe, that was most close to the centromere (hm-22-proximal), was located at a distance of 478 kb from the pericentromeric heterochromatin, the median one (hm-22-median) was located at a distance of 714 kb from the pericentromeric heterochromatin, and the distal DNA probe (hm-22-distal) furthest from the centromere was located at a distance of 1.2 Mb from the pericentromeric heterochromatin of chromosome 22 (Fig. 2B).

The results of FISH analysis of the pericentromeric euchromatic regions of sSMC originating from chromosomes

15 and 22 involving the designed homemade DNA probes is provided in Table 2; a total of 30 metaphase chromosome spreads were assessed in all cases.

As shown in Table 2, no pericentromeric euchromatin was found in four patients with sSMC 15 and eight patients with sSMC 22, i.e. the marker chromosomes comprised heterochromatic regions only.

In five patients (№ 3, 6–9; Table 2), pericentromeric euchromatin was found in the sSMC originating from chromosome 15, however, only the proximal DNA probe hybridization signal was detected, i.e. the euchromatic region size did not exceed 1.2 Mb from the chromosome 15 pericentromeric heterochromatin (Fig. 3).

In one case (11 in Table 2), hybridization with two homemade DNA probes, specifically proximal and median, revealed pericentromeric euchromatin in the sSMC 22. Therefore, the

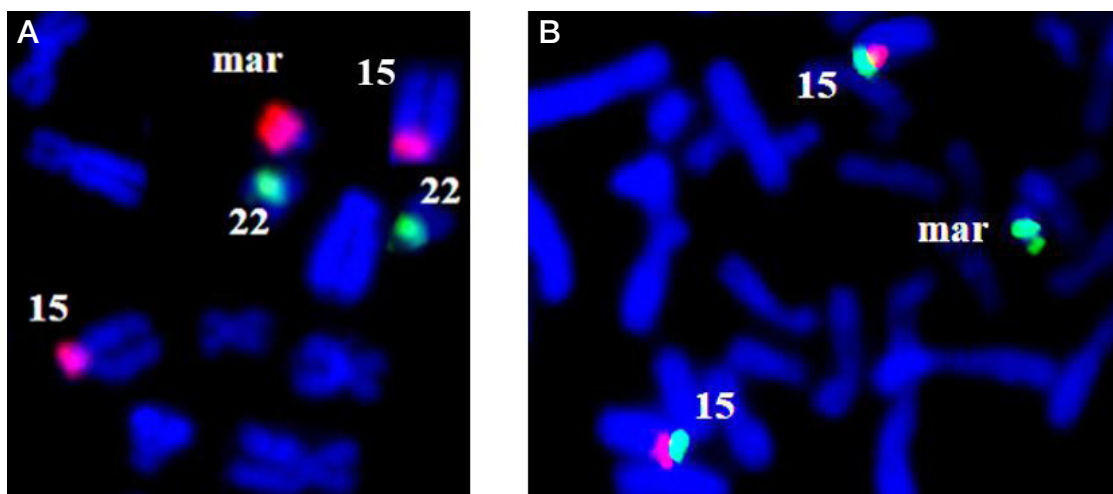


Fig. 1. Results of FISH with commercial DNA probes for chromosome 15. **A.** The marker chromosome originating from chromosome 15 in the form of inverted duplication (ish dic (15;15)(D15Z1+,D15Z1+)). Centromere of chromosome 15 (D15Z1) — red hybridization signal, pericentromeric region of chromosome 22 (CCP22-Pericentromeric) — green hybridization signal (control). **B.** The marker chromosome originating from chromosome 15 comprises no 15q11.2-q13 euchromatic region. Centromere of chromosome 15 (D15Z1) — green hybridization signal, LSI SNRPN — red hybridization signal

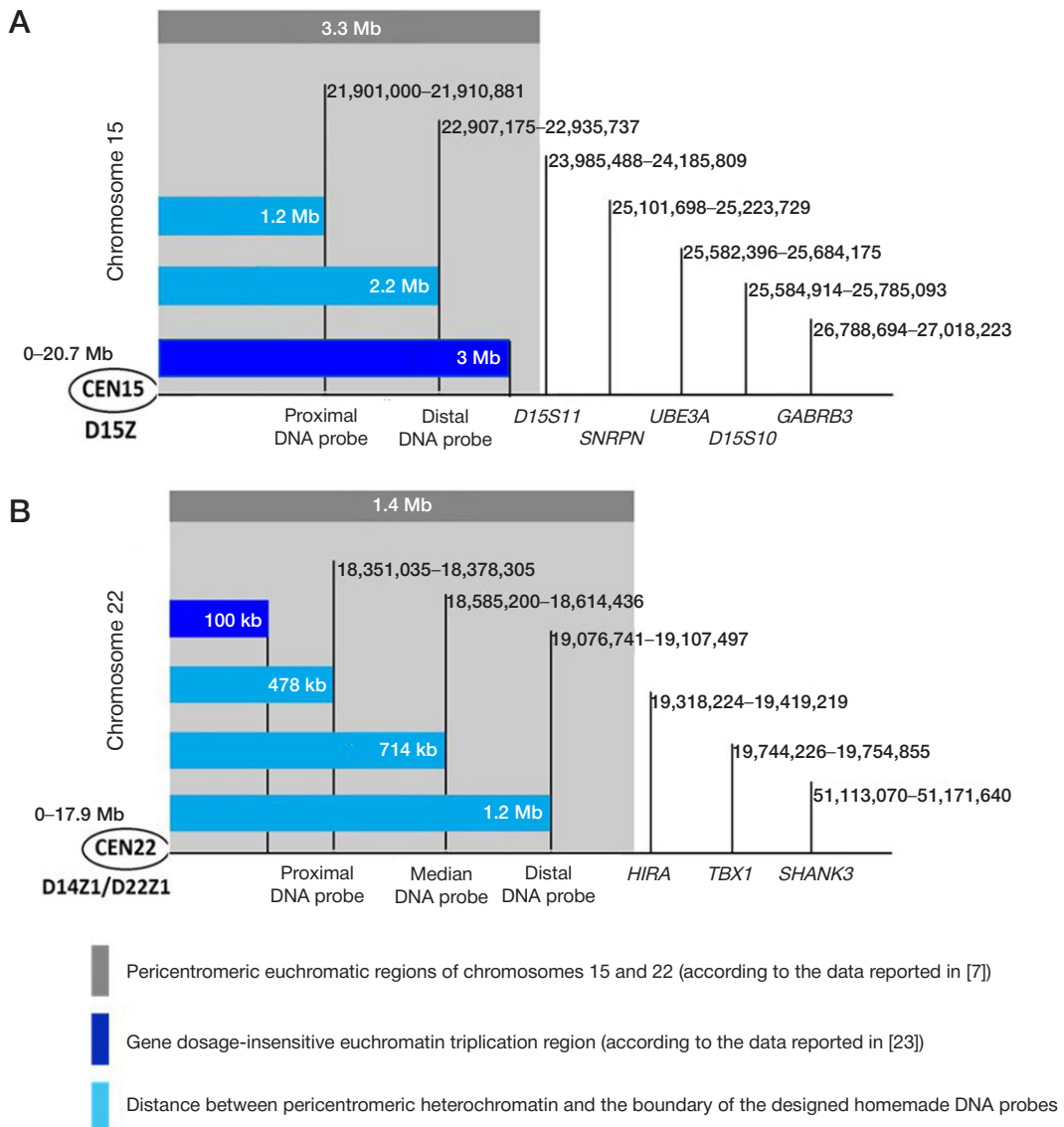


Fig. 2. A. Size and localization of homemade DNA probes within the pericentromeric euchromatic region of chromosome 15. **B.** Size and localization of homemade DNA probes within the pericentromeric euchromatic region of chromosome 22

overall size of the imbalance involved in the chromosomal rearrangement was 714 kb (Fig. 4).

Thus, in the carriers of the sSMC originating from chromosomes 15 and 22 having no apparent clinical manifestations, the marker chromosomes comprise heterochromatic regions only in 67% of cases (12/18); in 33% of cases, euchromatic regions were identified in the pericentromeric regions of the chromosomes 15 and 22 sized 1.2 Mb (chr15 [hg19]: 20,700,000–21,910,881) and 714 kb (chr22 [hg19]: 17,900,000–18,614,436), respectively.

DISCUSSION

Small supernumerary marker chromosomes represent a rare chromosomal abnormality, since these are both numerical and structural aberrations [18]. The clinical manifestations associated with sSMC vary, however, syndromal forms have been reported for some of those, such as cat eye syndrome (MIM#115470), Emanuel syndrome (MIM#609029), Pallister–Killian syndrome (MIM#601803), and isochromosome 18p syndrome (MIM#614290) [19].

The clinical features can be most often largely explained by euchromatin involvement in the chromosome imbalance, i.e. the presence/absence of dosage-sensitive genes in the

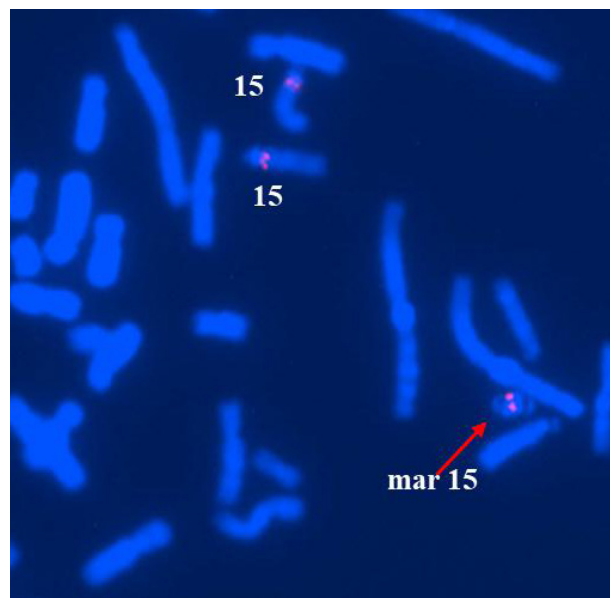


Fig. 3. Results of hybridization involving the homemade DNA probe for the chromosome 15 pericentromeric euchromatin — hm-15-prox

Table 2. Molecular cytogenetic characteristics of sSMC

№	Sex	FISH with commercial DNA probes	FISH with homemade DNA probes (hm)		
			Proximal	Median	Distal
1	M	ish dic(15;15)(D15Z1+,SNRPN-;SNRPN-,D15Z1+)	hm15-	Not provided for для sSMC 15	–
2	F	ish dic(15; 15)(D15Z1+,SNRPN-;SNRPN-,D15Z1+)	hm15-		–
3	F	ish dic(15; 15)(D15Z1+,D15S10-;D15S10-,D15Z1+)	hm15+		hm15-
4	F	ish dic(15; 15)(D15Z1+,SNRPN-;SNRPN-,D15Z1+)	hm15-		–
5	F	ish dic(15; 15)(D15Z1+,D15S10-;D15S10-,D15Z1+)	hm15-		–
6	F	ish dic(15; 15)(D15Z1+,D15S10-;D15S10-,D15Z1+)	hm15+		hm15-
7	M	ish dic(15; 15)(D15Z1+,D15S10-;D15S10-,D15Z1+)	hm15+		hm15-
8	M	ish dic(15; 15)(D15Z1+,D15S10-;D15S10-,D15Z1+)	hm15+		hm15-
9	F	ish dic(15; 15)(D15Z1+,D15S10-;D15S10-,D15Z1+)	hm15+		hm15-
10	F	ish dic(22; 22)(D14Z1/D22Z1+,TBX1-;TBX1-;D14Z1/D22Z1+)	hm22-	–	–
11	M	ish dic(22; 22)(D14Z1/D22Z1+,TBX1-;TBX1-;D14Z1/D22Z1+)	hm22++	hm22+	hm22-
12	M	ish r(22)(p13q11.1)(D14Z1/D22Z1+,TBX1-)	hm22-	–	–
13	F	ish dic(22; 22)(D14Z1/D22Z1+,TBX1-;TBX1-;D14Z1/D22Z1+)	hm22-	–	–
14	F	ish dic(22; 22)(D14Z1/D22Z1+,TBX1-;TBX1-;D14Z1/D22Z1+)	hm22-	–	–
15	M	ish i(22)(p10)(D14Z1/D22Z1+,acro-p++)	hm22-	–	–
16	F	ish dic(22; 22)(D14Z1/D22Z1+,TBX1-;TBX1-;D14Z1/D22Z1+)	hm22-	–	–
17	M	ish dic(22; 22)(D14Z1/D22Z1+,TBX1-;TBX1-;D14Z1/D22Z1+)	hm22-	–	–
18	M	ish dic(22; 22)(D14Z1/D22Z1+,TBX1-;TBX1-;D14Z1/D22Z1+)	hm22-	–	–

Note: hm (homemade) — homemade DNA probe.

pericentromeric euchromatic regions. However, no specific genes have been yet identified [7].

With the development of molecular cytogenetics methods, it became possible to determine the sSMC chromosomal origin and classify sSMC based on the presence or absence of euchromatic regions, thereby facilitating the analysis of the relationship between sSMC and clinical phenotypic abnormalities [6]. Laboratory approaches to the diagnosis and assessment of sSMC are well represented in the literature [20–22]. Fluorescent *in situ* hybridization and chromosomal microarray analysis are most often used to identify the structure and determine the gene content. The shortcomings of the latter include difficulties in interpreting the exact degree of mosaicism, which is a crucial point, given the high frequency of the sSMC mosaic forms [1]. It is more preferable to use FISH, however, the commercial DNA probes not always cover the chromosomal region of interest. Thus, the homemade DNA probes designed to solve specific problems become more and more important. In one of the studies, the possibility of using the PeCR-FISH kit for determination of pericentromeric euchromatin in sSMC developed by the authors is discussed; it has been shown that the locus specific homemade DNA probes based on the BAC clones can be used to accurately determine the sSMC size and the pericentromeric euchromatin involvement [7]. During the reported study, we have designed our own homemade oligonucleotide DNA probes for the pericentromeric euchromatin of chromosomes 15 and 22. The FISH analysis results demonstrate high quality of hybridization signals and, therefore, the possibility of using this approach to assess pericentromeric euchromatin in sSMC carriers.

Our data on the pericentromeric euchromatin size in asymptomatic carriers of sSMC 15 and 22 are consistent with the available literature data and complement these data. To date, there is a rather large number of reported cases of the presence of sSMC 15 in the karyotype of patients without phenotypic features, specifically 418 cases according

to the marker chromosome database (Chromosomes — Database, [23]), among which the majority of sSMC comprise heterochromatin only. The number of sSMC cases with euchromatin involvement, apart from prenatal cases, is small [18]. For example, it was found that in an asymptomatic carrier of sSMC15 with a history of infertility, the length of the gene dose-insensitive region is 3.8 Mb (15-Oq11.2/2-6 in the above database). It should be noted that high degree of mosaicism has been reported in the patient (74% based on the abnormal clone). The proximal pericentromeric euchromatic region revealed in five asymptomatic carriers of sSMC 15 in our sample turned out to be shorter (1.2 Mb) compared to the previously reported “non-critical” region, which makes it possible to significantly complement the database of the marker chromosome 15 region insensitive to the genes dosage.

The number of papers focused on studying sSMC 22 in asymptomatic carriers is much smaller, which correlates with the rate of this chromosomal abnormality [24]. To date, the data of 156 such patients have been reported (according to the website), among them the majority have sSMC comprising heterochromatin only [23]. It has been shown that the size of dosage-insensitive pericentromeric euchromatin region of chromosome 22 in case of triplication is about 100 kb. However, it is important to note that the reported case is unique, it is represented by detection of triplication in the fetus, i.e. identified during prenatal assessment, while normal phenotype has been reported after birth [7, 18]. In the case we have identified, the size of pericentromeric euchromatin of chromosome 22 in the sSMC 22 asymptomatic carrier was 714 kb, which far exceeded the reported size of the “non-critical” proximal region of the chromosome 22 q-arm. New data were obtained on the size of the proximal euchromatin of chromosome 22, which is insensitive to an increase in the dose of genes, may be important for the prenatal diagnosis of cases of the chromosome 22 genomic imbalances (duplication, triplication).

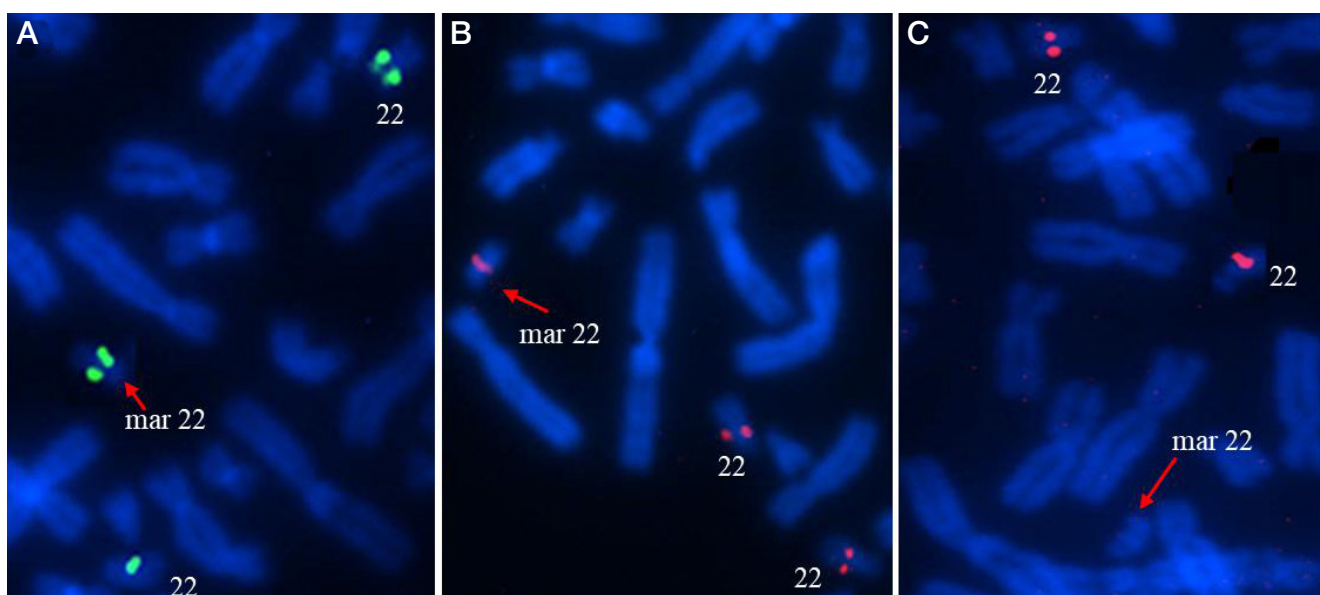


Fig. 4. Results of hybridization involving the homemade DNA probe for the chromosome 22 pericentromeric euchromatin. **A.** Proximal DNA probe. **B.** Median DNA probe. **C.** Distal DNA probe

CONCLUSIONS

Our research findings suggest that, in the pericentromeric euchromatin of the long arm of chromosome 15 (chr15(hg19): 20,700,000–21,910,881) and the long arm of chromosome 22 (chr22(hg19): 17,900,000–18,614,436), there is an apparent absence of genes that are potentially sensitive to an increase

in the copy number of DNA sections. The genomic imbalance resulting from duplication/triplication of these regions does not appear to have an adverse impact on intellectual development or cause developmental abnormalities. Our developed approach utilizing non-serial DNA probes has demonstrated the high sensitivity and specificity of the FISH method for analyzing the pericentromeric euchromatin of chromosomes 15 and 22.

References

- Liehr T. Small supernumerary marker chromosomes (sSMC) in humans. *Cytogenet Genome Res.* 2004; 107 (1–2): 55–67. PMID: 15305057.
- Liehr T, Weise A. Frequency of small supernumerary marker chromosomes in prenatal, newborn, developmentally retarded and infertility diagnostics. *Int J Mol Med.* 2007; 19 (5): 719–31. PMID: 17390076.
- Liehr T. Small Supernumerary Marker Chromosomes (sSMC). A Guide for Human Geneticists and Clinicians; With contributions by UNIQUE (The Rare Chromosome Disorder Support Group). Heidelberg: Springer, 2012; p. 220.
- Dalprà L, Giardino D, Finelli P, Corti C, Valtorta C, Ilardi P, et al. Cytogenetic and molecular evaluation of 241 small supernumerary marker chromosomes: cooperative study of 19 Italian laboratories. *Genet Med.* 2005; 7 (9): 620–5. PMID: 16301863.
- Liehr T. Small supernumerary marker chromosomes (sSMCs): a spotlight on some nomenclature problems. *J Histochem Cytochem.* 2009; 57 (11): 991–3. PMID: 19654102.
- Hamid A, Weise A, Voigt M, Bucksch M, Kosyakova N, Liehr T, et al. Clinical impact of proximal autosomal imbalances. *Balkan J Med Genet.* 2012; 15 (2): 15–22. PMID: 24052727.
- Al-Rikabi ABH, Pekova S, Fan X, Jančuřková T, Liehr T. Small Supernumerary Marker Chromosome May Provide Information on Dosage-insensitive Pericentric Regions in Human. *Curr Genomics.* 2018; 19 (3): 192–9. PMID: 29606906.
- Liehr T, Stumm M, Wegner RD, Bhatt S, Hickmann P, Patsalis PC, et al. 10p11.2 to 10q11.2 is a yet unreported region leading to unbalanced chromosomal abnormalities without phenotypic consequences. *Cytogenet Genome Res.* 2009; 124 (1): 102–5. PMID: 19372675.
- Ginter EK. Tsitogeneticheskie metody diagnostiki khromosomnykh bolezney. Metodicheskoe posobie dlya vrachey. M.: GEOTAR-Media, 2009; 81 p. Russian.
- Ye J, Coulouris G, Zaretskaya I, Cutcutache I, Rozen S, Madden TL. Primer-BLAST: a tool to design target-specific primers for polymerase chain reaction. *BMC Bioinformatics.* 2012; 13: 134. PMID: 22708584.
- UCSC Genome Browser. Available from: <http://genome.ucsc.edu>.
- OligoAnalyzer™ Tool. Available from: <https://eu.idtdna.com/pages/tools/oligoanalyzer/>.
- ООО «BiolabMiks»; Russia. Available from: <http://www.biolabmix.ru>. Russian.
- Minzhenkova ME, Yurchenko DA, Semenova NA, Markova ZG, Tarylcheva AA, Shilova NV. Characterization of a complex chromosomal rearrangement in a girl with PURA syndrome. *Genetics and Molecular Research.* 2022; 21 (4): GMR19065.
- Yurchenko DA, Minzhenkova ME, Tveleneva AA, Vorontsova EO, Kharchenko TV, Shilova NV. Cytogenomic approach in the diagnostics of inverted duplication/deletion rearrangements. *Medical Genetics.* 2023; 22 (5): 54–62. Russian.
- Liehr T. Fluorescence in Situ Hybridization (FISH) — Application Guide. Berlin: Springer, 2017; p. 606.
- Yurchenko DA. Molekulyarno-tsitogeneticheskie kharakteristiki i osobennosti diagnostiki variatsiy chisla kopiy uchastkov DNK (CNV) [dissertation]. M., 2022. Russian.
- Liehr T, Williams HE, Ziegler M, Kankel S, Padutsch N, Al-Rikabi A. Small supernumerary marker chromosomes derived from chromosome 14 and/or 22. *Mol Cytogenet.* 2021; 14 (1): 13. PMID: 33632263.
- OMIM — Online Mendelian Inheritance in Man. Available from: <https://www.omim.org/>.
- Hills LV, Nouri S, Slater HR. Pericentromeric euchromatin is conserved in minute human supernumerary chromosomes: a study using cross-species colour segmenting (RxFISH). *Chromosome Res.* 2003; 11 (4): 359–63. DOI: 10.1023/a:1024096024847.
- Liehr T, Weise A, Hamid AB, Fan X, Klein E, Aust N, et al. Multicolor FISH methods in current clinical diagnostics. *Expert Rev Mol Diagn.* 2013; 13 (3): 251–5.

22. Hamid AB, Kreskowski K, Weise A, Kosayakova N, Mrasek K, Voigt M, et al. How to narrow down chromosomal breakpoints in small and large derivative chromosomes — a new probe set. *J. Appl. Genet.* 2012; 53 (3): 259–9.
23. ChromosOmics — Database. Available from: <http://cs-tl.de/DB/CA/sSMC/15/a-Start.html>.
24. Tug E, Karaoguz MY, Ergun MA. Prenatal and Postnatal Clinical Spectrum of a Mosaic Small Supernumerary Marker Chromosome 22. *International Journal of Pediatrics and Child Health.* 2019; 7: 36–9.

Литература

1. Liehr T. Small supernumerary marker chromosomes (sSMC) in humans. *Cytogenet Genome Res.* 2004; 107 (1–2): 55–67. PMID: 15305057.
2. Liehr T, Weise A. Frequency of small supernumerary marker chromosomes in prenatal, newborn, developmentally retarded and infertility diagnostics. *Int J Mol Med.* 2007; 19 (5): 719–31. PMID: 17390076.
3. Liehr T. Small Supernumerary Marker Chromosomes (sSMC). A Guide for Human Geneticists and Clinicians; With contributions by UNIQUE (The Rare Chromosome Disorder Support Group). Heidelberg: Springer, 2012; p. 220.
4. Dalprà L, Giardino D, Finelli P, Corti C, Valtorta C, Iardi P, et al. Cytogenetic and molecular evaluation of 241 small supernumerary marker chromosomes: cooperative study of 19 Italian laboratories. *Genet Med.* 2005; 7 (9): 620–5. PMID: 16301863.
5. Liehr T. Small supernumerary marker chromosomes (sSMCs): a spotlight on some nomenclature problems. *J Histochem Cytochem.* 2009; 57 (11): 991–3. PMID: 19654102.
6. Hamid A, Weise A, Voigt M, Bucksch M, Kosyakova N, Liehr T, et al. Clinical impact of proximal autosomal imbalances. *Balkan J Med Genet.* 2012; 15 (2): 15–22. PMID: 24052727.
7. Al-Rikabi ABH, Pekova S, Fan X, Jančušková T, Liehr T. Small Supernumerary Marker Chromosome May Provide Information on Dosage-insensitive Pericentric Regions in Human. *Curr Genomics.* 2018; 19 (3): 192–9. PMID: 29606906.
8. Liehr T, Stumm M, Wegner RD, Bhatt S, Hickmann P, Patsalis PC, et al. 10p11.2 to 10q11.2 is a yet unreported region leading to unbalanced chromosomal abnormalities without phenotypic consequences. *Cytogenet Genome Res.* 2009; 124 (1): 102–5. PMID: 19372675.
9. Гинтер Е. К. Цитогенетические методы диагностики хромосомных болезней. Методическое пособие для врачей. М.: ГЭОТАР-Медиа, 2009; 81 с.
10. Ye J, Coulouris G, Zaretskaya I, Cutcutache I, Rozen S, Madden TL. Primer-BLAST: a tool to design target-specific primers for polymerase chain reaction. *BMC Bioinformatics.* 2012; 13: 134. PMID: 22708584.
11. UCSC Genome Browser. Available from: <http://genome.ucsc.edu>.
12. OligoAnalyzer™ Tool. Available from: <https://eu.idtdna.com/pages/tools/oligoanalyzer/>.
13. ООО «БиолабМикс»; Россия. Доступно по ссылке: <http://www.biolabmix.ru>.
14. Minzhenkova ME, Yurchenko DA, Semenova NA, Markova ZG, Tarlycheva AA, Shilova NV. Characterization of a complex chromosomal rearrangement in a girl with PURA syndrome. *Genetics and Molecular Research.* 2022; 21 (4): GMR19065.
15. Юрченко Д. А., Миньженкова М. Е., Твеленева А. А., Воронцова Е. О., Харченко Т. В., Шилова Н. В. Цитогеномный подход в диагностике инвертированных дупликаций со смежными терминальными делециями. *Медицинская генетика.* 2023; 22 (5): 54–62.
16. Liehr T. Fluorescence in Situ Hybridization (FISH) — Application Guide. Berlin: Springer, 2017; p. 606.
17. Юрченко Д. А. Молекулярно-цитогенетические характеристики и особенности диагностики вариаций числа копий участков ДНК (CNV) [диссертация]. М., 2022.
18. Liehr T, Williams HE, Ziegler M, Kankel S, Padutsch N, Al-Rikabi A. Small supernumerary marker chromosomes derived from chromosome 14 and/or 22. *Mol Cytogenet.* 2021; 14 (1): 13. PMID: 33632263.
19. OMIM — Online Mendelian Inheritance in Man. Available from: <https://www.omim.org/>.
20. Hills LV, Nouri S, Slater HR. Pericentromeric euchromatin is conserved in minute human supernumerary chromosomes: a study using cross-species colour segmenting (Rx-FISH). *Chromosome Res.* 2003; 11 (4): 359–63. DOI: 10.1023/a:1024096024847.
21. Liehr T, Weise A, Hamid AB, Fan X, Klein E, Aust N, et al. Multicolor FISH methods in current clinical diagnostics. *Expert Rev Mol Diagn.* 2013; 13 (3): 251–5.
22. Hamid AB, Kreskowski K, Weise A, Kosayakova N, Mrasek K, Voigt M, et al. How to narrow down chromosomal breakpoints in small and large derivative chromosomes — a new probe set. *J. Appl. Genet.* 2012; 53 (3): 259–9.
23. ChromosOmics — Database. Available from: <http://cs-tl.de/DB/CA/sSMC/15/a-Start.html>.
24. Tug E, Karaoguz MY, Ergun MA. Prenatal and Postnatal Clinical Spectrum of a Mosaic Small Supernumerary Marker Chromosome 22. *International Journal of Pediatrics and Child Health.* 2019; 7: 36–9.

FILAGGRIN LOSS-OF-FUNCTION MUTATIONS 2282DEL4, R501X, R2447X AND S3247X IN ATOPIC DERMATITIS

Verbenko DA , Karamova AE, Chikin VV, Kozlova IV, Aulova KM, Kubanov AA, Gorodnichev PV

State Research Center of Dermatovenereology and Cosmetology, Russian Ministry of Health, Moscow, Russia

Atopic dermatitis (AD) is a widespread multifactorial genetically determined inflammatory skin disease caused by, among other causes, impaired functions of the epidermal barrier. Loss-of-function mutations of the filaggrin gene (important part of the natural moisturizing factor system) that arrest production of the full-fledged precursor protein is associated with AD. This study investigated the frequency of the 2282delACTG (rs558269137), R501X (rs61816761), S3247X (rs150597413), R2447X (rs138726443) loss-of-function mutations of the filaggrin gene in adults of European origin with moderate to severe AD. The study involved 99 adult patients of both sexes aged 18–68 years. The mutations were identified with the help of the purpose-developed method of multiplex analysis of four single nucleotide polymorphisms that relies on the SNaPshot technique (minisequencing). The incidence of loss-of-function mutation of filaggrin 2282delACTG was 5.3%, that of R501X — 0.5%, R2447X — 1%. No S3247X mutation was detected in the sample. Collation of the results with Russian and European samples revealed a comparable level of the analyzed filaggrin gene mutations in adult patients with AD from different regions of the Russian Federation.

Keywords: atopic eczema, filaggrin, loss-of-function mutation, SNaPshot technique, SNP

Funding: the research was financially supported by the Ministry of Health of the Russian Federation (State Task for the State Research Center of Dermatovenereology and Cosmetology № 056-00116-21-00-6 for 2021–2023).

Author contribution: Karamova AE, Chikin VV, Aulova KM, Gorodnichev PV — examination of patients, diagnosing, SCORAD calculation, obtaining informed consent, sampling patients' biomaterial; Verbenko DA — research planning, molecular genetic experiments, manuscript authoring; Kozlova IV — analysis of uniqueness of the oligonucleotides hybridizing to the loss-of-function mutations in the *FLG* gene; Karamova AE — manuscript editing; Kubanov AA — general guidance, manuscript editing.

Compliance with ethical standards: the study was approved by the Ethics Committee of the State Research Center of Dermatovenereology and Cosmetology (Minutes #1 of January 29, 2021), and meets the standards of good clinical practice and evidence-based medicine. All patients included in the study have read and signed a voluntary informed consent to participate therein.

 **Correspondence should be addressed:** Dmitry A. Verbenko
Korolenko, 3/6, k. 320, Moscow, 117076, Russia; verbenko@gmail.com

Received: 12.01.2024 **Accepted:** 10.02.2024 **Published online:** 25.02.2024

DOI: 10.24075/brsmu.2024.006

МУТАЦИИ 2282DEL4, R501X, R2447X, S3247X ФИЛАГГРИНА ПРИ АТОПИЧЕСКОМ ДЕРМАТИТЕ

Д. А. Вербенко , А. Э. Карамова, В. В. Чикин, И. В. Козлова, К. М. Аулова, А. А. Кубанов, П. В. Городничев

Государственный научный центр дерматовенерологии и косметологии, Москва, Россия

Атопический дерматит (АтД) — широко распространенное мультифакторное генетически детерминированное воспалительное заболевание кожи, обусловленное среди прочих причин нарушением функций эпидермального барьера. Нулевые мутации гена филлагрина — важного компонента системы натурального увлажняющего фактора, приводящие к отсутствию выработки полноценного белка-предшественника, ассоциированы с АтД. Цель исследования — оценить частоту наиболее распространенных в европейских популяциях нулевых мутаций гена филлагрина 2282delACTG (rs558269137), R501X (rs61816761), S3247X (rs150597413), R2447X (rs138726443) у взрослых пациентов со среднетяжелой и тяжелой степенью АтД. Анализ проведен у 99 взрослых пациентов обоих полов в возрасте 18–68 лет, со среднетяжелым и тяжелым АтД. Идентификацию мутаций осуществляли с помощью разработанного метода мультиплексного анализа четырех однонуклеотидных полиморфизмов при использовании минисеквенирования. Частота встречаемости нулевой мутации филлагрина 2282delACTG оказалась на уровне 5,3%, R501X — на уровне 0,5%, R2447X — на уровне 1%. Нулевая мутация S3247X гена *FLG* в выборке пациентов не обнаружена. Сравнение результатов с российскими и европейскими выборками выявило сопоставимый уровень анализируемых мутаций гена филлагрина у взрослых пациентов с АтД из различных регионов Российской Федерации.

Ключевые слова: атопический дерматит, филлагрин, нулевые мутации, минисеквенирование, однонуклеотидный полиморфизм

Финансирование: исследования выполнены при финансовой поддержке Минздрава РФ (Государственное задание ГНЦДК № 056-00116-21-00-6 на 2021–2023 гг.).

Вклад авторов: А. Э. Карамова, В. В. Чикин, К. М. Аулова, П. В. Городничев — обследование пациентов, постановка диагноза, расчет клинического индекса SCORAD, получение информированного согласия и забор биоматериала пациентов; Д. А. Вербенко — планирование исследования, выполнение молекулярно-генетических экспериментов, написание рукописи; И. В. Козлова — анализ уникальности гибридизирующихся к нулевым мутациям олигонуклеотидов в гене *FLG*; А. Э. Карамова — редактирование рукописи; А. А. Кубанов — общее руководство, редактирование рукописи.

Соблюдение этических стандартов: исследование одобрено этическим комитетом при ФГБУ «Государственный научный центр дерматовенерологии и косметологии» (протокол заседания № 1 от 29 января 2021 г.), соответствует стандартам добросовестной клинической практики и доказательной медицины. Все включенные в исследование пациенты ознакомились и подписали добровольное информированное согласие на участие в его проведении.

 **Для корреспонденции:** Дмитрий Анатольевич Вербенко
ул. Короленко, 3/6, каб. 320, г. Москва, 117076, Россия; verbenko@gmail.com

Статья получена: 12.01.2024 **Статья принята к печати:** 10.02.2024 **Опубликована онлайн:** 25.02.2024

DOI: 10.24075/vrgmu.2024.006

Atopic dermatitis (AD) is a multifactorial genetically determined, chronic and recurrent inflammatory skin disease characterized by itching, age-dependent localizations and morphology of lesions. This is one of the most common skin diseases [1–2]. The prevalence and incidence of AD in the entire population of the Russian Federation (RF) in 2022 amounted to 384.7 and 157.1 cases per 100,000 population, respectively [3, 4]. In German-speaking countries, 25% of all referrals to a dermatovenerologist turn out to have moderate or severe AD [5].

A filaggrin gene mutation and change of function of the epidermal barrier are the genetic factors of AD development [2]. Hereditary determination plays an important role in its the pathogenesis, causing skin barrier disruptions, immunity defects (stimulation of Th2 cells with subsequent hyperproduction of IgE), hypersensitivity to allergens and non-specific stimuli, colonization by pathogenic microorganisms (*Staphylococcus aureus*, *Malassezia furfur*), and autonomic nervous system disbalance with increased production of inflammatory mediators [1, 6, 7]. Twin and family studies confirm the magnitude of effect of hereditary factors (72–90%) on the development of the disease. Eighty percent of children whose parents have AD suffer from the disease; this figure goes down to 50% if only one parent has AD, but the risk grows 1.5-fold if that parent is mother [8]. Thus, genes encoding structural and functional proteins of the epidermis and those managing innate and acquired immunity underly pathogenesis of the disease [1, 9, 10]. However, genome-wide association studies (GWAS) show that genomic regions associated with AD explain only about 15% of cases of the disease, and the remaining variability, the so-called "missing heritability" peculiar to complex diseases, may stem from its pronounced heterogeneity, cumulative effects of structural variations, and fluctuations of quantity of genomic copies, as well as epigenetic influences [8–10].

The size of the *FLG* gene is 2 kb; it is located on the 1st chromosome of the epidermal differentiation complex counting 70 genes [1, 11]. The gene consists of three exons, the first two of which regulate its expression, and the third contains from 10 to 13 tandemly arranged filaggrin repeats [12]. The product of the gene is profilaggrin, a protein expressed in the epidermis basal cells. Diffused into the upper layers of the outer skin, it undergoes a number of biochemical transformations that result in formation of filaggrin monomers, degradation of which produces components that are part of the natural moisturizing factor [8, 13].

Numerous studies have confirmed that loss-of-function mutations in the filaggrin gene, which stop production of the protein, are the key AD development factor [1, 2, 8, 11–18]. Carriers of such mutations run a 3.12-fold greater risk of having this disease, and in the Russian population, the ultimate risk may be 8.13 times greater [19, 20]. In the AD pathogenesis, *FLG* gene loss-of-function mutations compromise protective function of the skin barrier, which facilitates penetration of the epidermis by environmental factors that initiate inflammatory reactions and subsequent moderate-to-severe course of the disease.

The frequency of such mutations has been shown to be increased in AD patients, and their spectrum revealed to depend on these patients' ethnicity [15]. In European populations, the most common loss-of-function mutations are 2282del4, R501X, R2447X, S3247X, and in Asian populations - c.3321delA, c.6950del8, p.S2706X, p.K4022X, p.E2422X, p.Q2417X, p.S1515X, p.S406X, etc. [11–18]. There is evidence of a correlation between the frequency of *FLG* gene loss-of-function mutations and the severity of AD [16, 21].

The classic approach to identification of the *FLG* gene loss-of-function mutations involves a PCR with the considered

locus and a subsequent restriction analysis of the product of this reaction [22]. However, unstable performance of the restriction enzyme may produce a biased estimate of the frequency. Sanger sequencing of the *FLG* gene's third exon is complicated by repetitive sequences of filaggrin monomers [8, 11, 13]; the same reason is likely to be behind lack of common application of allele-specific hybridization as well as TaqMan real-time PCR [23, 24], which is also used to detect mutations of the filaggrin gene. Next-generation sequencing (NGS) can reveal the full spectrum of the *FLG* gene loss-of-function mutations [17]. However, NGS requires special equipment and large samples, since some loss-of-function mutations are rare; in addition, targeted filaggrin LOF sequencing kits are not yet commercially available in Russia. At the same time it is possible to set up single-tube studies (in any PCR laboratory equipped for fragment analysis) and identify such *FLG* gene mutations most common in the European populations.

This study aimed to estimate the frequency of 2282delACTG (rs558269137), R501X (rs61816761), S3247X (rs150597413), R2447X (rs138726443), most common *FLG* gene loss-of-function mutations in the European populations, using the new method based SNaPshot technique.

METHODS

The study was conducted in the State Research Center of Dermatovenerology and Cosmetology of the Ministry of Health of the Russian Federation. The study's inclusion and exclusion criteria have been described earlier [25].

The total number of AD patients participating in the study was 99, 50 female and 49 male, aged 18–68 years. The mean age of the patients was 31.07 ± 10.53 years; all of them have been diagnosed with AD before the study, and when included, had the disease confirmed as exhibiting features described by J.M. Hanifin and G. Rajka [2, 26]. Ninety-six patients were of European origin, three — Asian ethnics.

Table 1 gives the age of onset of AD in the participants.

The disease manifested primarily in childhood. Most often (49.5% of cases), the onset was registered in infancy, before the age of 1 year. Sixty-eight patients (68.7%) developed AD before the age of 3. In 88 patients, the disease first manifested when they were under 7 years of age. However, 5 (5.0%) patients reported the onset of AD in adulthood.

Allergic rhinitis was diagnosed in 17 (17.2%) patients, bronchial asthma in 15 (15.2%), pollinosis in 11 (11.1%), allergic conjunctivitis in 9 (9.1%).

The analysis of the family history considered blood-related siblings, parents and grandparents, and uncles and aunts; in 44 patients, it revealed atopic and allergic burdens. AD was diagnosed in relatives of 40 (40.4%) participants: fathers of 14, mothers of 13, grandparents of 6, siblings of 6, uncles/aunts of 7. Relatives of 8 (8.1%) AD patients suffered from bronchial asthma. Three patients reported that their fathers have been diagnosed with bronchial asthma, 2 patients pointed to this disease in their brothers, and 1 participant stated that this diagnosis was announced to his mother, grandfather and grandmother. Two (2.0%) patients mentioned relatives with pollinosis, a father of one and a grandmother of another. As for allergic rhinitis, this disorder affected both parents of one patient and father of another patient, which means there were 2 (2.0%) participants with it in their family medical history.

The severity of AD was established with the help of the SCORAD. The participants that who 25 through 50 points on its scale were considered to have moderate AD, those with the score above 50 — severe AD [27].

Table 1. Participating AD patients by the disease onset age

Number of patients	abc.	Infancy (1 month to 1 year)	Early childhood (1 to 3 years)	Preschool age (3 to 7 years)	Junior and senior school age (7 to 18 years)	Early adulthood (18 to 44 years)	Total
		%	49,5	19,2	20,2	6,1	5

Thus, 64 (64.6%) patients were diagnosed with moderate AD, and 35 (35.4%) with severe atopic dermatitis. The SCORAD scores in the sample ranged from 25.2 to 77.1 points (mean — 47.20 ± 12.57 points).

The participants donated venous blood samples, 4–5 ml of which were collected into VACUETTE® K3E K3EDTA tubes (Greiner Bio-One; Austria), and separated into cellular and plasma fractions at 3000 g for 10 minutes in an Allegra X-14 centrifuge (Beckman Coulter; USA), the results of separation then stored at -20 °C until DNA extraction.

Genomic DNA was isolated from cellular biomass with the help of QIAamp DNA Mini Kit (QIAGEN; Germany), as prescribed by the manufacturer. Resulting genomic DNA's concentration and purity were analyzed in a NanoVue 2000 spectrophotometer (GeneralElectric; France).

To detect loss-of-function mutations of the FLG gene, we carried out a two-stage multiplex PCR with intermediate purification and subsequent identification of single-nucleotide polymorphisms after separation in 3130 Genetic Analyzer according to the instructions of the manufacturer of the SNaPshot kit (Applied Biosystems; USA). The sequences of oligonucleotides and hybridization probes were selected based on the data from BLAST (USA) [28], using Ugene software v.44.0 (<http://ugene.net/>); the synthesis was performed by Syntol LLC (Russia).

The first stage of PCR involved four regions of the FLG gene and was done with primers; Table 2 shows their nucleotide sequence. PCR was followed by visualization of the successful reaction in VersaDoc gel documentation system (Bio-Rad; USA), with ethidium bromide staining after separation of fragments by electrophoresis in 2% agarose gel (TAE buffer, voltage — 180 V, time — 30 minutes). To determine the molecular weight of the amplified fragments, we used a 100-1000 bps lengths marker. (Thermo Fisher Scientific; CLLIA).

For PCR, we used in 0.1 ml tubes (Biologix; China); the volume of the mixture was 20 µl, including 10 µl of PCR

buffer from the QUAGEN Multiplex PCR Kit (Germany), 5 pM of each primer per 1 µl of the mixture, from 1 to 100 nM of DNA, and deionized water. The amplification program involved DNA melting and activation of Taq polymerase for 15 minutes at 95 °C, followed by 40 cycles that included annealing of primers at 57 °C for a minute, a minute long elongation at 72 °C, and melting at 95 °C for 30 seconds. When the reaction was over, we purified the PCR products by incubation at 37 °C for 45 minutes in the presence of exonuclease I and alkaline phosphatase enzymes: 0.5 µl of ExoI and 1 µl of FastUP (Thermo Fisher Scientific; USA) were added to 5 µl of the PCR product, and 15-minute enzymes inactivation at 85 °C.

The purified PCR products from the first stage were used in the hybridization PCR with oligonucleotides flanking single nucleotide polymorphisms, the sequences of which are shown in Table 3. The reaction occurred in 0.1 ml tubes (Biologix; China), the substance volume was 10 µl, including 5 µl of the finished mixture of 2x SNaPshot PCR ready Master Mix, 3 µl of water, 1 µl of mixed purified PCR products, and 1 µl of a primers mixture. At this stage, the amplification program included 25 cycles: primers annealing at 50 °C for 5 seconds, elongation at 60 °C for 30 seconds, and melting at 95 °C for 10 seconds. Once the reaction was over, PCR products were purified through incubation at 37 °C for 45 minutes in the presence of alkaline phosphatase: 1 µl of FastUP enzyme (Thermo Fisher Scientific; USA) was added to 5 µl of the PCR product, and subsequent inactivation at 85 °C for 15 minutes.

To 0.5 µl of the purified second-stage PCR product, we added 9 µl of deionized formamide and Gene Mapper LIZ-120 molecular weight marker (Applied Biosystems; USA), denatured the resulting mixture at 95 °C for 5 minutes, then cooled it on ice.

The mixture of products of the second stage of multiplex PCR was separated in an ABI 3130 Genetic Analyser (Applied Biosystems; USA), according to the SNaPshot kit protocol. For this operation, we used a standard 50 cm capillary tube filled

Table 2. Oligonucleotide sequences of primers for multiplex PCR of target regions of the FLG gene

Genome region	Primer direction	Nucleotide sequence 5'-3'
2282delACTG	direct	TGGTAGTCAGGCCACTGACAGTG
	reverse	GGTGACCAGCCTGTCCATGG
R501X	direct	GACCTATTTACCGATTGCTCGTGG
	reverse	GGACGTTCCAGGGTCTTCCCTCT
S3247X	direct	ACTGGACCCCCAGTGTCTACT
	reverse	GGTGGTCTGGGTCTGCTTCCAG
R2447X	direct	TGGGATGTGGTGTGGCTGTGATGAG
	reverse	CAAGGATCCCACCACAAGCAGGCA

Table 3. Detection of the FLG gene loss-of-function mutations 2282delACTG (rs558269137), R501X (rs61816761), S3247X (rs150597413), R2447X (rs138726443); oligonucleotide sequences of primers, second stage (hybridization PCR).

Mutation	Hybridizing primer 5'-3' nucleotide sequence	Amplicon size	Wild type allelic
2282delACTG (rs558269137)	(CT) ₂₂ ACCAGCCTGTCCATGGCCTGACACTG	71	A
R501X (rs61816761)	(CT) ₂₀ CGCTGAATGCCTGGAGCTGTCTC	64	G
S3247X (rs150597413)	(TC) ₁₁ TGGTGTCTGGAGCCGTGCCTT	44	G
R2447X (rs138726443)	(CT) ₁₃ CCGTTGAGTGCCTGGAGCTGTCTC	51	G

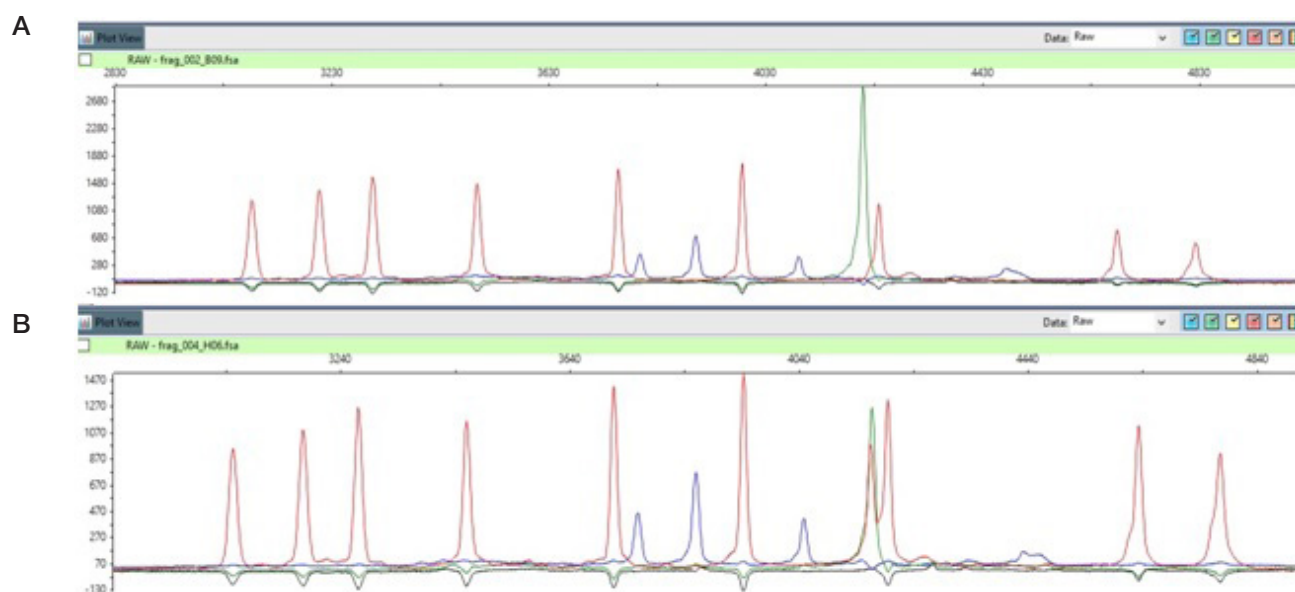


Fig. Electrophoregram of detection of the four single nucleotide polymorphisms of *FLG* gene loss-of-function mutations (minisequencing). Peak color signals the allelic variant, its size (retention time) indicates the specific polymorphism. Left to right: S3247X (rs150597413), R2447X (rs138726443), R501X (rs61816761), 2282delACTG (rs558269137). **A.** All allelic variants are wild-type, loss-of-function mutations not detected. **B.** An example of a 2282delACTG mutation heterozygote

with POP-7 polymer. The sample was introduced in the course of 7 seconds. We visualized the resulting chromatograms in Peak Scanner Software 2 (Applied Biosystems; USA), and decoded by comparing the retention time of the amplified fragments and Gene Mapper LIZ-120. The SNaPshot kit manufacturer (Applied Biosystems; USA) also offers Gene Mapper Software that can automatically decode single nucleotide polymorphisms. Comparison of the resulting data with wild-type alleles (enabled by electrophoregram imaging) allowed detecting presence of the filaggrin gene loss-of-function mutations against identification of the wild-type alleles.

To confirm detection of the 2282delACTG loss-of-function mutation by minisequencing, we analyzed an amplified fragment of the filaggrin gene (Table 1) using Ade I (Dra III) restrictase (SibEnzyme; Russia), as described in a previously published study [22]. 2282delACTG deletion creates a Dra III restrictase recognition site, which is visualized as two bands after separation of the hydrolysis products in an agarose gel.

For PCR, we used T100 (Bio-Rad; USA) and 96-well plates (Applied Biosystems; USA). The reaction was carried out in 10 μ l of a mixture comprising 0.1 μ l of each primer per 1 μ l, 5 μ l of the PCR reaction mixture from a commercially available Multiplex PCR mix kit (QIAGEN; Germany), deionized water, and a DNA matrix. The amplification program included DNA melting and polymerase activation for 15 minutes and subsequent 40 cycles of 30-second primer annealing at 54 $^{\circ}$ C, 30-second elongation, and mixture melting at 95 $^{\circ}$ C for 15 seconds.

The hydrolysis of the PCR fragment was enabled by T100 (Bio-Rad; USA) in 96-well plates (Applied Biosystems; USA); the procedure lasted for 3 hours at 37 $^{\circ}$ C, and involved 20 μ l of the reaction mixture containing 5 units of restriction endonuclease, 2 μ l of restriction buffer, 10 μ l of the PCR product, and deionized water. The restriction sites were detected after 30-minute separation in a chamber (Bio-Rad; USA) on 2% agarose gel at 180 V by visualization of ethidium bromide-stained fragments in UV light.

RESULTS

To estimate the frequency of the filaggrin gene loss-of-function mutations 2282delACTG (rs558269137), R501X (rs61816761),

S3247X (rs150597413), R2447X (rs138726443) in adult patients with moderate to severe AD, we developed a method based the detection of single-nucleotide polymorphisms that signal presence of such mutations. This method allows simultaneous identification of four *FLG* gene loss-of-function mutations; it is based on two consecutive PCRs, with the first reaction yielding the specific mutation locus, and second effecting single nucleotide elongation of the hybridizing primer with a special kit that allows determining allelic variants of a single nucleotide polymorphism. Simultaneous detection of the four considered single nucleotide polymorphisms is possible after separation in the capillary tube of 3130 Genetic Analyzer, performed as prescribed by the SNaPshot kit manufacturer (Applied Biosystems; USA); presence of the alleles different from the wild type allow conclusions about presence of loss-of-function mutations. Figure shows an example of the analysis of four loss-of-function mutations in the filaggrin gene.

The developed method of detection of loss-of-function mutations was verified by restriction analysis targeted at 2282delACTG in exon 3 of the filaggrin gene. The frequency of such mutations yielded by the analysis was 5.2%, which is comparable to the minisequencing data. Thus, the developed method of detection of the *FLG* gene loss-of-function mutations using minisequencing can be used to assess the prevalence thereof, including among the AD patients.

The study involved 99 adult patients with moderate to severe AD. In this sample, 6.8% of the participants had 2282delACTG, R501X, R2447X mutations, namely, 2282delACTG was detected in 5.05% of them, R501X — in 0.5%, R2447X — in 1%, and S3247X was not detected in any of the participating patients (Table 4). The loss-of-function mutation as a deletion of 4 p.o. in the heterozygous 2282delACTG was detected in 4% of patients, in the homozygous state — in one patient (1%), and along with R501X — in one patient, as a compound heterozygote.

DISCUSSION

The prevalence of the considered four mutations in the conditionally healthy populations represented in the 1000 Genomes catalog is below 1% [36]. The analysis of data describing adult AD patients revealed a slightly increased

Table 4. Frequency of occurrence of 2282delACTG, R501X, S3247X, R2447X in AD patients, Russian and European populations

	Sample size	2282delACTG	R501X	S3247X	R2447X	Reference
Patients with moderate to severe AD	99	5.05	0.5	0	1	
Residents of Novosibirsk	470	6.7	1.2	–	–	[29]
Russians of the central region of Russia	474	2.9	0.9	–	–	[30]
Russians of Bashkortostan	177	6.03	–	–	–	[31]
Tatars	126	9.35	–	–	–	[31]
Austrians and Germans	462	14.7	6.5	3	1.7	[32]
Germans	476	10.9	5.7	–	–	[33]
Italians	178	0.9	0.6	–	–	[34]
Finns	501	3.4	0.9	1.3	–	[35]

frequency of the *FLG* gene loss-of-function mutations (6.8%) compared with normal variability. In our study, the occurrence of R501X, S3247X and R2447X filaggrin gene mutations among AD patients was at the level of population variability for the cohort of conditionally healthy individuals. Thus, of the four studied *FLG* gene loss-of-function mutations, only 2282delACTG was associated with onset and development of AD in adult patients from the Russian Federation.

A comparison of the data on prevalence of the *FLG* gene loss-of-function mutations among adult AD patients in the Russian and European populations (Table 4) revealed slight fluctuations in the frequency of occurrence of the 2282delACTG mutation in different regions of the Russian Federation. The frequency variations, which, most likely, have evolutionary gene pool differences behind them, were twofold or less. The frequency of the 2282delACTG mutation in European adult AD patients varies more widely, and the value closest to that identified in our study was found in the respective reports from Finland. The data we obtained are comparable with the results of other studies investigating *FLG* gene loss-of-function mutations in Russian adult AD patients.

The integral frequency of the four *FLG* gene loss-of-function mutations (6.8%), as established in our study, was significantly lower than that registered in children with severe AD, which is 32.8% in the Russian population [21] and 42% in the comparable European patients [11]. A partial explanation of this phenomenon suggested by the researchers is that carriers of the loss-of-function mutations in the filaggrin gene have the

diseases onset at an earlier age (the odds ratio in the group under 20 years is 8.9; in the group under 5 years — 7.8) [37]. The detailed classification of AD types based on the specifics of immune pathways of development of the disease (Th2/retinol, skin homing, Th1/Th2/Th17/IL1, and Th1/IL1 with the influence of eosinophils) can also explain the differences in the frequency of the *FLG* gene loss-of-function mutations in patients of different age groups [38, 39]. The severity of the disease and the pathogenesis of AD in adults are associated only with the 'skin homing' inflammation pathway, which is consistent with data on the prevalence of AD in 20% of children and 2–8% of adults [40].

CONCLUSIONS

The technique for detection of the four *FLG* gene loss-of-function mutations most common in the European populations was developed based on the SNaPshot (minisequencing) approach. Examination of patients with moderate to severe AD with this technique revealed following frequencies of mutations: 2282delACTG — 5.05%, R501X — 0.5%, R2447X — 1%. No S3247X mutation was detected in the sample. The level of the *FLG* gene loss-of-function mutations is comparable to that reported in other studies examining adult AD patients from Russia. The data obtained suggest that the filaggrin gene loss-of-function mutations most common in the European populations contribute to the development of AD insignificantly.

References

- Zaslavskij DV, Svitich OA, Kudrjavceva AV. Atopicheskiy dermatit. Mezhdisciplinarnyj podhod k diagnostike i lecheniju: Rukovodstvo dlja vrachej. Moskva: GJeOTAR-Media, 2024; 288 s. Russian.
- Klinicheskie rekomendacii. Atopicheskiy dermatit. Utverzhdeny Minzdravom RF. Dostupno po ssylke: https://www.nrcii.ru/specialistam/klinrecommend/atopic_dermatitis_2020.pdf. Russian.
- Kubanov AA, Bogdanova EV. Resursy i rezul'taty dejatel'nosti medicinskih organizacij, okazyvajushhih medicinskuju pomoshh' po profilju «dermatovenerologija», v Rossijskoj Federacii v 2016–2022 gg. Vestnik dermatologii i venerologii. 2023; 99 (4): 18–40. Dostupno po ssylke: <https://doi.org/10.25208/vdv12385>. Russian.
- Kotova EG, Kobjakova OS, Kubanov AA, Starodubov VI, Aleksandrova GA, Bogdanova EV, i dr. Resursy i dejatel'nost' medicinskih organizacij dermatovenerologicheskogo profilja. Zabolevaemost' infekcijami, peredavaemymi polovym putem, zaraznymi kozhnymi boleznyami i boleznyami kozhi v 2022 godu: statisticheskie materialy. M.: FGBU «CNIIOIZ» Minzdrava Rossii, 2023; 209 s. DOI: 10.21045/978-5-94116-130-0-2023. Russian.
- Traidl S, Freimooser S, Werfel T. Janus kinase inhibitors for the therapy of atopic dermatitis. Allergol Select. 2021; 5: 293–304. DOI: 10.5414/ALX02272E.
- Gelezhe KA, Kudravtseva AV, Ryzhii E, Khachatryan LG, Bogdanova EA, Svitich OA. The role of the skin microbiome in the development of allergic inflammation in atopic dermatitis. New Armenian Medical Journal. 2021; 15 (1): 100–8.
- Gorskij VS, Bljumina VA. Sovremennye predstavlenija o patogeneze atopicheskogo dermatita. Immunopatologija, allergologija, infektologija. 2022; 3: 70–76. DOI: 10.14427/jipai.2022.3.70. Russian.
- Beljaeva TM, Ponomarenko IV, Churnosov MI. Molekuljarno-geneticheskie determinanty atopicheskogo dermatita (dannye polnogenomnyh issledovanij). Klinicheskaja dermatologija i venerologija. 2020; 19 (5): 615–21. DOI: 10.17116/klinderma202019051615. Russian.
- Svitich OA, Olisova OJu, Meremjanina EA., Rasskazova ND, Fomina VA, Potapova MB. Rol' polimorfnyh markerov v genah TLR2, TLR4 i TLR9 v riske razvitiya atopicheskogo dermatita. Medicinskaja immunologija. 2023; 25 (5): 1043–8. DOI: 10.15789/1563-0625-AOS-2807. Russian.
- Smolkina OJu, Bystrickaja EP, Svitich OA, Piruzjan AL, Denisova EV, Korsunskaja IM, i dr. Analiz metilirovanija DNK v porazhennoj

- i neporazhennoj kozhe u vzroslyh pacientov s atopicheskim dermatitom. *Molekuljarnaja medicina*, 2021; 19 (1): 53–58. DOI: 10.29296/24999490-2021-01-08. Russian.
11. Gupta J, Margolis DJ. Filaggrin gene mutations with special reference to atopic dermatitis. *Curr Treat Options Allergy*. 2020; 7 (3): 403–13. DOI: 10.1007/s40521-020-00271-x.
 12. Barker JN, Palmer CN, Zhao Y, Liao H, Hull PR, et al. Null mutations in the filaggrin gene (FLG) determine major susceptibility to early-onset atopic dermatitis that persists into adulthood. *J Invest Dermatol*. 2007; 127 (3): 564–7. DOI: 10.1038/sj.jid.5700587.
 13. Tamrazova OB, Gluhova EA. Unikal'naja molekula filaggrin v strukture jepidermisa i ee rol' v razvitii kseroza i patogeneza atopicheskogo dermatita. *Klinicheskaja dermatologija i venerologija*. 2021; 20 (6): 102–10. DOI: 10.17116/klinderma202120061102. Russian.
 14. Moosbrugger-Martinz V, Leprince C, Méchin M-C, Simon M, Blunder S, Gruber R, et al. Revisiting the roles of filaggrin in atopic dermatitis. *Int J Mol Sci*. 2022; 23: 5318. DOI: 10.3390/ijms23105318.
 15. Chiricozzi A, Maurelli M, Calabrese L, Peris K, Girolomoni G. Overview of atopic dermatitis in different ethnic groups. *J Clin Med*. 2023; 12: 2701. DOI: 10.3390/jcm12072701.
 16. Irvine AD, McLean WH, Leung DY. Filaggrin mutations associated with skin and allergic diseases. *N Engl J Med*. 2011; 365 (14): 1315–27. DOI: 10.1056/NEJMra1011040.
 17. X.F. Colin C. Wong, Simon L.I.J. Denil, Jia Nee Foo, Huijia Chen, Angeline Su Ling Tay, Rebecca L. Haines, et al. Array-based sequencing of filaggrin gene for comprehensive detection of disease-associated variants. *Journal of Allergy and Clinical Immunology*. 2018; 141 (2): 814–6. DOI: 10.1016/j.jaci.2017.10.001.
 18. Thyssen JP, Bikle DD, Elias PM. Evidence that loss-of-function filaggrin gene mutations evolved in northern Europeans to favor intracutaneous vitamin D3 production. *Evol Biol*. 2014; 41 (3): 388–96. DOI: 10.1007/s11692-014-9282-7.
 19. Rodríguez E, Baurecht H, Herberich E, Wagenpfeil S, Brown SJ, Cordell HJ, et al. Meta-analysis of filaggrin polymorphisms in eczema and asthma: robust risk factors in atopic disease. *J Allergy Clin Immunol*. 2009; 123 (6): 1361–70. DOI: 10.1016/j.jaci.2009.03.036.
 20. Makarova SI, Mitrofanov DV, Komova EG, Kaloshkin IV, Shintjapina AB, Kaznacheeva LF, i dr. Rol' mutacij gena filaggrina, vedushih k snizheniju kolichestva belka, v razvitii atopicheskogo dermatita i bronhial'noj astmy u detej. *Sibirskij nauchnyj medicinskij zhurnal*. 2021; 41 (3): 58–63. DOI: 10.18699/SSMJ20210308. Russian.
 21. Varlamov EE, Pampura AN. Pervichnaja profilaktika atopicheskogo dermatita u detej. *Rossijskij vestnik perinatologii i pediatrii*. 2015; 60 (5): 21–25. Russian.
 22. Gruber R, Janecke A, Fauth C, et al. Filaggrin mutations p.R501X and c.2282del4 in ichthyosis vulgaris. *Eur J Hum Genet*. 2007; 15, 179–84. DOI: 10.1038/sj.ejhg.5201742.
 23. Eremina AA, Gerlinger AV, Makeenko OA, Koh NV, Sergeeva IG. Vnedrenie sovremennyh genicheskikh i instrumental'nyh metodov obsledovanija v vedenii pacientov s vul'garnym ihtiozom i atopicheskim dermatitom. *Klinicheskaja dermatologija i venerologija*. 2023; 22 (4): 399–405. DOI: 10.17116/klinderma202322041399. Russian.
 24. Makeenko OA, Koh NV, Sergeeva IG. Klinicheskij razbor pacientov gomozigot po mutacii 2282del4 (rs558269137) v gene filaggrina. *Klinicheskaja dermatologija i venerologija*. 2022; 21 (3): 390–98. Dostupno po ssylke: <https://doi.org/10.17116/klinderma202221031390>. Russian.
 25. Chikin VV, Karamova AJe, Kubanov AA, Zhilova MB, Gorodnichev PV, Aulova KM. Uzkopolosnaja srednevolnovaja ul'traioletovaja terapija bol'nyh atopicheskim dermatitom: analiz faktorov, vlijajushih na vyrazhennost' terapevtsicheskogo jeffekta. *Vestnik dermatologii i venerologii*. 2023; 99 (5): 52–63. DOI: 10.25208/vdv15828. Russian.
 26. Hanifin JM, Rajka G. Diagnostic features of atopic dermatitis. *Acta DermVenereol*. 1980; 92 (Suppl): 44–47.
 27. Wollenberg A, Christen-Zäch S, Taieb A, Paul C, Thyssen JP, de Bruin-Weller M, et al. European Task Force on Atopic Dermatitis/EADV Eczema Task Force. ETFAD/EADV Eczema task force 2020 position paper on diagnosis and treatment of atopic dermatitis in adults and children. *J Eur Acad Dermatol Venereol*. 2020; 34 (12): 2717–44. DOI: 10.1111/jdv.16892.
 28. Standard Nucleotide BLAST. National Center for Biotechnology Information. U.S National Library of Medicine. Available from: https://blast.ncbi.nlm.nih.gov/Blast.cgi?PAGE_TYPE=BlastSearch.
 29. Maksimova JuV, Svechnikova EV, Maksimov VN, Lykva SG. Mutacii v gene filaggrina i atopicheskij dermatit. *Klinicheskaja dermatologija i venerologija*. 2014; 3: 58–62. Russian.
 30. Dvornyk V, Ponomarenko I, Belyaeva T, Reshetnikov E, Chumosov M. Filaggrin gene polymorphisms are associated with atopic dermatitis in women but not in men in the Caucasian population of Central Russia. *PLoS ONE*. 2021; 16 (12): e0261026. DOI: 10.1371/journal.pone.0261026.
 31. Gimalova GF, Karunas AS, Fedorova YY, Khusnutdinova EK. The study of filaggrin gene mutations and copy number variation in atopic dermatitis patients from Volga-Ural region of Russia. *Gene*. 2016; 591: 85–89. DOI: 10.1016/j.gene.2016.06.054.
 32. Greisenegger E, Novak N, Maintz L, Bieber T, Zimprich F, Haubenberger D, et al. Analysis of four prevalent filaggrin mutations (R501X, 2282del4, R2447X and S3247X) in Austrian and German patients with atopic dermatitis. *J Eur Acad Dermatol Venereol*. 2010; 24: 607–10. DOI: 10.1111/j.1468-3083.2009.03469.x.
 33. Weidinger S, Illig T, Baurecht H, Irvine AD, Rodriguez E, Diaz-Lacava A, et al. Loss-of-function variations within the filaggrin gene predispose for atopic dermatitis with allergic sensitizations. *J Allergy Clin Immunol*. 2006; 118 (1): 214–9. DOI: 10.1016/j.jaci.2006.05.004. Erratum in: *J Allergy Clin Immunol*. 2006; 118 (4): 922. Erratum in: *J Allergy Clin Immunol*. 2006; 118 (3): 724.
 34. Giardina E, Paolillo N, Sinibaldi C, Novelli G. R501X and 2282del4 filaggrin mutations do not confer susceptibility to psoriasis and atopic dermatitis in Italian patients. *Dermatology*. 2008; 216 (1): 83–4. DOI: 10.1159/000109365.
 35. Luukkonen TM, Kiiski V, Ahola M, Mandelin J, Virtanen H, Pöyhönen M, et al. The value of FLG null mutations in predicting treatment response in atopic dermatitis: an observational study in Finnish patients. *Acta Derm Venereol*. 2017; 97 (4): 456–63. DOI: 10.2340/00015555-2578.
 36. dbSNP Short Genetic Variations. Available from: https://www.ncbi.nlm.nih.gov/snp/rs558269137#frequency_tab (accessed 18 Dec 2023).
 37. Smieszek SP, Welsh S, Xiao C, et al. Correlation of age-of-onset of atopic dermatitis with filaggrin loss-of-function variant status. *Sci Rep*. 2020; 10: 2721. DOI: 10.1038/s41598-020-59627-7.
 38. Schuler CF, Allison C. Billi, Emanuel Maverakis, Lam C, Tsoi, Johann E. Gudjonsson, Novel insights into atopic dermatitis. *Journal of Allergy and Clinical Immunology*. 2023; 151 (5): 1145–54. DOI: 10.1016/j.jaci.2022.10.023.
 39. Bakker DS, de Graaf M, Nierkens S, Delemarre EM, Knol E, van Wijk F, et al. Unraveling heterogeneity in pediatric atopic dermatitis: identification of serum biomarker based patient clusters. *J Allergy Clin Immunol*. 2022; 149: 125–34. DOI: 10.1016/j.jaci.2021.06.029.
 40. Tokura Y, Hayano S. Subtypes of atopic dermatitis: From phenotype to endotype. *Allergology International*. 2022; 71 (1): 14–24. DOI: 10.1016/j.ait.2021.07.003.

Литература

1. Заславский Д. В., Свитич О. А., Кудрявцева А. В. Атопический дерматит. Междисциплинарный подход к диагностике и лечению: Руководство для врачей. Москва: ГЭОТАР-Медиа, 2024; 288 с.
2. Клинические рекомендации. Атопический дерматит.

- Утверждены Минздравом РФ. Доступно по ссылке: https://www.ncii.ru/specialistam/clinrecommend/atopic_dermatitis_2020.pdf
3. Кубанов А. А., Богданова Е. В. Ресурсы и результаты деятельности медицинских организаций, оказывающих медицинскую помощь по профилю «дерматовенерология»,

- в Российской Федерации в 2016–2022 гг. Вестник дерматологии и венерологии. 2023; 99 (4): 18–40. Доступно по ссылке: <https://doi.org/10.25208/vdv12385>.
4. Котова Е. Г., Кобякова О. С., Кубанов А. А., Стародубов В. И., Александрова Г. А., Богданова Е. В., и др. Ресурсы и деятельность медицинских организаций дерматовенерологического профиля. Заболеваемость инфекциями, передаваемыми половым путем, заразными кожными болезнями и болезнями кожи в 2022 году: статистические материалы. М.: ФГБУ «ЦНИИОИЗ» Минздрава России, 2023; 209 с. DOI: 10.21045/978-5-94116-130-0-2023.
 5. Traidl S, Freimooser S, Werfel T. Janus kinase inhibitors for the therapy of atopic dermatitis. *Allergol Select*. 2021; 5: 293–304. DOI: 10.5414/ALX02272E.
 6. Gelezhe KA, Kudravnitsa AV, Ryzhii E, Khachatryan LG, Bogdanova EA, Svitch OA. The role of the skin microbiome in the development of allergic inflammation in atopic dermatitis. *New Armenian Medical Journal*. 2021; 15 (1): 100–8.
 7. Горский В. С., Блюмина В. А. Современные представления о патогенезе атопического дерматита. *Имунопатология, аллергология, инфектология*. 2022; 3: 70–76. DOI: 10.14427/jipai.2022.3.70.
 8. Беляева Т. М., Пономаренко И. В., Чурносков М. И. Молекулярно-генетические детерминанты атопического дерматита (данные полногеномных исследований). *Клиническая дерматология и венерология*. 2020; 19 (5): 615–21. DOI: 10.17116/klinderma202019051615.
 9. Святнич О. А., Олисова О. Ю., Меремьянина Е. А., Рассказова Н. Д., Фомина В. А., Потапова М. Б. Роль полиморфных маркеров в генах TLR2, TLR4 и TLR9 в риске развития атопического дерматита. *Медицинская иммунология*. 2023; 25 (5): 1043–8. DOI: 10.15789/1563-0625-AOS-2807.
 10. Смолкина О. Ю., Быстрицкая Е. П., Святнич О. А., Пирузян А. Л., Денисова Е. В., Корсунская И. М., и др. Анализ метилирования ДНК в пораженной и непораженной коже у взрослых пациентов с атопическим дерматитом. *Молекулярная медицина*. 2021; 19 (1): 53–58. DOI: 10.29296/24999490-2021-01-08.
 11. Gupta J, Margolis DJ. Filaggrin gene mutations with special reference to atopic dermatitis. *Curr Treat Options Allergy*. 2020; 7 (3): 403–13. DOI: 10.1007/s40521-020-00271-x.
 12. Barker JN, Palmer CN, Zhao Y, Liao H, Hull PR, et al. Null mutations in the filaggrin gene (FLG) determine major susceptibility to early-onset atopic dermatitis that persists into adulthood. *J Invest Dermatol*. 2007; 127 (3): 564–7. DOI: 10.1038/sj.jid.5700587.
 13. Тамразова О. Б., Глухова Е. А. Уникальная молекула филаггрина в структуре эпидермиса и ее роль в развитии ксероза и патогенеза атопического дерматита. *Клиническая дерматология и венерология*. 2021; 20 (6): 102–10. DOI: 10.17116/klinderma202120061102.
 14. Moosbrugger-Martinz V, Leprince C, Méchin M-C, Simon M, Blunder S, Gruber R, et al. Revisiting the roles of filaggrin in atopic dermatitis. *Int J Mol Sci*. 2022; 23: 5318. DOI: 10.3390/ijms23105318/.
 15. Chiricozzi A, Maurelli M, Calabrese L, Peris K, Girolomoni G. Overview of atopic dermatitis in different ethnic groups. *J Clin Med*. 2023; 12: 2701. DOI: 10.3390/jcm12072701.
 16. Irvine AD, McLean WH, Leung DY. Filaggrin mutations associated with skin and allergic diseases. *N Engl J Med*. 2011; 365 (14): 1315–27. DOI: 10.1056/NEJMra1011040.
 17. X.F. Colin C. Wong, Simon L.I.J. Denil, Jia Nee Foo, Huijia Chen, Angeline Su Ling Tay, Rebecca L. Haines, et al. Array-based sequencing of filaggrin gene for comprehensive detection of disease-associated variants. *Journal of Allergy and Clinical Immunology*. 2018; 141 (2): 814–6. DOI: 10.1016/j.jaci.2017.10.001.
 18. Thyssen JP, Bikle DD, Elias PM. Evidence that loss-of-function filaggrin gene mutations evolved in northern Europeans to favor intracutaneous vitamin D3 production. *Evol Biol*. 2014; 41 (3): 388–96. DOI: 10.1007/s11692-014-9282-7.
 19. Rodríguez E, Baurecht H, Herberich E, Wagenpfeil S, Brown SJ, Cordell HJ, et al. Meta-analysis of filaggrin polymorphisms in eczema and asthma: robust risk factors in atopic disease. *J Allergy Clin Immunol*. 2009; 123 (6): 1361–70. DOI: 10.1016/j.jaci.2009.03.036.
 20. Макарова С. И., Митрофанов Д. В., Комова Е. Г., Калошкин И. В., Шинтяпина А. Б., Казначеева Л. Ф., и др. Роль мутаций гена филаггрина, ведущих к снижению количества белка, в развитии атопического дерматита и бронхиальной астмы у детей. *Сибирский научный медицинский журнал*. 2021; 41 (3): 58–63. DOI: 10.18699/SSMJ20210308.
 21. Варламов Е. Е., Пампура А. Н. Первичная профилактика атопического дерматита у детей. *Российский вестник перинатологии и педиатрии*. 2015; 60 (5): 21–25.
 22. Gruber R, Janecke A, Fauth C, et al. Filaggrin mutations p.R501X and c.2282del4 in ichthyosis vulgaris. *Eur J Hum Genet*. 2007; 15: 179–84. DOI: 10.1038/sj.ejhg.5201742.
 23. Еремина А. А., Герлингер А. В., Макеенко О. А., Кох Н. В., Сергеева И. Г. Внедрение современных генетических и инструментальных методов обследования в ведении пациентов с вульгарным ихтиозом и атопическим дерматитом. *Клиническая дерматология и венерология*. 2023; 22 (4): 399–405. DOI: 10.17116/klinderma202322041399.
 24. Макеенко О. А., Кох Н. В., Сергеева И. Г. Клинический разбор пациентов гомозигот по мутации 2282del4 (rs558269137) в гене филаггрина. *Клиническая дерматология и венерология*. 2022; 21 (3): 390–98. Доступно по ссылке: <https://doi.org/10.17116/klinderma202221031390>.
 25. Чикин В. В., Карамова А. Э., Кубанов А. А., Жилова М. Б., Городничев П. В., Аулова К. М. Узкополосная средневолновая ультрафиолетовая терапия больных атопическим дерматитом: анализ факторов, влияющих на выраженность терапевтического эффекта. *Вестник дерматологии и венерологии*. 2023; 99 (5): 52–63. DOI: 10.25208/vdv15828.
 26. Hanifin JM, Rajka G. Diagnostic features of atopic dermatitis. *Acta Derm Venereol*. 1980; 92 (Suppl): 44–47.
 27. Wollenberg A, Christen-Zäch S, Taieb A, Paul C, Thyssen JP, de Bruin-Weller M, et al. European Task Force on Atopic Dermatitis/EADV Eczema Task Force. ETFAD/EADV Eczema task force 2020 position paper on diagnosis and treatment of atopic dermatitis in adults and children. *J Eur Acad Dermatol Venereol*. 2020; 34 (12): 2717–44. DOI: 10.1111/jdv.16892.
 28. Standard Nucleotide BLAST. National Center for Biotechnology Information. U.S National Library of Medicine. Available from: https://blast.ncbi.nlm.nih.gov/Blast.cgi?PAGE_TYPE=BlastSearch.
 29. Максимова Ю. В., Свечникова Е. В., Максимов В. Н., Лыква С. Г. Мутации в гене филаггрина и атопический дерматит. *Клиническая дерматология и венерология*. 2014; 3: 58–62.
 30. Dvornyk V, Ponomarenko I, Belyaeva T, Reshetnikov E, Churnosov M. Filaggrin gene polymorphisms are associated with atopic dermatitis in women but not in men in the Caucasian population of Central Russia. *PLoS ONE*. 2021; 16 (12): e0261026. DOI: 10.1371/journal.pone.0261026.
 31. Gimalova GF, Karunas AS, Fedorova YY, Khusnutdinova EK. The study of filaggrin gene mutations and copy number variation in atopic dermatitis patients from Volga-Ural region of Russia. *Gene*. 2016; 591: 85–89. DOI: 10.1016/j.gene.2016.06.054.
 32. Greisenegger E, Novak N, Maintz L, Bieber T, Zimprich F, Haubenberger D, et al. Analysis of four prevalent filaggrin mutations (R501X, 2282del4, R2447X and S3247X) in Austrian and German patients with atopic dermatitis. *J Eur Acad Dermatol Venereol*. 2010; 24: 607–10. DOI: 10.1111/j.1468-3083.2009.03469.x.
 33. Weidinger S, Illig T, Baurecht H, Irvine AD, Rodriguez E, Diaz-Lacava A, et al. Loss-of-function variations within the filaggrin gene predispose for atopic dermatitis with allergic sensitizations. *J Allergy Clin Immunol*. 2006; 118 (1): 214–9. DOI: 10.1016/j.jaci.2006.05.004. Erratum in: *J Allergy Clin Immunol*. 2006; 118 (4): 922. Erratum in: *J Allergy Clin Immunol*. 2006; 118 (3): 724.
 34. Giardina E, Paolillo N, Sinibaldi C, Novelli G. R501X and 2282del4 filaggrin mutations do not confer susceptibility to psoriasis and atopic dermatitis in Italian patients. *Dermatology*. 2008; 216 (1): 83–4. DOI: 10.1159/000109365.
 35. Luukkainen TM, Kiiski V, Ahola M, Mandelin J, Virtanen H, Pöyhönen M, et al. The value of FLG null mutations in predicting treatment response in atopic dermatitis: an observational study in Finnish patients. *Acta Derm Venereol*. 2017; 97 (4): 456–63. DOI: 10.2340/00015555-2578.

36. dbSNP Short Genetic Variations. Available from: https://www.ncbi.nlm.nih.gov/snp/rs558269137#frequency_tab (accessed 18 Dec 2023).
37. Smieszek SP, Welsh S, Xiao C, et al. Correlation of age-of-onset of atopic dermatitis with filaggrin loss-of-function variant status. *Sci Rep.* 2020; 10: 2721. DOI: 10.1038/s41598-020-59627-7.
38. Schuler CF, Allison C. Billi, Emanuel Maverakis, Lam C. Tsoi, Johann E. Gudjonsson, Novel insights into atopic dermatitis. *Journal of Allergy and Clinical Immunology.* 2023; 151 (5): 1145–54. DOI: 10.1016/j.jaci.2022.10.023.
39. Bakker DS, de Graaf M, Nierkens S, Delemarre EM, Knol E, van Wijk F, et al. Unraveling heterogeneity in pediatric atopic dermatitis: identification of serum biomarker based patient clusters. *J Allergy Clin Immunol.* 2022; 149: 125–34. DOI: 10.1016/j.jaci.2021.06.029.
40. Tokura Y, Hayano S. Subtypes of atopic dermatitis: From phenotype to endotype. *Allergology International.* 2022; 71 (1): 14–24. DOI: 10.1016/j.alit.2021.07.003.

DETERMINING THE DIAGNOSTIC VALUE OF THE MARKERS OF CONGENITAL METABOLIC DISORDERS BY CHROMATOGRAPHY–MASS SPECTROMETRY

Mamedov IS¹, Zolkina IV²✉, Sukhorukov VS³, Krapivkin AI¹

¹ Voino-Yasenetsky Scientific and Practical Center for Specialized Assistance to Children, Moscow, Russia

² LLC Clinic of New Medical Technologies “ArchiMed”, Moscow, Russia

³ Research Center of Neurology, Moscow, Russia

Thorough investigation of metabolome by mass spectrometry is of great importance for personalized and preventive medicine. It is only timely laboratory diagnosis involving the use of high-tech chromatographic analysis methods that can help identify the patients with disorders of amino acid and acylcarnitine metabolism. The study was aimed to determine the efficacy of conventional and additional markers of metabolic disorders of amino acids and acylcarnitines detected by chromatography–mass spectrometry for the diagnosis of congenital metabolic disorders in children, as well as to create specific panels of the most effective indicators and determine the potential diagnostic efficacy of identification of the relationships between the levels of amino acids and acylcarnitines in pediatric patients with congenital metabolic disorders. We assessed amino acid and acylcarnitine profiles in blood spots by high-performance liquid chromatography–tandem mass spectrometry in patients aged 6 months to 16 years (48 boys and 32 girls) with suspected aminoacidopathy and organic aciduria/acidemia. The comparison group consisted of 35 children with suspected peroxisomal metabolic disorders, the control group included 40 generally healthy children of various age groups. The data obtained were used to conduct the analysis of correlations between the groups of markers. Strong correlation was revealed for the levels of metabolically most closely related compounds ($r < 0.8$, $p < 0.001$). However, a similar relationship between metabolically not closely related compounds (correlation coefficient 0.45–0.73 ($p < 0.001$)) was revealed for some groups of compounds. Thus, the acylcarnitine profile can be proposed as an additional potential marker to be used in cases of borderline phenylalanine levels, and the sum of normalized acylcarnitine levels (C12+C16) can be a potential secondary marker of phenylketonuria.

Keywords: mass-spectrometry, amino acids, acylcarnitines, hereditary metabolic diseases, correlation analysis, differential diagnosis

Author contribution: Mamedov IS — research idea; Mamedov IS, Zolkina IV — research methods and procedure, statistical data processing; Zolkina IV — manuscript writing; Mamedov IS, Sukhorukov VS, Zolkina IV, Krapivkin AI — manuscript editing; Krapivkin AI — research management.

Compliance with ethical standards: the study was approved by the Ethics Committee of the Pirogov Russian National Research Medical University (protocol № 94 dated 14 December 2009). All parents or caregivers of the subjects submitted the informed consent to participation in the study.

✉ **Correspondence should be addressed:** Irina V. Zolkina
Vavilova, 68, k. 2, Moscow, 119261, Russia; zolkina_ira@mail.ru

Received: 12.01.2024 **Accepted:** 29.01.2024 **Published online:** 15.02.2024

DOI: 10.24075/brsmu.2024.003

ОПРЕДЕЛЕНИЕ ДИАГНОСТИЧЕСКОЙ ЗНАЧИМОСТИ МАРКЕРОВ НАСЛЕДСТВЕННЫХ БОЛЕЗНЕЙ ОБМЕНА С ПРИМЕНЕНИЕМ МЕТОДА ХРОМАТО-МАСС-СПЕКТРОМЕТРИИ

И. С. Мамедов¹, И. В. Золкина²✉, В. С. Сухоруков³, А. И. Крапивкин¹

¹ Научно-практический центр специализированной помощи детям имени В. Ф. Войно-Ясенецкого, Москва, Россия

² ООО «Клиника новых медицинских технологий АрчиМед», Москва, Россия

³ Научный центр неврологии, Москва, Россия

Для развития персонализированной и превентивной медицины большое значение приобретает детальное изучение метаболома с применением масс-спектрометрии. Только своевременная лабораторная диагностика с помощью высокотехнологичных методов хроматографического анализа может помочь в выявлении пациентов с нарушениями метаболизма аминокислот и ацилкарнитинов. Целью работы было определить эффективность классических и дополнительных маркеров нарушений обмена аминокислот и ацилкарнитинов, детектируемых хромато-масс-спектрометрическими методами, в диагностике наследственных болезней обмена у детей, создать специфические панели наиболее эффективных показателей и определить потенциальную диагностическую эффективность выявления взаимосвязей между показателями аминокислот и ацилкарнитинов у педиатрических пациентов с врожденными нарушениями метаболизма. Были изучены профили аминокислот и ацилкарнитинов в пятках крови методом высокоэффективной хромато-масс-спектрометрии у пациентов в возрасте от 6 месяцев до 16 лет (48 мальчиков и 32 девочки) с подозрением на аминокислотапатии и органические ацидурии/ацидемии. Группа сравнения состояла из 35 детей с подозрением на пероксисомные болезни обмена, контрольная группа — из 40 практически здоровых детей разных возрастных групп. По полученным данным, между группами маркеров был проведен корреляционный анализ. Содержание метаболически наиболее близких соединений имело выраженную корреляционную взаимосвязь ($r < 0,8$, $p < 0,001$). Однако такая взаимосвязь проявилась и среди метаболически слабо связанных соединений (коэффициент корреляции варьировал от 0,45 до 0,73 ($p < 0,001$)) для некоторых групп соединений. Так, ацилкарнитиновый профиль может быть предложен в качестве потенциального дополнительного маркера при пограничных показателях фенилаланина, а сумма нормализованных показателей ацилкарнитинов (C12+C16) может быть потенциальным вторичным маркером фенилкетонурии.

Ключевые слова: масс-спектрометрия, аминокислоты, ацилкарнитины, наследственные болезни обмена, корреляционный анализ, дифференциальная диагностика

Вклад авторов: И. С. Мамедов — идея исследования; И. С. Мамедов, И. В. Золкина — методология и проведение исследования, статистическая обработка данных; И. В. Золкина — написание статьи; И. С. Мамедов, В. С. Сухоруков, И. В. Золкина, А. И. Крапивкин — редактирование статьи; А. И. Крапивкин — администрирование исследования.

Соблюдение этических стандартов: исследование одобрено этическим комитетом Российского государственного медицинского университета им. Н. И. Пирогова РГМУ (протокол № 94 от 14 декабря 2009 г.). Всеми родителями или опекунами участников исследования было подписано добровольное согласие на участие в исследовании.

✉ **Для корреспонденции:** Золкина Ирина Вячеславовна
ул. Вавилова, д. 68, к. 2, г. Москва, 119261, Россия; zolkina_ira@mail.ru

Статья получена: 11.01.2024 **Статья принята к печати:** 29.01.2024 **Опубликована онлайн:** 15.02.2024

DOI: 10.24075/vrgmu.2024.003

In the leading countries of the world mass spectrometry is among the newest and most popular laboratory medicine methods. Thorough investigation of metabolome is impossible without the use of mass spectrometry; the datasets acquired by this method are of great importance for the development of innovative personalized medicine technologies ensuring the switch from reactive to predictive and preventive medicine. Since introduction into practice of preventive check-ups and information technology for the development of the disease diagnosis algorithms is the most promising direction in solving the range of problems of personalized medicine, the tandem mass spectrometry is considered to be the method most suitable for fulfillment of these aspects [1–3].

Based on the prevalence, the disorders of amino acid and acylcarnitine metabolism are rather frequent compared to other congenital metabolic disorders. The prevalence of the majority of inherited metabolic disorders, many of which are acidemias that manifest themselves in the neonatal period, is 1:1000 – 1:5000 newborns. Individual pathogenetic pattern of amino acid and acylcarnitine metabolism disorders is complicated by the fact that certain clinical signs in various combinations having varying severity can emerge in individuals with different types of metabolic diseases. As a result, it is only timely laboratory diagnosis involving the use of high-tech chromatographic analysis methods that can help identify the patients with such disorders.

The study was aimed to determine the efficacy of the main (conventional) markers of amino acid and acylcarnitine metabolism disorders detected by chromatography–mass spectrometry for the diagnosis of congenital metabolic disorders, as well as to create specific panels of the most effective indicators and determine the potential diagnostic efficacy of identification of the relationships between mass spectrometry indicators in children with inherited metabolic disorders of amino acids and acylcarnitines.

METHODS

The study was carried out at the Veltischev Research and Clinical Institute for Pediatrics and Pediatric Surgery of the Pirogov Russian National Research Medical University and the Voyno-Yasenetsky Scientific and Practical Center for Specialized Assistance to Children in 2012–2023.

The group of affected individuals included children and adolescents with suspected aminoacidopathy and organic aciduria/acidemia, as well as patients with undifferentiated metabolic disorders. The age of patients included in the group was between 6 months and 16 years. The gender distribution of the group of patients was as follows: 48 boys and 32 girls. Inclusion criteria: children from birth to 18 years of age; history of the following symptoms: psychomotor and physical development retardation, cramps, muscle tone abnormality, ataxia, the combined symptoms including enlarged liver, decreased visual acuity, dermatitis. Exclusion criteria: age over 18 years, severe comorbidities (for example, cerebral palsy, congenital anomalies of the kidney and urinary tract, severe cardiovascular disorders) that could complicate fulfillment of the assessment conditions or cause harm to the patient. The comparison group for this group of affected individuals included 35 children with suspected peroxisomal metabolic disorders. Inclusion criteria for the comparison groups: age under 18 years, history of sharp typical neuronal migration defects, micronodular cirrhosis, kidney cysts, chondrodysplasia punctata, corneal opacity, cataract, glaucoma and retinopathy, congenital heart defects and dysmorphic features. The control group consisted of 40 generally healthy children of various age groups.

The study involved the use of the method for quantification of 12 amino acids and 30 acylcarnitines in dry blood spots by high-performance liquid chromatography–tandem mass spectrometry [4–7] modified in the following way: the mass spectrometry detection parameters for all analytes were optimized to increase sensitivity, the eluent flow rate was increased to reduce the single sample analysis time.

Reference samples: MassChrom®AminoAcids and Acylcarnitines lyophilized mixture of internal standards (Chromsystems; Germany).

Reagents: acetonitrile (LC/MS Grade) (Fisher Scientific; USA), butanol-1 (AR Grade; Chimmed, Russia), n-butyl acetate (AR Grade; Chimmed, Russia), hydrochloric acid (AR Grade; Chimmed, Russia), methanol (AR Grade; Sigma-Aldrich, Germany).

Laboratory glassware and materials: Whatman 903® filter paper for biomaterial sample collection (Whatman; USA), 96-well microplate with protective adhesive film (Eppendorf; Germany).

Laboratory equipment: DSB Puncher (PerkinElmer; USA), ST-3 thermal shaker (ELMI; Latvia), EVA EC-S evaporator (VLM; Germany), Sartorius Biohit Proline single-channel mechanical pipettes (Sartorius Biohit Liquid Handling Oy; Finland) having the volume of 0–100.0 µL, 0–200.0 µL with original disposable tips.

Biomaterial collection

The blood sample drawn from the newborn's heel or finger of the older patient was collected on the special Whatman 903® paper in the form of sheets for capillary blood collection and dried at room temperature until completely dry. Special paper soaked in biomaterial was stored at room temperature for up to one month.

Biomaterial sample preparation

To conduct the analysis, a circle with a diameter of 3.1 mm (corresponding to 3.2 µL of blood sample) was cut out from the dry blood spot with a puncher and placed in the microplate well. To ensure extraction, it was added 200.0 µL of the internal standard mixture (previously dissolved in acetonitrile); then the microplate was covered with protective adhesive film to avoid evaporation and splashing of the sample and mixed on the shaker at 600 rpm for 20 min at room temperature. To ensure evaporation, protective film was removed from the microplate, and the sample was evaporated at 60 °C in the air stream until dry. Sample derivatization was accomplished by adding 60.0 µL of the derivatization reagent (mixture of butanol-1, n-butyl acetate, hydrochloric acid in a volume ratio of 7:2:1) to the sample dry residue in the microplate, then the microplate was covered with the protective film and incubated at 60 °C and 600 rpm for 15 min. To concentrate the sample, the protective film was removed from the microplate, and the sample was evaporated in the air stream until dry. The final phase of sample preparation included dissolving the dry residue in 10.0 µL of methanol. After that the sample was mixed at 600 rpm for 1 min at room temperature. A total of 10.0 µL of the prepared sample were injected in the HPLC system.

Chromatographic conditions

The analysis was performed using the HPLC system consisting of the Agilent 1200 binary gradient pump, vacuum trap, column thermostat, and CTC HTS PAL autosampler connected to the Agilent 6410 QQQ MS detection system (Agilent Technologies; USA). The adaptor coupling was used as a column, and

Table. Diseases found in the group of patients with suspected aminoacidopathy and organic aciduria/acidemia based on the dry blood spot analysis by high-performance liquid chromatography–tandem mass spectrometry

Disease entity	Changes in marker levels	Number of patients
Disorders diagnosed by dry blood spot analysis by HPLC-MS/MS		
Phenylketonuria due to phenylalanine hydroxylase deficiency	Elevated phenylalanine levels, decreased tyrosine levels	7
Homocystinuria due to cobalamin metabolism disorders	Decreased methionine levels, presence of homocysteine	5
Argininemia	Elevated arginine levels	4
Cobalamin A type (cblA) and cobalamin B type (cblB) methylmalonic acidemia (MMA)	Elevated propionylcarnitine (C3) and methylmalonylcarnitine (C4DC) levels	5
Medium-chain acyl-coenzyme A dehydrogenase (MCAD) deficiency	Elevated levels of medium-chain acylcarnitines (C6, C8, C10)	3
Carnitine uptake defect (CUD)	Decreased free carnitine levels (C0)	1
Glutaric acidemia type I (GA I)	Elevated glutaryl carnitine levels (C5DC)	3
Tyrosinemia type I	Elevated levels of tyrosine, phenylalanine, and methionine	3
Tyrosinemia type II	Elevated tyrosine levels	1
Hyperammonemia due to N-acetylglutamate synthase deficiency	Elevated alanine levels	5
Citrullinemia	Elevated citrulline levels, decreased arginine levels	2
Isovaleric acidemia/aciduria (IVA)	Elevated isovalerylcarnitine levels (C5)	2
Propionic acidemia (PA)	Elevated propionylcarnitine levels (C3) and the C3/C2 ratio	2
Nonketotic hyperglycinemia	Elevated glycine levels	5
Maple syrup urine disease (leucinuria) (MSUD)	Elevated total indicator (leucine + isoleucine)	6

acetonitrile was used as a mobile phase and solution used to wash the injector needle. The HPLC system settings were as follows: injection volume — 10.0 µL, analysis time — 1.7 min, mobile phase flow rate during system equilibration — 0.5 mL/min.

Data processing

The data obtained were processed in MassHunter® (Agilent Technologies; USA).

The analytes were quantified by the internal standard method. The concentration of each analyte in the sample was calculated using the formula (1) as a ratio of its analytical signal intensity in the sample to the analytical signal intensity of the corresponding internal standard in the same sample multiplied by the concentration of this internal standard in the mixture of internal standards (calibration mixture):

$$c_{(A, \mu\text{mol/L})} = ([A_A]_{\text{sample}} / A_{\text{IS}} \times c_{(\text{IS, mmol/L})}, \quad (1)$$

where $c_{(A, \mu\text{mol/L})}$ was the concentration of analyte in the sample ($\mu\text{mol/L}$); A_A was the analyte analytical signal intensity in the sample; $c_{(\text{IS, mmol/L})}$ was the concentration of internal standard in the calibration mixture ($\mu\text{mol/L}$); A_{IS} was the internal standard analytical signal intensity in the sample.

The concentrations of all internal standards in the MassChrom®AminoAcids and Acylcarnitines mixture (Chromsystems; Germany, registration certificate № RZN 2018/7415 dated 27.07.2018) were provided in appropriate supporting documents.

Method validation characteristics

Depending on the analyte, the rate of amino acid and acylcarnitine extraction from dry blood spots was 69–97%; the detection limit for amino acids varied between 2.0 and 15.6 $\mu\text{mol/L}$, while that for acylcarnitines was 0.1–1.6 $\mu\text{mol/L}$;

the coefficients of variation for all analytes were within the range of 3.4–15.6%; the linearity range of amino acids was up to 2000 $\mu\text{mol/L}$, while that of acylcarnitines was up to 200 $\mu\text{mol/L}$.

To demonstrate the diagnostic value, ROC curves were plotted [8]. Hierarchical cluster analysis and the heatmaps based on Spearman's rank correlation were also used. The correlation analysis was performed using a programming language R, and the median values were compared with the interquartile ranges. The results were processed using the Morpheus statistical tool and the SPSS Statistics 23® (IBM Corporation; USA), Statistica 6.0® (StatSoftInc.; USA), Excel'2007® (Microsoft Corp.; USA) software packages.

RESULTS

Based on the analysis of dry blood spots collected from 80 children in the first group with suspected aminoacidopathy and organic aciduria/acidemia and clinical and laboratory characteristics, a total of 54 patients with the following monogenic disorders were identified: aminoacidopathies, organic acidemia, fatty acid oxidation defects, and carnitine transport defect. These diagnoses were later verified by molecular genetic methods (Table). Based on the analysis of dry blood spots collected from 35 individuals in the comparison group (patients with suspected peroxisomal disorders), low free carnitine levels (C0) in blood were revealed in five patients (within the range of 10–16 $\mu\text{mol/L}$, while the reference range was 19–45 $\mu\text{mol/L}$), which could be indicative of other metabolic disorder, such as secondary carnitine deficiency. In other patients, all the indicators were within reference ranges or at their high ends. The analysis of dry blood spots collected from 40 children in the control group confirmed the fact that the group included generally healthy children, since all the studied indicators were within reference ranges in all children.

When comparing the median values with the interquartile ranges of marker metabolites in the subjects of the comparison

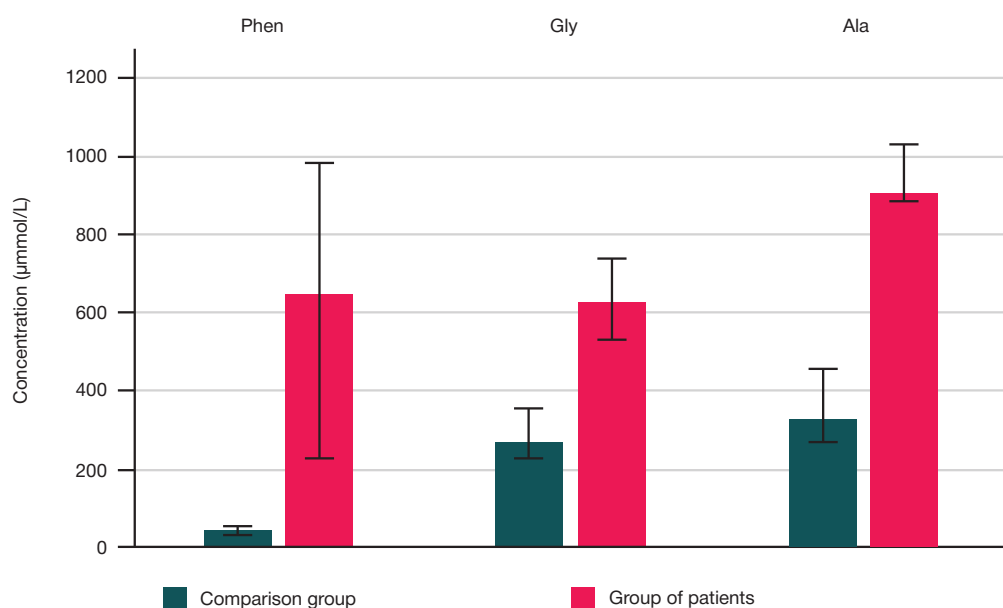


Fig. 1. Comparison of marker metabolite levels in surveyed individuals of the comparison group and the patients with phenylketonuria (diagnostic marker — phenylalanine (Phe)), nonketotic hyperglycinemia (diagnostic marker — glycine (Gly)), and hyperammonemia (diagnostic marker — alanine (Ala))

group and the patients diagnosed with metabolic disorders, significant (10–100-fold) differences become evident. This is exemplified by comparison of marker metabolite levels in surveyed individuals of the comparison group and the patients diagnosed with congenital amino acid metabolism disorders: phenylketonuria (more than 100-fold), nonketotic hyperglycinemia, and hyperammonemia (Fig. 1).

It is noteworthy that the levels of propionylcarnitine (C3) being the main marker of the disease are significantly higher in patients with methylmalonic acidemia than in surveyed individuals in the comparison group; the opposite trend is observed in patients with homocystinuria: the levels of the main marker, methionine (Met), are lower in affected patients than in individuals in the comparison group (Fig. 2).

The above examples confirm the diagnostic value of the biochemical markers determined by chromatography–mass spectrometry in this study when used to diagnose metabolic disorders of amino acids, acylcarnitines.

Fig. 3 presents a heatmap with a dendrogram for patients with identified metabolic disorders of amino acids and acylcarnitines, in the rows of which the data on each patient with identified disorder are provided, and the columns of which provide data on the tested metabolites; potential markers are clustered by cluster analysis.

The more detailed review of the data provided in the upper right corner of the heatmap shows the decreased blood levels of short-chain and long-chain acylcarnitines in patients with phenylketonuria compared to subjects in the comparison group, along with preserved levels of medium-chain acylcarnitines. These results have been confirmed for acylcarnitines C12, C14, C14:1, C16, C16:1, C18, C18:1, C5, C5OH using the nonparametric Mann–Whitney U test at $p < 0.05$. Thus, the acylcarnitine profile can be proposed as an additional potential marker to be used in cases of borderline phenylalanine levels.

A downward trend in different acylcarnitine profile indicators (short-, medium-, and long-chain acylcarnitines) is also observed

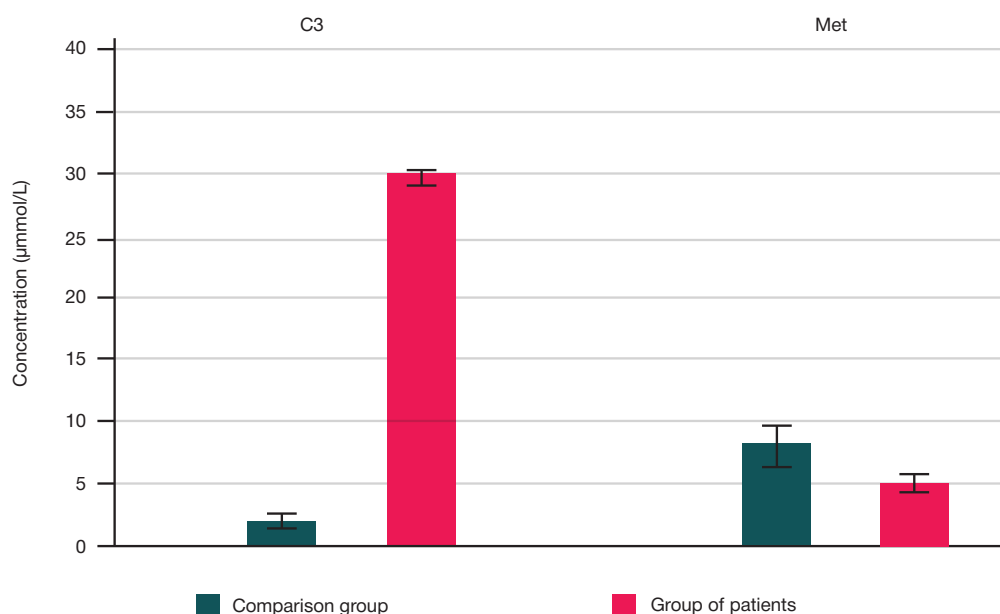


Fig. 2. Comparison of marker metabolite levels in surveyed individuals of the comparison group and the patients with methylmalonic acidemia (diagnostic marker — propionylcarnitine (C3)) and homocystinuria (diagnostic marker — methionine (Met))

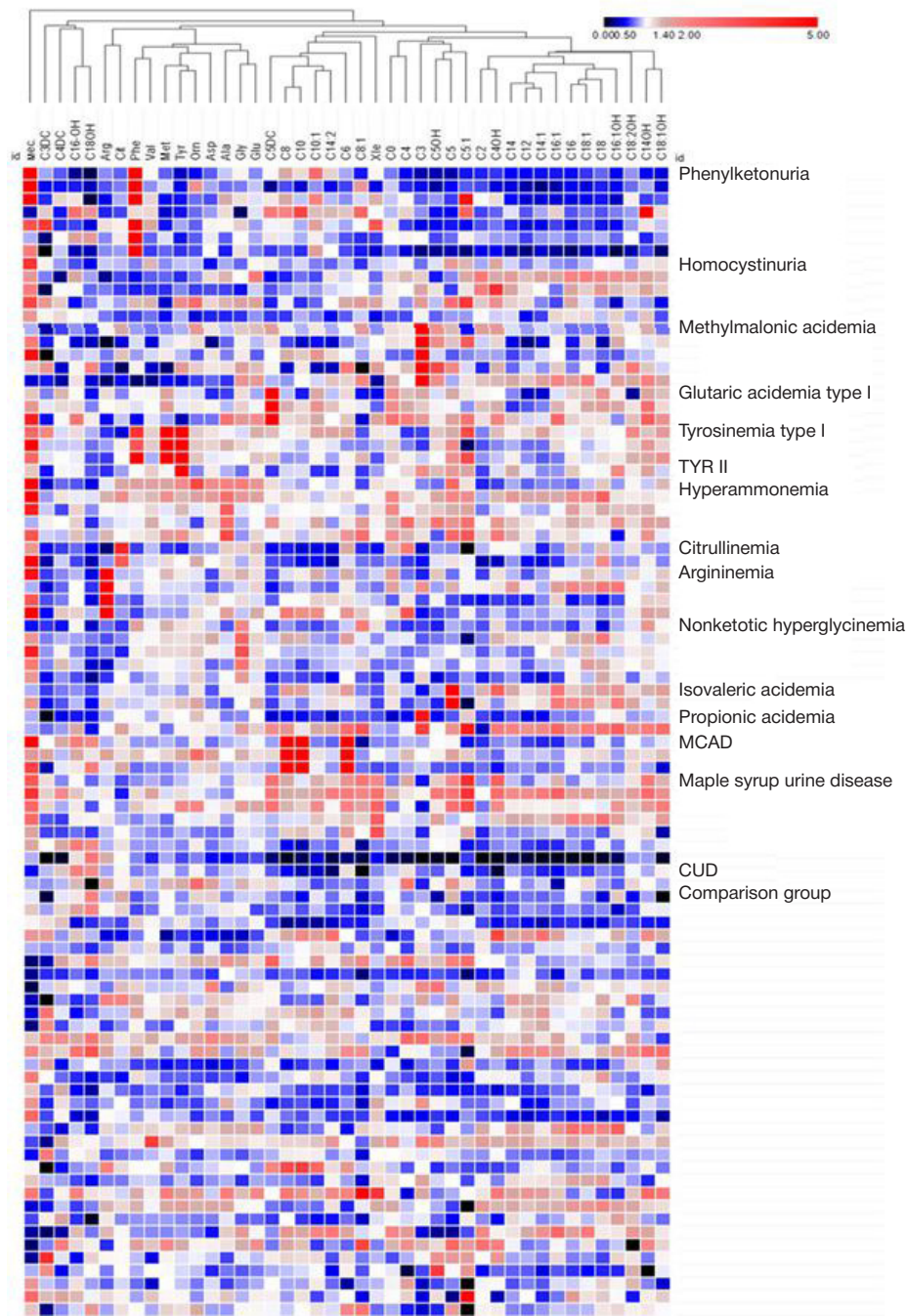


Fig. 3. Heatmap with a dendrogram of amino acid and acylcarnitine profile in patients with disturbed metabolism of these substances (the ratio of the diagnostic marker concentrations to the average concentration value in the control groups corresponds to the color chart)

in patients with citrullinemia and nonketotic hyperglycinemia. Despite the fact that these data are not enough to make statistically significant conclusions, the data definitely constitute the grounds for further research focused on identification of the groups of marker metabolites for the diagnosis of metabolic disorders of amino acids.

Specificity represents a far more important parameter for rare disorders than sensitivity, therefore, the tests having higher specificity show higher diagnostic efficacy [9]. Fig. 4 presents the ROC curve for the sum of normalized acylcarnitine levels (C12+C16). High values of area under the curve (> 0.9), specificity (almost 100%), and sensitivity (above 80%) make it possible to propose this parameter as a potential secondary marker of phenylketonuria.

It is obvious that phenylalanine levels represent one of the most important diagnostic markers of phenylketonuria

compared to others, but further study of the acylcarnitine profile will make it possible to differentiate phenylketonuria from other hyperphenylalaninurias with its help.

These examples allow us to say with certainty that hierarchical cluster analysis can be a reliable tool for physicians to be used in differential diagnosis of congenital metabolic disorders in children.

The analysis of correlations between certain markers and groups of markers selected based on the cluster analysis results was performed. The correlation analysis results are presented as the figures, in which the divisions mark the abscissa and ordinate axes for histograms; the concentration distribution graph for each marker metabolite is arranged diagonally; the graphs showing correlations between two variables are located under the diagonal, while the correlation coefficients and significance levels are located above the diagonal.

Predictably, the closest metabolically related substances, such as short-chain acylcarnitines, show the highest degree of correlation (Fig. 5).

However, the correlation between not metabolically closely related amino acids, such as methionine and tyrosine, was also observed ($r = 0.73$); the ornithine levels rather strongly correlated with the levels of aspartic acid, glycine, and glutamic acid ($r = 0.55$ and 0.43). The levels of the latter, in turn, were correlated to the levels of glycine, alanine, and ornithine ($r = 0.47$, 0.45 , and 0.48 , respectively) (Fig. 6).

High correlation of free carnitine (C0) with acetylcarnitine (C2) and butyrylcarnitine (C4) is confirmed by the correlation analysis results: $r = 0.46$ and 0.48 , respectively ($p < 0.001$). High correlation between all markers in the group of long-chain acylcarnitines (C12, C14, C16, C18) enables the complex use of this group of markers, i.e. in the form of the common profile: the correlation coefficient for these markers vary between 0.69 and 0.88 ($p < 0.001$).

DISCUSSION

In our country, chromatography–mass spectrometry has been introduced and used in clinical laboratory diagnosis for more than 10 years, and the reports published reflect the practical relevance of using the method by physicians of various specialties for the diagnosis of different disorders and disease entities, especially congenital metabolic disorders [10, 11]. The published papers contain information about the use of various developed qualitative and quantitative metabolic disorder marker determination methods for the diagnosis of different congenital and acquired metabolic disorders, however, no correlation analysis of indicators of various marker groups was performed, and different marker groups were not compared with each other. The published studies involved no big data analysis and no search for new statistically significant markers [12, 13]. At the same time, the tactics of big data analysis is currently being actively used in laboratory diagnosis. Large samples make it possible to create the datasets on their basis, allowing one to apply parametric tests used in statistical (cluster, correlation) analysis of various types. This represents an extra tool to be used to search for new laboratory markers and assess their diagnostic efficacy. Several papers were published, in which assessment of the entire set of data on the concentrations of

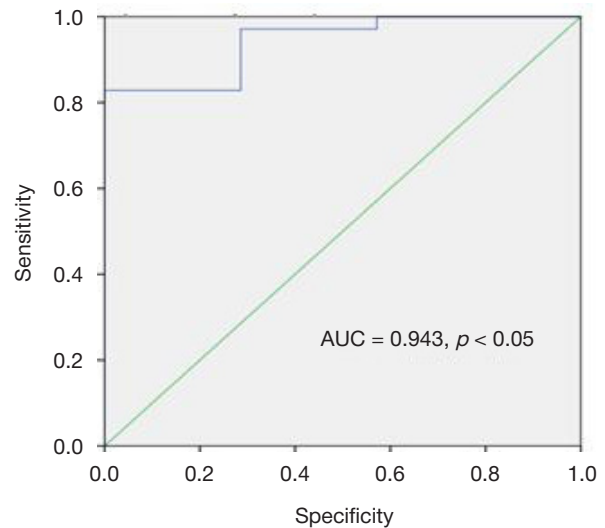


Fig. 4. ROC curve for the sum of normalized acylcarnitines (C12+C16)

amino acids and acetylcarnitines and the search for correlations between these groups of metabolites provided additional information and made it possible to determine the associations and develop the algorithms for the diagnosis of various metabolic disorders, such as type II diabetes mellitus and metabolic syndrome [14, 15]. Thus, a prognostic model containing a panel of acetylcarnitines and amino acids improved the classification of diabetes mellitus cases compared to the model comprising the identified risk factors only [15]. At the same time, no studies focused on assessing the sets of data on the concentrations of amino acids and acetylcarnitines in pediatric population were conducted; these groups of metabolites were always considered separately from each other.

CONCLUSIONS

The experimental data analysis confirmed the efficacy of conventional markers of the disorders of amino acid and acetylcarnitine metabolism when used for the diagnosis of congenital metabolic disorders. The statistical processing applied enabled identification of new markers and marker profiles, which would help ensure a more thorough differential diagnosis of congenital metabolic disorders. The identified

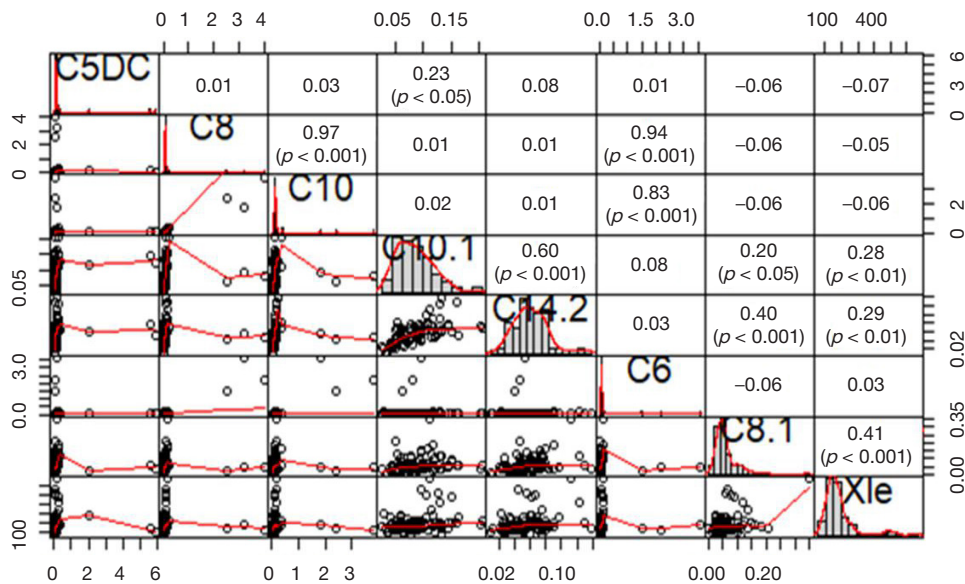


Fig. 5. Results of the correlation analysis performed in the group of marker short-chain acylcarnitines ($p < \text{significance level}$)

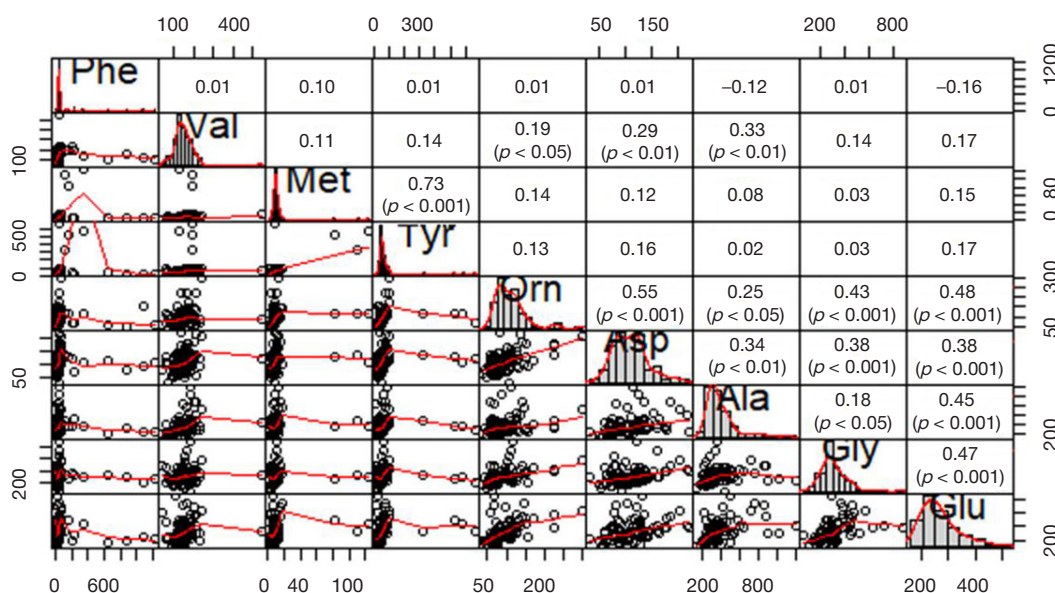


Fig. 6. Results of the correlation analysis performed in the group of marker amino acids ($p < \text{significance level}$)

relationships between mass spectrometry indicators of different groups (amino acids and acylcarnitines) demonstrate some potential diagnostic efficacy when testing children for congenital metabolic disorders. The acylcarnitine profile can be proposed as an additional potential marker to be used in cases of borderline phenylalanine levels, in patients with citrullinemia

and nonketotic hyperglycinemia; the sums of normalized acylcarnitine levels (C12+C16) can be proposed as a potential secondary marker of phenylketonuria, and high correlation between all markers belonging to the group of long-chain acylcarnitines (C12, C14, C16, C18) enables the complex use of this group of markers, i.e. as a common profile.

References

- Colby JM, Thoren KL. Applications of mass spectrometry in the clinical laboratory. In: Clarke W, Marzinko MA. Contemporary Practice in Clinical Chemistry (Fourth Edition). Academic press; 2020, p. 351–63. DOI: 10.1016/B978-0-12-815499-1.00021-1.
- Kilgore MB, Platis D, Lim T, Isenberg S, Pickens CA, Cuthbert C, et al. Development of a universal second-tier newborn screening LC-MS/MS Method for amino acids, lysophosphatidylcholines, and organic acids. *Analytical Chemistry*. 2023; 95 (6): 3187–94. DOI: 10.1021/acs.analchem.2c03098.
- Percenti L, Vickery GNC. Newborn Screening Follow-up. *Med J*. 2019; 80 (1): 37–414. DOI: 10.18043/ncm.80.1.37.
- Chace DH, Kalas T, Naylor EW. Use of tandem mass spectrometry for multianalyte screening of dried blood specimens from newborns. *Clin Chem*. 2003; 49 (11): 1797–817. DOI: 10.1373/clinchem.2003.022178.
- Mueller P, Schulze A, Schindler I. Validation of an ESI-MS/MS screening method for acylcarnitine profiling in urine specimens of neonates, children, adolescents and adults. *Clin Chim Acta*. 2003; 327: 47–57. DOI: 10.1016/S0009-8981(02)00327-3.
- Rashed MS. Clinical applications of tandem mass spectrometry: ten years of diagnosis and screening for inherited metabolic diseases. *J Chrom*. 2001; 758 (1): 27–48. DOI: 10.1016/S0378-4347(01)00100-1.
- Zoppa M, Gallo L, Zacchello F, Giordano G. Method for the quantification of underivatized amino acids on dry blood spots from newborn screening by HPLC-ESI-MS/MS. *J Chromatogr*. 2006; 831 (1–2): 267–73. DOI: 10.1016/j.jchromb.2005.12.015.
- Wong HB, Lim GS. Measures of diagnostic accuracy: sensitivity, specificity, PPV and NPV. *Proceedings of Singapore Healthcare*. 2011; 20 (4): 316–8. DOI: 10.1177/201010581102000411.
- Thomas LA. New era predicted for LC-MS in the clinical lab. *Clinical OMICS*. 2016; 3 (9): 12–15.
- Mamedov IS, Perevezencev OA, Zolkina IV, Vedenin AI, Moskaleva NE, Suhorukov VS, i dr. Bystraja diagnostika nasledstvennyh boleznej obmena veshhestv u detej. *Vestnik Rossijskogo gosudarstvennogo medicinskogo universiteta*. 2010; (3): 57–61. Russian.
- Mamedov IS, Zolkina IV, Suhorukov VS. Diagnostika nasledstvennyh boleznej metabolizma u detej. *Klinicheskaja laboratornaja diagnostika*. 2011; 10: 20–21. Russian.
- Mamedov IS, Suhorukov VS, Zolkina IV, Savina MI, Nikolaeva EA. Ocenka mass-spektrometricheskikh pokazatelej dlja differencial'noj diagnostiki nasledstvennyh naruszenij obmena organicheskikh kislot u detej. *Rossiiskij vestnik perinatologii i pediatrii*. 2019; 64 (1): 61–67. Russian.
- Baranova PV. Organicheskie acidurii: osnovnye principy analiza organicheskikh kislot metodom gazovoj hromatografii s mass-spektrometrijei: uchebno-metodicheskoe posobie. M.: Triumf, 2023; 80 s. Russian.
- Hananeh T, Solaleh E, Shaghayegh H, Babak A, Negar R, Arezou D-M. The association between acylcarnitine and amino acids profile and metabolic syndrome and its components in Iranian adults. *Frontiers in Endocrinology*. 2023 [cited 2023 Nov 29]; 14: [10 p.]. Available from: <https://www.frontiersin.org/articles/10.3389/fendo.2023.1058952/full> DOI: 10.3389/fendo.2023.1058952.
- Gunther SH, Khoo CM, Tai E-S, et al. Serum acylcarnitines and amino acids and risk of type 2 diabetes in a multiethnic Asian population. *BMJ Open Diab Res Care*. 2020 [cited 2023 Nov 29]; 8: e001315 [10 p.]. Available from: <https://drc.bmj.com/content/bmjdr/8/1/e001315.full.pdf> DOI: 10.1136/bmjdr-2020-001315.

Литература

- Colby JM, Thoren KL. Applications of mass spectrometry in the clinical laboratory. In: Clarke W, Marzinke MA. *Contemporary Practice in Clinical Chemistry (Fourth Edition)*. Academic press; 2020, p. 351–63. DOI: 10.1016/B978-0-12-815499-1.00021-1.
- Kilgore MB, Platis D, Lim T, Isenberg S, Pickens CA, Cuthbert C, et al. Development of a universal second-tier newborn screening LC–MS/MS Method for amino acids, lysophosphatidylcholines, and organic acids. *Analytical Chemistry*. 2023; 95 (6): 3187–94. DOI: 10.1021/acs.analchem.2c03098.
- Perenti L, Vickery GNC. Newborn Screening Follow-up. *Med J*. 2019; 80 (1): 37–414. DOI: 10.18043/hcm.80.1.37.
- Chace DH, Kalas T, Naylor EW. Use of tandem mass spectrometry for multianalyte screening of dried blood specimens from newborns. *Clin Chem*. 2003; 49 (11): 1797–817. DOI: 10.1373/clinchem.2003.022178.
- Mueller P, Schulze A, Schindler I. Validation of an ESI-MS/MS screening method for acylcarnitine profiling in urine specimens of neonates, children, adolescents and adults. *Clin Chim Acta*. 2003; 327: 47–57. DOI: 10.1016/S0009-8981(02)00327-3.
- Rashed MS. Clinical applications of tandem mass spectrometry: ten years of diagnosis and screening for inherited metabolic diseases. *J Chrom*. 2001; 758 (1): 27–48. DOI: 10.1016/S0378-4347(01)00100-1.
- Zoppa M, Gallo L, Zacchello F, Giordano G. Method for the quantification of underivatized amino acids on dry blood spots from newborn screening by HPLC–ESI-MS/MS. *J Chromatogr*. 2006; 831 (1–2): 267–73. DOI: 10.1016/j.jchromb.2005.12.015.
- Wong HB, Lim GS. Measures of diagnostic accuracy: sensitivity, specificity, PPV and NPV. *Proceedings of Singapore Healthcare*. 2011; 20 (4): 316–8. DOI: 10.1177/201010581102000411.
- Thomas LA. New era predicted for LC-MS in the clinical lab. *Clinical OMICS*. 2016; 3 (9): 12–15.
- Мамедов И. С., Перевезенцев О. А., Золкина И. В., Веденин А. И., Москалева Н. Е., Сухоруков В. С., и др. Быстрая диагностика наследственных болезней обмена веществ у детей. *Вестник Российского государственного медицинского университета*. 2010; (3): 57–61.
- Мамедов И. С., Золкина И. В., Сухоруков В. С. Диагностика наследственных болезней метаболизма у детей. *Клиническая лабораторная диагностика*. 2011; 10: 20–21.
- Мамедов И. С., Сухоруков В. С., Золкина И. В., Савина М. И., Николаева Е. А. Оценка масс-спектрометрических показателей для дифференциальной диагностики наследственных нарушений обмена органических кислот у детей. *Российский вестник перинатологии и педиатрии*. 2019; 64 (1): 61–67.
- Баранова П. В. Органические ацидурии: основные принципы анализа органических кислот методом газовой хроматографии с масс-спектрометрией: учебно-методическое пособие. М.: Триумф, 2023; 80 с.
- Hananeh T, Solaleh E, Shaghayegh H, Babak A, Negar R, Arezou D-M. The association between acylcarnitine and amino acids profile and metabolic syndrome and its components in Iranian adults. *Frontiers in Endocrinology*. 2023 [cited 2023 Nov 29]; 14: [10 p.]. Available from: <https://www.frontiersin.org/articles/10.3389/fendo.2023.1058952/full> DOI: 10.3389/fendo.2023.1058952.
- Gunther SH, Khoo CM, Tai E-S, et al. Serum acylcarnitines and amino acids and risk of type 2 diabetes in a multiethnic Asian population. *BMJ Open Diab Res Care*. 2020 [cited 2023 Nov 29]; 8: e001315 [10 p.]. Available from: <https://drc.bmj.com/content/bmjdr/8/1/e001315.full.pdf> DOI: 10.1136/bmjdr-2020-001315.

INFORMATION CAPACITY OF THE NF- κ B AND AP-1 SIGNALING ACTIVATION SENSORS IN *IN VITRO* ASSESSMENT OF DERMATOTOXIC EFFECTS

Tolstova TV , Pureczcky VK, Kozhin PM, Luzgina NG, Rusanov AL

Institute of Biomedical Chemistry, Moscow, Russia

Toxicity testing, including testing for skin toxicity, is essential for certification of novel pharmaceutical, chemical, and skincare products. The *in vitro* assessment models are considered to be the most promising; a number of such tests have been introduced into practice of approval testing. The new possibilities of detecting the early cellular response to damage can be provided by the cell-based sensors built upon visual quantification of the changes in activity of the signaling pathways involved in realization of such response. NF- κ B and AP-1 represent two important protein transcription factors, the increase in activity of which in the cell is associated with damage, inflammation or redox balance alteration. The study was aimed to develop the cell-based sensors built upon the HaCaT immortalized human keratinocyte cell line that express green fluorescent protein (GFP) when the NF- κ B (HaCaT/NF- κ B) or AP-1 (HaCaT/AP-1) signaling pathway is activated, as well as to assess their information capacity when recording the dose-dependent response to the exposure to inducers of appropriate signaling pathways. The findings showed that the HaCaT/NF- κ B cell fluorescence levels changed by 6.05 ± 0.51 and 5.53 ± 0.52 times upon exposure to TNF α or LPS (at a concentration of 0–80 ng/mL) in a dose dependent manner. The HaCaT/AP-1 biosensor also responded to the exposure to Cd (NO $_3$) $_2$ (at a concentration of 0–40 μ M) and ultraviolet A (UVA) (0–40 J/cm 2), however, it enabled qualitative, but not quantitative detection. The sensor cell fluorescence increased by 1.51 ± 0.24 and 1.66 ± 0.43 times, respectively. The cell-based sensors developed can be used to assess cytotoxic effects of the test substances on the human skin cells *in vitro* and study the cytotoxicity mechanisms.

Keywords: keratinocytes, biosensor, skin toxicity

Funding: the work was performed within the framework of the Program for Basic Research in the Russian Federation for a long-term period (2021–2030) (№ 122022800481-0).

Author contribution: Tolstova TV — experimental procedure, data acquisition, analysis, and interpretation, manuscript writing, illustrations; Pureczcky VK — experimental procedure, illustrations; Kozhin PM — literature review, manuscript writing, illustrations; Luzgina NG — study concept and design, manuscript writing; Rusanov AL — study planning, manuscript writing, overall guidance for the study.

✉ **Correspondence should be addressed:** Tatiana V. Tolstova
Pogodinskaya, 10, s. 8, Moscow, 119121, Russia; tolstova@ibmc.msk.ru

Received: 11.12.2023 **Accepted:** 16.02.2024 **Published online:** 27.02.2024

DOI: 10.24075/brsmu.2024.007

ИНФОРМАТИВНОСТЬ СЕНСОРОВ АКТИВАЦИИ СИГНАЛЬНЫХ ПУТЕЙ NF- κ B И AP-1 ПРИ ОЦЕНКЕ ДЕРМАТОТОКСИЧЕСКИХ ЭФФЕКТОВ *IN VITRO*

T. V. Толстова , В. К. Пурецкий, П. М. Кожин, Н. Г. Лузгина, А. Л. Русанов

Научно-исследовательский институт биомедицинской химии имени В. Н. Ореховича, Москва, Россия

Для сертификации новых фармацевтических, химических или косметических продуктов необходимо тестирование на токсичность, в том числе дерматотоксичность. Модели *in vitro* исследований считают наиболее перспективными, и ряд таких тестов внедрен в практику сертификационных испытаний. Новые возможности для регистрации раннего ответа клеток на повреждение могут предоставить клеточные сенсоры, основанные на визуальной количественной регистрации изменений активности сигнальных путей, задействованных в реализации такого ответа. NF- κ B и AP-1 — два важных фактора транскрипции белков, активность которых возрастает в клетке при повреждении, воспалении и изменении редокс-баланса. Целью исследования было разработать клеточные сенсоры на основе immortalized кератиноцитов человека линии HaCaT, которые экспрессируют зеленый флуоресцентный белок (GFP) при активации сигнальных путей NF- κ B (HaCaT/NF- κ B) или AP-1 (HaCaT/AP-1), и изучить их информативность при регистрации дозозависимого ответа на воздействие индукторов соответствующих сигнальных путей. Результаты показали, что уровень флуоресценции клеток HaCaT/NF- κ B дозозависимо изменялся в $6,05 \pm 0,51$ и $5,53 \pm 0,52$ раз при воздействии TNF α или LPS (в концентрациях от 0 до 80 нг/мл). Биосенсор HaCaT/AP-1 также реагировал на воздействие Cd (NO $_3$) $_2$ (в концентрациях от 0 до 40 мкМ) и ультрафиолетового излучения типа А (УФ-А) (от 0 до 40 Дж/см 2), однако позволял регистрировать его качественно, но не количественно. Флуоресценция клеток сенсора возрастала в $1,51 \pm 0,24$ и $1,66 \pm 0,43$ раз соответственно. Разработанные клеточные сенсоры могут быть использованы для оценки цитотоксического действия тестируемых веществ на клетки кожи человека *in vitro* и изучения механизмов цитотоксичности.

Ключевые слова: кератиноциты, биосенсор, дерматотоксичность

Финансирование: работа выполнена в рамках Программы фундаментальных научных исследований в Российской Федерации на долгосрочный период (2021–2030 годы) (№ 122022800481-0).

Вклад авторов: Т. В. Толстова — проведение эксперимента, сбор, анализ и интерпретация данных, написание статьи, оформление рисунков; В. К. Пурецкий — проведение эксперимента, оформление рисунков; П. М. Кожин — анализ литературы, написание статьи, оформление рисунков; Н. Г. Лузгина — концепция и дизайн работы, написание статьи; А. Л. Русанов — планирование исследования, написание статьи, общее руководство исследованием.

✉ **Для корреспонденции:** Татьяна Викторовна Толстова
ул. Погодинская, д. 10, с. 8, г. Москва, 119121, Россия; tolstova@ibmc.msk.ru

Статья получена: 11.12.2023 **Статья принята к печати:** 16.02.2024 **Опубликована онлайн:** 27.02.2024

DOI: 10.24075/vrgmu.2024.007

The risk of skin injury or irritation represents one of the restrictions for implementation of novel pharmaceutical substances, chemical compounds, and skincare products. In this regard, the approval safety testing of such products involves mandatory skin toxicity testing.

There is a number of routine *in vivo* tests approved by the Organization for Economic Cooperation and Development (OECD) and regulated by GOST of the RF. In particular, the OECD protocol № 429 based on the murine local lymph node assay [1], protocol № 406 (Guinea Pig Maximisation Test

(GPMT) of Magnusson and Kligman) [2], as well as methods for “Testing of Chemicals of Human Hazard”, including “Skin Sensitisation Testing” (GOST 32375-2013) [3] and “Repeated Dose Dermal Toxicity Testing. 21/28-day Study” (GOST 32642-2014) [4], etc., are widely used to assess skin toxicity.

However, the animal studies of adverse drug effects acquire more and more restrictions [5], while the *in vitro* tests based on using human cells are species-specific, show higher reproducibility and sufficient reliability [6, 7]. In particular, assessment of the eye injury and/or irritation can be performed using the reconstructed human cornea-like epithelium (EpiOcular™ (MatTek; USA), MCTT HCE™ (Biosolution; South Korea)) [8, 9], while the corrosion properties can be assessed using the reconstructed human epidermis (EpiSkin™ (L'Oréal; France), epiCS® (Phenion; Germany)) [10, 11].

Cytotoxicity testing, for example, involving the HaCaT immortalized human keratinocytes, by colorimetry or fluorimetry (MTT assay, Annexin V or trypan blue stain) represents one of the stages of the test substance biosafety testing [12]. However, cytotoxic effects may be represented not only by metabolic activity alterations or cell death, but also activation of certain signaling pathways. The use of genetically modified cells carrying the reporter genes controlled by the stress sensitive promoters is a promising approach to detection of cytotoxic effects [13–15]. For example, the KeratinoSens™ assay representing the cell line carrying a luciferase reporter gene controlled by the antioxidant response component (*AKR1C2* gene) is widely used to assess the test substances' skin sensitizing potential [16].

The transcription factors, such as NF-κB and AP-1, are involved in the cells' response to a wide range of stimuli: heavy metals, ultraviolet radiation, cytokines, infectious agents, etc., and may be of interest as biomarkers of cytotoxic effects [15, 17]. Thus, the important NF-κB transcription factor regulates transcription of proteins involved in inflammation, immune response, oxidative stress, apoptosis. AP-1 plays a key role in the cells' proliferation, differentiation, aging and death. A fluorescent biosensor based on the 3T3-L1 preadipocyte cell line, showing stable GFP expression when the NF-κB pathway was activated, was earlier used to detect the anti-inflammatory effects of the plant-derived antioxidants [18]. The previously developed cell-based model of human small intestine wall built upon the Caco-2 cell line ensured the dose-dependent detection of the NF-κB transcription factor activation under exposure to cadmium [15]. The cell-based biosensor built upon HT-29 with the regulatory element for AP-1 transcription factor and the gene encoding the mCherry fluorescent protein was successfully used for screening of heavy metal toxicity [17]. However, the cell-based sensors detecting activation of the NF-κB and AP-1 signaling pathways have not yet been studied when used to assess dermatotoxic effects during *in vitro* testing.

The study was aimed to develop the cell-based sensors built upon the HaCaT immortalized human keratinocyte cell line that express green fluorescent protein (GFP) when the NF-κB (HaCaT/NF-κB) or AP-1 (HaCaT/AP-1) signaling pathway is activated, as well as to assess their information capacity when detecting the dose-dependent cell damage.

METHODS

HaCaT cell line transduction with a lentiviral construct comprising the regulatory elements of the NF-κB/AP-1 transcription factors and the gene encoding green fluorescent protein

The HaCaT cells (CLS Cell Lines Service, 300493; Germany) were cultured in the DMEM/F12 (Gibco; USA) culture medium

supplemented with 10% fetal bovine serum (Gibco; USA), 0.1% GlutaMAX™, and penicillin/streptomycin at a concentration of 100 U/mL and 100 µg/mL, respectively (Gibco; USA), in the CO₂ incubator (MCO-20AIC Sanyo; Japan) at a temperature of 37 ± 1 °C, 90 ± 10% humidity, and CO₂ concentration of 5.0 ± 1.0%. The culture medium was replaced with fresh medium every 48 h. Upon reaching 80% confluence, the cells were dissociated with the 0.25% trypsin-EDTA solution (PanEco; Russia) and resuspended in the fresh culture medium.

The cell transduction was performed using the Signal Lenti Reporter Assay kits (QIAGEN; USA) containing lentiviral particles with the NF-κB/AP-1-induced GFP reporter. The concentration of lentiviral particles was 2 × 10⁷ particles/mL. For transduction, the cells were plated in the 24-well plate (Corning; USA), 4 × 10⁴ cells per well, and incubated overnight in the CO₂ incubator (MCO-20AIC Sanyo; Japan).

After 18 h the medium was collected; 80 µL of lentiviral particles were added, which corresponded to multiplicity of vector uptake of 40, together with 6 µL of SureENTRY Transduction Reagent (QIAGEN; USA) for transfection efficacy improvement. The total volume of the solution was brought to 600 µL. The 24 h incubation was carried out in the CO₂ incubator (MCO-20AIC Sanyo; Japan). In the control well, the medium was replaced with 600 µL of complete culture medium. After that the medium with lentiviral particles was replaced with DMEM/F12 (Gibco; USA) supplemented with 10% fetal bovine serum (Gibco; USA), penicillin/streptomycin at a concentration of 100 U/mL and 100 µg/mL, respectively, and 0.1% GlutaMAX™ (Gibco; USA).

Selection of transduced cells with the NF-κB/AP-1-induced GFP reporter

Selection involved the use of puromycin antibiotic (InvivoGen; USA), to which the transduced cells were resistant. The MTT assay was used to assess puromycin resistance of the non-transduced (wild type) HaCaT cells. For that the cells were plated in the 96-well plates (Corning; USA), 2 × 10³ cells in 200 µL of the medium per well, with DMEM/F12 containing 10% fetal bovine serum and GlutaMAX™ (Gibco; USA). Then 0; 0.5; 1.0; 2.0; 4.0, and 8.0 µg/mL of puromycin were added, and the cells were cultured for 10 days with the medium in the wells replaced every 96 h. The cells were examined with the Primovert phase contrast light microscope (Carl Zeiss; Germany) every day.

At the end of the exposure period, the culture medium with puromycin (experiment) or the culture medium (control) was drawn from the wells, washed with phosphate-buffered saline, pH 7.4 (PBS; PanEco, Russia), and added 200 µL of fresh complete culture medium containing 0.5 mg/mL MTT. The 2 h incubation was carried out in the MCO-20AIC CO₂ incubator (Sanyo; Japan) at a temperature of 37 °C with 5% CO₂. Then the medium was collected, washing with 200 µL of PBS was performed, and 100 µL of dimethyl sulfoxide (DMSO; Helicon, Russia) were added to each well. After the 15 min mixing on a shaker (150–200 rpm, in the dark), the optical density was measured at a wavelength of 595 nm (minus background absorbance at a wavelength of 655 nm) using the iMark microplate reader (BioRad; USA). Viability was determined using the following formula:

$$\frac{\text{OD of experimental wells} - \text{OD of the medium}}{\text{OD of control wells} - \text{OD of the medium}} \times 100\%$$

where OD was optical density.

Table 1. Sequences of PCR primers

Gene	Sequence of primer 1 (Forward)	Sequence of primer 2 (Reverse)
<i>GAPDH</i>	TCGACAGTCAGCCGCATCTTCTTT	ACCAAATCCGTTGACTCCGACCTT
<i>NFKB1</i>	CATGGCAGACGATGATCCC	ATTTGAAGGTATGGCCAT
<i>RelA</i>	CTGTCCCTTCTCATCCATCTT	TCCTCTTTCTGCACCTTGTC
<i>C-JUN</i>	ATGGTCAGGTTATACTCCTCCTC	CCTCCTGAAACATCGCACTATC

Sorting of transduced cells with the NF- κ B/AP-1-induced GFP reporter

Cell sorting was accomplished by plating the transduced cells obtained by selection in the population in the Petri dish with a diameter of 100 mm (Corning; USA) or the T75 flask (Corning; USA), 4×10^5 cells per dish. Upon reaching 70–80% confluence, the medium was replaced with the medium containing the NF- κ B signaling pathway activator (20 ng/mL of tumor necrosis factor alpha (TNF α), purity > 95%; Elabscience, China) or AP-1 signaling pathway activator (Cd(NO₃)₂ at a concentration of 10 μ M). After the 24 h incubation the cells were treated with the 0.25% trypsin-EDTA solution, precipitated at 300 g for 5 min, and resuspended in 1 mL of fresh culture medium for further sorting of GFP-positive cells.

The GFP-positive cells were sorted using the BD FACSMelody™ Cell Sorter (BD Biosciences; USA). The test population of cells was determined based on the parameters of forward and side light scatter in order to avoid debris and doubles. The non-transduced cells were used as negative controls (autofluorescence control). Cell sorting resulted in obtaining the transduced cell lines with the maximum levels of fluorescent protein generated in response to induction.

Assessment of dose-dependent changes in the HaCaT transduced cell fluorescence intensity associated with the NF- κ B/AP-1 pathway activation.

The transduced HaCaT cells were plated in the 96-well plate, 7×10^3 cells per well, and incubated overnight in the MCO-20AIC CO₂ incubator (Sanyo; Japan) at a temperature of 37 °C. The cells were added various concentrations of test substances: TNF α and lipopolysaccharide (LPS) (purity \geq 99%; Servicebio, China) for NF- κ B activation; Cd(NO₃)₂ for AP-1 activation. The effects of ultraviolet radiation (UVA) with the wavelength of 365 nm on the HaCaT/AP-1 transduced cells' fluorescence levels were also assessed. Fluorescence intensity was recorded using the Infinite M200 multimode plate reader (Tecan; Switzerland) with the excitation wavelength of 477 nm and emission wavelength of 507 nm for fluorescence and the wavelength of 600 nm for absorbance. We calculated average fluorescence intensity in the cells (minus average background fluorescence intensity with no cells) relative to the control cells with no inducers (100%). Micrographs of the intact and activated biosensor were acquired with the ZOE fluorescence microscope (Bio-Rad; USA). The resulting images were processed with the ImageJ tool (NIH; USA).

Assessing the target gene expression by polymerase chain reaction

The fluorescence intensities acquired were compared with the gene expression assessment results obtained by the real-time polymerase chain reaction (real-time PCR) method for the genes encoding various subunits of NF- κ B (*RelA* — p65 subunit; *NFKB1* — p50 subunit) and AP-1 (*C-JUN*) proteins. For that RNA was extracted using the kit for column-based RNA isolation (Biolabmix; Russia) in accordance with the manufacturer's protocol, and RNA was quantified using the

NanoDrop 2000c unit (Thermo Scientific; USA). The reverse transcription reaction with 1 μ g of RNA was performed with the use of the MMLV RT kit (Evrogen; Russia) in accordance with the manufacturer's protocol. PCR was carried out using qPCRmix-HS SYBR+LowROX (Evrogen; Russia). Primers are provided in Table 1. *GAPDH* was used as a reference gene.

Data analysis

The results obtained were processed using the R programming language for statistical data processing. The differences between groups were determined using the Student's *t*-test with Benjamini–Hochberg adjustment. The differences were considered significant at $p < 0.05$. The data were presented as $M \pm m$.

RESULTS

HaCaT cell transduction, selection and sorting

The HaCaT cells were transduced using the Cignal Lenti Reporter Assay lentiviral construct (QIAGEN; USA) containing lentiviral particles with the NF- κ B/AP-1-induced GFP reporter. Assessment of puromycin cytotoxic effects by MTT assay resulted in selection of the antibiotic exposure level (minimal concentration causing death of all original cells) corresponding to 1000 ng/mL for selection of transduced cells. Selection was carried out for 10 days, and the culture medium was replaced every three days.

During the next phase we performed selection of transduced cells after activation with 20 ng/mL TNF α for HaCaT/NF- κ B and 10 μ M Cd(NO₃)₂ for HaCaT/AP-1 for 24 h. Activation of appropriate signaling pathways resulted in the fact that the functional transduced cells started producing GFP, as detected by flow cytometry. Sorting of GFP-positive cells was accomplished by using the BD FACSMelody™ Cell Sorter (BD Biosciences; USA). The test population of cells was determined based on the parameters of forward and side light scatter in order to avoid debris and doubles (Fig. 1). The non-transduced cells were used as negative controls (autofluorescence control) (Fig. 1A, C). The transduced cell line showing maximum fluorescence levels in response to induction (gate *P1*, Fig. 1B; gate *P2*, Fig. 1D) were selected for further biosensor function assessment.

Assessing the dose-dependent changes in the HaCaT transduced cell fluorescence intensity associated with the NF- κ B signaling pathway activation using TNF α and LPS

The HaCaT cells transduced with the lentiviral construct containing the NF- κ B-induced GFP reporter obtained by selection and subsequent sorting were tested for the dose-dependent changes in fluorescence intensity by fluorometry using various concentrations of the well-known inducers of this signaling pathway, TNF α and LPS (hereinafter, inducers). The transduced cells were added various concentrations of inducers; then the sensor cell fluorescence intensity was

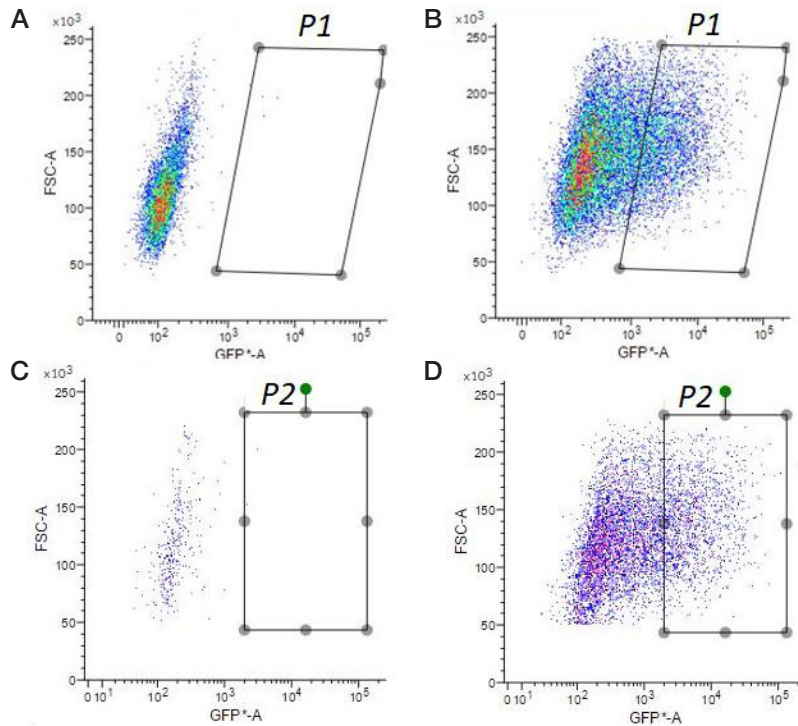


Fig. 1. Fluorescence intensity of transduced cells: control cells (**A, C**) and transduced cells showing high fluorescence intensity (**B, D**) in response to stimulation with 20 ng/mL TNF α for HaCaT/NF- κ B (gate P1) and 10 μ M Cd(NO $_3$) $_2$ for HaCaT/AP-1 (gate P2) throughout 24 h

recorded with the Infinite M200 multimode plate reader (Tecan; Switzerland), and the micrographs obtained with the ZOE fluorescence microscope (Bio-Rad; USA) were examined. Thus, to ensure NF- κ B activation, the cells were added TNF α and LPS at a concentration of 0–80 ng/mL for both substances. The changes in fluorescence intensity were detected after incubation with inducers (Fig. 2). Furthermore, the NF- κ B signaling pathway activation was detected based on the emergence of cells exhibiting green fluorescence when exposed to TNF α with a concentration as low as 5 ng/mL. The fluorescence intensity and the number of cells exhibiting

fluorescence increased with increasing TNF α concentration (up to 10 ng/mL) (Fig. 2A, B).

Under exposure to LPS, a significant fluorescence intensity increase and, therefore, the NF- κ B signaling pathway activation were also detected at the minimum test concentration of 5 ng/mL. The relationship between the fluorescence intensity and the concentrations of both inducers used reached the plateau when the concentration exceeded 20 ng/mL (Fig. 2C, D).

The fluorescence intensity measurement results were compared with the results of assessing the expression of genes encoding various NF- κ B protein subunits (*RelA* — subunit p65;

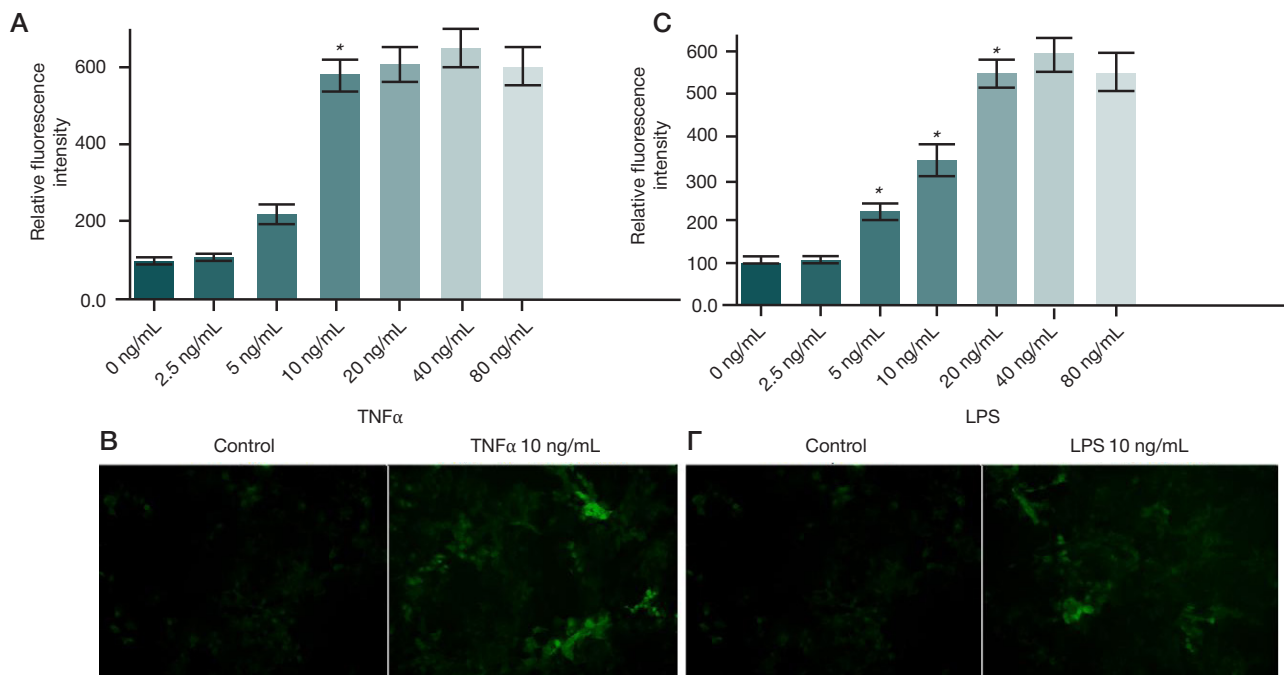


Fig. 2. Changes in the HaCaT/NF- κ B cells' relative fluorescence intensity under exposure to TNF α (**A, B**) and LPS (**C, D**). Fluorometry results (**A, C**) and fluorescence microscopy (**B, D**). * — significant differences from the previously reported concentration, $p < 0.05$.

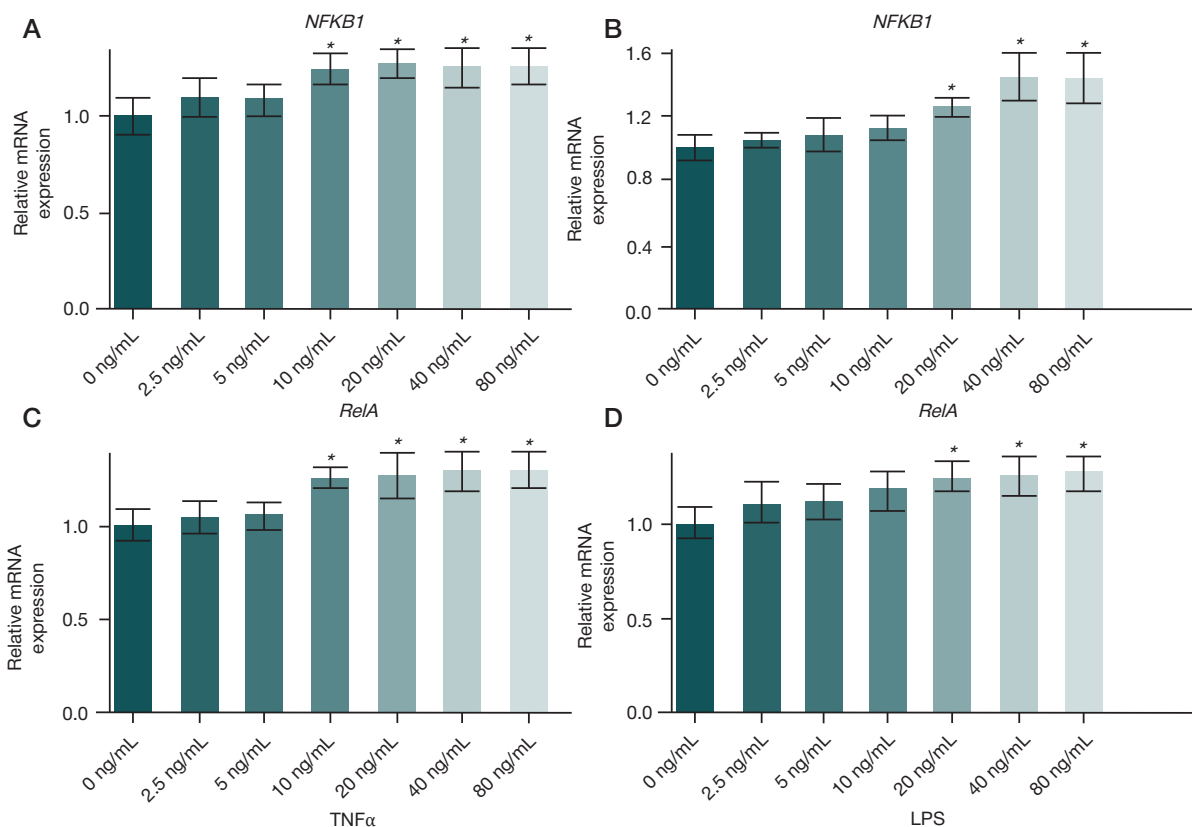


Fig. 3. Assessing activation of the genes encoding the NF-κB transcription factor subunits. Relative expression of *RelA* and *NFKB1* mRNA under exposure to TNFα (A, B) and LPS (C, D). * — significant differences from the control group, $p < 0.05$

NFKB1 — subunit p50) (Fig. 3). It was shown that exposure to TNFα resulted in the increased expression of *RelA* and *NFKB1* mRNA, however, significant differences from controls were obtained for the concentration of 10 ng/mL only, without further expression increase (Fig. 3A). A similar trend was observed under exposure to LPS (Fig. 3B): a significant increase in the *RelA* and *NFKB1* mRNA expression was observed only under exposure to LPS at a concentration of 20 ng/mL, without significant changes in expression with further concentration increase.

Assessing the dose-dependent changes in the HaCaT transduced cell fluorescence intensity associated with the AP-1 signaling pathway activation

We used Cd(NO₃)₂ and UVA, the inducers causing redox imbalance in the cells, to estimate information capacity of the cell-based sensor enabling detection of the AP-1 signaling pathway activity. We recorded the biosensor fluorescence intensity as a function of the Cd(NO₃)₂ concentration or radiation intensity (Fig. 4; Table 2). The findings about the AP-1 pathway activation were compared with the results of assessing the expression of gene *C-JUN* encoding the AP-1 protein subunit.

It was shown that exposure to Cd(NO₃)₂ resulted in the increase in fluorescence exhibited by the HaCaT/AP-1 cells, when the concentration was between 20 μM and 40 μM. However, the changes in fluorescence were not dose-dependent. Perhaps, the cytotoxic effects of this inducer manifested themselves, when the Cd(NO₃)₂ concentration increased, which resulted in the decrease in the number of viable cells exhibiting fluorescence. Furthermore, the *C-JUN* mRNA expression increased under exposure to the concentration as low as 5 μM, however, it did not depend on the exposure dose when the concentration increased (Table 2; Fig. 4A).

We also assessed the sensor cells' response to the 24 h exposure to various doses of ultraviolet radiation with the wavelength of 365 nm. The fluorescence intensity measurement results were also compared with the results of assessing the expression of gene *C-JUN* encoding the AP-1 subunit. A significant increase in the sensor cell fluorescence intensity was observed when the UV radiation exposure dose was 12–18 J/cm² (significant compared to control cells). The fluorescence intensity significantly differed from control when the exposure dose increased up to 18 J (Table 2; Fig. 4B). At the same time, the increase in the *C-JUN* mRNA expression was observed, when the cells were exposed to the studied UVA doses. However, the changes were not dose-dependent.

Table 2. Changes in the HaCaT/AP-1 cell fluorescence associated with exposure to Cd(NO₃)₂

Cd(NO ₃) ₂ , μM	Relative fluorescence intensity, %	UVA, J/cm ²	Relative fluorescence intensity, %
0	100 ± 13	0	100 ± 16
5	115 ± 18	6	135 ± 18
10	121 ± 16	12	168 ± 21*
20	172 ± 49*	18	151 ± 24*
40	166 ± 43*		

Note: * — significant differences from the control group, $p < 0.05$

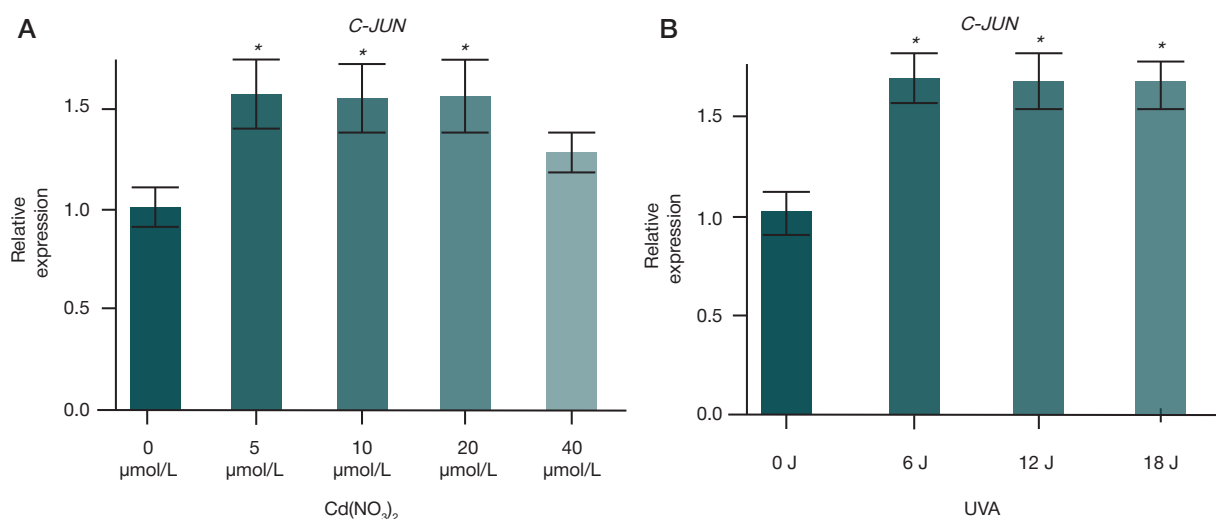


Fig. 4. Assessing activation of the gene encoding the AP-1 transcription factor subunit. Relative expression of the C-JUN mRNA under exposure to Cd(NO₃)₂ (A) and UVA (B). * — significant differences from the control group, $p < 0.05$

DISCUSSION

The development of *in vitro* tests for estimation of the chemical compound (CC) biosafety is an urgent task, since nowadays the animal studies become increasingly constrained [5, 19]. Keratinocytes are the first to contact the damaging agents and are involved in immune response, therefore, they represent a promising screening model for dermatological effects. Furthermore, the HaCaT immortalized keratinocyte cell line is a convenient alternative to primary cells for *in vitro* toxicology studies [12]. Thus, the HaCaT cells demonstrate normal morphogenesis and express all surface markers of primary keratinocytes. These cells can also differentiate when stimulated and express specific differentiation markers, such as keratin 14, keratin 10, and involucrin. Furthermore, the HaCaT cells can switch between the differentiated and basal states due to changes in the Ca²⁺ concentration in the culture medium [20, 21]. However, it is important to consider the presence of GOF (gain-of-function) mutations in the gene *TP53* resulting in the increased proliferation rate and abnormal terminal differentiation, when using HaCaT cells [22]. Nevertheless, in contrast to primary keratinocytes, the HaCaT cells do not require growth and/or differentiation factors in the culture medium, have boundless proliferation potential, and demonstrate a stable phenotype regardless of the number of passages [23]. Thus, the HaCaT cell line is a promising experimental model for investigation of various physiological processes occurring in human keratinocytes, including when assessing the CC toxicological effects.

When developing test systems for identification of irritation, providing the possibility of testing specific biomarkers associated with injury is considered to be promising [6, 24]. This makes it possible to draw a conclusion about the test substance potential cytotoxicity and the molecular mechanisms underlying realization of cytotoxicity.

Today, the focus is on the approaches aimed at studying the early cellular response to damage, preferably by real-time monitoring. Such approaches represent a promising alternative to the routine measurement of finite exposure effect, for example, based on the detection of specific metabolic processes using colorimetric and fluorometric assays (MTT assay, trypan blue stain, etc.). Thus, today the tests enabling the high-throughput real-time analysis of the cell damage process dynamics, such as STACK (scalable time-lapse analysis of cell death kinetics), are well known [25]. In particular, fluorescence

is used for identification of the population of viable and dead cells by fluorescence microscopy and thorough optimization of the image analysis procedures. However, the cytotoxic effects not only include cell death, but can be associated with the skin sensitization, one of the key events in the development of which, according to OECD-approved tests, is represented by activation of specific signaling pathways in keratinocytes (such as Keap1/Nrf2-ARE, NF-κB, etc.) [26].

To assess potential damaging effects of the test substances in the cellular response tests when assessing their potential biosafety at the molecular biological level, in this study we developed the cell-based sensors built upon the HaCaT immortalized human keratinocytes having regulatory elements for the NF-κB and AP-1 transcription factors and the gene encoding green fluorescent protein (GFP). After the delivery of these genetic constructs, the cells produced GFP, when appropriate signaling pathway was activated. In this case, fluorescence intensity was quantified. Despite the fact that peak GFP expression in the cells is achieved 24 h after the event detected using the protein, the GFP expression dynamics is well understood and accurately described. In this regard, the cell-based sensors built upon GFP make it possible to assess the dynamics of cellular response to the test exposure. In this case, it is necessary to consider the delayed effect of fluorescence and the cellular event itself [15].

Despite the fact, that the NF-κB and AP-1 transcription factors are among the most abundant actors of the cell damage process realization at the molecular level, the instrumental assessment performed has shown various possibilities of using the HaCaT/NF-κB and HaCaT/AP-1 sensors developed for detection of the dose-dependent effects of the well-known inducers of appropriate signaling pathways in the cells. The acquired cell-based sensor with the reporter construct associated with NF-κB activation demonstrated the possibility of sensitive dose-dependent *in vitro* detection of this signaling pathway activity in the model human epidermal cells. The GFP expression level of the biosensor construct associated with activation of the NF-κB signaling pathway strongly correlated with the changes in expression of target mRNA measured by real-time PCR. In turn, the HaCaT/AP-1 cell-based sensor made it possible to fix the fact of appropriate signaling pathway activation by inducers, however, detection of the inducer dose-dependent effects turned out to be impossible.

It is also worth noting that the information capacity of the testing results obtained using both sensors decreased with

increasing concentration of the inducers employed. This was probably due to a significant decrease in the number of viable sensor cells under these conditions, which did not allow to correctly estimate the fluorescence measurement results. In this regard, it is reasonable to perform MTT assay or other similar assay allowing one to determine the test substance concentrations causing death of sensor cells before conducting the tests involving the HaCaT/NF- κ B and HaCaT/AP-1 sensors. This will make it possible to more correctly estimate early cellular events occurring in response to the effects of test substances, including subtoxic ones.

CONCLUSIONS

In this study we developed biosensors based on the HaCaT immortalized keratinocytes containing genetic systems involved in activation of the GFP fluorescent reporter protein, the dose-dependent increase in expression of which was associated with activation of the AP-1 and NF- κ B signaling

pathways associated with damage to human epidermal cells. Experimental detection of the developed biosensors' sensitivity was conducted. We assessed the possibility of quantifying the intensity of sensor cell activation in response to exposure to inducers. It was found that the changes in HaCaT/NF- κ B fluorescence was observed under exposure to low concentrations of TNF α or LPS, which was in line with the changes in expression of genes *RelA* and *NFKB1* and had a dose-dependent nature. The cells with the HaCaT/AP-1 biosensor also responded to the Cd(NO₃)₂ and UVA exposure by increasing the fluorescence intensity and the target gene expression, however, we failed to detect the dose-dependent effects of these inducers on the sensor cells. The cell-based sensors developed can be used for *in vitro* assessment of cytotoxic effects of the test substances on human skin cells, as well as for fundamental studies of cytotoxicity mechanisms. Moreover, the HaCaT/NF- κ B sensor seems to be the most promising in terms of the possibility of detecting the dose-dependent effects of the damaging substances.

References

1. OECD, Test No. 429: Skin Sensitisation: Local Lymph Node Assay. Paris: Organisation for Economic Co-operation and Development, 2010. Accessed: Dec. 07, 2023. Available from: https://www.oecd-ilibrary.org/environment/test-no-429-skin-sensitisation_9789264071100-en.
2. OECD, Test No. 406: Skin Sensitisation. Paris: Organisation for Economic Co-operation and Development, 2022. Accessed: Dec. 06, 2023. Available from: https://www.oecd-ilibrary.org/environment/test-no-406-skin-sensitisation_9789264070660-en.
3. Metody ispytaniya po vozdeystviyu himicheskoy produkcii na organizm cheloveka. Ispytaniya po ocenke kozhnoj sensibilizacii: GOST 32375-2013. Vved. 01-08-2014. M.: Izd-vo standartov, 2014. Russian.
4. Metody ispytaniya po vozdeystviyu himicheskoy produkcii na organizm cheloveka. Opredelenie toksichnosti pri povtornom/mnogokratnom nakozhnom postuplenii. 28/21-dnevnyy test. GOST 32642-2014. Vved. 01-08-2014. M.: Izd-vo standartov, 2014. Russian.
5. Caloni F, De Angelis I, Hartung T. Replacement of animal testing by integrated approaches to testing and assessment (IATA): a call for *in vitro* studies. *Arch Toxicol*. 2022; 96 (7): 1935–1950. DOI: 10.1007/s00204-022-03299-x.
6. Test Methods, PETA Science Consortium International e.V. Accessed: Jul. 25, 2023. Available from: <https://www.thepsci.eu/test-methods/>.
7. Bergmann MM, Caubet J-C. Role of *in vivo* and *in vitro* Tests in the Diagnosis of Severe Cutaneous Adverse Reactions (SCAR) to Drug. *Curr Pharm Des*. 2019; 25 (36): 3872–80. DOI: 10.2174/1381612825666191107104126.
8. OECD, Test No. 492: Reconstructed human Cornea-like Epithelium (RhCE) test method for identifying chemicals not requiring classification and labelling for eye irritation or serious eye damage. Paris: Organization for Economic Co-operation and Development, 2023. Accessed: Dec. 06, 2023. Available from: https://www.oecd-ilibrary.org/environment/test-no-492-reconstructed-human-cornea-like-epithelium-rhce-test-method-for-identifying-chemicals-not-requiring-classification-and-labelling-for-eye-irritation-or-serious-eye-damage_9789264242548-en.
9. Metody ispytaniya po vozdeystviyu himicheskoy produkcii na organizm cheloveka. Metody ispytaniya s primeneniem rekonstruirovannogo rogovogo jepitelija cheloveka (RhCE) dlja opredeleniya himicheskoy produkcii, ne trebujushhej klassifikacii opasnosti kak vyzyvajushhej razdrazhenie ili ser'eznoe povrezhdenie glaz. GOST 34735-2021. Vved. 01.05.2024. M.: Izd-vo standartov, 2021. Russian.
10. OECD, Test No. 431: *In vitro* skin corrosion: reconstructed human epidermis (RHE) test method. Paris: Organisation for Economic Co-operation and Development, 2019. Accessed: Dec. 06, 2023. Available from: https://www.oecd-ilibrary.org/environment/test-no-431-in-vitro-skin-corrosion-reconstructed-human-epidermis-rhe-test-method_9789264264618-en.
11. Metody ispytaniya po vozdeystviyu himicheskoy produkcii na organizm cheloveka. Raz'edanie kozhi *in vitro*. Metody s ispol'zovaniem rekonstruirovannogo chelovecheskogo jepidermisa. GOST 32634-2020. Vved. 01.07.2021. M.: Standartinform, 2021. Russian.
12. Rusanov AL, Luzgina NG, Lisica AV. Citotoksichnost' dodecilsul'fata natrija v otnoshenii keratinocitov linii HaCaT: sravnitel'nyy analiz razlichnykh metodov ocenki zhiznesposobnosti kletok. *Bjulleten' jeksperimental'noj biologii i mediciny*. 2017; 163 (2): 256–60. Russian.
13. Arslanbaeva LR, Zherdeva VV, Ivashina TV, Vinokurov LM, Rusanov AL, Savickij AP. Geneticheski kodiruemaja FRET-para na osnove terbijsvjazyvajushhego peptida i krasnogo fluorescentnogo belka. *Prikladnaja biohimija i mikrobiologija*. 2010; 46 (2): 166–71. Russian.
14. Rusanov AL, Savitsky AP. Fluorescence resonance energy transfer between fluorescent proteins as powerful toolkits for *in vivo* studies. *Laser Physics Letters*. 2011; 8 (2): 91–102. DOI: 10.1002/lapl.201010107.
15. Rusanov AL, Luzgina ED, Vahrushev IV, Nahod KV, Luzgina NG. Kletochnaja model' stenki tonkogo kishechnika cheloveka na osnove geneticheski modifitsirovannykh kletok linii Saco-2. *Kletochnye tehnologii v biologii i medicine*. 2018; 3: 201–4. Russian.
16. Emter R, van der Veen JW, Adamson G, Ezendam J, van Loveren H, Natsch A. Gene expression changes induced by skin sensitizers in the KeratinoSens™ cell line: Discriminating Nrf2-dependent and Nrf2-independent events. *Toxicol In Vitro*. 2013; 27 (8): 2225–32. DOI: 10.1016/j.tiv.2013.09.009.
17. Guo H, Ji J, Sun J, Zhang Y, Sun X. Development of a living mammalian cell-based biosensor for the monitoring and evaluation of synergetic toxicity of cadmium and deoxyvalenol. *Science of the Total Environment*. 2021; 771: 144823. DOI: 10.1016/j.scitotenv.2020.144823.
18. Shen Q, et al. Adipocyte reporter assays: Application for identification of anti-inflammatory and antioxidant properties of mangostin xanthones. *Mol Nutr Food Res*. 2014; 58 (2): 239–47. DOI: 10.1002/mnfr.201300181.
19. Buchanan V. H.R.2565 — 117th Congress (2021-2022): FDA Modernization Act of 2021. Accessed: Jul. 25, 2023. Available from: <http://www.congress.gov/bill/117th-congress/house-bill/2565>.
20. Deyrieux AF, Wilson VG. *In vitro* culture conditions to study keratinocyte differentiation using the HaCaT cell line. *Cytotechnology*. 2007; 54 (2): 77–83. DOI: 10.1007/s10616-007-9076-1.

21. Micallef L, et al. Effects of extracellular calcium on the growth-differentiation switch in immortalized keratinocyte HaCaT cells compared with normal human keratinocytes. *Exp Dermatol.* 2009; 18 (2): 143–51. DOI: 10.1111/j.1600-0625.2008.00775.x.
22. Rusanov AL, et al. Impact of p53 Knockout on Protein Data Set of HaCaT Cells in Confluent and Subconfluent Conditions. *Data.* 2022; 7 (3). DOI: 10.3390/data7030027.
23. Rusanov AL, Romashin DD, Zgoda VG, Butkova TV, Luzgina NG. Protein dataset of immortalized keratinocyte HaCaT cells and normal human keratinocytes. *Data in Brief.* 2021; 35: 106871. DOI: 10.1016/j.dib.2021.106871.
24. Sergachev I, Rusanov A, Trushkin E, Sakharov D, Marx U, Tonevitsky A. Fluorescent optical fiber sensors for cell viability monitoring. *Analyst.* 2013; 138 (14): 4066–9. DOI: 10.1039/c3an00248a.
25. Forcina GC, Conlon M, Wells A, Cao JY, Dixon SJ. Systematic quantification of population cell death kinetics in mammalian cells. *Cell Syst.* 2017; 4 (6): 600–10. DOI: 10.1016/j.cels.2017.05.002.
26. OECD, Test No. 442D: In Vitro Skin Sensitisation: ARE-Nrf2 Luciferase Test Method. Paris: Organisation for Economic Co-operation and Development, 2022. Accessed: Jul. 25, 2023. Available from: https://www.oecd-ilibrary.org/environment/test-no-442d-in-vitro-skin-sensitisation_9789264229822-en.

Литература

1. OECD, Test No. 429: Skin Sensitisation: Local Lymph Node Assay. Paris: Organisation for Economic Co-operation and Development, 2010. Accessed: Dec. 07, 2023. Available from: https://www.oecd-ilibrary.org/environment/test-no-429-skin-sensitisation_9789264071100-en.
2. OECD, Test No. 406: Skin Sensitisation. Paris: Organisation for Economic Co-operation and Development, 2022. Accessed: Dec. 06, 2023. Available from: https://www.oecd-ilibrary.org/environment/test-no-406-skin-sensitisation_9789264070660-en.
3. Методы испытания по воздействию химической продукции на организм человека. Испытания по оценке кожной сенсбилизации: ГОСТ 32375-2013. Введ. 01-08-2014. М.: Изд-во стандартов, 2014.
4. Методы испытания по воздействию химической продукции на организм человека. Определение токсичности при повторном/многократном нахождении на коже. 28/21-дневный тест. ГОСТ 32642-2014. Введ. 01-08-2014. М.: Изд-во стандартов, 2014.
5. Caloni F, De Angelis I, Hartung T. Replacement of animal testing by integrated approaches to testing and assessment (IATA): a call for in vivitrosi. *Arch Toxicol.* 2022; 96 (7): 1935–1950. DOI: 10.1007/s00204-022-03299-x.
6. Test Methods, PETA Science Consortium International e.V. Accessed: Jul. 25, 2023. Available from: <https://www.thepsci.eu/test-methods/>.
7. Bergmann MM, Caubet J-C. Role of in vivo and in vitro Tests in the Diagnosis of Severe Cutaneous Adverse Reactions (SCAR) to Drug. *Curr Pharm Des.* 2019; 25 (36): 3872–80. DOI: 10.2174/1381612825666191107104126.
8. OECD, Test No. 492: Reconstructed human Cornea-like Epithelium (RhCE) test method for identifying chemicals not requiring classification and labelling for eye irritation or serious eye damage. Paris: Organization for Economic Co-operation and Development, 2023. Accessed: Dec. 06, 2023. Available from: https://www.oecd-ilibrary.org/environment/test-no-492-reconstructed-human-cornea-like-epithelium-rhce-test-method-for-identifying-chemicals-not-requiring-classification-and-labelling-for-eye-irritation-or-serious-eye-damage_9789264242548-en.
9. Методы испытаний по воздействию химической продукции на организм человека. Методы испытаний с применением реконструированного рогового эпителия человека (RhCE) для определения химической продукции, не требующей классификации опасности как вызывающей раздражение или серьезное повреждение глаз. ГОСТ 34735-2021. Введ. 01.05.2024. М.: Изд-во стандартов, 2021.
10. OECD, Test No. 431: In vitro skin corrosion: reconstructed human epidermis (RHE) test method. Paris: Organisation for Economic Co-operation and Development, 2019. Accessed: Dec. 06, 2023. Available from: https://www.oecd-ilibrary.org/environment/test-no-431-in-vitro-skin-corrosion-reconstructed-human-epidermis-rhe-test-method_9789264264618-en.
11. Методы испытаний по воздействию химической продукции на организм человека. Разъедание кожи in vitro. Методы с использованием реконструированного человеческого эпидермиса. ГОСТ 32634-2020. Введ. 01.07.2021. М.: Стандартинформ, 2021.
12. Русанов А. Л., Лузгина Н. Г., Лисица А. В. Цитотоксичность додецилсульфата натрия в отношении кератиноцитов линии HaCaT: сравнительный анализ различных методов оценки жизнеспособности клеток. *Бюллетень экспериментальной биологии и медицины.* 2017; 163 (2): 256–60.
13. Арсланбаева Л. П., Жердева В. В., Ивашина Т. В., Винокуров Л. М., Русанов А. Л., Савицкий А. П. Генетически кодируемая Fret-пара на основе тербийсвязывающего пептида и красного флуоресцентного белка. *Прикладная биохимия и микробиология.* 2010; 46 (2): 166–71.
14. Rusanov AL, Savitsky AP. Fluorescence resonance energy transfer between fluorescent proteins as powerful toolkits for in vivo studies. *Laser Physics Letters.* 2011; 8 (2): 91–102. DOI: 10.1002/lapl.201010107.
15. Русанов А. Л., Лузгина Е. Д., Вахрушев И. В., Наход К. В., Лузгина Н. Г. Клеточная модель стенки тонкого кишечника человека на основе генетически модифицированных клеток линии Saso-2. *Клеточные технологии в биологии и медицине.* 2018; 3: 201–4.
16. Emter R, van der Veen JW, Adamson G, Ezendam J, van Loveren H, Natsch A. Gene expression changes induced by skin sensitizers in the KeratinoSens™ cell line: Discriminating Nrf2-dependent and Nrf2-independent events. *Toxicol In Vitro.* 2013; 27 (8): 2225–32. DOI: 10.1016/j.tiv.2013.09.009.
17. Guo H, Ji J, Sun J, Zhang Y, Sun X. Development of a living mammalian cell-based biosensor for the monitoring and evaluation of synergistic toxicity of cadmium and deoxynivalenol. *Science of the Total Environment.* 2021; 771: 144823. DOI: 10.1016/j.scitotenv.2020.144823.
18. Shen Q, et al. Adipocyte reporter assays: Application for identification of anti-inflammatory and antioxidant properties of mangostin xanthenes. *Mol Nutr Food Res.* 2014; 58 (2): 239–47. DOI: 10.1002/mnfr.201300181.
19. Buchanan V. H.R.2565 — 117th Congress (2021-2022): FDA Modernization Act of 2021. Accessed: Jul. 25, 2023. Available from: <http://www.congress.gov/bill/117th-congress/house-bill/2565>.
20. Deyrieux AF, Wilson VG. In vitro culture conditions to study keratinocyte differentiation using the HaCaT cell line. *Cytotechnology.* 2007; 54 (2): 77–83. DOI: 10.1007/s10616-007-9076-1.
21. Micallef L, et al. Effects of extracellular calcium on the growth-differentiation switch in immortalized keratinocyte HaCaT cells compared with normal human keratinocytes. *Exp Dermatol.* 2009; 18 (2): 143–51. DOI: 10.1111/j.1600-0625.2008.00775.x.
22. Rusanov AL, et al. Impact of p53 Knockout on Protein Data Set of HaCaT Cells in Confluent and Subconfluent Conditions. *Data.* 2022; 7 (3). DOI: 10.3390/data7030027.
23. Rusanov AL, Romashin DD, Zgoda VG, Butkova TV, Luzgina NG. Protein dataset of immortalized keratinocyte HaCaT cells and normal human keratinocytes. *Data in Brief.* 2021; 35: 106871. DOI: 10.1016/j.dib.2021.106871.
24. Sergachev I, Rusanov A, Trushkin E, Sakharov D, Marx U, Tonevitsky A. Fluorescent optical fiber sensors for cell viability monitoring. *Analyst.* 2013; 138 (14): 4066–9. DOI: 10.1039/c3an00248a.
25. Forcina GC, Conlon M, Wells A, Cao JY, Dixon SJ. Systematic quantification of population cell death kinetics in mammalian cells. *Cell Syst.* 2017; 4 (6): 600–10. DOI: 10.1016/j.cels.2017.05.002.
26. OECD, Test No. 442D: In Vitro Skin Sensitisation: ARE-Nrf2 Luciferase Test Method. Paris: Organisation for Economic Co-operation and Development, 2022. Accessed: Jul. 25, 2023. Available from: https://www.oecd-ilibrary.org/environment/test-no-442d-in-vitro-skin-sensitisation_9789264229822-en.

COMPARISON OF LIPID ALTERATIONS IN ASTROCYTOMAS WITH INCREASING GRADE

Pekov SI^{1,2,3}, Bocharov KV^{2,4}, Bormotov DS², Eliferov VA², Parochkina EV², Sorokin AA², Nikolaev EN¹, Popov IA^{2,3} ✉¹ Skolkovo Institute of Science and Technology, Moscow, Russia² Moscow Institute of Physics and Technology, Dolgoprudny, Russia³ Siberian State Medical University, Tomsk, Russia⁴ Semenov Federal Research Center for Chemical Physics, Moscow, Russia

The use of ambient ionization mass spectrometry methods is one of the promising approaches to the improvement of glial tumor resection completeness by using an additional method to improve the tumor margin identification accuracy during the neurosurgical intervention itself. The amounts of data accumulated when testing such techniques can be also used in fundamental research to identify metabolic alterations associated with the tumor growth. The study was aimed to assess changes in the cell membrane lipid composition of diffuse and anaplastic astrocytomas based on the data acquired by ambient ionization mass spectrometry profiling of the tissues excised during the elective neurosurgical intervention. The lipid profiles obtained when assessing the tumor tissue samples ($n = 43$) by flow microextraction in a cartridge were subjected to shrinkage linear discriminant analysis enabling extraction of a number of lipids, the levels of which changed with increasing tumor grade. The lipid diversity decreased with increasing grade. Thus, the levels of 13 phospholipids belonging to six different subclasses turned out to be decreased in anaplastic tumors compared to diffuse ones. Both average size of the polar lipid fatty acid residues and their degree of unsaturation decrease with increasing tumor grade. The findings agree well with the data of the earlier study of high-grade glial tumors and confirm the biochemical view of metabolic reprogramming associated with malignant transformation of neuroglia.

Keywords: mass spectrometry, lipids, astrocytoma, neurosurgery, molecular diagnosis

Funding: the study was performed within the framework of the state assignment of the Ministry of Science and Higher Education of the Russian Federation (agreement № 075-03-2022-107, project № 0714-2020-0006). The study involved the use of equipment of the Semenov Federal Research Center for Chemical Physics RAS.

Author contribution: Pekov SI — concept, data analysis, manuscript writing; Bocharov KV — experimental procedure, resource provision; Bormotov DS — experimental procedure, data analysis; Eliferov VA — experimental procedure, communication with surgeons; Parochkina EV — experimental procedure; Sorokin AA — data analysis, concept; Nikolaev EN — resource provision; Popov IA — search of funding sources, research management.

Compliance with ethical standards: the study was approved by the Ethics Committee of the Burdenko Research Institute of Neurosurgery (protocols № 40 dated 12 April 2016 and № 131 dated 17 July 2018) and conducted in accordance with the principles of the Declaration of Helsinki (2000) and its subsequent revisions. All patients submitted the informed consent to study participation and the use of biomaterial for scientific purposes.

✉ **Correspondence should be addressed:** Igor A. Popov
Institutskiy per., 9, str. 7, Dolgoprudny, 141701, Russia; popov.ia@mipt.ru

Received: 11.01.2024 **Accepted:** 07.02.2024 **Published online:** 24.02.2024

DOI: 10.24075/brsmu.2024.008

СРАВНЕНИЕ ЛИПИДНЫХ ИЗМЕНЕНИЙ В АСТРОЦИТОМАХ ПО МЕРЕ РОСТА ИХ ЗЛОКАЧЕСТВЕННОСТИ

С. И. Пеков^{1,2,3}, К. В. Бочаров^{2,4}, Д. С. Бормотов², В. А. Елиферов², Е. В. Парочкина², А. А. Сорокин², Е. Н. Николаев¹, И. А. Попов^{2,3} ✉¹ Сколковский институт науки и технологий, Москва, Россия² Московский физико-технический институт, Долгопрудный, Россия³ Сибирский государственный медицинский университет, Томск, Россия⁴ Федеральный исследовательский центр химической физики имени Н. Н. Семенова, Москва, Россия

Применение методов прямой масс-спектрометрии является одним из перспективных подходов к улучшению полноты резекции глиальных опухолей за счет использования дополнительного способа повышения точности определения границ опухоли непосредственно в ходе нейрохирургического вмешательства. Массивы данных, накапливаемые в ходе апробации подобных технологий, могут быть использованы и для проведения фундаментальных исследований с целью выявления метаболических изменений, сопровождающих рост опухоли. Целью работы было провести анализ изменений в липидном составе клеточных мембран диффузных и анапластических астроцитом на основе данных, собранных в ходе прямого масс-спектрометрического профилирования тканей, иссеченных в ходе планового нейрохирургического вмешательства. Липидные профили, полученные в ходе исследования образцов опухолевых тканей ($n = 43$) методом проточной микроэкстракции в картридже, анализировали с использованием линейного дискриминантного анализа со сжатием, что позволило выделить набор липидов, содержание которых изменяется при увеличении степени злокачественности опухоли. Разнообразие липидов снижается по мере повышения степени злокачественности, так, содержание 13 фосфолипидов, принадлежащих к 6 различным подклассам, оказывается сниженным в анапластических опухолях по сравнению с диффузными. С ростом злокачественности опухоли уменьшаются как средний размер жирнокислотных остатков полярных липидов, так и степень их ненасыщенности. Полученные результаты хорошо согласуются с данными, полученными ранее в рамках исследования высокозлокачественных глиальных опухолей, и подтверждают биохимические представления о перепрограммировании метаболизма в ходе малигнизации нейроглии.

Ключевые слова: масс-спектрометрия, липиды, астроцитомы, нейрохирургия, молекулярная диагностика

Финансирование: работа выполнена в рамках государственного задания Министерства науки и высшего образования (соглашение № 075-03-2022-107, проект № 0714-2020-0006). Исследование выполнено с использованием оборудования ЦКП ФИЦ ХФ имени Н. Н. Семенова РАН.

Вклад авторов: С. И. Пеков — концепция, анализ данных, написание статьи; К. В. Бочаров — проведение эксперимента, предоставление ресурсов; Д. С. Бормотов — проведение эксперимента, анализ данных; В. А. Елиферов — проведение эксперимента, взаимодействие с хирургами; Е. В. Парочкина — проведение эксперимента; А. А. Сорокин — анализ данных, концепция; Е. Н. Николаев — предоставление ресурсов; И. А. Попов — поиск источников финансирования, руководство исследованием.

Соблюдение этических стандартов: исследование одобрено этическим комитетом НМИЦН имени Н. Н. Бурденко (протоколы № 40 от 12 апреля 2016 г. и № 131 от 17 июля 2018 г.), проведено в соответствии с принципами Хельсинкской декларации (2000 г.) и ее последующих пересмотров. Все пациенты подписали добровольное информированное согласие на участие в исследовании и использование биоматериалов в исследовательских целях.

✉ **Для корреспонденции:** Игорь Алексеевич Попов
Институтский пер., д. 9, стр. 7, Долгопрудный, 141701, Россия; popov.ia@mipt.ru

Статья получена: 11.01.2024 **Статья принята к печати:** 07.02.2024 **Опубликована онлайн:** 24.02.2024

DOI: 10.24075/vrgmu.2024.008

Tumors of the central nervous system are considered to be the most demanding to precision of surgical intervention. The resection completeness and volume are the key parameters affecting the outcome of complex treatment and the long-term overall survival [1–3]. Thus, the tumor margin identification accuracy is the most important parameter controlled during surgery, and the surgeon has to balance between the need to remove the maximum amount of the affected tissue and preservation of adjacent non-affected functional regions of the brain. In this regard, glial tumors characterized by diffuse tumor cell invasion are particularly challenging. Intraoperative computed tomography, magnetic resonance imaging, and rapid histological analysis are widely used as the methods to facilitate the surgeon's decision-making, however, their substantially time-consuming nature limits the use of the methods for continuous monitoring of the resection area [4, 5]. Ultrasound guidance and fluorescence imaging are convenient and effective, however, the accuracy and specificity of these methods drop to 50% for some tumors [6, 7]. Today, the mass-spectrometry-based molecular profiling methods rapidly transform into a quick universal tool to support neurosurgical procedures [4, 8]. Regardless of the nature of the specific method for the sample collection and ionization, the mass spectrometry methods are based on assessing the features of tumor tissues addressing both changes in the lipid composition of proliferating cells and the set and concentration of specific metabolites, such as N-acetylaspartate, 2-hydroxyglutarate, and glutamic acid [9–11].

The mass spectrometry profiles acquired when developing such methods enable the building of classification and regression models distinguishing cancerous and non-cancerous tissue with high sensitivity and specificity [12, 13]. It should be noted that such methods are generally based not on a single marker, but on the combination of multiple peaks in the spectra reflecting metabolic reprogramming occurring during malignant transformation of the tissue [14]. To proliferate, the cancer cells need large amounts of biomass, however, tumor hypovascularization results in the lack of nutrients. Activation of anaerobic glycolysis, even in the presence of oxygen (Warburg effect) [15], also leads to activation of fatty acid synthesis and acceleration of lipogenesis. The synthesis of saturated fatty acids and the lack of dietary unsaturated fatty acids result in significant changes in the lipid composition of cells, including redistribution of fatty acid residues among triglycerides and phospholipids [16]. Despite the fact that the biochemical basis explaining the differences in the lipid composition between glioma cells and healthy glial cells is well known, no thorough tumor lipidome investigation has yet been carried out, since such studies usually involve cell lines or xenografts, which do not fully reflect the tumors' natural biological variability and physiological environment [17]. Diffuse tumors are still challenging for metabolomic studies due to difficulty in obtaining enough tumor material containing no incorporated cells of other types for assessment.

A substantial amount of data obtained by mass spectrometry-based molecular profiling enables investigation of metabolic alterations even in heterogeneous samples, since the use of advanced mathematical approaches makes it possible to identify the characteristic features of molecular profiles distinguishing the tissues, by separating these features from natural biological variability and the contributions of other cells present in the sample [16, 18]. The study was aimed to identify the differences in the lipid composition of grade 2 and 3 astrocytomas in order to confirm the suspected metabolic alterations associated with malignant transformation of tissues.

METHODS

All the samples included in the study were collected by the neurosurgeon, who monitored the progress of surgical procedure using the neuronavigation systems or visually. Composition of the sample that had to consist mostly of tumor tissue was the main selection criterion. The areas showing signs of necrosis and comprising a large number of blood vessels were not selected for the study. The tissue samples were washed with sterile saline to remove the remaining blood and divided into two visually similar parts. The first part was frozen and stored at -80°C prior to the study. The second part was used by a professional pathologist to conduct histological assessment using the routine protocol. The samples containing less than 75% tumor cells and the samples showing signs of necrosis were excluded from the study based on the pathology report. Thus, a total of 28 anaplastic astrocytoma tissue samples (grade 3; collected from 23 patients) and 15 diffuse astrocytoma tissue samples (grade 2; collected from 12 patients) were selected.

All the collected samples were analyzed at random. Furthermore, different samples obtained from the same patient were not analyzed on the same day in order to minimize possible bias. Each tissue sample was thawed just before the analysis and divided into 2–4 parts depending on the size. These parts were immediately subjected for mass spectrometry-based profiling. A total of 81 mass spectrometry profiles of anaplastic astrocytoma samples and 46 mass spectrometry profiles of diffuse astrocytoma samples were acquired.

All the samples were analyzed using Inline Cartridge Extraction (ICE) [19]. The tissue sample of about 1 mm^3 was placed in a disposable cartridge, which was a stainless steel tube having a fused silica electrospray emitter on one end and sealed with an input polyether ether ketone (PEEK) capillary on the other end. The fused silica emitter was sealed against entry of tissue particles with a glass microfiber filter. The sample in the cartridge was washed with $100\ \mu\text{L}$ of the solution containing isopropanol, methanol, acetonitrile, and water (3 : 3 : 3 : 1 v/v) supplemented with 0.1% formic acid (v/v), then the cartridge was mounted into the ion source of a mass spectrometer. Extraction was performed by continuously supplying the above solvent with the flow rate of $3\ \mu\text{L}/\text{min}$. Mass spectra were acquired using the LTQ XL Orbitrap ETD mass spectrometer (Thermo Fisher Scientific; San Jose, USA) with the 30,000 resolution (at $m/z\ 400$) within the range of $m/z\ 500\text{--}1000$, in both polarities consequently.

Peaks with the signal-to-noise ratio less than 2 were removed from mass spectra, then the peaks found in less than 25% of individual scans in each group were removed. Then, only peaks with intensity values exceeding the median were selected for further analysis. Extraction of the peaks characterizing each group of samples was performed by shrinkage discriminant analysis (SDA) [20]. Significance of each extracted peak was assessed using the *lfdr* criterion (local false discovery rate) showing the probability that an individual peak would not have an impact on the sample classification. The *lfdr* threshold value of 33% was selected.

Two tissue samples with the maximum volume in each group were also used for identification of lipids. For that approximately 10 mg of the tissue were homogenized in $400\ \mu\text{L}$ of the above solution on ice. The homogenate was processed in the ultrasonic bath for 5 min and centrifuged at $21,000\text{ g}$ for 15 min at a temperature of 4°C . Supernatant was transferred to the chromatography vial and subjected to vacuum evaporation. Lipids were redissolved in $20\ \mu\text{L}$ of the solution

Table. Significance of polar lipid ions when attributing spectra to the groups of diffuse or anaplastic astrocytoma. The analysis results for positively and negatively charged ions are combined

CAT-score	m/z	Ion
Ions typical for diffuse astrocytoma samples		
71.4	742.55	[PE(36:2)-H] ⁻
61.9	782.58	[PC(34:1)+Na] ⁺
53	786.57	[PS(36:2)-H] ⁻
52.3	780.57	[PC(34:2)+Na] ⁺
47.3	700.53	[PA(36:2)-H] ⁻
46.3	857.59	[PI(36:4)-H] ⁻
45.9	754.55	[PC(32:1)+Na] ⁺
45.3	794.55	[PE(40:4)-H] ⁻
44	797.61	[PG(38:4)-H] ⁻
43	820.57	[PC(34:0)-H] ⁻
40.8	792.53	[PC(32:0)-H] ⁻
39.6	920.71	[PC(44:2)+Na] ⁺
39.4	808.56	[PC(36:2)+Na] ⁺
Ions typical for anaplastic astrocytoma samples		
48	772.53	[PE(38:1)-H] ⁻
44.1	762.58	[PC(30:1)-H] ⁻
40.2	646.62	[PA(32:1)-H] ⁻

containing n-butanol, isopropanol, and water (8 : 21 : 69 v/v) supplemented with 5 mM phosphoric acid. The analysis of lipids was performed by the reverse phase nanoHPLC–HRMS/MS using the above mass spectrometer. Lipids were identified using the LipiDex software.

RESULTS

The limited dynamic range of mass analyzers does not allow us to draw firm quantitative conclusions about the levels of molecules in the original biological sample. However, relative peak intensities change in proportion to changes in the levels of appropriate molecules against the background of other compounds of the selected class. The mixture of solvents used in the study effectively dissolves lipids, especially polar lipids of the cell membranes, which are easy to ionize and detect in the selected mass range. Thus, the molecular profiles acquired during this study correspond mainly to the lipid component of the cell. The use of SDA [20], the subtype of linear discriminant analysis considering internal correlations caused by natural distribution of stable isotopes in biological molecules (mainly ¹³C for lipids), makes it possible to identify ions, the intensities of which vary between samples of the assessed groups. The CAT score (correlation-adjusted *t*-score) calculated during this procedure represents an analogue of Student's *t*-test considering both internal correlations together with the higher dimension of raw data and the peak intensity distribution deviation from normal. The CAT score demonstrates the individual peak intensity deviation from the average towards appropriate group. As a result, a total of 13 ions of lipids were identified, the levels of which were higher in the diffuse astrocytoma samples than in the anaplastic astrocytoma samples, along with three ions of lipids, the levels of which were elevated based on spectra corresponding to the anaplastic astrocytoma samples (Table). Chemical identification of the ions was performed by chromatography–tandem mass spectrometry based on the lipid extraction from the largest tissue samples, which was likely to be impossible for the majority of samples due to small amounts of available

biomaterial. Thus, the problem of preserving natural biological variability of the assessed tumors and interpatient variability recording was solved through mass spectrometry-based tissue profiling without sample preparation.

All the extracted peaks are not among the most intense in the mass spectra; these are considered the second and third quartiles of the intensity distribution. This is due to the fact that the most and the least intense peaks strongly correlate with the natural variability and can vary considerably between patients, which makes their intragroup variability comparable with the intergroup variability in the sample of this size. However, the results obtained demonstrate the decrease in the diversity of lipid composition with increasing grade, which is in line with the overall pattern reported earlier when comparing grade 4 glial tumors with the non-cancerous control samples [16].

DISCUSSION

The reported differences in lipid composition between grade 2 and 3 astrocytomas demonstrate the decrease in the levels of phospholipids containing polyunsaturated fatty acids, which suggests the increase in the share of fatty acids de novo synthesized in the glioma cell membranes with increasing glioma grade. A decrease in the levels of phospholipids with fully saturated fatty acid residues is observed, because, according to the previous studies, the most aggressive glioma cells accumulate fatty acids in the lipid droplets to use them to maintain metabolic activity in the later stages of the disease, when the nutrient availability is reduced even more [15, 21].

It should be noted that the relative content of phosphatidylcholines PC(32:1), PC(34:1), and PC(34:2) is not fully compliant with the overall pattern of astrocytoma growth. Thus, it has been shown that these lipids largely characterize the high-grade cancerous, but not non-cancerous, brain tissue [16], while comparison of diffuse and anaplastic astrocytomas has shown that these lipids are typical for the less malignant form. This observation suggests irregular pattern of the decrease in the levels of various classes of lipids with increasing grade, which results in the increase in the observed

share of the above lecithins in diffuse astrocytomas and demonstrates the restriction imposed by the ambient ionization mass spectrometry-based profiling on the possibility of assessing lipid composition without applying more informative chromatography–mass spectrometry methods. The analysis of the overall fatty acid composition of certain lipids that can be performed by ambient ionization mass spectrometry does not enable distinguishing isomeric lipids. Thus, for example, the PC(34:1) phospholipid can consist of palmitoleic and stearic acid residues or palmitic and oleic acid residues. Among fatty acids, it is palmitic acid that is the most accessible for incorporation into lipids with increasing grade, since it is the main product released due to functioning of the NADPH-dependent fatty acid synthase [14]. It should be noted that the pentose phosphate pathway activated due to Warburg effect results in the increased NADPH generation by the tumor cell [22]. Thus, the increasing grade can be associated with both spending the pool of phospholipids containing 32–34 carbon atoms in their

fatty acid chains [21, 23] and active replacement of those with the isomeric lipids containing fatty acid chains synthesized *de novo* in cases of astrocytoma progression to grade 4.

CONCLUSIONS

The use of molecular profiling methods makes it possible to study changes in the lipid composition of cancerous tissues of various grades considering their natural biological variability. The trend towards reducing the diversity of polar lipids contained in the cell membranes is observed during the astrocytoma progression to a higher grade. The length and degree of unsaturation of the fatty acid residues constituting these lipids are also reduced. Such an effect is associated with the fatty acid synthesis activation due to metabolic reprogramming of glial cells during their malignant transformation; it is also associated with activation of fatty acid beta-oxidation required to maintain the cells' vital activity in cases of high-grade glial tumors.

References

- Kreatsoulas D, Damante M, Gruber M, et al. Supratotal surgical resection for low-grade glioma: a systematic review. *Cancers (Basel)*. 2023; 15 (9): 2493.
- Karschnia P, Vogelbaum MA, van den Bent M, et al. Evidence-based recommendations on categories for extent of resection in diffuse glioma. *Eur J Cancer*. 2021; 149: 23–33.
- Chanbour H, Chotai S. Review of intraoperative adjuncts for maximal safe resection of gliomas and its impact on outcomes. *Cancers (Basel)*. 2022; 14: 22.
- Bogusiewicz J, Bojko B. Insight into new opportunities in intrasurgical diagnostics of brain tumors. *TrAC — Trends Anal Chem. Elsevier B.V.* 2023; 162: 117043.
- Cordova JS, Gurbani SS, Olson JJ, et al. A systematic pipeline for the objective comparison of whole-brain spectroscopic MRI with histology in biopsy specimens from grade 3 glioma. *Tomography*. 2016; 2 (2): 106–16.
- Schupper AJ, Rao M, Mohammadi N, et al. Fluorescence-guided surgery: a review on timing and use in brain tumor surgery. *Front Neurol*. 2021; 12.
- Behbahaninia M, Martirosyan NL, Georges J, et al. Intraoperative fluorescent imaging of intracranial tumors: a review. *Clin Neurol Neurosurg. Elsevier B.V.* 2013; 115 (5): 517–28.
- Pekov SI, Bormotov DS, Nikitin PV, et al. Rapid estimation of tumor cell percentage in brain tissue biopsy samples using inline cartridge extraction mass spectrometry. *Anal Bioanal Chem. Analytical and Bioanalytical Chemistry*. 2021; 413 (11): 2913–22.
- Brown HM, Alfaro CM, Pirro V, et al. Intraoperative mass spectrometry platform for IDH mutation status prediction, glioma diagnosis, and estimation of tumor cell infiltration. *J Appl Lab Med*. 2021; 6 (4): 902–16.
- Eberlin LS, Dill AL, Golby AJ, et al. Discrimination of human astrocytoma subtypes by lipid analysis using desorption electrospray ionization imaging mass spectrometry. *Angew Chemie - Int Ed*. 2010; 49 (34): 5953–6.
- Bormotov D, Shamraeva M, Kuzin A, et al. Ambient ms profiling of meningiomas: intraoperative oncometabolite-based monitoring. *Bull Russ State Med Univ*. 2022; 2022 (6): 74–81.
- King ME, Lin M, Spradlin M, et al. Advances and emerging medical applications of direct mass spectrometry technologies for tissue analysis. *Annu Rev Anal Chem*. 2023; 16: 1–25.
- Eberlin LS, Margulis K, Planell-Mendez I, et al. Pancreatic cancer surgical resection margins: molecular assessment by mass spectrometry imaging. *PLOS Med*. 2016; 13 (8): e1002108.
- Sorokin A, Shurkhay V, Pekov S, et al. Untangling the metabolic reprogramming in brain cancer: discovering key molecular players using mass spectrometry. *Curr Top Med Chem*. 2019; 19 (17): 1521–34.
- Duraj T, García-Romero N, Carrión-Navarro J, et al. Beyond the Warburg effect: oxidative and glycolytic phenotypes coexist within the metabolic heterogeneity of glioblastoma. *Cells*. 2021; 10 (2): 202.
- Pekov SI, Sorokin AA, Kuzin AA, et al. Analysis of phosphatidylcholines alterations in human glioblastomas *ex vivo*. *Biochem Suppl Ser B Biomed Chem* 2021; 15 (3): 241–7.
- McNeill RS, Vitucci M, Wu J, et al. Contemporary murine models in preclinical astrocytoma drug development. *Neuro Oncol*. 2015; 17 (1): 12–28.
- Mason SE, Manoli E, Alexander JL, et al. Lipidomic profiling of colorectal lesions for real-time tissue recognition and risk-stratification using rapid evaporative ionization mass spectrometry. *Ann Surg*. 2023; 277 (3): e569–e577.
- Bormotov DS, Eliferov VA, Peregudova OV, et al. Incorporation of a disposable ESI emitter into inline cartridge extraction mass spectrometry improves throughput and spectra stability. *J Am Soc Mass Spectrom*. 2023; 34 (1): 119–22.
- Ahdesmäki M, Strimmer K. Feature selection in omics prediction problems using cat scores and false nondiscovery rate control. *Ann Appl Stat*. 2010; 4 (1): 503–19.
- Wu X, Geng F, Cheng X, et al. Lipid droplets maintain energy homeostasis and glioblastoma growth via autophagic release of stored fatty acids. *Science. Elsevier Inc.*, 2020; 23 (10): 101569.
- Jaraíz-Rodríguez M, del Prado L, Balsa E. Metabolic remodeling in astrocytes: paving the path to brain tumor development. *Neurobiol Dis*. 2023; 188: 106327.
- Panov A, Orynbayeva Z, Vavilin V, et al. Fatty acids in energy metabolism of the central nervous system. *Biomed Res Int*. 2014; 2014.

Литература

- Kreatsoulas D, Damante M, Gruber M, et al. Supratotal surgical resection for low-grade glioma: a systematic review. *Cancers (Basel)*. 2023; 15 (9): 2493.
- Karschnia P, Vogelbaum MA, van den Bent M, et al. Evidence-based recommendations on categories for extent of resection in diffuse glioma. *Eur J Cancer*. 2021; 149: 23–33.
- Chanbour H, Chotai S. Review of intraoperative adjuncts for maximal safe resection of gliomas and its impact on outcomes.

- Cancers (Basel). 2022; 14: 22.
4. Bogusiewicz J, Bojko B. Insight into new opportunities in intra-surgical diagnostics of brain tumors. *TrAC — Trends Anal Chem.* Elsevier B.V. 2023; 162: 117043.
 5. Cordova JS, Gurbani SS, Olson JJ, et al. A systematic pipeline for the objective comparison of whole-brain spectroscopic MRI with histology in biopsy specimens from grade 3 glioma. *Tomography.* 2016; 2 (2): 106–16.
 6. Schupper AJ, Rao M, Mohammadi N, et al. Fluorescence-guided surgery: a review on timing and use in brain tumor surgery. *Front Neurol.* 2021; 12.
 7. Behbahaniinia M, Martirosyan NL, Georges J, et al. Intraoperative fluorescent imaging of intracranial tumors: a review. *Clin Neurol Neurosurg.* Elsevier B.V. 2013; 115 (5): 517–28.
 8. Pekov SI, Bormotov DS, Nikitin PV, et al. Rapid estimation of tumor cell percentage in brain tissue biopsy samples using inline cartridge extraction mass spectrometry. *Anal Bioanal Chem.* Analytical and Bioanalytical Chemistry. 2021; 413 (11): 2913–22.
 9. Brown HM, Alfaro CM, Pirro V, et al. Intraoperative mass spectrometry platform for IDH mutation status prediction, glioma diagnosis, and estimation of tumor cell infiltration. *J Appl Lab Med.* 2021; 6 (4): 902–16.
 10. Eberlin LS, Dill AL, Golby AJ, et al. Discrimination of human astrocytoma subtypes by lipid analysis using desorption electrospray ionization imaging mass spectrometry. *Angew Chemie - Int Ed.* 2010; 49 (34): 5953–6.
 11. Bormotov D, Shamraeva M, Kuzin A, et al. Ambient ms profiling of meningiomas: intraoperative oncometabolite-based monitoring. *Bull Russ State Med Univ.* 2022; 2022 (6): 74–81.
 12. King ME, Lin M, Spradlin M, et al. Advances and emerging medical applications of direct mass spectrometry technologies for tissue analysis. *Annu Rev Anal Chem.* 2023; 16: 1–25.
 13. Eberlin LS, Margulis K, Planell-Mendez I, et al. Pancreatic cancer surgical resection margins: molecular assessment by mass spectrometry imaging. *PLOS Med.* 2016; 13 (8): e1002108.
 14. Sorokin A, Shurkhay V, Pekov S, et al. Untangling the metabolic reprogramming in brain cancer: discovering key molecular players using mass spectrometry. *Curr Top Med Chem.* 2019; 19 (17): 1521–34.
 15. Duraj T, García-Romero N, Carrión-Navarro J, et al. Beyond the Warburge effect: oxidative and glycolytic phenotypes coexist within the metabolic heterogeneity of glioblastoma. *Cells.* 2021; 10 (2): 202.
 16. Pekov SI, Sorokin AA, Kuzin AA, et al. Analysis of phosphatidylcholines alterations in human glioblastomas ex vivo. *Biochem Suppl Ser B Biomed Chem* 2021; 15 (3): 241–7.
 17. McNeill RS, Vitucci M, Wu J, et al. Contemporary murine models in preclinical astrocytoma drug development. *Neuro Oncol.* 2015; 17 (1): 12–28.
 18. Mason SE, Manoli E, Alexander JL, et al. Lipidomic profiling of colorectal lesions for real-time tissue recognition and risk-stratification using rapid evaporative ionization mass spectrometry. *Ann Surg.* 2023; 277 (3): e569–e577.
 19. Bormotov DS, Eliferov VA, Peregudova OV, et al. Incorporation of a disposable ESI emitter into inline cartridge extraction mass spectrometry improves throughput and spectra stability. *J Am Soc Mass Spectrom.* 2023; 34 (1): 119–22.
 20. Ahdesmäki M, Strimmer K. Feature selection in omics prediction problems using cat scores and false nondiscovery rate control. *Ann Appl Stat.* 2010; 4 (1): 503–19.
 21. Wu X, Geng F, Cheng X, et al. Lipid droplets maintain energy homeostasis and glioblastoma growth via autophagic release of stored fatty acids. *Science.* Elsevier Inc., 2020; 23 (10): 101569.
 22. Jaraíz-Rodríguez M, del Prado L, Balsa E. Metabolic remodeling in astrocytes: paving the path to brain tumor development. *Neurobiol Dis.* 2023; 188: 106327.
 23. Panov A, Orynbayeva Z, Vavilin V, et al. Fatty acids in energy metabolism of the central nervous system. *Biomed Res Int.* 2014; 2014.

EFFECT OF PROBENECID ON ASTROCYTE ACTIVATION *IN VITRO*Babkina II¹, Mazeeva VV², Morozova MP¹, Gorbacheva LR^{1,2}✉¹ Pirogov Russian National Research Medical University, Moscow, Russia² Lomonosov Moscow State University, Moscow, Russia

Both acute brain injuries and neurodegenerative diseases are accompanied by neuroinflammation. The outcome of neuroinflammation and the prognosis of brain functional status depend on the balance of pro-inflammatory and anti-inflammatory factors. Many studies are aimed at finding possible therapeutic targets allowing to shift inflammatory response processes towards anti-inflammatory mechanisms. It has been shown that channels formed by pannexin proteins are expressed in all brain cells including astrocytes. However, their role in the processes of neuroinflammation is still unclear. Channels formed by pannexin 1 (Panx1) may be involved in proinflammatory activation of astrocytes induced by thrombin and/or lipopolysaccharide (LPS). The aim of this study was to assess thrombin- and LPS-induced activation of primary mouse cortical astrocytes under Panx1 blockade by probenecid. Functional profile of astrocytes, their proliferation and secretory activity changed both in case of thrombin application (50 nM and 100 nM) and in case of incubating cells with LPS. The observed increasing of nitric oxide (NO), β -hexosaminidase HEX and IL6 secretion stopped after the cells were treated with probenecid. Based on the obtained results, probenecid can be considered as a potential agent influencing the inflammatory process in brain tissue by stabilizing astrocytes through inactivation of Panx1 and reduction of astrogliosis.

Keywords: neuroinflammation, probenecid, pannexin 1, astrocytes, thrombin, lipopolysaccharide, astrogliosis

Funding: The study was supported by the Russian Science Foundation, Project № 22-25-00848.

Author contribution: Babkina II, Morozova MP — obtaining and maintaining primary culture of astrocytes; collection, interpretation and statistical analysis of data, manuscript writing; Mazeeva VV — obtaining and maintaining primary culture of astrocytes, interpretation and statistical analysis of data; Gorbacheva LR — conception and design of the experiment, interpretation of data, project management, manuscript writing.

Compliance with ethical standards: the study was approved by the Ethical Committee of Pirogov Russian National Research Medical University (Protocol № 23/2021 dated December 13, 2021).

✉ **Correspondence should be addressed:** Lyubov R. Gorbacheva, Ostrovitianova, 1, Moscow, 117997, Russia; gorb67@mail.ru

Received: 13.12.2023 **Accepted:** 24.01.2024 **Published online:** 26.02.2024

DOI: 10.24075/brsmu.2024.005

ВЛИЯНИЕ ПРОБЕНЕЦИДА НА АКТИВАЦИЮ АСТРОЦИТОВ *IN VITRO*И. И. Бабкина¹, В. В. Мазеева², М. П. Морозова¹, Л. Р. Горбачева^{1,2}✉¹ Российский национальный исследовательский медицинский университет имени Н. И. Пирогова, Москва, Россия² Московский государственный университет имени М. В. Ломоносова, Москва, Россия

Нейровоспаление развивается в мозговой ткани как при острых повреждениях мозга, так и при нейродегенеративных заболеваниях. От баланса провоспалительных и противовоспалительных факторов будет зависеть исход нейровоспаления и прогноз функционального состояния мозга. Поэтому целью многих исследований является поиск возможных терапевтических мишеней, позволяющих сдвигать ход воспалительной реакции в пользу реализации противовоспалительных механизмов. Показано, что каналы, образованные белками паннексинами экспрессируются во всех клетках мозга, в том числе и в астроцитах. Однако их роль в процессах нейровоспаления пока не ясна. Каналы, сформированные паннексином 1 (Panx1), могут быть вовлечены в провоспалительную активацию астроцитов, индуцируемую тромбином и/или липополисахаридом (ЛПС). Целью исследования было оценить тромбин- и ЛПС-вызванную активацию первичных кортикальных астроцитов мыши в условиях блокады Panx1 пробенецидом. Установлено, что и в случае аппликации тромбина (50 и 100 нМ), и в случае инкубации клеток с ЛПС, происходит изменение функционального профиля астроцитов, изменяется их пролиферация и секреторная активность. Наблюдаемое при этом увеличение секреции NO, β -гексозаминидазы (БГА) и IL6 прекращалось на фоне обработки клеток пробенецидом. Полученные результаты свидетельствуют о возможности рассматривать пробенецид в качестве потенциального агента, влияющего на воспалительный процесс в мозговой ткани путем стабилизации астроцитов через инактивацию Panx1 и снижение астроглиоза.

Ключевые слова: нейровоспаление, пробенецид, паннексин 1, Panx1, астроциты, тромбин, липополисахарид, астроглиоз

Финансирование: работа поддержана Российским научным фондом, грант 22-25-00848.

Вклад авторов: И. И. Бабкина, М. П. Морозова — получение и ведение первичной культуры астроцитов; сбор, интерпретация и статистическая обработка данных, написание рукописи; В. В. Мазеева — получение и ведение первичной культуры астроцитов, интерпретация и статистическая обработка данных; Л. Р. Горбачева — концепция и дизайн эксперимента, интерпретация данных, руководство проектом, написание рукописи.

Соблюдение этических стандартов: исследование одобрено этическим комитетом РНИМУ имени Н. И. Пирогова (протокол № 23/2021 от 13 декабря 2021 г.).

✉ **Для корреспонденции:** Любовь Руфэлевна Горбачева ул. Островитянова, д. 1, г. Москва, 117997; gorb67@mail.ru

Статья получена: 13.12.2023 **Статья принята к печати:** 24.01.2024 **Опубликована онлайн:** 26.02.2024

DOI: 10.24075/vrgmu.2024.005

Inflammatory response is aimed at removing the damaging agent and restoring the structural and functional integrity of the tissue and can be accompanied by both pathogenetic and adaptive changes. Triggering of an acute inflammatory response in the nervous tissue can activate the processes of neurogenesis, angiogenesis and functional plasticity of neurons. However, the chronic inflammation potentiates further cell alteration and

exacerbates neurodegenerative diseases increasing the risk of complications and disabilities.

Astrocytes are among the most abundant CNS cells involved in neuroinflammation. The level of astrocyte activity largely determines the outcome of neuroinflammation. Activated resident and immunocompetent CNS cells including microglia and astrocytes are the source of proinflammatory factors. As

a result, there is an increase in BBB permeability, infiltration of immune cells into brain tissue, additional alteration, activation of host defense system and thrombin formation.

Development of neurodegenerative processes was shown to be associated with thrombin-dependent enhancement of microglia activation and is mediated by iNOS stimulation, secretion of reactive oxygen species (ROS) and proinflammatory factors COX-2, TNF α , IL1 β , IL6 [1]. In addition, thrombin potentiates astrocyte proliferation through activation of PAR1/MARK cascade.

Neuroinflammation can also be triggered by exogenous factors such as lipopolysaccharides (LPS), a component of bacterial cell wall. The main target of LPS is TLR4 receptor expressed by astrocytes, microglia and endothelium, and its activation triggers the formation of proinflammatory mediators.

The channels formed by pannexin proteins play an important role in the development of the inflammatory response involving astrocytes. The pannexins not only provide transport but also form complexes with other ionic and metabotropic receptors regulating the activity of these receptors [2]. A special role is played by pannexin 1 (Panx1) which is widely present in the CNS and expressed by neurons, astrocytes, microglia, cerebral endothelium and smooth muscle cells [3]. Panx1 contributes to development of neurodegeneration by regulating the release of ATP and other nucleotides from cells, inflammasome assembly and cytokine secretion. Panx1 is thereby a potential target for pharmacotherapy of neurodegenerative diseases and acute brain injuries [4, 5].

Probenecid having a broad spectrum of action including Panx1 inhibition, might be a potential neuroprotective agent. It has been shown that probenecid can specifically activate TRPV2 in sensory neurons and block ATP release from both astrocytes and microglia [5, 6]. Therefore, it can be considered as a promising drug for treatment of neurodegenerative and psychiatric diseases.

The aim of the present study was to evaluate the effect of probenecid, a Panx1 blocker, on thrombin- and LPS-induced proinflammatory activation of mouse astrocytes *in vitro*.

METHODS

Reagents

10 \times HBSS without Ca²⁺ and Mg²⁺ (Gibco; USA), 1M HEPES (Gibco; USA), 10 \times PBS (Gibco; USA), BSA (Sigma; USA), DMEM/F12 cell culture medium (Gibco; USA), inactivated fetal bovine serum HI FBS (Gibco; USA), penicillin-streptomycin (Invitrogen; USA), trypsin-EDTA (Gibco; USA), Versen solution (PanEco; Russia); probenecid (BioQuest; USA); thrombin (Sigma; USA), lipopolysaccharide *Escherichia coli* O111: B4 (L3024; Sigma, USA), Griess reagent (Sigma; USA), Cell Proliferation Reagent WST-1 (Sigma; USA), Mouse IL6 ELISA kit (abcam ab 222503), Triton \times 100 (Sigma; USA), RIPA lysis buffer (Sigma; USA), Complete Protease Inhibitor Cocktail (Roche; USA), Bradford reagent (Bio-Rad; USA).

Obtaining and maintaining primary astrocyte culture

Primary cortical astrocytes were isolated from the cerebral hemispheres obtained from 0 to 3-day-old C57BL/6 mice. Cell cultures were prepared as described in [7]. Brain hemispheres were extracted and placed in buffer (1 \times HBSS, 100 mM sodium pyruvate and 1M HEPES), washed and cut into pieces. The brain homogenate was incubated with 0.5 mg/mL papain (1 \times PBS, L-Cystein-HCl, BSA, glucose, 8 min, 37 °C). The

homogenate was then resuspended in buffer containing DNase (0.01 mg/mL) followed by centrifugation at 1,500 g for 5 min at +4 °C. The resulting precipitate was resuspended in buffer (1 \times HBSS with Ca²⁺ и Mg²⁺, 100 mM sodium pyruvate, 1M HEPES) and recentrifuged. The precipitate was resuspended in 1 ml of culture medium (DMEM/F12, 10% FBS, antibiotic-antimycotic, GlutaMAX). Cells were placed in 25 cm² culture flasks and cultured for 10–12 days at 37 °C and 5% CO₂. Complete medium replacement was performed on day 2 and day 7 by removing microglia, placing flasks with cells in a shaker for 6–8 h, with further medium replacement with a fresh one. Four days before starting the experiment, the cells were removed from the flasks by 0.05% trypsin solution in phosphate buffered saline and placed in 48-well plates. Before experimental exposure, the culture medium was replaced with serum-free medium for 3 h followed by addition of thrombin at a final concentration of 50 nM or 100 nM or LPS at a concentration of 100 ng/mL or 1 μ g/mL. Probenecid 0.1 mM was added 30 min before thrombin or LPS exposure. Measurements were performed 6 h, 24 h, and 48 h following exposure.

Astrocyte survival assessment (WST-1 Assay)

Cell survival was assessed 24 h after astrocyte activation using the WST-1 test according to the manufacturer's protocol. Optical density was measured at $\lambda = 450$ nm using iMarkTM microplate absorbance reader (BioRad; USA). The obtained data were interpreted as cell proliferation, assuming that contribution of cellular hyperplasia under these conditions is not significant, and guided by the manufacturer's information presenting this test as WST-1-proliferative reagent.

Assessment of nitrite accumulation in astrocyte culture medium

Nitric oxide (NO) secretion was assessed by nitrite accumulation in the culture medium 24 h after incubation with inflammatory inducers, using the Griess reagent. The Griess reagent forms colored nitrogen compounds when interacting with nitrite — the absorbance intensity of the compounds was evaluated at 530 nm using iMarkTM microplate absorbance reader (BioRad; USA). The results were presented in relative values as NO secretion by one cell using the ratio of nitrite level in the culture medium to the number of cells in the corresponding well estimated by WST-1 assay.

Assessment of β -hexosaminidase activity

β -Hexosaminidase (HEX) activity was assessed 24 and 48 h after astrocyte activation using the modified method proposed by Schwartz LB et al. [8] in supernatant and intracellularly for subsequent calculation of enzyme secretion as follows:

$$A(A + B) \times 100\%$$

where A is the optical density of the sample reflecting the enzyme activity in the culture medium minus the background optical density; B is the optical density of the sample reflecting the activity of the intracellular pool of enzyme minus the background optical density.

Further, HEX secretion was represented in relative units in relation to control taken as 1.

Assessment of IL6 secretion by astrocytes

IL6 secretion by astrocytes 6 h after exposure was assessed using Mouse IL6 ELISA kit (abcam, Cat. № ab222503)

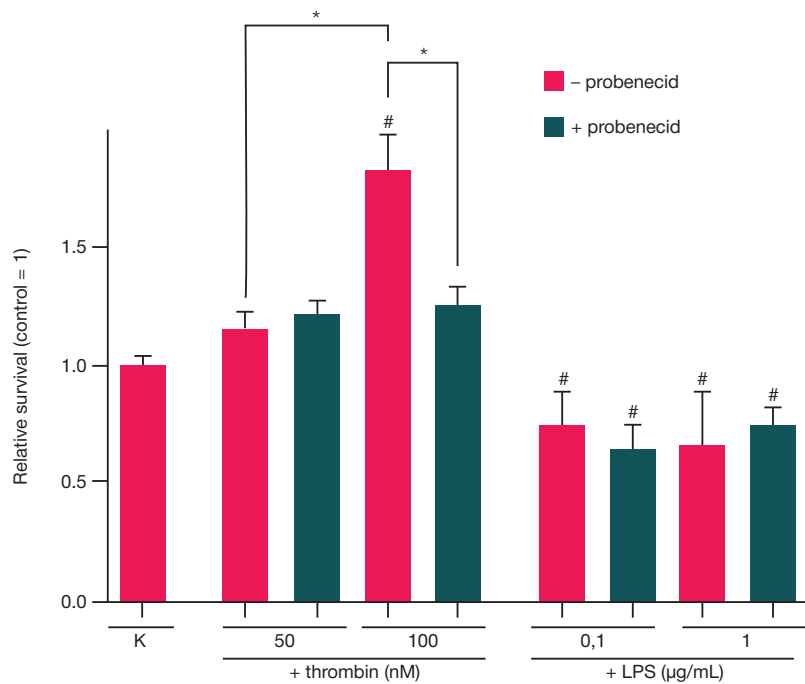


Fig. 1. Effect of Panx1 blockade on survival of thrombin- or LPS-activated astrocytes. * — $p < 0.05$, # — $p < 0.05$ (compared to control); C — control; $n \geq 8$

according to the manufacturer's protocol. The sensitivity limit of IL6 was 30 pg/ml. IL6 content was determined in exposed culture medium samples using the kit. Cells in the wells were washed with phosphate buffered saline and lysed with RIPA buffer with protease inhibitors. Lysates were centrifuged at 14,000g for 15 min at 4 °C, after that total protein content was measured in the supernatant using the Bradford kit. IL6 secretion was represented in pg/mg of total protein.

Statistical Analysis

Statistical analysis was performed using GraphPad Prism 8 (GraphPad Software Inc.; USA). Normality of sample distribution was assessed using the Shapiro-Wilk test. To compare

groups, two-factor ANOVA of variance followed by a posteriori analysis using Tukey's criterion was applied. Data were presented as arithmetic mean \pm standard error (SEM), differences were considered statistically significant (*, #) at $p < 0.05$. The number of experiments (n , number of astrocytes plantings) was indicated in each case separately.

RESULTS

Effect of probenecid on the survival of thrombin- and LPS-activated astrocytes

Thrombin is involved in the inflammatory response since the hemostasis system in the first place reacts to tissue damage. In

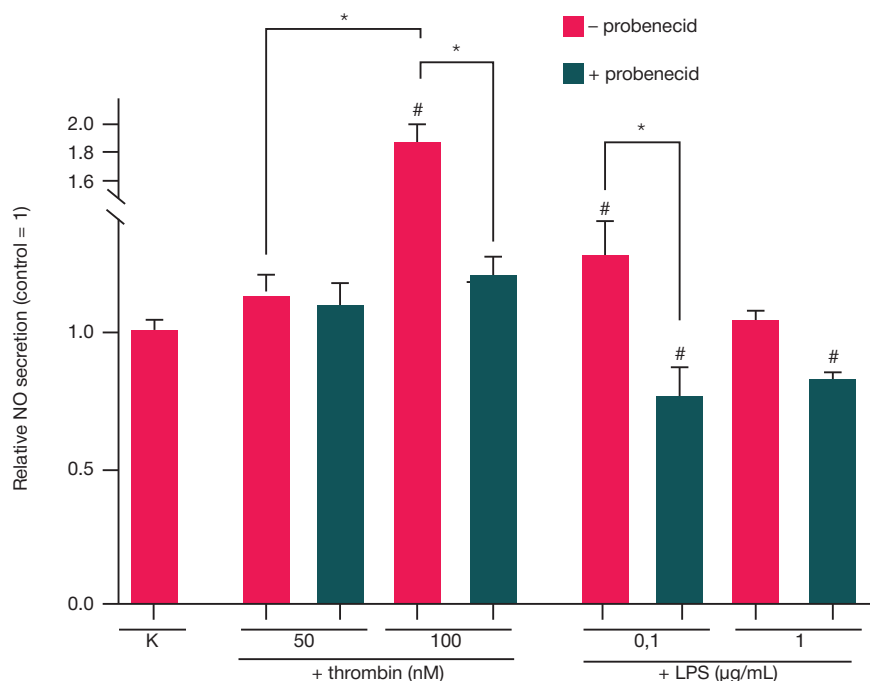


Fig. 2. Effect of blockade of Panx1 channels by probenecid on NO secretion by astrocytes during their incubation with thrombin/LPS. C — control; * — $p < 0.05$ and # — $p < 0.05$ (compared to control), $n \geq 6$

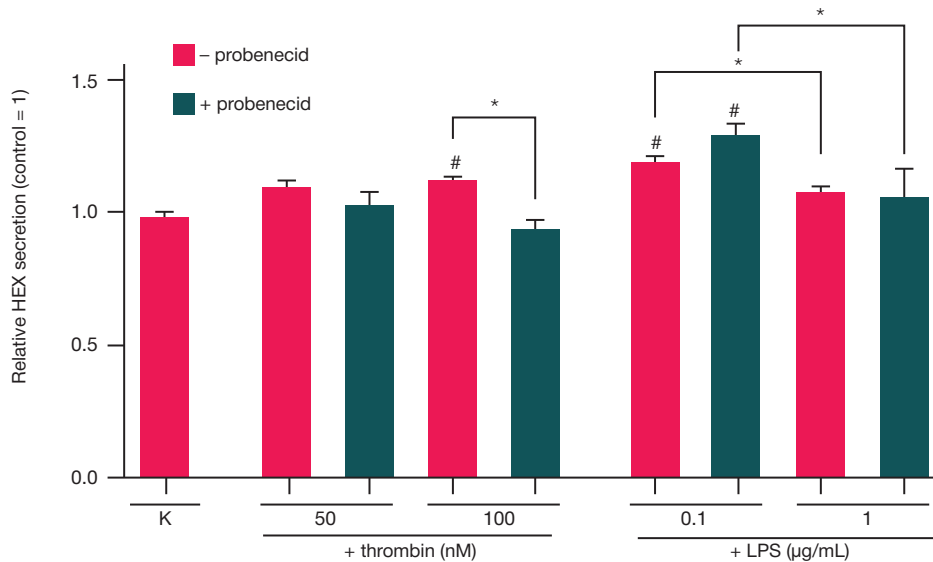


Fig. 3. Effect of Panx1 blockade on thrombin/LPS-induced HEX secretion by mouse astrocytes. HEX secretion was assessed 24 h after thrombin/LPS exposure. C — control; * — $p < 0.05$, # — $p < 0.05$ (compared with control), $n \geq 6$

the first series of experiments, neuroinflammation was modeled by adding thrombin to the culture medium of mouse astrocytes. It was demonstrated that thrombin at a concentration of 100 nM significantly ($p < 0.05$) increased the number of living astrocytes, while treatment of cells with probenecid reduced this index to control values which may indicate the participation of Panx1 channels in thrombin-induced astrocyte proliferation (Fig. 1). In contrast to thrombin, LPS caused a decrease in survival under the same conditions at all concentrations used, which may indicate its toxic effect on astrocytes (Fig. 1). Probenecid did not alter the effect of LPS (Fig. 1).

Effect of probenecid on NO secretion by activated astrocytes

Increased NO production is a sign of neuroinflammation. In this study, it was observed that 24 hours after application of 100 nM thrombin (not 50 nM), there was a significant accumulation of

nitrites in the culture medium of astrocytes while probenecid stopped thrombin-induced NO secretion, indicating the Panx1 involvement in this process (Fig. 2). In case of 24-hour incubation of cells with LPS, the most significant increase in NO secretion was observed at 0.1 µg/mL LPS concentration which was terminated using Panx1 blockade. In case of 1 µg/mL LPS concentration, NO secretion did not differ from control values and did not depend on Panx1 (Fig. 2).

Effect of probenecid on β -hexosaminidase secretion by activated astrocytes

Release of the lysosomal enzyme β -hexosaminidase (HEX) from cells may also be considered as a marker of proinflammatory activation of astrocytes.

The effect of probenecid on HEX secretion by astrocytes was assessed 24 and 48 h after their activation by thrombin (concentrations 50 nM and 100 nM) and LPS (concentrations

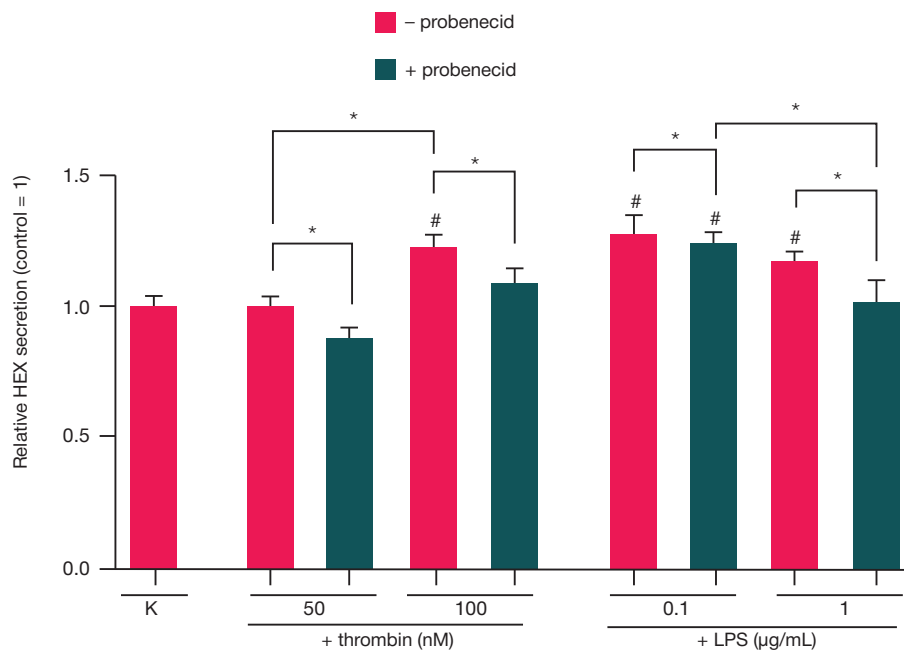


Fig. 4. Effect of Panx1 blockade on thrombin/LPS-induced HEX secretion by mouse astrocytes. HEX secretion was assessed 48 h after thrombin/LPS exposure. C — control; * — $p < 0.05$, # — $p < 0.05$ (compared to control), $n \geq 6$

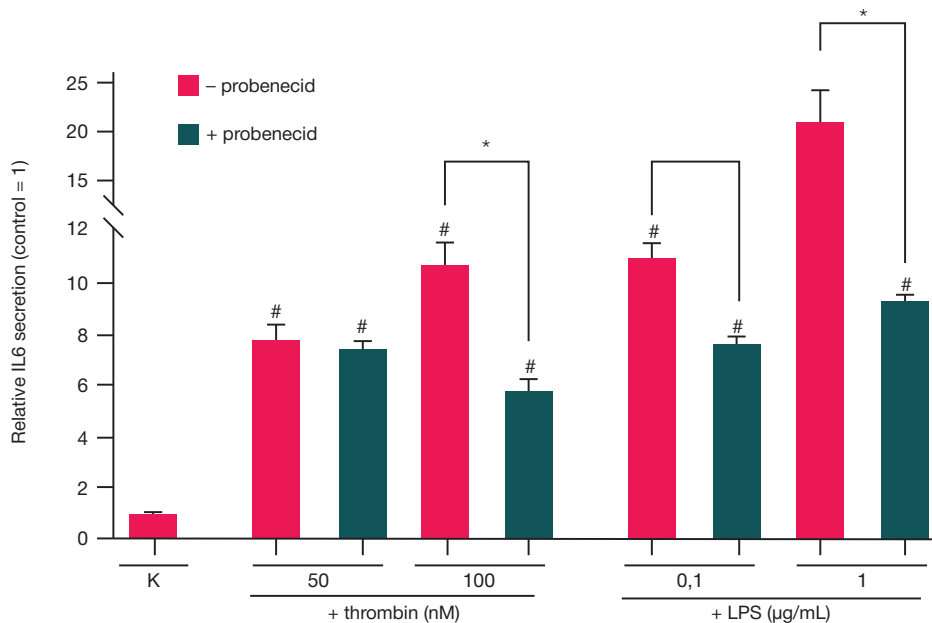


Fig. 5. Effect of Panx1 blockade on IL6 secretion by mouse astrocytes exposed to thrombin/LPS for 6 hours. C — control; * $p < 0.05$, # $p < 0.05$ (compared to control), $n \geq 3$

0.1 $\mu\text{g/mL}$ and 1 $\mu\text{g/mL}$). After 24 h we observed the proinflammatory effect of thrombin at the concentration of 100 nM and the involvement of Panx1 in the realization of this effect since its blockade by probenecid significantly reduced HEX secretion (Fig. 3). Application of 0.1 $\mu\text{g/mL}$ LPS caused cell activation after 24 h, in contrast to the effect of 1 $\mu\text{g/mL}$ LPS (Fig. 3). In both cases, blockade of Panx1 channels by probenecid did not change the effect of endotoxin (Fig. 3).

The increase of thrombin exposure time from 24 to 48 h resulted in a more significant increase in HEX secretion by astrocytes and was mediated by Panx1 since this index decreases to control values when probenecid was applied (Fig. 4). HEX secretion on the background of LPS, similarly to thrombin, was higher 48 h after exposure. At the same time, the anti-inflammatory effect of probenecid was manifested only against LPS at a concentration of 1 $\mu\text{g/mL}$ — HEX secretion decreases to control level (Fig. 4).

Effect of probenecid on IL6 secretion by activated astrocytes

Astrocyte activation is associated with the secretion of proinflammatory cytokines, particularly IL6. High concentrations of thrombin and LPS increased the levels of IL6 secretion 6 h after induction. Effect of LPS was 2-fold more significant compared with the effect of thrombin ($p < 0.05$). Thus, LPS appeared to be a more specific proinflammatory agent. Probenecid in both cases had an anti-inflammatory effect and stopped the proinflammatory activation of astrocytes caused by both thrombin and LPS, significantly reducing the level of IL6 secretion (Fig. 5) and indicating the involvement of Panx1 in secretory function of reactive astrocytes.

DISCUSSION

Chronic neuroinflammation is a pathogenetic factor that triggers neurodegeneration processes and increases the risk of irreversible CNS damage. Astrocytes, the most abundant brain cells contributing to neuron-glia interaction, may be involved in regulating neuroinflammation. Proinflammatory activation of astrocytes is associated with an increase in their proliferative

and secretory activity and may be accompanied by opening of Panx1 channels [9].

Releasing ATP from cells including ATP release through Panx1 channels is a signal for a variety of processes starting from migration, proliferation and growth in physiological conditions to triggering neuroinflammation and neurodegeneration in pathological conditions. ATP effects are realized through purinergic receptors — ligand-gated ion channels (P2X) and G protein-coupled metabotropic receptors (P2Y). P2X7 receptors play an important role in triggering neuroinflammation. Panx1 blockade by probenecid can limit ATP release from cells and — mediately — purinergic signaling [6]. However, probenecid was also reported to be able to block P2X7 receptors directly [10].

Interestingly, Panx1 co-expressed with P2Y1 and P2Y2 receptors via PLC-cascade caused an increase in intracellular Ca^{2+} levels which enhanced Panx1 activation [11]. Calcium-induced activation of Panx1 supposedly occurred through CaMKII phosphorylation, Panx1 opening and ATP release [12].

In brain ischemia and excitotoxicity, NMDAR overactivation occurs which activates Panx1 and triggers proapoptotic signaling pathways [13]. Panx1 activation initiates the assembly of inflammasomes, multimeric protein complexes in the cytosol of all cells that control the inflammatory response. Inflammasome activation provides an active form of pro-inflammatory caspase-1 cleaving pro-IL1 β and pro-IL18 to form mature cytokines IL1 β and IL18 [3, 6]. Pyroptosis, a pro-inflammatory form of cell death accompanied by release of pro-inflammatory signals, is also caspase-1-dependent. ATP release, e.g. via Panx1, into the environment and subsequent activation of P2X7R also results in activation of inflammatory processes, inflammasome assembly and IL1 β production [6].

In a neuron-astrocyte co-culture system, ATP and glutamate released from astrocytes treated with conditioned medium from activated microglia, were shown to cause neuronal death through activation of Panx1 neurons [14]. Panx1 regulated the release of ATP and other nucleotides, inflammasome assembly and cytokine secretion, which may determine its contribution to neurodegeneration. Panx1 is therefore a potential target for pharmacotherapy of neurodegenerative diseases and acute brain injuries. Possible conjugation of PAR1 with Panx1 channels was described in [15].

In this study, we demonstrated that quantity of astrocytes increased under the action of thrombin (Fig. 1). Such effect may be associated with thrombin/PAR1-mediated phosphorylation of ERK1/2 or activation of PLC ϵ , which in turn regulates MAPK/NF κ B-intracellular cascade [16]. This effect may also be associated with triggering thrombin/PAR1-dependent IL6 secretion by astrocytes and further signaling through the IL6/STAT3 pathway, development of astrogliosis including increased levels of glial fibrillary acidic protein (GFAP) and vimentin. In the present study, probenecid was shown to inhibit the thrombin-mediated increase in the number of astrocytes and to return this index to control values indicating that Panx1-channels may be involved in this process. This is consistent with the data obtained for lung epithelial cells and human endothelialocytes where thrombin-dependent activation of Panx1 channels was demonstrated [15, 17]. However, the mechanisms of such cooperation are still unknown.

LPS proinflammatory factor is widely used to model the inflammatory response. LPS-induced proinflammatory activation is known to be mediated by TLR4. TLR4 triggers activation of a complex of factors including NF- κ B through MyD88-IRAK-TRAF6-TAK1 signaling complex [18]. As a result, astrocyte proliferation may be altered and pro-inflammatory cytokines may be expressed through MAPK/NF- κ B activation [19]. In addition, it was shown that the Akt/ERK/JNK cascade may be involved in LPS-mediated inflammation since its blockade decreased the secretion of proinflammatory cytokines [20]. Some data is available on LPS/TLR4-dependent increase in the level of mouse astrocyte proliferation.

In the present study, LPS was shown to reduce cell survival but activate the secretion of primary cultured mouse cortical astrocytes. LPS-induced activation of astrocytes expectedly resulted in a persistent increase in secretion of the proinflammatory interleukin IL6 (Fig. 5) and, to a less extent, NO and HEX (Figs. 3, 4). Remarkably, blockade of Panx1 channels by probenecid significantly reduced LPS-induced proinflammatory secretion of astrocytes.

Proinflammatory activation of astrocytes is accompanied by an increase in production of many chemokines and cytokines

as well as activation of inducible NO synthase (iNOS) and NO secretion [21, 22]. Increased NO levels are shown to accompany many neurodegenerative diseases such as Alzheimer's and Parkinson's diseases and can also contribute to formation of reactive nitrogen species having cytotoxic effect on neurons [23, 24]. In astrocytes, both endogenous and exogenous proinflammatory factors can act as inducers of NO production [21, 24]. We have observed an increase in NO secretion by primary mouse astrocytes under the action of thrombin and LPS (Fig. 3). PAR1-mediated NO secretion and iNOS activation were previously demonstrated on astrocytoma cells [25]. The observed thrombin-induced NO production by cultured astrocytes reduced under Panx1 blockade with probenecid (Fig. 3). This may be an evidence of possible interaction between thrombin receptor PAR1 and Panx1. Activation of Panx1 channels can be induced by high concentration of intracellular Ca²⁺ which, in turn, can be a consequence of the thrombin/PAR1/Gq/RCS/IP3 signaling pathway activation [4]. Panx1-dependent ATP release via P2X7 enhances thrombin-induced increase of intracellular calcium [26] and activation of nNOS and eNOS in astrocytes.

We have demonstrated that LPS-stimulated NO secretion by astrocytes as well as thrombin-induced NO secretion stopped in the presence of probenecid (Fig. 2). Panx1-dependent effects of LPS on HK-2 cells were described in other investigations. In particular, under Panx1 inhibition, LPS-induced inflammation was alleviated with inhibition of NLRP3 and decreased expression of Bax and Bcl2 [27].

Level of activation of immunocompetent cells (macrophages, mast cells) can be estimated based on HEX secretion level. In our study, we used substrate-enzyme reaction to evaluate the activity of HEX in astrocyte cultivation medium in 24 h and 48 h after thrombin and LPS application. Both in case of thrombin and LPS, the increase in HEX secretion was more significant after 48 hours that can probably be explained by delayed activation of astrocytes on the principle of positive feedback. These results are consistent with the data on thrombin-dependent increase in HEX secretion in thrombocytes and

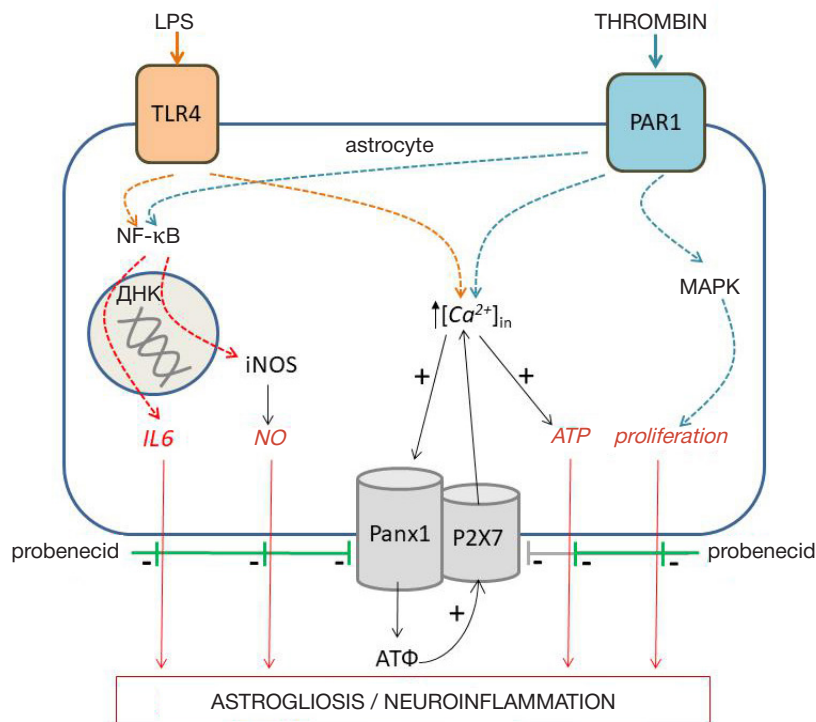


Fig. 6. Effect of probenecid on thrombin/LPS-induced activation of astrocytes

most cells demonstrating the involvement of P2X7 receptors in activating degranulation [28].

Proinflammatory cytokine IL6 is one of the specific markers of inflammation. Analysis of IL6 level in the astrocyte cultures confirmed the proinflammatory effect of both thrombin and, to a greater extent, LPS (Fig. 5). Similar proinflammatory effect of thrombin was previously observed for astrocytes [29]. This protease effect is attributed to thrombin/PAR1-dependent activation of G12/13 protein triggering the RhoGEF/RhoA/phospholipase C ϵ — DAG and PKC — PKD cascade, culminating in increased expression of IL6, COX-2 and other proinflammatory genes [30]. Clear proinflammatory effect of LPS on astrocytes with induction of IL6 secretion was also demonstrated by other researchers [31]. In the present study, we have shown for the first time a probenecid-dependent decrease in thrombin- and LPS-induced IL6 production for primary astrocyte cultures (Fig. 6). Probenecid-induced inhibition of TNF α , IL6, IL1 β and IL8 expression including in the presence of LPS was observed by Z. Zhang et al. on hippocampal cells in sepsis, and by L. Wei et al. on U87-MG cells [19, 32]. At the same time, the results of some other investigations do not confirm the participation of Panx1 and potential heterodimers P2X4/P2X7 in P2X7-dependent release of IL6, CCL2 and TNF α in microglia [33].

We investigated the effects of probenecid having a broad spectrum of activity as a potential neuroprotective agent. Owing to its high lipid solubility, probenecid freely penetrates to the BBB. It is able to interact with TRPV2 membrane protein channels and organic anion transporters (OAT1-3) and cation transporters (OST1-3) as well as Panx1 channels which indicates its potential therapeutic use, e.g. as an adjuvant to increase the bioavailability of some drugs in the CNS. Using probenecid as a blocker of Panx1 channels seems to be promising to suppress neuroinflammation, a neurodegenerative component of many CNS diseases [6]. With a great number of Panx1 activating stimuli and functionally diverse effects, probenecid exhibits dual

activities — on the one hand, it may trigger anti-inflammatory effects by inhibiting inflammasome activation while on the other hand, reduced glial-neuronal interaction and plasticity increases the risk of additional tissue damage. Decreased levels of AQP4, NLRP3 and caspase-1 expression in astrocyte culture under oxygen-glucose deprivation evidences about anti-inflammatory and neuroprotective effect of probenecid [34]. Probenecid increased astrocyte survival by reducing ROS production and suppressing the expression of NLRP3, caspase-1, and IL1 β [6].

Thus, using Panx1 inhibitor probenecid as an anti-inflammatory agent (Fig. 6) may be considered for developing new approaches for effective control of neuroinflammation, one of the important factors potentiating brain damage in trauma and neurodegenerative diseases [35, 36].

CONCLUSIONS

Proinflammatory activation of mouse astrocytes by application of thrombin (50 nM, 100 nM) and lipopolysaccharide (0.1 μ g/mL, 1 μ g/mL) changed their functional profile as well as cell proliferation and secretory activity. LPS induced a significant increase in secretion of IL6 while thrombin had a more significant effect on NO production and astrocyte proliferation. The induced production of NO, HEX and IL6 was observed to be terminated by the Panx1 channel blocker probenecid. Remarkably, probenecid abolished the effect of thrombin on astrocyte proliferation but not the effect of LPS. Inhibition of IL6 and HEX secretion by probenecid also differed in case of LPS as compared with thrombin. The obtained results indicate the possible involvement of Panx1 channels in thrombin- and lipopolysaccharide-induced proinflammatory activation of astrocytes and induction of astrogliosis. Identifying mechanisms and key participants of the signalling cascade triggered in thrombin- and LPS-induced neuroinflammation under pretreatment of cell cultures with probenecid is subject to further investigation.

References

- Choi SH, Da YL, Seung UK, Byung KJ. Thrombin-induced oxidative stress contributes to the death of hippocampal neurons in vivo: Role of microglial NADPH oxidase. *Journal of Neuroscience*. 2005; 25: 4082–90.
- D'hondt C, Ponsaerts R, De Smedt H, Vinken M, De Vuyst E, De Bock M, et al. Pannexin channels in ATP release and beyond: An unexpected rendezvous at the endoplasmic reticulum. *Cellular Signalling*. 2011; 23: 305–16.
- Koval M, Cwiek A, Carr T, Good ME, Lohman AW, Isakson BE. Pannexin 1 as a driver of inflammation and ischemia-reperfusion injury. *Purinergic Signalling*. 2021; 17: 521–31.
- Galkov MD, Surin AM, Lisina OYu, Gorbacheva LR. Neurodegeneration and Neuroinflammation: The Role of Pannexin 1. *Neurochemical Journal*. 2023; 17: 727–39.
- Rusiecka OM, Tournier M, Molica F, Kwak BR. Pannexin1 channels — a potential therapeutic target in inflammation. *Front Cell Dev Biol*. 2022; 10: 1020826.
- García-Rodríguez C, Mujica P, Illanes-González J, López A, Vargas C, Sáez JC, et al. Probenecid, an Old Drug with Potential New Uses for Central Nervous System Disorders and Neuroinflammation. *Biomedicines*. 2023; 11.
- Ivanova AE, Gorbacheva LR, Strukova SM, Pinelic VG, Rajzer G. Uchastie aktivirovannogo proteina S i trombina v reguljacii funkcij astrocitov. *Biol membrany*. 2013; 30: 387–97.
- Schwartz LB, Austen KF, Wasserman SI. Immunologic Release of β -Hexosaminidase and β -Glucuronidase from Purified Rat Serosal Mast Cells. *The Journal of Immunology*. 1979; 123: 1445–50.
- Penuela S, Gehi R, Laird DW. The biochemistry and function of pannexin channels. *Biochimica et Biophysica Acta — Biomembranes*. 2013; 1828: 15–22.
- Bhaskaracharya A, Dao-Ung P, Jalilian I, Spildrejorde M, Skarratt KK, Fuller SJ, et al. Probenecid Blocks Human P2X7 Receptor-Induced Dye Uptake via a Pannexin-1 Independent Mechanism. *PLoS ONE*. 2014; 9: e93058.
- Locovei S, Wang J, Dahl G. Activation of pannexin 1 channels by ATP through P2Y receptors and by cytoplasmic calcium. *FEBS Letters*. 2006; 580: 239–44.
- Yang K, Xiao Z, He X, Weng R, Zhao X, Sun T. Mechanisms of Pannexin 1 (PANX1) Channel Mechanosensitivity and Its Pathological Roles. *International Journal of Molecular Sciences*. 2022; 23.
- Szydłowska K, Tymianski M. Calcium, ischemia and excitotoxicity. *Cell Calcium*. 2010; 47: 122–9.
- Orellana JA, Froger N, Ezan P, Jiang JX, Bennett MVL, Naus CC, et al. ATP and glutamate released via astroglial connexin 43 hemichannels mediate neuronal death through activation of pannexin 1 hemichannels. *Journal of Neurochemistry*. 2011; 118: 826–40.
- Gödecke S, Roderigo C, Rose CR, Rauch BH, Gödecke A, Schrader J. Thrombin-induced ATP release from human umbilical vein endothelial cells. *Am J Physiol Cell Physiol*. 2012; 302: 915–23.
- Chen X, Zhang H, Hao H, Zhang X, Song H, He B, et al. Thrombin induces morphological and inflammatory astrocytic responses via activation of PAR1 receptor. *Cell Death Discovery*. 2022; 8.
- Seminario-Vidal L, Kreda S, Jones L, O'Neal W, Trejo JA, Boucher

- RC, et al. Thrombin promotes release of ATP from lung epithelial cells through coordinated activation of Rho- and Ca²⁺-dependent signaling pathways. *Journal of Biological Chemistry*. 2009; 284: 20638–48.
18. Fiebich BL, Batista CRA, Saliba SW, Yousif NM, de Oliveira ACP. Role of microglia TLRs in neurodegeneration. *Frontiers in Cellular Neuroscience*. 2018; 12.
 19. Zhang Z, Lei Y, Yan C, Mei X, Jiang T, Ma Z, et al. Probenecid Relieves Cerebral Dysfunction of Sepsis by Inhibiting Pannexin 1-Dependent ATP Release. *Inflammation*. 2019; 42: 1082–92.
 20. Yu D-K, Lee B, Kwon M, Yoon N, Shin T, Kim N-G, et al. Phlorofucofuroeckol B suppresses inflammatory responses by down-regulating nuclear factor κ B activation via Akt, ERK, and JNK in LPS-stimulated microglial cells. *International Immunopharmacology*. 2015; 28: 1068–75.
 21. Kozuka N, Itofusa R, Kudo Y, Morita M. Lipopolysaccharide and proinflammatory cytokines require different astrocyte states to induce nitric oxide production. *J of Neuroscience Research*. 2005; 82: 717–28.
 22. Chen Q, Liang Z, Yue Q, Wang X, Siu SWI, Pui-Man Hoi M, et al. A Neuropeptide Y/F-like Polypeptide Derived from the Transcriptome of *Turbinaria peltata* Suppresses LPS-Induced Astrocytic Inflammation. *J Nat Prod*. 2022; 85: 1569–80.
 23. Liu B, Gao H-M, Wang J-Y, Jeohn G-H, Cooper CL, Hong J-S. Role of nitric oxide in inflammation-mediated neurodegeneration. *Ann N Y Acad Sci*. 2002; 962: 318–31.
 24. Li T, Xu T, Zhao J, Gao H, Xie W. Depletion of iNOS-positive inflammatory cells decelerates neuronal degeneration and alleviates cerebral ischemic damage by suppressing the inflammatory response. *Free Radic Biol Med*. 2022; 181: 209–20.
 25. Boven LA, Vergnolle N, Henry SD, Silva C, Imai Y, Holden J, et al. Up-Regulation of Proteinase-Activated Receptor 1 Expression in Astrocytes During HIV Encephalitis. *The Journal of Immunology*. 2003; 170: 2638–46.
 26. Isakson BE, Thompson RJ. Pannexin-1 as a potentiator of ligand-gated receptor signaling. *Channels*. 2014; 8: 118–23.
 27. Huang G, Bao J, Shao X, Zhou W, Wu B, Ni Z, et al. Inhibiting pannexin-1 alleviates sepsis-induced acute kidney injury via decreasing NLRP3 inflammasome activation and cell apoptosis. *Life Sciences*. 2020; 254.
 28. Wareham KJ, Seward EP. P2X7 receptors induce degranulation in human mast cells. *Purinergic Signalling*. 2016; 12: 235–46.
 29. Ponath G, Park C, Pitt D. The role of astrocytes in multiple sclerosis. *Frontiers in Immunology*. 2018; 9.
 30. Okada S, Nakamura M, Mikami Y, Shimazaki T, Mihara M, Ohsugi Y, et al. Blockade of interleukin-6 receptor suppresses reactive astrogliosis and ameliorates functional recovery in experimental spinal cord injury. *Journal of Neuroscience Research*. 2004; 76 (2): 265–76.
 31. Krasovska V, Doering LC. Regulation of IL6 secretion by astrocytes via TLR4 in the fragile X mouse model. *Frontiers in Molecular Neuroscience*. 2018; 11: 272.
 32. Wei L, Sheng H, Chen L, Hao B, Shi X, Chen Y. Effect of pannexin-1 on the release of glutamate and cytokines in astrocytes. *Journal of Clinical Neuroscience*. 2016; 23: 135–41.
 33. Shieh CH, Heinrich A, Serchov T, van Calker D, Biber K. P2X7-dependent, but differentially regulated release of IL6, CCL2, and TNF- α in cultured mouse microglia. *GLIA*. 2014; 62: 592–607.
 34. Jian Z, Ding S, Deng H, Wang J, Yi W, Wang L, et al. Probenecid protects against oxygen–glucose deprivation injury in primary astrocytes by regulating inflammasome activity. *Brain Research*. 2016; 1643: 123–9.
 35. Hainz N, Wolf S, Tschernig T, Meier C. Probenecid Application Prevents Clinical Symptoms and Inflammation in Experimental Autoimmune Encephalomyelitis. *Inflammation*. 2016; 39: 123–8.
 36. Wang Q, Li H, Ling Z, Chen G, Wei Z-Y. Inhibition of Schwann cell pannexin 1 attenuates neuropathic pain through the suppression of inflammatory responses. *J Neuroinflammation*. 2022; 19: 244.

Литература

1. Choi SH, Da YL, Seung UK, Byung KJ. Thrombin-induced oxidative stress contributes to the death of hippocampal neurons in vivo: Role of microglial NADPH oxidase. *Journal of Neuroscience*. 2005; 25: 4082–90.
2. D'hondt C, Ponsaerts R, De Smedt H, Vinken M, De Vuyst E, De Bock M, et al. Pannexin channels in ATP release and beyond: An unexpected rendezvous at the endoplasmic reticulum. *Cellular Signalling*. 2011; 23: 305–16.
3. Koval M, Cwiek A, Carr T, Good ME, Lohman AW, Isakson BE. Pannexin 1 as a driver of inflammation and ischemia–reperfusion injury. *Purinergic Signalling*. 2021; 17: 521–31.
4. Galkov MD, Surin AM, Lisina OYu, Gorbacheva LR. Neurodegeneration and Neuroinflammation: The Role of Pannexin 1. *Neurochemical Journal*. 2023; 17: 727–39.
5. Rusiecka OM, Tournier M, Molica F, Kwak BR. Pannexin1 channels — a potential therapeutic target in inflammation. *Front Cell Dev Biol*. 2022; 10: 1020826.
6. García-Rodríguez C, Mujica P, Illanes-González J, López A, Vargas C, Sáez JC, et al. Probenecid, an Old Drug with Potential New Uses for Central Nervous System Disorders and Neuroinflammation. *Biomedicines*. 2023; 11.
7. Иванова А. Е., Горбачева Л. Р., Струкова С. М., Пинелис В. Г., Райзер Г. Участие активированного протеина С и тромбина в регуляции функций астроцитов. *Биол мембраны*. 2013; 30: 387–97.
8. Schwartz LB, Austen KF, Wasserman SI. Immunologic Release of β -Hexosaminidase and β -Glucuronidase from Purified Rat Serosal Mast Cells. *The Journal of Immunology*. 1979; 123: 1445–50.
9. Penuela S, Gehi R, Laird DW. The biochemistry and function of pannexin channels. *Biochimica et Biophysica Acta — Biomembranes*. 2013; 1828: 15–22.
10. Bhaskaracharya A, Dao-Ung P, Jalilian I, Spildrejrde M, Skarratt KK, Fuller SJ, et al. Probenecid Blocks Human P2X7 Receptor-Induced Dye Uptake via a Pannexin-1 Independent Mechanism. *PLoS ONE*. 2014; 9: e93058.
11. Locovei S, Wang J, Dahl G. Activation of pannexin 1 channels by ATP through P2Y receptors and by cytoplasmic calcium. *FEBS Letters*. 2006; 580: 239–44.
12. Yang K, Xiao Z, He X, Weng R, Zhao X, Sun T. Mechanisms of Pannexin 1 (PANX1) Channel Mechanosensitivity and Its Pathological Roles. *International Journal of Molecular Sciences*. 2022; 23.
13. Szydłowska K, Tymianski M. Calcium, ischemia and excitotoxicity. *Cell Calcium*. 2010; 47: 122–9.
14. Orellana JA, Froger N, Ezan P, Jiang JX, Bennett MVL, Naus CC, et al. ATP and glutamate released via astroglial connexin 43 hemichannels mediate neuronal death through activation of pannexin 1 hemichannels. *Journal of Neurochemistry*. 2011; 118: 826–40.
15. Gödecke S, Roderigo C, Rose CR, Rauch BH, Gödecke A, Schrader J. Thrombin-induced ATP release from human umbilical vein endothelial cells. *Am J Physiol Cell Physiol*. 2012; 302: 915–23.
16. Chen X, Zhang H, Hao H, Zhang X, Song H, He B, et al. Thrombin induces morphological and inflammatory astrocytic responses via activation of PAR1 receptor. *Cell Death Discovery*. 2022; 8.
17. Seminario-Vidal L, Kreda S, Jones L, O'Neal W, Trejo JA, Boucher RC, et al. Thrombin promotes release of ATP from lung epithelial cells through coordinated activation of Rho- and Ca²⁺-dependent signaling pathways. *Journal of Biological Chemistry*. 2009; 284: 20638–48.
18. Fiebich BL, Batista CRA, Saliba SW, Yousif NM, de Oliveira ACP. Role of microglia TLRs in neurodegeneration. *Frontiers in Cellular Neuroscience*. 2018; 12.
19. Zhang Z, Lei Y, Yan C, Mei X, Jiang T, Ma Z, et al. Probenecid Relieves Cerebral Dysfunction of Sepsis by Inhibiting Pannexin 1-Dependent ATP Release. *Inflammation*. 2019; 42: 1082–92.
20. Yu D-K, Lee B, Kwon M, Yoon N, Shin T, Kim N-G, et al. Phlorofucofuroeckol B suppresses inflammatory responses by down-regulating nuclear factor κ B activation via Akt, ERK, and JNK in LPS-stimulated microglial cells. *International*

- Immunopharmacology. 2015; 28: 1068–75.
21. Kozuka N, Itofusa R, Kudo Y, Morita M. Lipopolysaccharide and proinflammatory cytokines require different astrocyte states to induce nitric oxide production. *J of Neuroscience Research*. 2005; 82: 717–28.
 22. Chen Q, Liang Z, Yue Q, Wang X, Siu SWI, Pui-Man Hoi M, et al. A Neuropeptide Y/F-like Polypeptide Derived from the Transcriptome of *Turbinaria peltata* Suppresses LPS-Induced Astrocytic Inflammation. *J Nat Prod*. 2022; 85: 1569–80.
 23. Liu B, Gao H-M, Wang J-Y, Jeohn G-H, Cooper CL, Hong J-S. Role of nitric oxide in inflammation-mediated neurodegeneration. *Ann N Y Acad Sci*. 2002; 962: 318–31.
 24. Li T, Xu T, Zhao J, Gao H, Xie W. Depletion of iNOS-positive inflammatory cells decelerates neuronal degeneration and alleviates cerebral ischemic damage by suppressing the inflammatory response. *Free Radic Biol Med*. 2022; 181: 209–20.
 25. Boven LA, Vergnolle N, Henry SD, Silva C, Imai Y, Holden J, et al. Up-Regulation of Proteinase-Activated Receptor 1 Expression in Astrocytes During HIV Encephalitis. *The Journal of Immunology*. 2003; 170: 2638–46.
 26. Isakson BE, Thompson RJ. Pannexin-1 as a potentiator of ligand-gated receptor signaling. *Channels*. 2014; 8: 118–23.
 27. Huang G, Bao J, Shao X, Zhou W, Wu B, Ni Z, et al. Inhibiting pannexin-1 alleviates sepsis-induced acute kidney injury via decreasing NLRP3 inflammasome activation and cell apoptosis. *Life Sciences*. 2020; 254.
 28. Wareham KJ, Seward EP. P2X7 receptors induce degranulation in human mast cells. *Purinergic Signalling*. 2016; 12: 235–46.
 29. Ponath G, Park C, Pitt D. The role of astrocytes in multiple sclerosis. *Frontiers in Immunology*. 2018; 9.
 30. Okada S, Nakamura M, Mikami Y, Shimazaki T, Mihara M, Ohsugi Y, et al. Blockade of interleukin-6 receptor suppresses reactive astrogliosis and ameliorates functional recovery in experimental spinal cord injury. *Journal of Neuroscience Research*. 2004; 76 (2): 265–76.
 31. Krasovska V, Doering LC. Regulation of IL6 secretion by astrocytes via TLR4 in the fragile X mouse model. *Frontiers in Molecular Neuroscience*. 2018; 11: 272.
 32. Wei L, Sheng H, Chen L, Hao B, Shi X, Chen Y. Effect of pannexin-1 on the release of glutamate and cytokines in astrocytes. *Journal of Clinical Neuroscience*. 2016; 23: 135–41.
 33. Shieh CH, Heinrich A, Serchov T, van Calker D, Biber K. P2X7-dependent, but differentially regulated release of IL6, CCL2, and TNF- α in cultured mouse microglia. *GLIA*. 2014; 62: 592–607.
 34. Jian Z, Ding S, Deng H, Wang J, Yi W, Wang L, et al. Probenecid protects against oxygen–glucose deprivation injury in primary astrocytes by regulating inflammasome activity. *Brain Research*. 2016; 1643: 123–9.
 35. Hainz N, Wolf S, Tschernig T, Meier C. Probenecid Application Prevents Clinical Symptoms and Inflammation in Experimental Autoimmune Encephalomyelitis. *Inflammation*. 2016; 39: 123–8.
 36. Wang Q, Li H, Ling Z, Chen G, Wei Z-Y. Inhibition of Schwann cell pannexin 1 attenuates neuropathic pain through the suppression of inflammatory responses. *J Neuroinflammation*. 2022; 19: 244.

DEEP LEARNING IN MODELLING THE PROTEIN–LIGAND INTERACTION: NEW PATHWAYS IN DRUG DEVELOPMENT

Barykin AD^{1,2}, Chepurnykh TV¹, Osipova ZM^{1,3}✉

¹ Shemyakin–Ovchinnikov Institute of Bioorganic Chemistry of the Russian Academy of Sciences, Moscow, Russia

² Moscow Institute of Physics and Technology (MIPT), Dolgoprudny, Russia

³ Pirogov Russian National Research Medical University, Moscow, Russia

The deep learning technologies have become the driver of the revolutionary changes in scientific research in various fields. The AlphaFold-2 neural network software development that has solved the semicentennial problem of 3D protein structure prediction based on primary amino acid sequence is the most obvious example of using such technologies in structural biology and biomedicine. The use of deep learning methods for the prediction of protein–ligand interactions can considerably simplify predicting, speed up the development of new effective pharmaceuticals and change the concept of drug design.

Keywords: docking, protein–ligand interaction, neural networks, deep learning

Funding: the study was supported by the Russian Science Foundation grant, project № 22-44-02024 (<https://rscf.ru/project/22-44-02024/>).

Author contribution: Barykin AD — literature review, manuscript writing, Chepurnykh TV — concept, literature review, manuscript writing and editing, Osipova ZM — project management, manuscript editing.

✉ **Correspondence should be addressed:** Zinaida M. Osipova
Miklukho-Maklaya, 16/10, Moscow, 117997, Russia; zkaskova@ibch.ru

Received: 06.12.2023 **Accepted:** 22.01.2024 **Published online:** 08.02.2024

DOI: 10.24075/brsmu.2024.002

ГЛУБОКОЕ ОБУЧЕНИЕ В МОДЕЛИРОВАНИИ БЕЛОК-ЛИГАНДНОГО ВЗАИМОДЕЙСТВИЯ: НОВЫЕ ПУТИ В РАЗРАБОТКЕ ЛЕКАРСТВЕННЫХ ПРЕПАРАТОВ

А. Д. Барыкин^{1,2}, Т. В. Чепурных¹, З. М. Осипова^{1,3}✉

¹ Институт биоорганической химии имени М. М. Шемякина и Ю. А. Овчинникова Российской академии наук, Москва, Россия

² Московский физико-технический институт, Долгопрудный, Россия

³ Российский национальный исследовательский медицинский университет имени Н. И. Пирогова, Москва, Россия

Технологии глубокого обучения стали драйвером революционных изменений в научных исследованиях разных областей. Наиболее ярким примером их применения в области структурной биологии и биомедицины является программная разработка нейросеть AlphaFold-2, решившая полувековую проблему предсказания 3D-структуры белков по первичной аминокислотной последовательности. Использование методов глубокого обучения для предсказания белок-лигандных взаимодействий сможет значительно упростить предсказание, ускорить разработку новых эффективных лекарственных препаратов и поменять концепцию драг-дизайна.

Ключевые слова: докинг, белок-лигандное взаимодействие, алгоритм нейросети, глубокое обучение

Финансирование: исследование выполнено за счет гранта Российского научного фонда № 22-44-02024, <https://rscf.ru/project/22-44-02024/>.

Вклад авторов: А. Д. Барыкин — анализ литературы, написание рукописи, Т. В. Чепурных — идея, анализ литературы, написание и редактирование рукописи, З. М. Осипова — руководство проектом, редактирование рукописи.

✉ **Для корреспонденции:** Зинаида Михайловна Осипова
ул. Миклухо-Маклая, 16/10, г. Москва, 117997, Россия; zkaskova@ibch.ru

Статья получена: 06.12.2023 **Статья принята к печати:** 22.01.2024 **Опубликована онлайн:** 08.02.2024

DOI: 10.24075/vrgmu.2024.002

Computer (*in silico*) modelling of protein–ligand interaction plays a key role in biomedical research and represents one of the fundamental challenges of the ongoing process of developing new pharmaceuticals. The higher is the affinity and selectivity of the bioactive molecule binding with the receptor or enzyme, the more effective and safe the resulting drug candidate will be. The model reliability determines the quantity and quality of the candidate molecules, which will undergo the expensive procedure of chemical synthesis and testing *in vitro* and *in vivo*. Modelling often represents the key phase: this to the great extent determines the time and cost of the design, as well as the final price of the drug [1]. Until recently, there was no highly effective method for automated bioinformatics analysis of the protein–ligand interaction.

Conventional computer modelling methods

Molecular docking is a molecular modelling method predicting the best position of the ligand relative to the target protein that

uses their 3D structures and the molecular interaction energy scoring functions. The scoring function learning (Fig. 1A) is usually based on the set of the experimentally determined affinity values of protein binding to the ligands similar to the studied one. Thus, the prediction accuracy will depend directly on the similarity of the studied new candidate to the known ligands from the database.

The great diversity of scoring functions can be explained by insufficient reliability of each of these functions in case of solving a specific problem. Various scoring functions are more appropriate for various classes of ligands, however, there is no absolute guarantee of the result even when the method is selected correctly. That is why consensus assessment (using the data of several scoring functions at once) increases the likelihood of successful docking [2].

In case of rigid docking, the algorithms consider the ligand and target molecules as solids, while in case of dynamic docking the programs admit the possibility of conformational changes in the ligand associated with binding. The methods

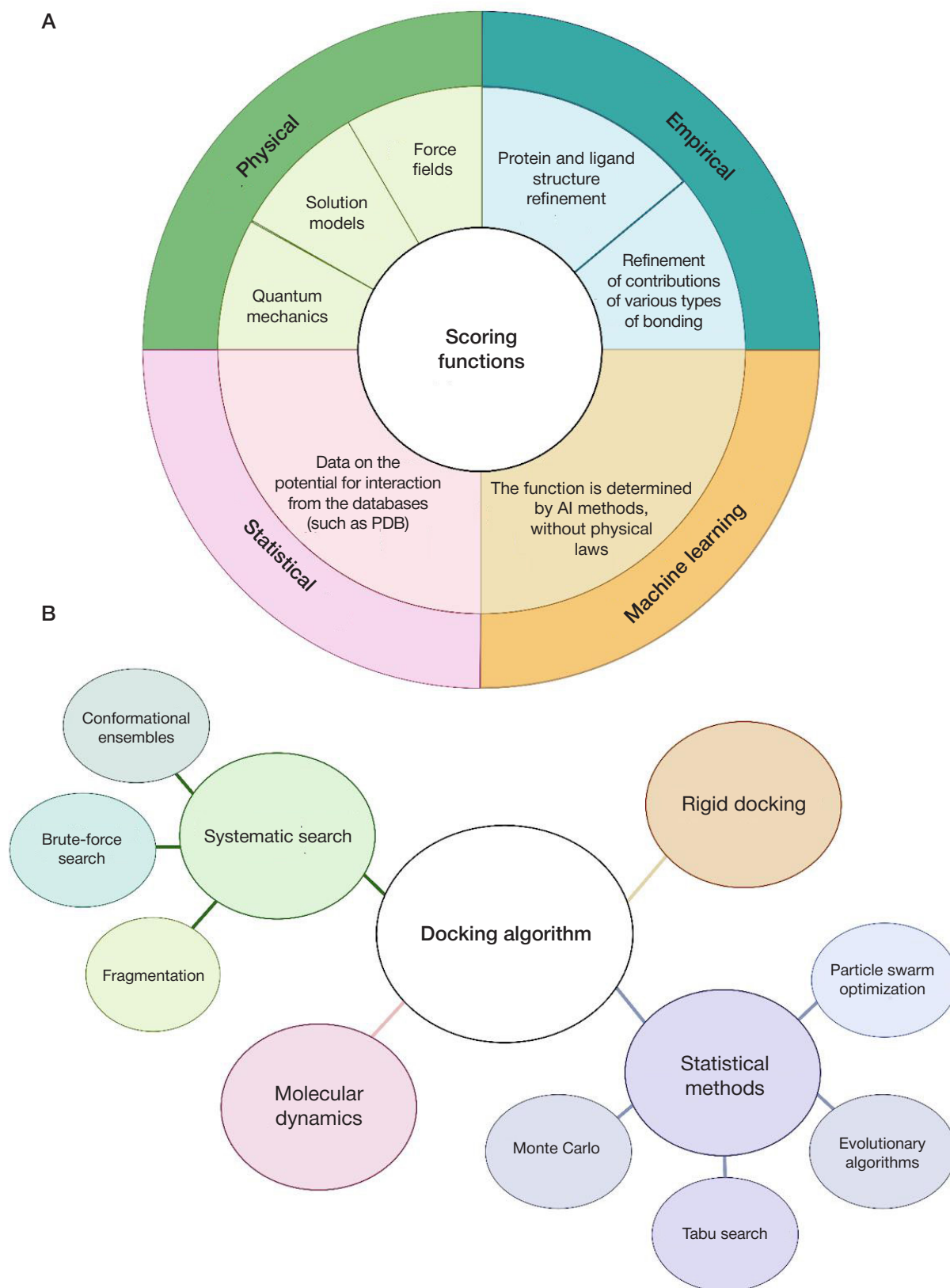


Fig. 1. Molecular docking algorithms. **A.** Types of scoring functions for molecular docking. **B.** Variants of molecular docking algorithms and molecular dynamics

underlying the docking algorithms (Fig. 1B) can be divided roughly into systematic and statistical. The systematic methods split molecule into several parts, thereby allowing one to assess affinity of interaction for each part, and then ensure covalent cross-linking of the parts in order to reassemble the ligand. Statistical methods to find the global energy minimum generate random changes, for each of which the thermodynamic

state is estimated [3]. Statistical methods include the Monte Carlo method, tabu search, particle swarm optimization, and evolutionary algorithms. The systematic algorithms guarantee achievement of results in a finite number of steps (usually very large), while the statistical ones can “miss” the energy state of interest. However, in practice, statistical algorithms more often yield more reliable results than systematic ones.

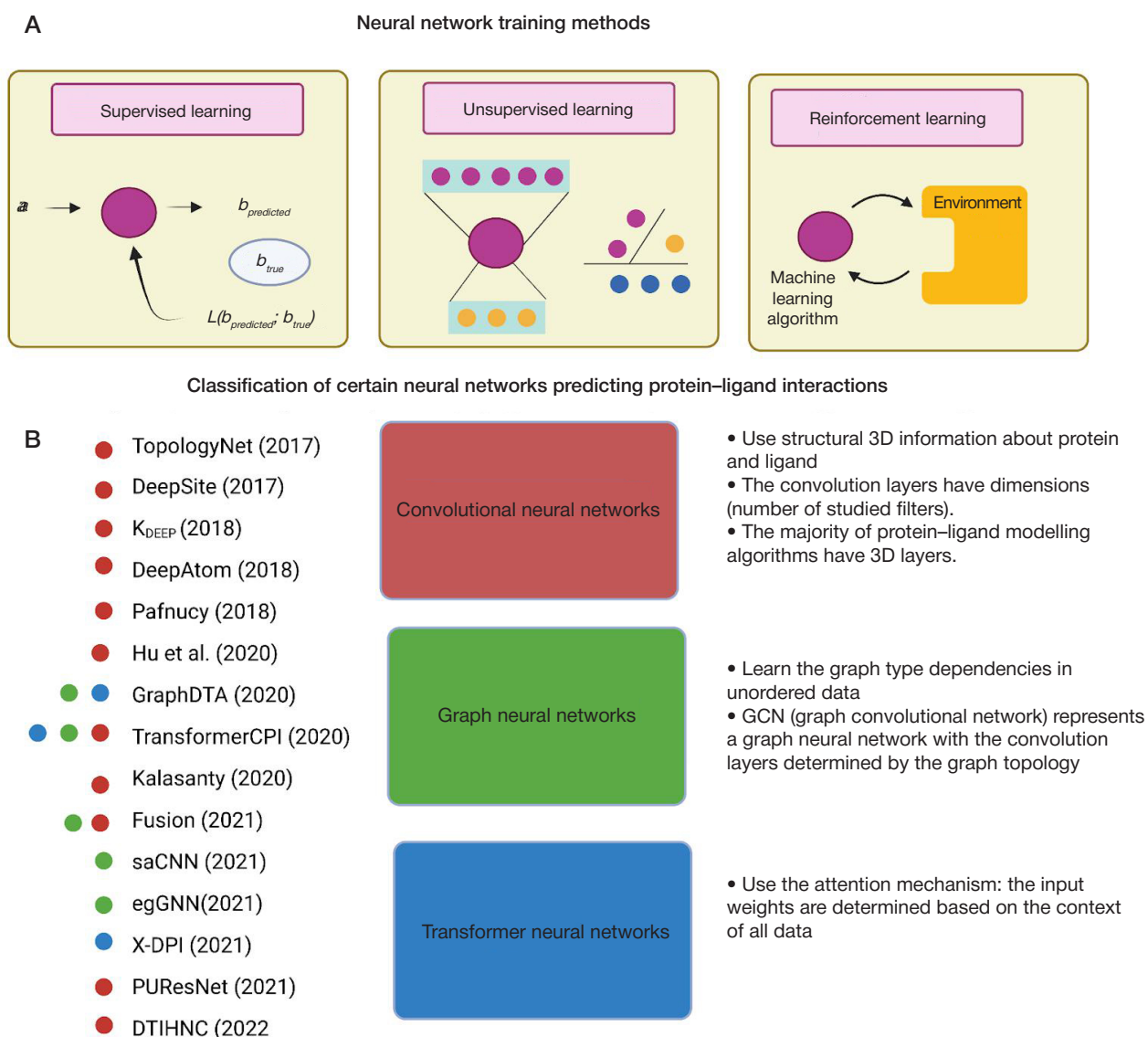


Fig. 2. Neural network operation algorithms. A. Neural network training methods. B. Major types of neural networks predicting the protein–ligand interactions

In the last two decades, dozens of free and commercially available molecular docking programs have emerged: DOCK, AutoDock, Surflex, LigandFit, MCDock, LeDock, AutoDock Vina, rDock, UCSF Dock, and many more [4]. The programs usually use several algorithms at once, allowing one to adapt docking for specific enzyme–ligand pairs.

In the majority of cases, the modern protein–ligand docking methods correctly determine the ligand binding site and binding mechanism, however, these are unable to define its affinity accurately enough [5]. This significantly reduces the method applicability for discovery of new pharmaceuticals, since the candidate molecules are selected based specifically on the binding energy.

The molecular dynamics (MD) method is based on the use of the equations of atom motion and the empirical potential energy functions for calculation of interatomic interactions and characterization of the molecular system evolution over time. The interatomic interactions include elastic interactions (corresponding to covalent bonds) and Van der Waals forces. The most important post-processing methods to calculate free energy of the bond in the protein–ligand interaction complex also use the principles of molecular mechanics involving the Poisson–Boltzmann equation / Generalized Born model, as well as some additional approaches, such as thermodynamic integration and free analysis [6].

The molecular trajectory length determined by the number of simulation steps is the main limitation of the molecular dynamics method. The simulation time step should be comparable with the fastest motion in the system, i.e. with the bond fluctuations (1–2 fs). Thus, modelling slow processes, such as large domain motions and binding (μs – ms), requires many MD steps, which significantly increases the amount of computation. That is why detection of actual protein–ligand binding is a very rare phenomenon [7]. It was expected that the MD modelling based on the binding computation involving the use of molecular mechanics and the Poisson–Boltzmann equation would contribute significantly to the solution of real problems, such as identification of the most advantageous combination for the protein–ligand pairs with their further optimization.

Deep learning: another chapter in modelling the protein–ligand interaction

The first deep learning methods emerged in the mid-1960s, however, these became popular by the mid-2000s due to the increase in processing power and the emergence of large experimental data sets. Today, application of deep learning technologies to problems in various disciplines has yielded the

results that are not inferior, and sometimes even superior, to the results yielded by conventional methods. Creation of the AlphaFold-2 algorithm predicting the protein tertiary structure based on the primary amino acid sequence within only a few minutes is the most obvious example [8], which has become a revolution in the field of structural biology.

The deep learning models were proposed for the prediction of protein–ligand interaction as an alternative to conventional docking based on the search for the free energy minimum [9]. The advantage of deep learning is that there is a possibility of studying the protein–ligand interaction based directly on the spatial arrangement of atoms, without selecting the mathematical parameters that not always reflect the actual binding mechanism. This method to predict protein–ligand interaction is currently developing rapidly: the DeepSite neural network model published in 2017 [10] correctly determined 23.8% of ligand binding sites in the specific dataset, while the Kalasanty neural network published in 2020 yielded the result of 44.6% for the same sample. In 2021, PURESNet significantly improved the prediction results (53% success for PURESNet vs. 51% for Kalasanty) [11].

To date, a wide variety of the neural network operation and training algorithms has been developed (Fig. 2). Convolutional neural networks (CNN), graph neural networks (GNN), and transformer neural networks are usually used to study protein–ligand interactions. Convolutional neural networks consider the relationships between pairs of atoms through the prism of their relative spatial positions. The operation principle of graph neural networks is based on recording the threshold values aimed to determine the type of interaction between atoms (covalent or non-covalent). The use of the lower number of parameters represents the potential advantage of this approach. The combinations of several algorithms are also used, or the other modules (such as denoising autoencoder) that improve the outcome are added [12].

CONCLUSION

No definite leader has been revealed among various neural network architectures: accuracy of the results yielded by each algorithm depends on the types of proteins and ligands,

affinity, and binding mechanism. According to the latest data, the egGNN and saCNN graph neural networks turned out to be the most successful in terms of ligand affinity prediction [13, 14], however, the differences from convolutional neural networks are not critical. We believe that this is due to the fact that no optimal prediction algorithm has yet been developed. Creating such an algorithm, judging by the pace of AI development in computational biology, is more likely to take years, not decades. Just like AlphaFold-2 changed the paradigm in the area of protein structure investigation in 2020, the use of artificial intelligence in biomedical research opens a new chapter in pharmaceutical industry and drug design.

The prospects of using AI for drug discovery have become apparent for the industry, since the use of AI significantly accelerates and reduces the cost of the conventional 12-year lifecycle of drug development. Over the past five years, almost all large pharmaceutical companies announced a partnership with the leading AI companies (Sanofi — Aily Labs, Pfizer — IBM, Novartis — Microsoft, AstraZeneca — Benevolent, etc.). The research details are likely to be protected by trade secret for a long time, however, press releases are being regularly issued that suggest introduction of deep learning into the ongoing R&D processes. Furthermore, more and more reports appear of the success of drug candidates designed using AI that are being prepared for or are through clinical trials. The examples include halicin (the promising broad-spectrum antibiotic, preclinical trial) [15], INS018_055 (drug for idiopathic pulmonary fibrosis, phase 2 clinical trial), REC-2282, REC-994, REC-4881, BEN-2293, EXS-21546, RLY-4008, EXS-4318, BEN-8744, etc. [16].

We believe that the search for the pool of new bioactive molecules will accelerate dramatically in the near future, and deep learning will become an essential element of the process of developing new pharmaceuticals. However, competent selection of the data that are used to train a neural network model still represents one of the topical problems on the path to the widespread use of deep learning for drug discovery, since the quality of these data is critical for reliability of predictions made by the model. In this regard, the task of the most effective training involving the use of incomplete or small datasets remains the main challenge faced by AI in the field of drug design [17].

References

- Lazo JS. Rear-view mirrors and crystal balls: a brief reflection on drug discovery. *Mol Interv.* 2008; 8 (2): 60–3. DOI: 10.1124/mi.8.2.1.
- Blanes-Mira C, Fernández-Aguado P, de Andrés-López J, Fernández-Carvajal A, Ferrer-Montiel A, Fernández-Ballester G. Comprehensive survey of consensus docking for high-throughput virtual screening. *Molecules.* 2023; 28 (1): 175. DOI: 10.3390/molecules28010175.
- Zhao L, Zhu Y, Wang J, Wen N, Wang C, Cheng L. A brief review of protein–ligand interaction prediction. *Comput Struct Biotechnol J.* 2022; 20: 2831–8. DOI: 10.1016/j.csbj.2022.06.004.
- Pagadala NS, Syed K, Tuszynski J. Software for molecular docking: a review. *Biophys Rev.* 2017; 9: 91–102. DOI: 10.1007/s12551-016-0247-1. PubMed PMID: 28510083.
- Wang Z, Sun H, Yao X, Li D, Xu L, Li Y, et al. Comprehensive evaluation of ten docking programs on a diverse set of protein–ligand complexes: the prediction accuracy of sampling power and scoring power. *Phys Chem Chem Phys.* 2016; 18: 12964–75. DOI: 10.1039/c6cp01555g.
- Perez JJ, Perez RA, Perez A. Computational modeling as a tool to investigate PPI: from drug design to tissue engineering. *Front Mol Biosci.* 2021; 8: 681617. DOI: 10.3389/fmolb.2021.681617. PubMed PMID: 34095231.
- Santos LHS, Ferreira RS, Caffarena ER. Integrating molecular docking and molecular dynamics simulations. *Methods Mol Biol.* 2019; 2053: 13–34. DOI: 10.3389/fmolb.2021.681617.
- Jumper J, Evans R, Pritzel A, Green T, Figurnov M, Ronneberger O, et al. Highly accurate protein structure prediction with AlphaFold. *Nature.* 2021; 596: 583–9. DOI: 10.1038/s41586-021-03819-2.
- Crampon K, Giorkallos A, Deldossi M, Baud S, Steffanel LA. Machine-learning methods for ligand–protein molecular docking. *Drug Discov Today.* 2021; 27(1): 151–64. DOI: 10.1016/j.drudis.2021.09.007.
- Jiménez J, Doerr S, Martínez-Rosell G, Rose AS, De Fabritiis G. DeepSite: protein-binding site predictor using 3D-convolutional neural networks. *Bioinformatics.* 2017; 33 (19): 3036–42. DOI: 10.1093/bioinformatics/btx350.
- Kandel J, Tayara H, Chong KT. PURESNet: prediction of protein–ligand binding sites using deep residual neural network. *J Cheminform.* 2021; 13: 65. DOI: 10.1186/s13321-021-00547-7.
- Greener JG, Kandathil SM, Moffat L, Jones DT. A guide to machine learning for biologists. *Nat Rev Mol Cell Biol.* 2022; 23: 40–55. DOI: 10.1038/s41580-021-00407-0.

13. Wang Y, Jiao Q, Wang J, Cai X, Zhao W, Cui X. Prediction of protein-ligand binding affinity with deep learning. *Comput Struct Biotechnol J.* 2023; 21: 5796–806. DOI: 10.1016/j.csbj.2023.11.009.
14. Zhao L, Zhu Y, Wang J, Wen N, Wang C, Cheng L. A brief review of protein–ligand interaction prediction. *Comput Struct Biotechnol J.* 2022; 20: 2831–8. DOI: 10.1016/j.csbj.2022.06.004.
15. Stokes JM, Yang K, Swanson K, Jin W, Cubillos-Ruiz A, Donghia NM, et al. A deep learning approach to antibiotic discovery. *Cell.* 2020; 180: P688–702.E13. DOI: 10.1016/j.cell.2020.01.021.
16. Arnold C. Inside the nascent industry of AI-designed drugs. *Nat Med.* 2023; 29: 1292–5. DOI: 10.1038/s41591-023-02361-0.
17. Yang B, Li K, Zhong X, Zou J. Implementation of deep learning in drug design. *MedComm — Fut Med.* 2022; 1: e18. DOI: 10.1002/mef2.18.

Литература

1. Lazo JS. Rear-view mirrors and crystal balls: a brief reflection on drug discovery. *Mol Interv.* 2008; 8 (2): 60–3. DOI: 10.1124/mi.8.2.1.
2. Blanes-Mira C, Fernández-Aguado P, de Andrés-López J, Fernández-Carvajal A, Ferrer-Montiel A, Fernández-Ballester G. Comprehensive survey of consensus docking for high-throughput virtual screening. *Molecules.* 2023; 28 (1): 175. DOI: 10.3390/molecules28010175.
3. Zhao L, Zhu Y, Wang J, Wen N, Wang C, Cheng L. A brief review of protein–ligand interaction prediction. *Comput Struct Biotechnol J.* 2022; 20: 2831–8. DOI: 10.1016/j.csbj.2022.06.004.
4. Pagadala NS, Syed K, Tuszynski J. Software for molecular docking: a review. *Biophys Rev.* 2017; 9: 91–102. DOI: 10.1007/s12551-016-0247-1. PubMed PMID: 28510083.
5. Wang Z, Sun H, Yao X, Li D, Xu L, Li Y, et al. Comprehensive evaluation of ten docking programs on a diverse set of protein–ligand complexes: the prediction accuracy of sampling power and scoring power. *Phys Chem Chem Phys.* 2016; 18: 12964–75. DOI: 10.1039/c6cp01555g.
6. Perez JJ, Perez RA, Perez A. Computational modeling as a tool to investigate PPI: from drug design to tissue engineering. *Front Mol Biosci.* 2021; 8: 681617. DOI: 10.3389/fmolb.2021.681617. PubMed PMID: 34095231.
7. Santos LHS, Ferreira RS, Caffarena ER. Integrating molecular docking and molecular dynamics simulations. *Methods Mol Biol.* 2019; 2053: 13–34. DOI: 10.3389/fmolb.2021.681617.
8. Jumper J, Evans R, Pritzel A, Green T, Figurnov M, Ronneberger O, et al. Highly accurate protein structure prediction with AlphaFold. *Nature.* 2021; 596: 583–9. DOI: 10.1038/s41586-021-03819-2.
9. Crampon K, Giorkallos A, Deldossi M, Baud S, Steffanel LA. Machine-learning methods for ligand–protein molecular docking. *Drug Discov Today.* 2021; 27(1): 151–64. DOI: 10.1016/j.drudis.2021.09.007.
10. Jiménez J, Doerr S, Martínez-Rosell G, Rose AS, De Fabritiis G. DeepSite: protein-binding site predictor using 3D-convolutional neural networks. *Bioinformatics.* 2017; 33 (19): 3036–42. DOI: 10.1093/bioinformatics/btx350.
11. Kandel J, Tayara H, Chong KT. PUPResNet: prediction of protein–ligand binding sites using deep residual neural network. *J Cheminform.* 2021; 13: 65. DOI: 10.1186/s13321-021-00547-7.
12. Greener JG, Kandathil SM, Moffat L, Jones DT. A guide to machine learning for biologists. *Nat Rev Mol Cell Biol.* 2022; 23: 40–55. DOI: 10.1038/s41580-021-00407-0.
13. Wang Y, Jiao Q, Wang J, Cai X, Zhao W, Cui X. Prediction of protein-ligand binding affinity with deep learning. *Comput Struct Biotechnol J.* 2023; 21: 5796–806. DOI: 10.1016/j.csbj.2023.11.009.
14. Zhao L, Zhu Y, Wang J, Wen N, Wang C, Cheng L. A brief review of protein–ligand interaction prediction. *Comput Struct Biotechnol J.* 2022; 20: 2831–8. DOI: 10.1016/j.csbj.2022.06.004.
15. Stokes JM, Yang K, Swanson K, Jin W, Cubillos-Ruiz A, Donghia NM, et al. A deep learning approach to antibiotic discovery. *Cell.* 2020; 180: P688–702.E13. DOI: 10.1016/j.cell.2020.01.021.
16. Arnold C. Inside the nascent industry of AI-designed drugs. *Nat Med.* 2023; 29: 1292–5. DOI: 10.1038/s41591-023-02361-0.
17. Yang B, Li K, Zhong X, Zou J. Implementation of deep learning in drug design. *MedComm — Fut Med.* 2022; 1: e18. DOI: 10.1002/mef2.18.

EMERGING PREDICTION OF PREECLAMPSIA BASED ON THE EXPRESSION OF EXOSOMAL SUMO PROTEINS

Gusar VA [✉], Timofeeva AV, Fedorov IS, Tarasova AM, Sukhova YuV, Ivanets TYu

Kulakov National Medical Research Center for Obstetrics, Gynecology and Perinatology, Moscow, Russia

The cellular response to various types of stress underlying placental vascular dysfunction is under the sumoylation control. Consequently, SUMO homeostasis is closely related to the maintenance of angiogenic balance, the disruption of which is a feature of preeclampsia (PE). The goal of the research is to search for exosomal markers of such a disorder. The expression and prognostic potential of exosomal SUMO 1–4, UBC9 and hnRNP2/B1 were evaluated in 39 pregnant women (cohort I) in the first trimester using Western blotting technology. The expression of these proteins in the placenta (cohort II, 27 pregnant women) at the time of delivery was also assessed. The expression of their conjugated forms was significantly changed in pregnant women with early-onset (SUMO 1, $p = 0.03$; SUMO 2/3/4, $p = 0.03$) and late-onset PE (SUMO 1, $p = 0.03$; SUMO 2/3/4, $p = 0.04$; UBC9 and hnRNP2/B1, $p < 0.0001$, respectively). This change may be due to the functional specificity of SUMO isoforms in the context of their subcellular targets upon exposure to stressful stimuli. Significant changes in the expression of these proteins were also found in the placenta. Significant correlations were established between the expression of exosomal SUMO 2/3/4 ($r = -0.59$; $p = 0.01$) and UBC9 ($r = -0.88$; $p = 0.0001$) with PIGF in early-onset PE. In late-onset PE, hnRNP2/B1 ($r = -0.48$; $p = 0.03$) and UBC9 ($r = -0.48$; $p = 0.03$) was correlated with β -hCG, and SUMO 2/3/4 with PAPP-A ($r = -0.60$; $p = 0.006$) in the blood serum of pregnant women. The analyzed proteins also significantly correlated with uterine artery pulsation index (SUMO 1 ($r = 0.59$; $p = 0.01$), SUMO 2/3/4 ($r = 0.54$; $p = 0.02$), hnRNP2/B1 ($r = 0.75$; $p = 0.0001$)) and mean arterial pressure (UBC9 ($r = 0.53$; $p = 0.03$)). Based on the data the logistic models have been created to predict the risk of developing early-onset (UBC9 (AUC = 0.88; Se-0.72; Sp-1)) and late-onset PE (SUMO 1 (AUC = 0.79; Se-0.8; Sp-0.77)) at 11–14 weeks of pregnancy.

Keywords: exosomes, sumoylation, SUMO, prediction, placental dysfunction, preeclampsia

Funding: the study was supported by the RSF grant [22-15-00363 "Epigenetic and biochemical aspects of abnormal pregnancy in disturbances of the trophoblast invasive properties: from early diagnosis to prevention of maternal and perinatal morbidity"].

Author contribution: Gusar VA, Timofeeva AV — study concept; Fedorov IS — statistical analysis, graphic design; Gusar VA, Tarasova AM — research procedure (western blotting); Sukhova YuV, Ivanets TYu — providing the clinical basis, assessment of hormones; Gusar VA — data analysis/interpretation, manuscript writing; Timofeeva AV — editing.

Compliance with ethical standards: the study was approved by the Ethics Committee of the Kulakov National Medical Research Center for Obstetrics, Gynecology and Perinatology (protocol № 13 dated 12 October 2015); the informed consent was obtained from all the patients enrolled.

✉ **Correspondence should be addressed:** Vladoslava A. Gusar
Akademika Oparina, 4, Moscow, 117997, Russia; v_gusar@mail.ru

Received: 29.01.2024 **Accepted:** 20.02.2024 **Published online:** 29.02.2024

DOI: 10.24075/brsmu.2024.010

НОВЫЕ ВОЗМОЖНОСТИ ПРОГНОЗИРОВАНИЯ ПРЕЭКЛАМПСИИ НА ОСНОВЕ ЭКСПРЕССИИ ЭКЗОСОМНЫХ БЕЛКОВ SUMO

В. А. Гусар [✉], А. В. Тимофеева, И. С. Федоров, А. М. Тарасова, Ю. В. Сухова, Т. Ю. Иванец

Национальный медицинский исследовательский центр акушерства, гинекологии и перинатологии имени В. И. Кулакова, Москва, Россия

Клеточная реакция на стресс, лежащий в основе сосудистой дисфункции плаценты, находится под контролем сумоилирования. Следовательно, SUMO-гомеостаз тесно связан с поддержанием ангиогенного баланса, нарушение которого характерно для преэклампсии (ПЭ). Цель работы — поиск экзосомных маркеров подобного нарушения. Оценивали экспрессию и прогностический потенциал экзосомных SUMO 1–4, UBC9 и hnRNP2/B1 у 39 беременных (когорты I) в первом триместре с помощью вестерн-блоттинга. В когорте II (27 беременных) оценивали экспрессию данных белков в плаценте на момент родов. Экспрессия экзосомных конъюгированных форм значимо изменялась у беременных с ранней (SUMO 1, $p = 0,03$; SUMO 2/3/4, $p = 0,03$) и поздней ПЭ (SUMO 1, $p = 0,03$; SUMO 2/3/4, $p = 0,04$; UBC9 и hnRNP2/B1, $p < 0,0001$ соответственно), что может быть обусловлено функциональной специфичностью изоформ SUMO в контексте их субклеточных мишеней при воздействии стрессовых стимулов. В плаценте также обнаружены значимые изменения экспрессии конъюгированных форм данных белков. При ранней ПЭ установлены значимые корреляционные связи экспрессии экзосомных SUMO 2/3/4 ($r = -0,59$; $p = 0,01$) и UBC9 ($r = -0,88$; $p = 0,0001$) с уровнем PIGF, а при поздней ПЭ — hnRNP2/B1 ($r = -0,48$; $p = 0,03$), UBC9 ($r = -0,48$; $p = 0,03$) с β -ХГЧ, и SUMO 2/3/4 ($r = -0,60$; $p = 0,006$) с концентрацией PAPP-A в сыворотке крови беременных. Анализируемые белки достоверно коррелировали с пульсационным индексом маточной артерии (SUMO 1 ($r = 0,59$; $p = 0,01$), SUMO 2/3/4 ($r = 0,54$; $p = 0,02$), hnRNP2/B1 ($r = 0,75$; $p = 0,0001$)) и средним артериальным давлением (UBC9 ($r = 0,53$; $p = 0,03$)). На основе полученных данных созданы логистические модели прогнозирования риска развития ранней (UBC9 (AUC = 0,88; Se-0,72; Sp-1)) и поздней ПЭ (SUMO 1 (AUC = 0,79; Se-0,8; Sp-0,77)) на сроке 11–14 недель беременности.

Ключевые слова: экзосомы, сумоилирование, SUMO, прогнозирование, плацентарная дисфункция, преэклампсия

Финансирование: работа выполнена при поддержке гранта РНФ [22-15-00363 «Эпигенетические и биохимические аспекты патологии беременности при нарушениях инвазивных свойств трофобласта: от ранней диагностики к профилактике материнской и перинатальной заболеваемости»].

Вклад авторов: В. А. Гусар, А. В. Тимофеева — концепция исследования; И. С. Федоров — статистический анализ, графическое оформление; В. А. Гусар, А. М. Тарасова — проведение исследований (вестерн-блоттинг); Ю. В. Сухова, Т. Ю. Иванец — формирование клинической базы, гормональные исследования; В. А. Гусар — анализ/интерпретация данных, подготовка статьи; А. В. Тимофеева — редактирование.

Соблюдение этических стандартов: исследование одобрено этическим комитетом ФГБУ «Национальный медицинский исследовательский центр акушерства, гинекологии и перинатологии им. академика В. И. Кулакова» Минздрава России (№ 13 от 12 октября 2015 г.); добровольное информированное согласие получено от всех пациентов, включенных в исследование.

✉ **Для корреспонденции:** Владислава Анатольевна Гусар
ул. Академика Опарина, д. 4, г. Москва, 117997; v_gusar@mail.ru

Статья получена: 29.01.2024 **Статья принята к печати:** 20.02.2024 **Опубликована онлайн:** 29.02.2024

DOI: 10.24075/vrgmu.2024.010

The role of placental dysfunction proven by numerous studies in the basis of adverse pregnancy outcomes, including preeclampsia (PE) and fetal growth restriction (FGR), is undeniable. The molecular component of these syndromes is represented by key processes combined with stress — hypoxic, oxidative/nitrate, mitochondrial and endoplasmic reticulum [1–4], resulting from abnormal endovascular invasion of spiral arteries by trophoblasts. As a result, various pro-inflammatory factors that disturb the angiogenic balance are released into the mother's bloodstream [5]. The resulting therefrom pathological changes lead to a higher risk of metabolic, cardiovascular and nephrological diseases in women and their fetuses in the long term [6, 7].

In general, PE is defined as a multisystem disease, with new onset hypertension with (or without) significant proteinuria after 20 weeks of gestation [8, 9]. Over the past three decades, this definition has been expanded. Nowadays the definition include timing of symptom onset in early or late pregnancy, with delivery before or after 34 weeks, and different phenotypes due to adverse effects on the fetus (PE with or without IGR) [8]. Of note is the recent discussion that argues that the maternal cardiovascular system is the etiological cause of PE [5,10]. However, the linking mechanism between placental dysfunction and maternal cardiovascular maladaptation is angiogenic-antiangiogenic imbalance [10]. During physiological pregnancy, the levels of angiogenic placental growth factor (PLGF) and anti-angiogenic factor sFlt-1 (soluble fms-like tyrosine kinase 1) are balanced, but under conditions of hypoxia and oxidative stress, there is an increase in the secretion of sFlt-1 by cytotrophoblasts, leading to impaired angiogenesis. There are propose various pathways modulating PLGF expression [11]. One of them is mediated by the transcription factor GCM-1, which plays a critical role in maintaining the balance between proliferation and differentiation of syncytiotrophoblast in the first trimester of pregnancy [12] and its upstream target DREAM [13]. It is important to emphasize that the modulation of the activity of the latter occurs at the post-translational level, including through sumoylation [14]. Interestingly, this modification is also a key player in controlling cellular responses to heat shock, inflammation, and various types of stress (oxidative, hypoxic, mitochondrial) underlying placental dysfunction [15–18].

Sumoylation is a dynamic reversible process carried out by SUMO (Small Ubiquitin-like MOdifier) proteins, which have four isoforms. Their conjugation (the formation of an isopeptide bond between SUMO and the target protein) is performed by the UBC9 enzyme [19]. Sumoylation has attracted increasing attention in the context of regulating the expression of molecules mediating placental function and angiogenesis. However, data on the study of sumoylation in placental diseases are essentially limited. In particular, Baczyk et al. revealed a significant increase of SUMO 1 and SUMO 2/3 in the placenta in severe early-onset PE [20]. And the WGCNA evolutionary approach has identified gene co-expression modules that play a critical role in the pathogenesis of PE, including SUMO 1 and the heterogeneous nuclear protein (hnRNP), as candidates genes for positive selection [21].

The coordinated interface between the fetoplacental and maternal systems is a complex multidimensional array of tissues, resident and circulating factors, covering the developing fetus, placenta, decidua, and the mother's dynamic cardiovascular system [1]. It is carried out through extracellular vesicles (exosomes, microvesicles, apoptotic vesicles), which are secreted by various types of cells, carry a certain cargo (proteins, lipids, mRNA transcripts), and also have the ability to modulate the function of target cells and have therapeutic

potential [22, 23]. In particular, exosomes are selectively packaged with signaling molecules such as microRNAs (miRNAs). Their secretion by syncytiotrophoblast increases with placental dysfunction [24–26]. Most notably, the selectivity and loading of miRNAs into exosomes is mediated by sumoylation of the heterogeneous nuclear protein hnRNP2/B1 [27].

Progress in understanding the molecular processes consociating placental dysfunction and the maternal cardiovascular system suggests that disturbances in the angiogenic-antiangiogenic balance may be a target for the search for exosomal prognostic markers. Our previous studies demonstrated a regulatory mechanism along the miR-652-3p/ SUMO 2/3/4/ UBC9/ GCM-1/ PIGF axis in the placenta of pregnant women with early-onset PE [28] and changes in SUMO 1–4 and UBC9 expression in exosomes of pregnant women with early-onset PE at the time of delivery [29]. Further to these studies, we focused our attention on evaluating the expression of exosomal SUMO 1–4, UBC9, and hnRNP2/B1 proteins as predictors of placental dysfunction at early gestational periods (11–14 weeks) before the manifestation of clinical signs of this pathology. Beyond that, to the best of the authors' knowledge, such studies have not previously been conducted.

METHODS

Study Design and Patient Cohort

This study included pregnant women who were under observation at the “National Medical Research Center for Obstetrics, Gynecology, and Perinatology named after Academician V. I. Kulakov” of the Ministry of Healthcare of the Russian Federation. The total sample of patients of reproductive age consisted of 66 pregnant women, divided into 2 cohorts (Fig. 1). Inclusion criteria are singleton pregnancy, patients aged from 25 to 40 years, delivered vaginally and by cesarean section. The study of both cohorts did not include pregnant women with multiple pregnancies, resulting from assisted reproductive technologies, positive somatic history and genetic pathologies in the mother and fetus. Cohort I included 39 pregnant women and was divided into groups: pregnant women who subsequently developed early-onset (11 pregnant women) and late-onset (10 pregnant women) PE; pregnant women with a high risk of developing PE according to combined prenatal screening in the first trimester and a favorable pregnancy outcome (9 pregnant women); pregnant women with a physiological course of pregnancy (9 pregnant women). The expression of SUMO, UBC9 and hnRNP2/B1 proteins was assessed in exosomes of pregnant women at 11–14 weeks of gestation. Cohort II included 27 pregnant women with early-onset (7 pregnant women), late-onset PE (7 pregnant women) and a control group of the corresponding period (7 and 6 pregnant women, respectively) to assess protein expression in placental samples. The detailed clinical characteristics of pregnant women included in study are presented in Table 1–2.

Exosome Purification from the Serum Blood Samples of Pregnant Women

Whole blood samples were collected from pregnant women at 11–14 weeks of pregnancy (cohort I). Previously, the samples were centrifuged for 20 minutes, +4 °C at 300 g. The upper phase was then carefully transferred into a clean conical bottom tube and centrifuged again for 10 min at +4 °C at

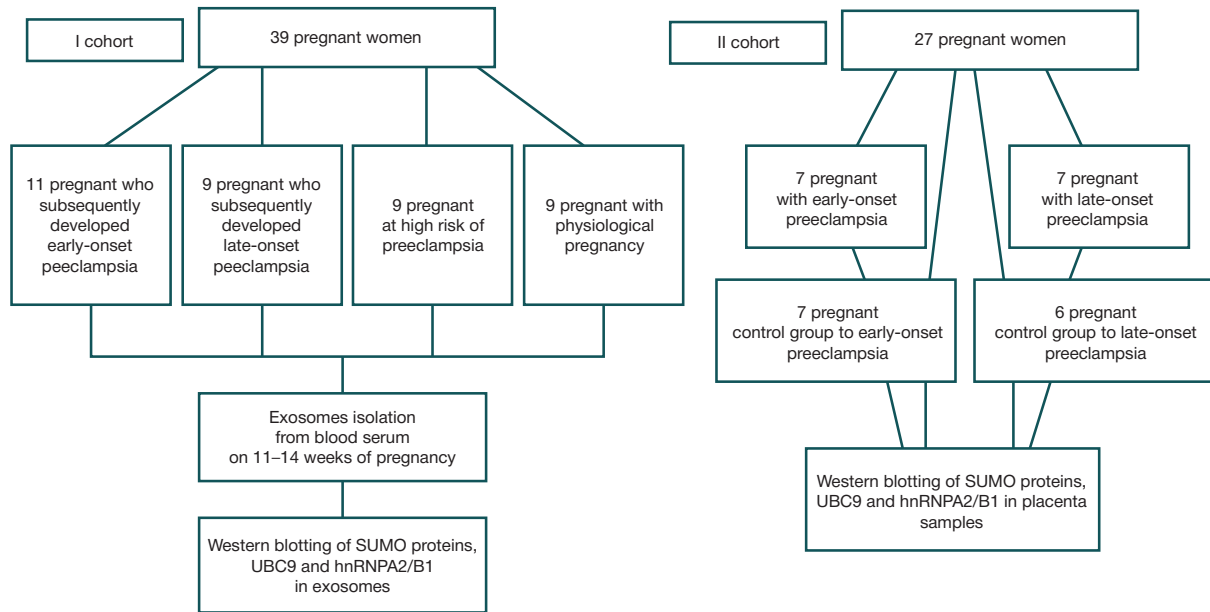


Fig. 1. Flowchart of the study population

16,000 g to remove cell debris. From the prepared samples, 600 μ l was used for purification of exosomes using miRCURY Exosome Serum/Plasma Kit (cat. no. 76603; Germany, Qiagen) according to the manufacturer's instructions, and subsequent Western blotting.

Western Blotting of exosomal and tissue proteins

A placental tissue (a cross-section through the maternal and fetal part of the placenta no more than 5 mm in thickness, obtained immediately after delivery) from pregnant women (cohort II) was used for protein extraction. Powdered tissue samples preliminarily ground in liquid nitrogen were homogenized in a RIPA Lysis Buffer System (sc-24948; Santa Cruz Biotechnology, Inc.; Dallas, Texas, USA). Separation of proteins (20 μ g per gel lane) was performed in Tris/Tricine/SDS Buffer (12.5%). Exosome and tissue protein transfer to nitrocellulose membrane (0.45 μ m, cat. no: 1620115; Bio-Rad, USA) was performed using Trans-Blot SD™ (cat. #. 170-3957; Bio-Rad, USA) in 10 mM CAPS + 10% C_2H_5OH , pH = 11. The membranes were blocked with 5% NFD/MTBST for 2 h. Incubation with primary antibodies: SUMO 1 (1:500; sc-5308; Santa Cruz Biotechnology, USA), SUMO 2/3/4 (1:500; sc-393144; Santa Cruz Biotechnology, USA), UBC9 (1:500; sc-271057; Santa Cruz Biotechnology, USA), hnRNPA2/B1 (1:500; sc-374053; Santa Cruz Biotechnology, USA), and Actin (1:100; sc-376421; Santa Cruz Biotechnology, USA) were performed for 2h (RT). Secondary HRP-conjugated antibodies (goat anti-mouse IgG-HRP: sc-2031; Santa Cruz Biotechnology, USA) were incubated for 1 h (RT) in 1% NFD/MTBST. A SuperSignal West Femto Maximum Sensitivity Substrate Kit (cat. no: 34096, Thermo Scientific™, USA) was used as a detection reagent. Densitometric analysis was performed using Bio-Rad ImageLab 6.0 software. The expression of tissue proteins SUMO 1–4, UBC9 and hnRNP A2/B1 was normalized to that of actin, and the level of SUMO 1–4, UBC9 and hnRNP A2/B1 in exosomes was normalized to the concentration of total protein.

Evaluation of biochemical parameters of prenatal screening in blood serum of pregnant women

The concentration of placental factors (sFlt-1, PLGF) and hormones (PAPP-A, b-HCG) in the blood serum of pregnant

women at 11–14 weeks of gestation was determined by immunochemical analyzer "Cobas e411" (Roche Diagnostics GmbH; Germany) using commercial kits of this manufacturer.

Statistical Analysis

The statistical significance of the difference between the clinical parameters and the proteins expression in study groups was assessed by the Wilcoxon–Mann–Whitney test using scripts written in the R language (<https://www.R-project.org/>). The Spearman nonparametric rank correlation method was used to evaluate the relationship between the protein expression and clinical parameters of pregnant women. Logistic regression models for proteins expression were created to test their predictive ability. The efficiency of the created models was evaluated by ROC analysis.

RESULTS

SUMO 1–4, UBC9 and hnRNPA2/B1 Expression in Exosomes at 11–14 weeks of pregnancy

The expression of SUMO 1–4, UBC9, and hnRNPA2/B1 in exosomes isolated from the serum blood of pregnant women with physiological pregnancy, which subsequently manifested early-onset and late-onset PE, as well as pregnant women with a high risk of developing PE according to combined prenatal screening at 11–14 weeks of gestation, was assessed by Western blotting. There were several conjugated forms of these proteins differing in molecular weights detected, while no free forms were found in exosomes (Fig. 2 A–D).

Comparative analysis revealed that in the exosomes of pregnant women with early-onset PE, the expression of the conjugated form SUMO 1 (~50–52 kDa) was significantly reduced ($p = 0.03$), and SUMO 2/3/4 (~55–58 kDa) was increased relative to physiological pregnancy ($p = 0.03$). Expression of approximately molecular weight conjugated UBC9 (~54–63 kDa) and hnRNPA2/B1 (~51–55 kDa) was also increased, but without statistically significant differences ($p = 0.07$; $p = 0.3$, respectively). Presumably, these forms are a SUMO 1 + UBC9 conjugate, as the molecular weight of their free forms is ~12 kDa and ~18 kDa, respectively. And if

Table 1. The clinical characteristics of pregnant women (cohort I)

	11–14 weeks of pregnancy						
	Pregnant who subsequently developed EPE (n = 11)	Pregnant who subsequently developed LPE (n = 10)	Pregnant at high risk of PE (n = 9)	Pregnant with PP (n = 9)	p-value EPE vs.PP	p-value LPE vs.PP	p-value high risk vs.PP
Gestational age at the time of screening, weeks	12.1 (11.8; 12.25)	12.15 (12.1; 12.47)	12.1 (11.6; 12.3)	12.35 (12.03; 12.9)	0.1	0.3	0.3
History of PE, n (%)	0	0	0	0	–	–	–
Mean arterial pressure, MoM	1.06 (1; 1.11)	0.98 (0.94; 1.1)	0.96 (0.95; 0.98)	1 (0.96; 1.04)	0.08	1	0.07
PIGF (17.6–70.0, pg/ml; 12 week of gestation)	11.7 (6.3; 18.0)	15.8 (15.6; 23.08)	18.8 (18.8; 18.8)	18.05 (16.01; 26.5)	0.001	0.2	0.8
β-hCG (0.5–2.0, MoM)	0.92 (0.65; 1.07)	0.72 (0.52; 0.8)	0.74 (0.58; 1.22)	1.38 (1.18; 1.8)	<0.001	<0.001	0.07
PAPP-A (0.5–2.0, MoM)	0.9 (0.72; 1.1)	0.65 (0.57; 1.17)	1.07 (0.9; 1.32)	0.87 (0.74; 1.28)	0.7	0.3	0.5
Ultrasonography:							
CRL (43–84 mm)	57.7 (56.5; 60.2)	58.6 (57.7; 62.5)	57.6 (56; 61.2)	64.4 (55.7; 66.0)	0.11	0.3	0.4
NTS (1.6–1.7 mm)	1.6 (1.38; 1.73)	1.5 (1.42; 1.85)	1.5 (1.29; 1.9)	1.25 (1.2; 1.6)	0.2	0.1	0.6
PI UtA (0.76–1.1, MoM)	1.14 (1; 1.21)	0.99 (0.76; 1.3)	1.1 (1.02; 1.19)	1.02 (0.91; 1.13)	0.3	0.7	0.3
PI DV	0.98 (0.98; 0.98)	0.97 (0.97; 0.97)	0.95 (0.95; 0.95)	1.06 (0.99; 1.14)	0.02	0.02	0.03
	Clinical characteristics at the time of delivery						
Gestational age at the time of delivery, weeks	32.1 (30.7; 33.35)	37.2 (36.47; 38.27)	38.3 (37.6; 39.2)	38.8 (38.35; 39.35)	<0.001	0.01	0.4
Systolic blood pressure (110–130 mmHg)	150 (145; 160)	140 (130; 150)	140 (115; 147)	115 (110; 131.2)	<0.001	0.006	0.08
Diastolic blood pressure (65–80 mmHg)	100 (90; 100)	90 (90; 95)	90 (75; 90)	77.5 (71.2; 85.2)	<0.001	0.003	0.1
Proteinuria (0–0.2 g/L)	1.98 (1.08; 2.5)	0.27 (0.13; 0.95)	0.09 (0; 0.1)	0 (0; 0.1)	<0.001	0.01	0.5
Peripheral edema, n (%)	5 (45.4)	4 (40.0)	1 (11.1)	3 (33.3)	–	–	–
Ratio of placental dysfunction markers (sFLT-1/PIGF; 1.5–7)	316.6 (116.7; 433.9)	120.1 (78.8; 156.9)	133.7 (117.9; 173.4)	54.4 (54.4; 54.4)	0.01	<0.001	<0.001
Platelet level (150–400 × 10 ⁹ c/L)	220 (146; 233)	244 (142; 262.5)	212 (186; 234)	247.5 (235.7; 270.2)	0.03	0.07	0.07
ALT level (0–40 u/L)	30.9 (21.7; 68.05)	20.6 (15.4; 22.3)	19.2 (18.1; 26.1)	31.8 (18.2; 31.8)	0.09	1	0.7
AST level (0–40 u/L)	27.3 (21.7; 43.15)	25.1 (20.05; 32.6)	17.4 (16.3; 34.5)	19.7 (19.7; 20.6)	0.08	0.3	0.8
Ultrasonography PI UtA (average value)	1.24 (1.05; 1.38)	0.9 (0.74; 0.99)	0.68 (0.55; 0.85)	0.57 (0.52; 0.6)	<0.001	0.001	0.1
Birth weight, grams	1350 (1195; 1572)	2721 (2409.25; 2992.5)	3040 (2750; 3266)	3320 (3257; 3612.5)	<0.001	0.01	0.05
Apgar 1 score	7 (7; 7)	8 (8; 8)	8 (8; 8)	8 (8; 8)	<0.001	1	0.2
Apgar 5 score	8 (7; 8)	9 (9; 9)	9 (9; 9)	9 (9; 9)	<0.001	0.3	0.8
Newborns outcomes:							
IP, n (%)	7 (63.6)	0	0	0	–	–	–
IVH, n (%)	5 (45.4)	0	0	0	–	–	–
RDS, n (%)	2 (18.1)	0	0	0	–	–	–

Note: EPE is early-onset preeclampsia; LPE is late-onset preeclampsia; PP is physiological pregnancy; PIGF is a placental growth factor; sFLT-1 is a soluble Fms-like tyrosine kinase 1; PAPP-A is a pregnancy-associated protein A; β-hCG is a human chorionic gonadotropin, subunit β; CRL is a crown-to-rump length; NTS is a nuchal translucency scan; PI UtA is a Pulsatility Index of the uterine artery; PI DV is a Pulsatility Index of ductus venosus; IP is an intrauterine pneumonia; IVH is an intraventricular hemorrhage; RDS is a respiratory distress syndrome; The median (Me) and quartiles Q₁, Q₃ in the format Me (Q₁–Q₃) were used in the case of non-normal distribution.

hnRNPA2/B1 (free form ~36/38 kDa) is attached as a SUMO 1 target, their total molecular weight may be ~50–56 kDa.

There is also a significant decrease in the expression of the conjugated SUMO 1 (~50–52 kDa; $p = 0.03$) in late-onset PE. While the expression of the conjugated SUMO 2/3/4 (~55–58 kDa; $p = 0.04$), UBC9 (~54–63 kDa; $p < 0.0001$) and hnRNPA2/B1 (~51–55 kDa; $p < 0.0001$) significantly increased relative to normal pregnancy (Fig. 3 A–D).

Interestingly, the analysis of the studied proteins expression in the group of pregnant women with a high risk of developing PE also revealed a significant decrease in the conjugated SUMO 1 expression (~50–52 kDa; $p = 0.007$) and an increase in the conjugated UBC9 (~54–63 kDa), hnRNPA2 /B1 (~51–55 kDa) relative to physiological pregnancy ($p = 0.01$ and $p = 0.001$, respectively).

SUMO 1–4, UBC9 and hnRNPA2/B1 Expression in Placenta Tissue in early-onset and late-onset PE

Taking into account significant changes in the conjugated SUMO 1–4, UBC9 and hnRNPA2/B1 expression in exosomes of pregnant women secreted by syncytiotrophoblasts at 11–14 weeks of gestation, their expression in the placenta in pregnant women with early-onset and late-onset PE was evaluated. Western blotting identified conjugated fragments of these proteins, differing in molecular weights, corresponding to those found in exosomes.

Comparative analysis revealed a significant decrease in the conjugated SUMO 1 expression (~50–55 kDa, $p = 0.04$; $p = 0.04$, respectively), SUMO 2/3/4 (~55–59 kDa; $p = 0.008$, $p = 0.05$, respectively) and hnRNPA2/B1 (~54 kDa; $p = 0.01$,

Table 2. The clinical characteristics of pregnant women (cohort II)

	Pregnant with EPE (n = 7)	Control group (n = 7)	<i>p</i>	Pregnant with LPE (n = 7)	Control group (n = 6)	<i>p</i>
Gestational age at the time of delivery, weeks	29 (27; 30)	30 (26.7; 30.5)	0.5	37 (36; 37.5)	38 (38; 38.75)	0.03
Manifestation PE, weeks	25 (23.5; 25)	absent	–	36 (36; 36)	absent	–
Systolic blood pressure (110–130 mmHg)	150 (145; 170)	115 (109.2; 117.5)	0.002	140 (140; 147.5)	110 (110; 113.7)	0.03
Diastolic blood pressure (65–80 mmHg)	100 (92.5; 106.5)	70 (67.5; 72.9)	0.002	100 (90; 100)	70 (70; 70)	0.005
Proteinuria (0–0.2 g/L)	2.08 (0.82; 3.72)	absent	–	1.07 (0.39; 1.81)	absent	–
Peripheral edema, <i>n</i> (%)	1 (14.2)	absent	–	5 (71.4)	absent	–
Ratio of placental dysfunction markers (sFLT-1/PLGF; 1.5–7)	413 (315.65; 546.43)	NA	–	219.79 (80.9; 289.9)	NA	–
Platelet level (150–400 × 10 ⁹ c/L)	129 (102.5; 185)	246 (190.5; 269)	0.01	233 (219; 254.5)	233.5 (192; 287.7)	1
ALT level (0–40 u/L)	64.3 (22.15; 91.22)	NA	–	22.6 (20; 28.65)	NA	–
AST level (0–40 u/L)	37.4 (24; 48.37)	NA	–	28.3 (22.6; 32.95)	NA	–
Birth weight, grams	826.17 (590; 1068.5)	VLBW	–	2725 (2495; 2774.5)	3325 (2892.5; 3401.2)	0.1

Note: EPE is early-onset preeclampsia; LPE is late-onset preeclampsia; NA here means “not analyzed”; VLBW is very low birth weight; The median (Me) and quartiles Q_1 , Q_3 in the format Me (Q_1 – Q_3) were used in the case of non-normal distribution.

$p = 0.009$, respectively) in the placenta in early-onset and late-onset PE. Their conjugated forms approximately correspond to the molecular weights of fragments detected in exosomes. Meanwhile, the expression of conjugated UBC9 (~53–55 kDa; $p = 0.04$) is significantly reduced only in late-onset PE relative to the comparison group of the corresponding gestational age (Fig. 4 A–D).

Correlation of exosomal SUMO 1–4, UBC9 and hnRNPA2/B1 expression with clinical assessments of pregnant women screening. Predictive ability

Considering the significant change in the expression of the studied proteins in exosomes, we assessed the relationship of these changes with the indices of combined prenatal screening of the first trimester in pregnant women with manifestations of

early and late forms of PE using the Spearman nonparametric rank correlation method (Table 3).

The exosomal SUMO 1 levels ($r = 0.59$; $p = 0.01$), SUMO 2/3/4 ($r = 0.54$; $p = 0.02$), and hnRNPA2/B1 ($r = 0.75$; $p = 0.0001$) were significantly correlated with the pulsation index of the uterine artery of pregnant women with early-onset PE. Whereas the UBC9 level is correlated with the mean arterial pressure ($r = 0.53$; $p = 0.03$). Moreover, a high invert correlation of SUMO 2/3/4 ($r = -0.59$; $p = 0.01$) and UBC9 ($r = -0.88$; $p = 0.0001$) with the concentration of PIGF was observed. Interestingly, a correlation was established with the biochemical parameters of combined screening in pregnant women with late-onset PE: the concentration of β -hCG with the exosomal UBC9 ($r = -0.48$; $p = 0.03$) and hnRNPA2/B1 ($r = -0.48$; $p = 0.03$), as well as PAPP-A concentrations with a SUMO 2/3/4 level ($r = -0.60$; $p = 0.006$).

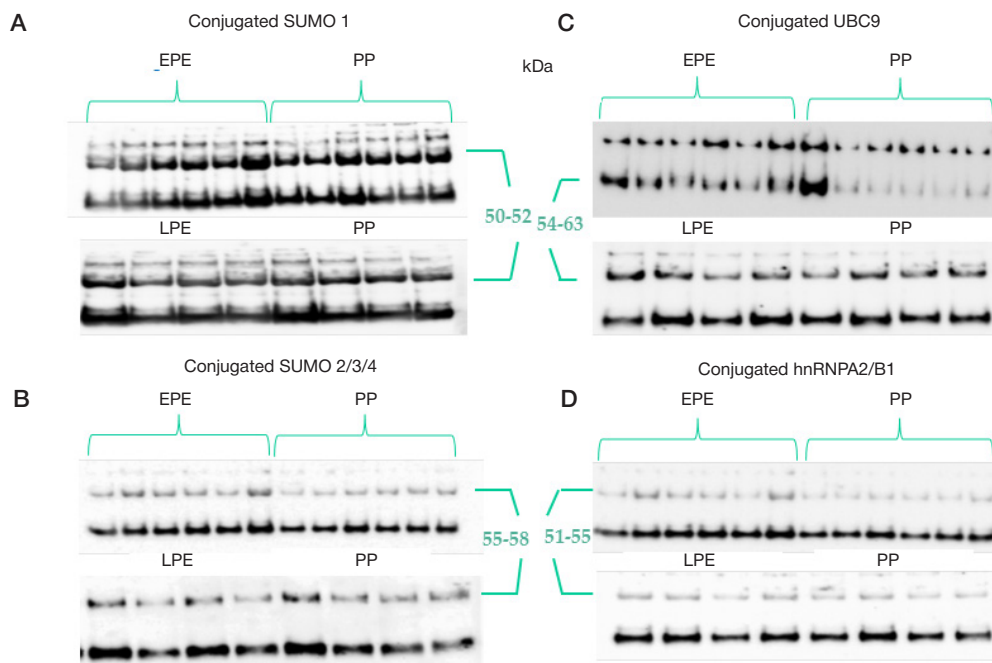


Fig. 2. Western blot of membrane with conjugated exosomal forms of SUMO 1 (A), SUMO 2/3/4 (B), UBC9 (C) and hnRNPA2/B1 (D) in pregnant women with subsequently developed early-onset PE (EPE), late-onset PE (LPE), and physiological pregnancy (PP)

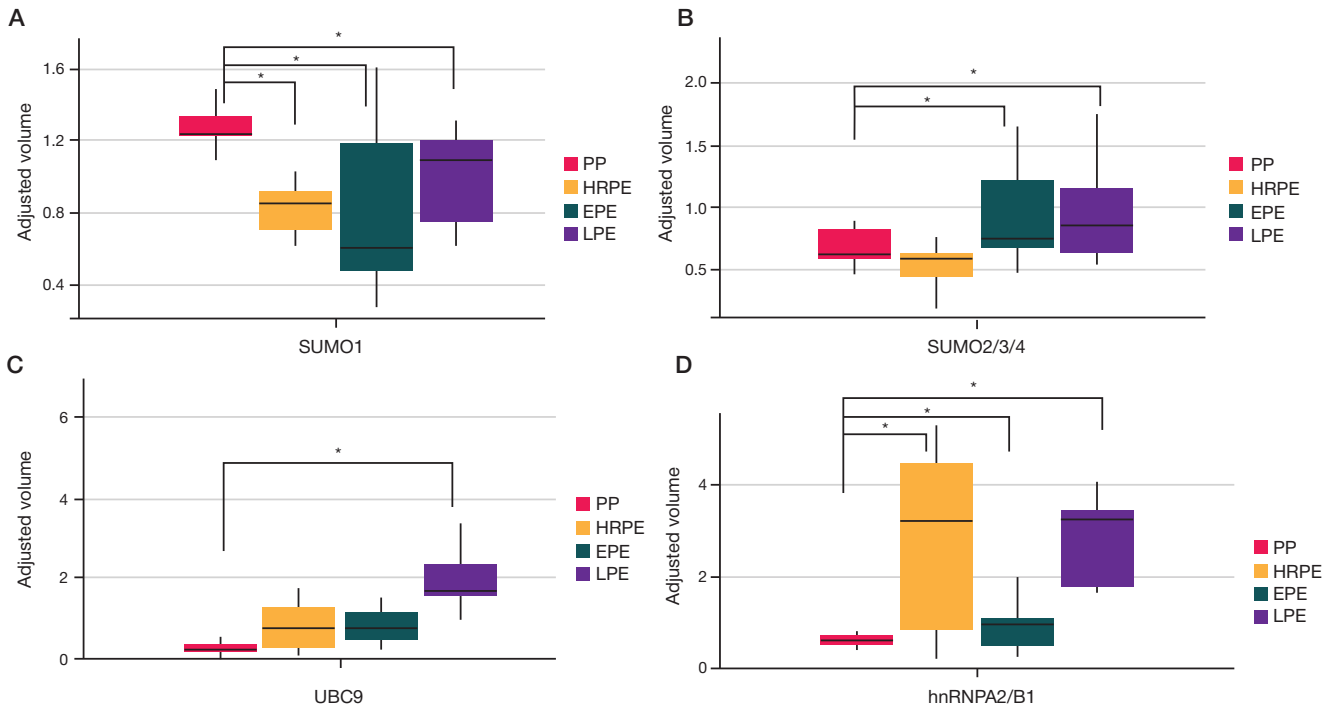


Fig. 3. Comparative analysis of SUMO 1 (A), SUMO 2/3/4 (B), UBC9 (C) and hnRNPA2/B1 (D) expression in exosomes in pregnant women with physiological pregnancy (PP), who subsequently developed early-onset PE (EPE), late-onset PE (LPE), and high risk of PE (HRPE). Total densitometry of proteins was quantified and normalized to loading control sample. Data presented in the format Me (Q₁; Q₃); *: significance level $p \leq 0.05$ when compared with PP

The logistic regression models were created with the view to assess the possibility of using exosomal SUMO 1–4, UBC9 and hnRNPA2/B1 as potential predictors of the development of PE in early pregnancy (Fig. 5 A–D, Table 4).

ROC curves for logistic models are represented by various combinations, among which significant ones were chosen (the formulas for them are given below the Table 4). Importantly, the selected models also make it possible to differentiate pregnant women at high risk of developing PE according to the combined

prenatal screening of the first trimester from pregnant women with PE and pregnant women with a normal pregnancy.

DISCUSSION

The progress of a successful pregnancy is based on the mechanism of communication between the fetoplacental and maternal compartments, which is carried out through the release of bioactive molecules and extracellular vesicles

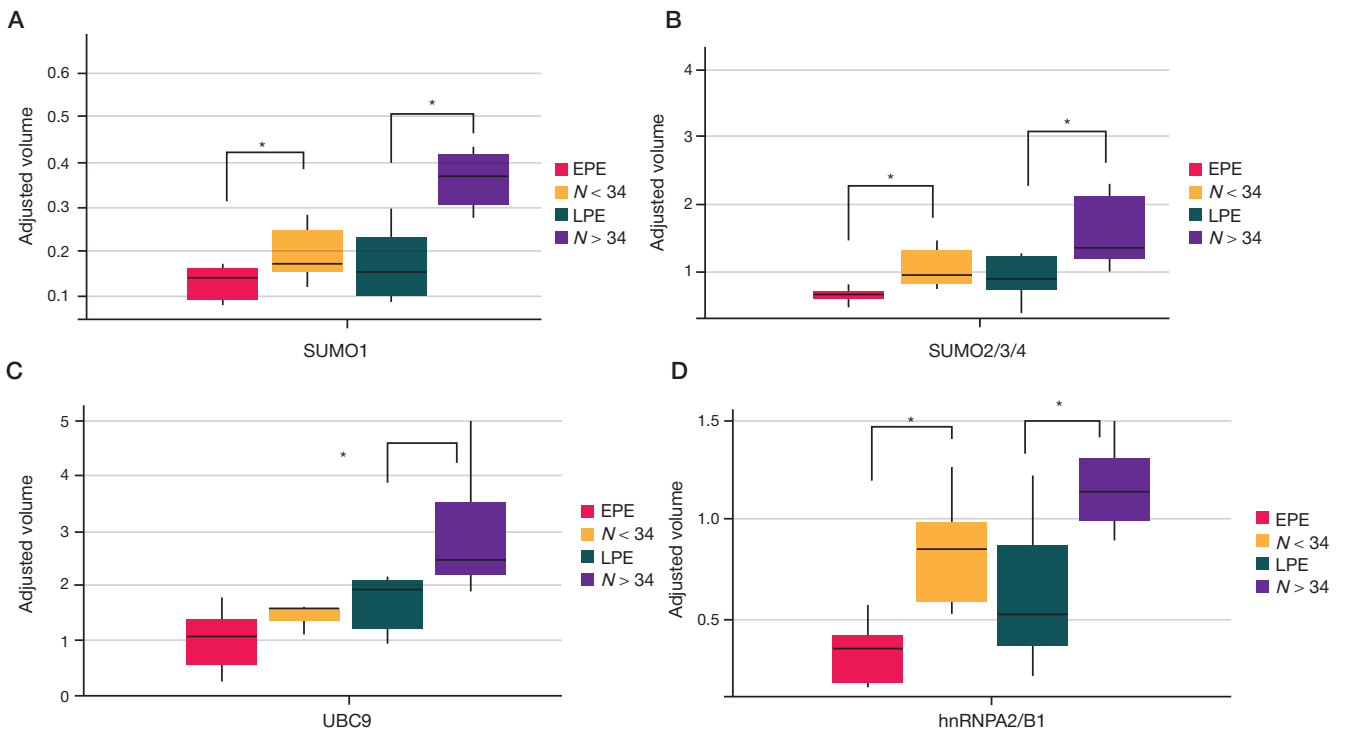


Fig. 4. Comparative analysis of SUMO 1 (A), SUMO 2/3/4 (B), UBC9 (C) and hnRNPA2/B1 (D) expression in placental tissue in pregnant women with early-onset (EPE) and late-onset (LPE) PE, and age-matched controls ($N < 34$, $N > 34$). Total densitometry of proteins was quantified and normalized to loading control actin. Data presented in the format Me (Q₁; Q₃); *: significance level $p \leq 0.05$ when compared with age-matched controls

Table 3. The results of a correlation of protein expression in exosomes with indices of combined prenatal screening of pregnant women with early-onset and late-onset PE

Parameter	SUMO 1		SUMO 2/3/4		UBC9		hnRNPA2/B1	
	<i>r</i> *	<i>p</i> **						
Early-onset PE								
Mean arterial pressure, MoM	ns	ns	ns	ns	0.53	0.03	ns	ns
PI UtA, MoM	0.59	0.01	0.54	0.02	ns	ns	0.75	0.0001
PIGF	ns	ns	-0.59	0.01	-0.88	0.0001	ns	ns
Late-onset PE								
β-hCG, MoM	ns	ns	ns	ns	-0.48	0.03	-0.63	0.004
PAPP-A, MoM	ns	ns	-0.60	0.006	ns	ns	ns	ns

Note: * *r* is a Spearman rank correlation coefficient; ** *p* is the statistical significance of correlation; Ns is not statistically significant.

reflecting the pathophysiological state of donor cells and can modulate the functions of target cells [30]. It is known that placental exosomes mediate the adaptation of maternal vessels to pregnancy, and their plasma concentration increases with the progression of pregnancy and correlates with blood flow in the uterine arteries [31]. Such functional uniqueness allows them to be considered as dynamic biomarkers capable of real-time monitoring of placental dysfunction. [32].

An interesting aspect that attracts attention is exosomal content, which determines the bioactivity of exosomes, and its loading is controlled by one of the posttranslational modifications, sumoylation [27]. Reversible conjugation of the small SUMO peptide with target proteins is critical for cell function and various cellular processes, including transcription, DNA repair, cell cycle regulation, chromatin remodeling, nucleocytoplasmic transport, and apoptosis [33]. The expression of SUMO 2 and SUMO 3 isoforms, which are 97% identical to each other, and SUMO 1 by 46%, was found in all eukaryotic cells [19, 34]. Recent discoveries have demonstrated that another isoform, SUMO 4, is expressed in the placenta [35]. At the same time, disorders of sumoylation homeostasis are associated with various pathological conditions [36, 37]. Despite the available

data on the involvement of sumoylation in placental dysfunction [13, 20], there are no data of the exosomal SUMO proteins expression in this pathology.

In the context of the above, we evaluated the SUMO proteins expression in exosomes of pregnant women at 11–14 weeks of gestation (cohort I). It should be noted that we have previously revealed an increase in conjugated SUMO 1–4 and UBC9 expression in exosomes of pregnant women with early-onset PE at the time of delivery [29] and free forms of SUMO 1–4, UBC9 in the placenta in early-onset PE [28]. In the present study, the conjugated SUMO 1 expression in exosomes of pregnant women with early-onset PE at 11–14 weeks of gestation was significantly reduced, while the SUMO 2/3/4 expression was increased relative to normal pregnancy. A similar picture was observed with regard to direction of the conjugated SUMO 1 and SUMO 2/3/4 expression in exosomes in pregnant women with late-onset PE. As previously shown by Baczyk D. et al., the expression pattern of SUMO proteins may be due to their unique spatiotemporal distribution in trophoblast layers during pregnancy, as well as their activity in response to oxidative stress and inflammation. In particular, free SUMO 1 and SUMO 4 are predominantly expressed in cytotrophoblasts

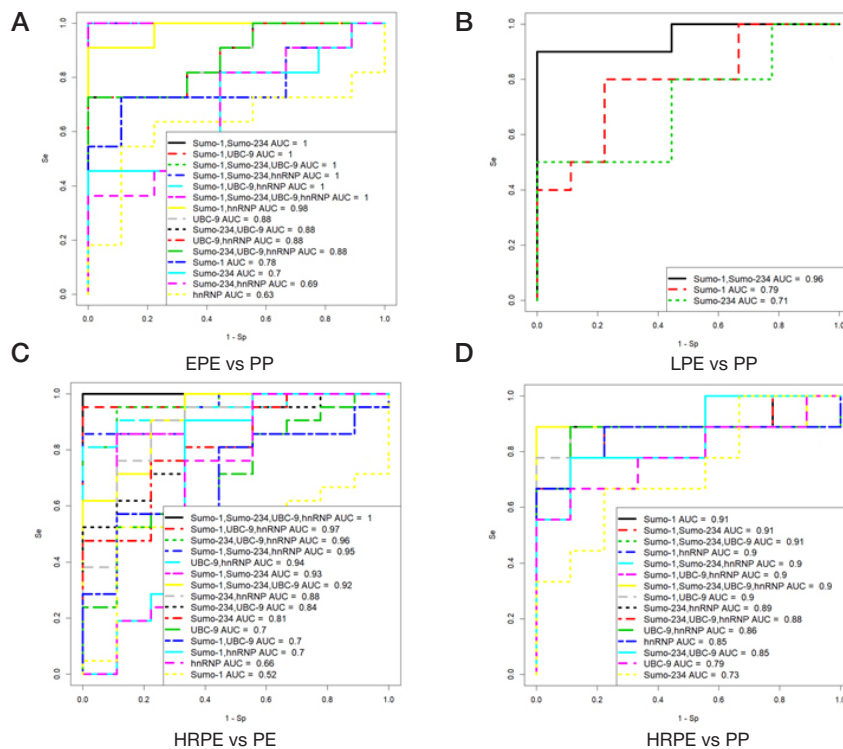


Fig. 5. ROC curves for a logistic model for the risk assessment of PE at early gestation by SUMO 1–4, UBC9 and hnRNPA2/B1 expression in exosomes (A–D). EPE is early-onset PE; LPE is late-onset PE; HRPE is high risk of PE; PP is physiological pregnancy

Table 4. Predictive values with parameters of logistic models for SUMO 1–4, UBC9 and hnRNPA2/B1

	AUC	Sensitivity	Specificity	Cutoff	p-value	Parameters	Formulas
EPE vs. PP							
UBC9	0.88	0.72	1	0.72	0.03	i — 2.65 UBC9 — 6.73	$\frac{1}{1+e^{0.65-6.73x_1}}$
LPE vs. PP							
SUMO 1	0.79	0.8	0.77	0.43	0.05	i — 7.4 SUMO1 — 6.29	$\frac{1}{1+e^{7.4+6.29x_1}}$
HRPE vs. PE							
UBC9; hnRNPA2/B1	0.94	0.80	1	0.79	0.02/0.01	i — 0.18 UBC9 — 6.23 hnRNPA2/B1 — 2.19	$\frac{1}{1+e^{0.18-6.23x_1+2.19x_2}}$
HRPE vs. PP							
SUMO 1	0.91	0.88	1	0.58	0.02	i — 9.78 SUMO1 — 9.073	$\frac{1}{1+e^{9.78+9.073x_1}}$

Note: EPE is early-onset PE; LPE is late-onset PE; HRPE is high risk of PE; PP is physiological pregnancy; AUC is area under curve.

in the first and second trimesters of pregnancy, with a shift to the syncytiotrophoblast in the third trimester. In particular, free SUMO 1 and SUMO 4 are predominantly expressed in cytotrophoblasts in the first and second trimesters of pregnancy, with a shift to the syncytiotrophoblast in the third trimester. SUMO 2/3 stable expression throughout the trophoblast layer during pregnancy. However, the activity and redistribution of SUMO 1 and SUMO 4 into syncytium from the cytotrophoblast is observed in response to hypoxic/oxidative stress, and the SUMO 2/3 expression increases during inflammatory stress [38]. It is noteworthy that the results of our study, in general, are consistent with the above data of Baczyk D. et al., demonstrating multidirectional activation of the expression of exosomal conjugated SUMO 1 and SUMO 2/3/4 in response to cellular stress in placental dysfunction. Nevertheless, the all SUMO isoforms expression and respectively their subsequent secretion should increase in cells under the influence of various stress stimuli. However, SUMO 1 expression in exosomes was reduced in both early-onset and late-onset PE in our study. Previously, Saitoh H. et al. found a decrease in pool of the SUMO 2/3 free in cells and the accumulation of its high molecular weight conjugates in response to cellular stress, in contrast to SUMO 1 [39]. Taking into account these data, we hypothesized that hypoxic and oxidative stress that occurs with early placental dysfunction activates the SUMO 2/3 free to form a large number of conjugates with target proteins and induce stress-sensitive signaling cascades through exosomes. Whereas, SUMO 1 is able to selectively conjugate to targets in response to stress. This is evidenced by a decrease in the expression of its conjugated form in exosomes. Interestingly, we did not find free forms of these proteins in exosomes. And the molecular weight of the conjugated forms, presumably, conforms to the total weight of their free form with UBC9. Moreover, the conjugated UBC9 expression was also significantly increased only in late-onset PE relative to normal pregnancy. It should be noted that UBC9 is the only enzyme that conjugates SUMO 1–4 with target proteins, in contrast to the ubiquitination system [19]. Therefore, its expression level is critical for sumoylation. Based on the previously demonstrated spatiotemporal distribution of SUMO 1–4 in trophoblast cells (38), we suggested a certain specificity of UBC9 conjugation with SUMO 1 and SUMO 2/3 in the context of their subcellular targets. Even more so, evidence of its different immunoreactivity with SUMO proteins has already been obtained on model objects depending on the cell population [40].

Sumoylation is known to modulate the transcriptional activity and localization of many nuclear [41] and cytoplasmic proteins

(42), thereby regulating a wide range of biological processes. And certain interest is the recent discovery of the sumoylation of the heterogeneous nuclear ribonucleoprotein (hnRNPs) family members, which provides a universal mechanism for regulating their RNA-binding activity and subsequent selective sorting of transcripts into exosomes [27, 43]. Sumoylation of hnRNPA2/B1 by SUMO 1 is a necessary condition for its binding to specific miRNA exomotifs and their subsequent loading into exosomes. At the same time, inhibition of sumoylation can impair protein binding to miRNA. In our previous study, exomotifs of a number of microRNAs sensitive to hypoxia were identified, and their expression correlated with the of SUMO 2/3/4 level in the placenta of pregnant women with early-onset PE [29]. Based on this relationship, we assessed the hnRNPA2/B1 expression. It was significantly increased in exosomes of pregnant women with late-onset PE at 11–14 weeks, similarly to UBC9. Since hnRNPA2/B1 is a SUMO substrate [44], it is likely that its expression in exosomes may also be regulated by SUMO 2/3/4, if the level of SUMO 1 is reduced. Moreover, providing the specificity of UBC9 conjugation, it may be suppose that the hnRNPA2/B1 expression is activated by conjugation with UBC9 in late-onset PE. And this is necessary for loading microRNAs into exosomes that regulate targets associated with vascular dysfunction. It is worth noting no less interesting results on protein expression in pregnant women with a high risk of developing PE according to the combined prenatal screening of the first trimester. Despite the presence of markers of placental dysfunction, the outcome of their pregnancies was favorable. However, the direction of the conjugated SUMO 1, UBC9 and hnRNPA2/B1 expression coincided with that in early-onset and late-onset PE, the exclusion of SUMO 2/3/4, the level of which did not change.

Considering the revealed changes in the expression of conjugated proteins in the exosomes of pregnant women with PE at 11–14 weeks of gestation, it seemed interesting to evaluate their expression in the placenta of pregnant women with early-onset and late-onset PE (cohort II). In the placenta, we found a decrease in the conjugated SUMO 1–4 and hnRNPA2/B1 expression in both early-onset and late-onset PE. And the level of UBC9 significantly decreases only in late-onset PE. The results were unexpected, just as intriguing. As noted earlier, the process of sumoylation, being the most important regulator of the cellular response to stress, includes an increase in the level of high-molecular-weight SUMO conjugates, as well as free forms. Moreover, a previous study found an increase in SUMO free in early-onset PE [28]. Such multidirectional

expression of free and conjugated forms of the studied proteins in the placenta may be explained by the fact that free forms are expressed exclusively in response to stressful stimuli, performing an adaptive function. While, the formation of SUMO conjugates is necessary to trigger regulatory cascades. Thereby, the change in their expression depends on what is needed at a given time — sumoylation or desumoylation of the target protein. Our assumption has been confirmed in a number of studies. In particular, Bhattacharjee J. et al. demonstrated that the level of SUMO free increases in early pregnancy (9–10 weeks), and this coincides with physiological placental hypoxia. However, overexpression of the SUMO 2/3 can inhibit the activity of HIF 1A (hypoxia inducible factor) at 10–12 weeks of gestation. In order to preserve the stability of latter, the SENP 3 desumoylation protein reduces the expression of SUMO 2/3 [45]. Other authors provide evidence for the role of the SENP 1 desumoylation protein in endothelial cells as a positive regulator of hypoxia-induced VEGF expression and angiogenesis [46, 47]. With regard to placental dysfunction, changes in GCM-1 expression induced by hypoxia and regulated by the p45 NF-E2 transcription factor [48] are associated, among other things, with desumoylation [49,50]. It is important to note that factors that increase global sumoylation do not necessarily lead to changes in sumoylation of all SUMO substrates. Sumoylation of individual proteins occurs in a substrate-specific manner and often without global changes [51].

The discovery of placental factors has contributed to a surge in research on their use as biomarkers for diagnosing and predicting the risk of developing PE and FGR since 2003 [52]. However, the most reliable results were obtained when predicting the early-onset PE. Researchers attribute this to the fact that a change in their level is a reflection of syncytiotrophoblast stress, that is, placental dysfunction in general, and not a biomarker of PE [53]. In addition, the provided diagnostically significant level of pro- and anti-angiogenic factors circulating in the mother's blood can be achieved at the onset of a pathological condition, and not at the initial stage of impaired endovascular invasion of spiral arteries by trophoblast [54]. In this regard, it is necessary to look for specific markers. Interestingly, a decrease in angiogenic PLGF and an increase in anti-angiogenic sFlt-1 during the third trimester correlate with changes in the redistribution of SUMO 1 and SUMO 4 from the cytotrophoblast to the syncytium. The given type of placental cell is the only which directly contacts with the maternal circulation [38]. As previously reported, we found a correlation between changes in miR-423-3p, miR-652-3p expression, the level of SUMO 2/3/4, UBC9 in the placenta and a decrease in the concentration of PLGF in the blood of pregnant women with early-onset PE at the time of delivery [28]. Based on the results, a search was made for correlations with indices of combined prenatal screening of pregnant women in the first trimester. An increased level of exosomal SUMO 2/3/4 and UBC9 correlated inversely with the PLGF in the blood serum of pregnant women in the early gestation, that is in good agreement with our previous data. Moreover, the relationship confirms the regulation of placental factor through

sumoylation and indicates the specificity of SUMO 2/3/4 and UBC9 in relation to PLGF. Interestingly, this relationship was revealed only for the early-onset PE. It is noteworthy that, beyond the association with the placental factor, significant correlations were found the expression of all conjugated SUMO isoforms and hnRNPA2/B1 with the uterine artery pulsation index. And UBC9 correlated with mean arterial pressure. The highlight was an increased level of SUMO 2/3/4 was inversely correlated with PAPP-A, while UBC9 and hnRNPA2/B1 were inversely correlated with the concentration of β -hCG in the late-onset PE. At the same time, no correlation was found between SUMO 1 and any of the indices. Low concentrations of β -hCG and PAPP-A in the first trimester of pregnancy are associated with the risk of developing PE and FGR [55–57].

Given the correlation results, as well as the lack of data on the predictive potential of SUMO modifications, we created logistic regression models with ROC-curves to assess the possibility of using the studied exosomal proteins as potential predictors of the risk of developing PE. Significant coefficients were determined for UBC9 (AUC = 0.88; Se-0.72; Sp-1) in early-onset PE prediction model, and for SUMO 1 (AUC = 0.79; Se-0.8; Sp-0.77) in late-onset PE. In addition, it is possible to differentiate pregnant women with a high risk of developing PE from pregnant women with PE and with physiological pregnancy based on the assessment of UBC9, hnRNPA2/B1 expression (AUC = 0.94; Se-0.80; Sp-1) and SUMO 1 (AUC = 0.91; Se-0.88; Sp-1), respectively. We payed attention to SUMO 2/3/4 did not reach a significant level in any of the models. Nevertheless, the results suggest a differential specificity of UBC9 and SUMO 1 in the pathogenesis of PE subtypes, as well as a different functional role of SUMO proteins in placental dysfunction in general, that is important for a preventive therapeutic strategy. Undoubtedly, the use of predictive models will require subsequent validation in a large cohort of pregnant women with relevant clinical outcomes, including isolated PE and FGR.

CONCLUSIONS

The primary value of this research is that it opens up several avenues for predicting conditions associated with placental dysfunction based on the study of the exosomal contents sumoylation pattern. This is the first data on the exosomal expression of conjugated SUMO 1–4, as well as UBC9 and hnRNPA2/B1 that differentially change in early gestation in pregnant women with PE. The possibility of predicting this pathology may be due to the functional specificity of SUMO isoforms, as well as the conjugation/deconjugation mechanism that coordinates the signaling pathways. It is worth noting that our study has limitations due to the small cohorts. We brought this to our attention because the validation of predictive models requires an expansion of the pregnant women cohort. Moreover, we did not evaluate desumoylating protein expression in exosomes. But this is rather seen as a prospect for future research, as well as the study of the SUMO substrates involved in the regulation of placental dysfunction.

References

1. Ilekis JV, Tsilou E, Fisher S, et al. Placental origins of adverse pregnancy outcomes: potential molecular targets: an Executive Workshop Summary of the Eunice Kennedy Shriver National Institute of Child Health and Human Development. *American Journal of Obstetrics and Gynecology*. 2016; 215 (1): S1–S46.
2. Rana S, Lemoine E, Granger JP, Karumanchi SA. Preeclampsia: pathophysiology, challenges, and perspectives. 2019; *Circ Res*. 124 (7): 1094–112.
3. Staff AC. The two-stage placental model of preeclampsia: An update. *Journal of Reproductive Immunology*. 2019; 134–35: 1–10.

4. Tenório MB, Ferreira RC, Moura FA, Bueno NB, de Oliveira ACM, Goulart MOF. Cross-Talk between Oxidative Stress and Inflammation in Preeclampsia. *Oxidative Medicine and Cellular Longevity*. 2019; 2019: 1–26.
5. Melchiorre K, Giorgione V, Thilaganathan B. The placenta and preeclampsia: villain or victim? *American Journal of Obstetrics and Gynecology*. 2022; 226 (2): S954–S962.
6. Chen CW, Jaffe IZ, Karumanchi SA. Pre-eclampsia and cardiovascular disease. *Cardiovascular Research*. 2014; 101 (4): 579–86.
7. Ritz E, Amann K, Koleganova N, Benz K. Prenatal programming—effects on blood pressure and renal function. *Nat Rev Nephrol*. 2011; 7 (3): 137–44.
8. Poon LC, Shennan A, Hyett JA, et al. The International Federation of Gynecology and Obstetrics (FIGO) initiative on preeclampsia: a pragmatic guide for first-trimester screening and prevention. *Int J Gynecol Obstet*. 2019; 145 (S1): 1–33.
9. ACOG. *Obstetrics & Gynecology*. 2019; 133 (1): 1–1.
10. Yagel S, Cohen SM, Goldman-Wohl D. An integrated model of preeclampsia: a multifaceted syndrome of the maternal cardiovascular-placental-fetal array. *American Journal of Obstetrics and Gynecology*. 2022; 226 (2): S963–S972.
11. Gobble RM, Groesch KA, Chang M, Torry RJ, Torry DS. Differential regulation of human PlGF gene expression in trophoblast and nontrophoblast cells by oxygen tension. *Placenta*. 2009; 30 (10): 869–75.
12. Chang M, Mukherjee D, Gobble RM, Groesch KA, Torry RJ, Torry DS. Glial cell missing regulates Placental Growth Factor (PGF) gene transcription in human trophoblast. *Biology of Reproduction*. 2008; 78 (5): 841–51.
13. Baczyk D, Kibschull M, Mellstrom B, et al. DREAM mediated regulation of GCM1 in the human placental trophoblast. *PLoS ONE*. 2013; 8 (1): e51837.
14. Chou C-C, Chang C, Liu J-H, Chen L-F, Hsiao C-D, Chen H. Small ubiquitin-like modifier modification regulates the DNA binding activity of glial cell missing Drosophila Homolog a. *Journal of Biological Chemistry*. 2007; 282 (37): 27239–49.
15. Enserink JM. Sumo and the cellular stress response. *Cell Div*. 2015; 10 (1): 4.
16. He J, Cheng J, Wang T. SUMOylation-Mediated Response to Mitochondrial Stress. *IJMS*. 2020; 21 (16): 5657.
17. Kunz K, Wagner K, Mendler L, Hölper S, Dehne N, Müller S. SUMO signaling by hypoxic inactivation of SUMO-specific isopeptidases. *Cell Reports*. 2016; 16 (11): 3075–86.
18. Karhausen J, Ulloa L, Yang W. SUMOylation connects cell stress responses and inflammatory control: lessons from the gut as a model organ. *Front Immunol*. 2021; 12: 646633.
19. Chang H-M, Yeh ETH. SUMO: from bench to bedside. *Physiological Reviews*. 2020; 100 (4): 1599–619.
20. Baczyk D, Drewlo S, Kingdom JCP. Emerging role of SUMOylation in placental pathology. *Placenta*. 2013; 34 (7): 606–12.
21. Kondoh K, Akahori H, Muto Y, Terada T. Identification of key genes and pathways associated with preeclampsia by a WGCNA and an evolutionary approach. *Genes*. 2022; 13 (11): 2134.
22. Gurung S, Perocheau D, Touramanidou L, Baruteau J. The exosome journey: from biogenesis to uptake and intracellular signalling. *Cell Commun Signal*. 2021; 19 (1): 47.
23. Robbins PD, Morelli AE. Regulation of immune responses by extracellular vesicles. *Nat Rev Immunol*. 2014; 14 (3): 195–208.
24. Salomon C, Kobayashi M, Ashman K, Sobrevia L, Mitchell MD, Rice GE. Hypoxia-induced changes in the bioactivity of cytotrophoblast-derived exosomes. *PLoS ONE*. 2013; 8 (11): e79636.
25. Tannetta DS, Dragovic RA, Gardiner C, Redman CW, Sargent IL. Characterisation of syncytiotrophoblast vesicles in normal pregnancy and pre-eclampsia: expression of Fit-1 and Endoglin. *PLoS ONE*. 2013; 8 (2): e56754.
26. Salomon C, Guanzone D, Scholz-Romero K, et al. Placental exosomes as early biomarker of preeclampsia: potential role of exosomal microRNAs across gestation. *The Journal of Clinical Endocrinology & Metabolism*. 2017; 102 (9): 3182–94.
27. Villarroya-Beltri C, Gutiérrez-Vázquez C, Sánchez-Cabo F, et al. Sumoylated hnRNP A2B1 controls the sorting of miRNAs into exosomes through binding to specific motifs. *Nat Commun*. 2013; 4 (1): 2980.
28. Gusar VA, Timofeeva AV, Chagovets VV, Kan NE, Ivanets TYu, Sukhikh GT. Regulation of the placental growth factor mediated by sumoylation and expression of miR-652-3p in pregnant women with early-onset preeclampsia. *Bull Exp Biol Med*. 2022; 174 (1): 174–8.
29. Gusar V, Timofeeva A, Chagovets V, et al. Diagnostic potential of exosomal hypoxamiRs in the context of hypoxia–sumoylation–hypoxamiRs in early onset preeclampsia at the preclinical stage. *Life*. 2022; 12 (1): 101.
30. Chiarello DI, Salsoso R, Toledo F, Mate A, Vázquez CM, Sobrevia L. Foetoplacental communication via extracellular vesicles in normal pregnancy and preeclampsia. *Molecular Aspects of Medicine*. 2018; 60: 69–80.
31. Salomon C, Torres MJ, Kobayashi M, et al. A Gestational Pprofile of placental exosomes in maternal plasma and their effects on endothelial cell migration. *PLoS ONE*. 2014; 9 (6): e98667.
32. Tannetta D, Collett G, Vatish M, Redman C, Sargent I. Syncytiotrophoblast extracellular vesicles — Circulating biopsies reflecting placental health. *Placenta*. 2017; 52: 134–8.
33. Hendriks IA, D'Souza RCJ, Yang B, Verlaan-de Vries M, Mann M, Vertegeal ACO. Uncovering global SUMOylation signaling networks in a site-specific manner. *Nat Struct Mol Biol*. 2014; 21 (10): 927–36.
34. Hay RT. SUMO. *Molecular Cell*. 2005; 18 (1): 1–12.
35. Baczyk D, Audette MC, Drewlo S, Levytska K, Kingdom JC. SUMO-4: a novel functional candidate in the human placental protein SUMOylation machinery. *PLoS ONE*. 2017; 12 (5): e0178056.
36. Anderson DB, Wilkinson KA, Henley JM. Protein SUMOylation in neuropathological conditions. *Drug News & Perspectives*. 2009; 22 (5): 255.
37. Bawa-Khalife T, Yeh ETH. SUMO losing balance: SUMO proteases disrupt SUMO homeostasis to facilitate cancer development and Progression. *Genes & Cancer*. 2010; 1 (7): 748–52.
38. Baczyk D, Audette MC, Coyaud E, Raught B, Kingdom JC. Spatiotemporal distribution of small ubiquitin-like modifiers during human placental development and in response to oxidative and inflammatory stress: Placental distribution of small ubiquitin-like modifiers. *J Physiol*. 2018; 596 (9): 1587–600.
39. Saitoh H, Hinchey J. Functional heterogeneity of small ubiquitin-related protein modifiers SUMO-1 versus SUMO-2/3. *Journal of Biological Chemistry*. 2000; 275 (9): 6252–8.
40. Hasegawa Y, Yoshida D, Nakamura Y, Sakakibara S. Spatiotemporal distribution of SUMOylation components during mouse brain development: Sumo-ylation during brain development. *J Comp Neurol*. 2014; 522 (13): 3020–36.
41. Chalkiadaki A, Talianidis I. SUMO-dependent compartmentalization in promyelocytic leukemia protein nuclear bodies prevents the access of LRF-1 to chromatin. *Molecular and Cellular Biology*. 2005; 25 (12): 5095–105.
42. Snider NT, Omary MB. Post-translational modifications of intermediate filament proteins: mechanisms and functions. *Nat Rev Mol Cell Biol*. 2014; 15 (3): 163–77.
43. Vassileva MT, Matunis MJ. SUMO modification of heterogeneous nuclear ribonucleoproteins. *Molecular and Cellular Biology*. 2004; 24 (9): 3623–32.
44. Vertegeal ACO, Ogg SC, Jaffray E, et al. A Proteomic study of SUMO-2 target proteins. *Journal of Biological Chemistry*. 2004; 279 (32): 33791–8.
45. Bhattacharjee J, Alahari S, Sallais J, Tagliaferro A, Post M, Caniggia I. Dynamic regulation of HIF1A stability by SUMO2/3 and SENP3 in the human placenta. *Placenta*. 2016; 40: 8–17.
46. Xu Y, Zuo Y, Zhang H, et al. Induction of SENP1 in endothelial cells contributes to hypoxia-driven VEGF expression and angiogenesis. *Journal of Biological Chemistry*. 2010; 285 (47): 36682–8.
47. Zhou HJ, Xu Z, Wang Z, et al. SUMOylation of VEGFR2 regulates its intracellular trafficking and pathological angiogenesis. *Nat Commun*. 2018; 9 (1): 3303.
48. McCaig D, Lyall F. Hypoxia upregulates GCM1 in human placenta explants. hypertension in pregnancy. 2009; 28 (4): 457–72.
49. Kohli S, Hoffmann J, Lochmann F, et al. p45 NF-E2 regulates syncytiotrophoblast differentiation by post-translational GCM1 modifications in human intrauterine growth restriction. *Cell Death Dis*. 2017; 8 (4): e2730–e2730.

50. Chang C-W, Chang G-D, Chen H. A novel cyclic AMP/Epac1/CaMKI signaling cascade promotes GCM1 desumoylation and placental cell fusion. *Molecular and Cellular Biology*. 2011; 31 (18): 3820–31.
51. Luo J, Ashikaga E, Rubin PP, et al. Receptor trafficking and the regulation of synaptic plasticity by SUMO. *Neuromol Med*. 2013; 15 (4): 692–706.
52. Maynard SE, Min J-Y, Merchan J, et al. Excess placental soluble fms-like tyrosine kinase 1 (sFlt1) may contribute to endothelial dysfunction, hypertension, and proteinuria in preeclampsia. *J Clin Invest*. 2003; 111 (5): 649–58.
53. Redman CWG, Staff AC. Preeclampsia, biomarkers, syncytiotrophoblast stress, and placental capacity. *American Journal of Obstetrics and Gynecology*. 2015; 213 (4): S9.e1–S9.e4.
54. Dymara-Konopka W, Laskowska M, Grywalska E, Hymos A, Błażewicz A, Leszczyńska-Gorzela B. Similar pro- and antiangiogenic profiles close to delivery in different clinical presentations of two pregnancy syndromes: preeclampsia and fetal growth restriction. *IJMS*. 2023; 24 (2): 972.
55. Keikkala E, Vuorela P, Laivuori H, Romppanen J, Heinonen S, Stenman U-H. First trimester hyperglycosylated human chorionic gonadotrophin in serum — a marker of early-onset preeclampsia. *Placenta*. 2013; 34 (11): 1059–65.
56. Morris RK, Bilagi A, Devani P, Kilby MD. Association of serum PAPP-A levels in first trimester with small for gestational age and adverse pregnancy outcomes: systematic review and meta-analysis: Systematic review association serum PAPP-A and adverse pregnancy outcome. *Prenat Diagn*. 2017; 37 (3): 253–65.
57. Krantz D, Goetzl L, Simpson JL, et al. Association of extreme first-trimester free human chorionic gonadotropin-β, pregnancy-associated plasma protein A, and nuchal translucency with intrauterine growth restriction and other adverse pregnancy outcomes. *American Journal of Obstetrics and Gynecology*. 2004; 191 (4): 1452–8.

Литература

1. Ilekis JV, Tsilou E, Fisher S, et al. Placental origins of adverse pregnancy outcomes: potential molecular targets: an Executive Workshop Summary of the Eunice Kennedy Shriver National Institute of Child Health and Human Development. *American Journal of Obstetrics and Gynecology*. 2016; 215 (1): S1–S46.
2. Rana S, Lemoine E, Granger JP, Karumanchi SA. Preeclampsia: pathophysiology, challenges, and perspectives. 2019; *Circ Res*. 124 (7): 1094–1112.
3. Staff AC. The two-stage placental model of preeclampsia: An update. *Journal of Reproductive Immunology*. 2019; 134–135: 1–10.
4. Tenório MB, Ferreira RC, Moura FA, Bueno NB, de Oliveira ACM, Goulart MOF. Cross-Talk between Oxidative Stress and Inflammation in Preeclampsia. *Oxidative Medicine and Cellular Longevity*. 2019; 2019: 1–26.
5. Melchiorre K, Giorgione V, Thilaganathan B. The placenta and preeclampsia: villain or victim? *American Journal of Obstetrics and Gynecology*. 2022; 226 (2): S954–S962.
6. Chen CW, Jaffe IZ, Karumanchi SA. Pre-eclampsia and cardiovascular disease. *Cardiovascular Research*. 2014; 101 (4): 579–86.
7. Ritz E, Amann K, Koleganova N, Benz K. Prenatal programming—effects on blood pressure and renal function. *Nat Rev Nephrol*. 2011; 7 (3): 137–44.
8. Poon LC, Shennan A, Hyett JA, et al. The International Federation of Gynecology and Obstetrics (FIGO) initiative on preeclampsia: a pragmatic guide for first-trimester screening and prevention. *Int J Gynecol Obstet*. 2019; 145 (S1): 1–33.
9. ACOG. *Obstetrics & Gynecology*. 2019; 133 (1): 1–1.
10. Yagel S, Cohen SM, Goldman-Wohl D. An integrated model of preeclampsia: a multifaceted syndrome of the maternal cardiovascular-placental-fetal array. *American Journal of Obstetrics and Gynecology*. 2022; 226 (2): S963–S972.
11. Gobble RM, Groesch KA, Chang M, Torry RJ, Torry DS. Differential regulation of human PIGF gene expression in trophoblast and nontrophoblast cells by oxygen tension. *Placenta*. 2009; 30 (10): 869–75.
12. Chang M, Mukherjee D, Gobble RM, Groesch KA, Torry RJ, Torry DS. Glial cell missing regulates Placental Growth Factor (PGF) gene transcription in human trophoblast. *Biology of Reproduction*. 2008; 78 (5): 841–51.
13. Baczyk D, Kibschull M, Mellstrom B, et al. DREAM mediated regulation of GCM1 in the human placental trophoblast. *PLoS ONE*. 2013; 8 (1): e51837.
14. Chou C-C, Chang C, Liu J-H, Chen L-F, Hsiao C-D, Chen H. Small ubiquitin-like modifier modification regulates the DNA binding activity of glial cell missing *Drosophila* Homolog a. *Journal of Biological Chemistry*. 2007; 282 (37): 27239–49.
15. Enserink JM. Sumo and the cellular stress response. *Cell Div*. 2015; 10 (1): 4.
16. He J, Cheng J, Wang T. SUMOylation-Mediated Response to Mitochondrial Stress. *IJMS*. 2020; 21 (16): 5657.
17. Kunz K, Wagner K, Mendler L, Hölper S, Dehne N, Müller S. SUMO signaling by hypoxic inactivation of SUMO-specific isopeptidases. *Cell Reports*. 2016; 16 (11): 3075–86.
18. Karhausen J, Ulloa L, Yang W. SUMOylation connects cell stress responses and inflammatory control: lessons from the gut as a model organ. *Front Immunol*. 2021; 12: 646633.
19. Chang H-M, Yeh ETH. SUMO: from bench to bedside. *Physiological Reviews*. 2020; 100 (4): 1599–619.
20. Baczyk D, Drewlo S, Kingdom JCP. Emerging role of SUMOylation in placental pathology. *Placenta*. 2013; 34 (7): 606–12.
21. Kondoh K, Akahori H, Muto Y, Terada T. Identification of key genes and pathways associated with preeclampsia by a WGCNA and an evolutionary approach. *Genes*. 2022; 13 (11): 2134.
22. Gurung S, Perocheau D, Touramanidou L, Baruteau J. The exosome journey: from biogenesis to uptake and intracellular signalling. *Cell Commun Signal*. 2021; 19 (1): 47.
23. Robbins PD, Morelli AE. Regulation of immune responses by extracellular vesicles. *Nat Rev Immunol*. 2014; 14 (3): 195–208.
24. Salomon C, Kobayashi M, Ashman K, Sobrevia L, Mitchell MD, Rice GE. Hypoxia-induced changes in the bioactivity of cytotrophoblast-derived exosomes. *PLoS ONE*. 2013; 8 (11): e79636.
25. Tannetta DS, Dragovic RA, Gardiner C, Redman CW, Sargent IL. Characterisation of syncytiotrophoblast vesicles in normal pregnancy and pre-eclampsia: expression of Flt-1 and Endoglin. *PLoS ONE*. 2013; 8 (2): e56754.
26. Salomon C, Guanzon D, Scholz-Romero K, et al. Placental exosomes as early biomarker of preeclampsia: potential role of exosomal microRNAs across gestation. *The Journal of Clinical Endocrinology & Metabolism*. 2017; 102 (9): 3182–94.
27. Villarroya-Beltri C, Gutiérrez-Vázquez C, Sánchez-Cabo F, et al. Sumoylated hnRNPA2B1 controls the sorting of miRNAs into exosomes through binding to specific motifs. *Nat Commun*. 2013; 4 (1): 2980.
28. Gusar VA, Timofeeva AV, Chagovets VV, Kan NE, Ivanets TYu, Sukhikh GT. Regulation of the placental growth factor mediated by sumoylation and expression of miR-652-3p in pregnant women with early-onset preeclampsia. *Bull Exp Biol Med*. 2022; 174 (1): 174–8.
29. Gusar V, Timofeeva A, Chagovets V, et al. Diagnostic potential of exosomal hypoxamiRs in the context of hypoxia–sumoylation–hypoxamiRs in early onset preeclampsia at the preclinical stage. *Life*. 2022; 12 (1): 101.
30. Chiarello DI, Salsoso R, Toledo F, Mate A, Vázquez CM, Sobrevia L. Foetoplacental communication via extracellular vesicles in normal pregnancy and preeclampsia. *Molecular Aspects of Medicine*. 2018; 60: 69–80.
31. Salomon C, Torres MJ, Kobayashi M, et al. A Gestational Pprofile of placental exosomes in maternal plasma and their effects on endothelial cell migration. *PLoS ONE*. 2014; 9 (6): e98667.
32. Tannetta D, Collett G, Vatish M, Redman C, Sargent I. Syncytiotrophoblast extracellular vesicles — Circulating biopsies reflecting placental health. *Placenta*. 2017; 52: 134–8.

33. Hendriks IA, D'Souza RCJ, Yang B, Verlaan-de Vries M, Mann M, Vertegaal ACO. Uncovering global SUMOylation signaling networks in a site-specific manner. *Nat Struct Mol Biol.* 2014; 21 (10): 927–36.
34. Hay RT. SUMO. *Molecular Cell.* 2005; 18 (1): 1–12.
35. Baczyk D, Audette MC, Drewlo S, Levytska K, Kingdom JC. SUMO-4: a novel functional candidate in the human placental protein SUMOylation machinery. *PLoS ONE.* 2017; 12 (5): e0178056.
36. Anderson DB, Wilkinson KA, Henley JM. Protein SUMOylation in neuropathological conditions. *Drug News & Perspectives.* 2009; 22 (5): 255.
37. Bawa-Khalife T, Yeh ETH. SUMO losing balance: SUMO proteases disrupt SUMO homeostasis to facilitate cancer development and Progression. *Genes & Cancer.* 2010; 1 (7): 748–52.
38. Baczyk D, Audette MC, Coyaud E, Raught B, Kingdom JC. Spatiotemporal distribution of small ubiquitin-like modifiers during human placental development and in response to oxidative and inflammatory stress: Placental distribution of small ubiquitin-like modifiers. *J Physiol.* 2018; 596 (9): 1587–600.
39. Saitoh H, Hinchey J. Functional heterogeneity of small ubiquitin-related protein modifiers SUMO-1 versus SUMO-2/3. *Journal of Biological Chemistry.* 2000; 275 (9): 6252–8.
40. Hasegawa Y, Yoshida D, Nakamura Y, Sakakibara S. Spatiotemporal distribution of SUMOylation components during mouse brain development: Sumo-ylation during brain development. *J Comp Neurol.* 2014; 522 (13): 3020–36.
41. Chalkiadaki A, Talianidis I. SUMO-dependent compartmentalization in promyelocytic leukemia protein nuclear bodies prevents the access of LRH-1 to chromatin. *Molecular and Cellular Biology.* 2005; 25 (12): 5095–105.
42. Snider NT, Omary MB. Post-translational modifications of intermediate filament proteins: mechanisms and functions. *Nat Rev Mol Cell Biol.* 2014; 15 (3): 163–77.
43. Vassileva MT, Matunis MJ. SUMO modification of heterogeneous nuclear ribonucleoproteins. *Molecular and Cellular Biology.* 2004; 24 (9): 3623–32.
44. Vertegaal ACO, Ogg SC, Jaffray E, et al. A Proteomic study of SUMO-2 target proteins. *Journal of Biological Chemistry.* 2004; 279 (32): 33791–8.
45. Bhattacharjee J, Alahari S, Sallais J, Tagliaferro A, Post M, Caniggia I. Dynamic regulation of HIF1A stability by SUMO2/3 and SENP3 in the human placenta. *Placenta.* 2016; 40: 8–17.
46. Xu Y, Zuo Y, Zhang H, et al. Induction of SENP1 in endothelial cells contributes to hypoxia-driven VEGF expression and angiogenesis. *Journal of Biological Chemistry.* 2010; 285 (47): 36682–8.
47. Zhou HJ, Xu Z, Wang Z, et al. SUMOylation of VEGFR2 regulates its intracellular trafficking and pathological angiogenesis. *Nat Commun.* 2018; 9 (1): 3303.
48. McCaig D, Lyall F. Hypoxia upregulates GCM1 in human placenta explants. hypertension in pregnancy. 2009; 28 (4): 457–72.
49. Kohli S, Hoffmann J, Lochmann F, et al. p45 NF-E2 regulates syncytiotrophoblast differentiation by post-translational GCM1 modifications in human intrauterine growth restriction. *Cell Death Dis.* 2017; 8 (4): e2730–e2730.
50. Chang C-W, Chang G-D, Chen H. A novel cyclic AMP/Epac1/CaMKI signaling cascade promotes GCM1 desumoylation and placental cell fusion. *Molecular and Cellular Biology.* 2011; 31 (18): 3820–31.
51. Luo J, Ashikaga E, Rubin PP, et al. Receptor trafficking and the regulation of synaptic plasticity by SUMO. *Neuromol Med.* 2013; 15 (4): 692–706.
52. Maynard SE, Min J-Y, Merchan J, et al. Excess placental soluble fms-like tyrosine kinase 1 (sFlt1) may contribute to endothelial dysfunction, hypertension, and proteinuria in preeclampsia. *J Clin Invest.* 2003; 111 (5): 649–58.
53. Redman CWG, Staff AC. Preeclampsia, biomarkers, syncytiotrophoblast stress, and placental capacity. *American Journal of Obstetrics and Gynecology.* 2015; 213 (4): S9.e1-S9.e4.
54. Dymara-Konopka W, Laskowska M, Grywalska E, Hymos A, Błazewicz A, Leszczyńska-Gorzela B. Similar pro- and antiangiogenic profiles close to delivery in different clinical presentations of two pregnancy syndromes: preeclampsia and fetal growth restriction. *IJMS.* 2023; 24 (2): 972.
55. Keikkala E, Vuorela P, Laivuori H, Romppanen J, Heinonen S, Stenman U-H. First trimester hyperglycosylated human chorionic gonadotrophin in serum — a marker of early-onset preeclampsia. *Placenta.* 2013; 34 (11): 1059–65.
56. Morris RK, Bilagi A, Devani P, Kilby MD. Association of serum PAPP-A levels in first trimester with small for gestational age and adverse pregnancy outcomes: systematic review and meta-analysis: Systematic review association serum PAPP-A and adverse pregnancy outcome. *Prenat Diagn.* 2017; 37 (3): 253–65.
57. Krantz D, Goetzl L, Simpson JL, et al. Association of extreme first-trimester free human chorionic gonadotropin-β, pregnancy-associated plasma protein A, and nuchal translucency with intrauterine growth restriction and other adverse pregnancy outcomes. *American Journal of Obstetrics and Gynecology.* 2004; 191 (4): 1452–8.

SPECIFICS OF GUT MICROBIOTA IN WOMEN WITH IDIOPATHIC RECURRENT MISCARRIAGE

Gumenyuk LN , Bordyugov MD, Sarchuk EV, Knyazeva SV, Zastavskii VA, Krickaya DV, Saitibragimova SE, Kurtvelieva AI

Medical Academy named after S. I. Georgievsky of Vernadsky Crimean Federal University, Simferopol, Russia

Currently, researchers show considerable interest in the link between gut microbiota and idiopathic recurrent miscarriage (IRM). This study aimed to analyze taxonomic changes of gut microbiota and assess its relationship with plasma levels of cortisol, melatonin, TNF α and IL17 in women with IRM. We invited 55 women with IRM and 60 women with normal pregnancy, studied their gut microbiota, and registered serum concentrations of cortisol, melatonin, TNF α and IL17. Women with IRM had changed gut microbiota: significantly decreased — diversity (Chao1 $p = 0.014$), significantly decreased abundance of *Bifidobacterium* ($p < 0.001$), *Lachnospira* ($p = 0.032$), *Roseburia* ($p = 0.003$), *Coprococcus* ($p = 0.012$), and significantly increased abundance of *Ruminococcus* ($p < 0.001$) and *Klebsiella* ($p = 0.002$). We have shown a statistically significant relationship between cortisol level and abundance of *Lachnospira* ($r = -0.51$; $p = 0.002$), melatonin level and abundance of *Coprococcus* ($r = -0.49$; $p = 0.012$), and identified connections between TNF and IL17 concentrations and Chao1 index ($r = -0.51$; $p = 0.002$, $r = -0.54$; $p = 0.001$, respectively), TNF concentration and abundance of *Ruminococcus* ($r = 0.51$; $p = 0.002$), IL17 concentration and abundance of *Bifidobacterium* ($r = -0.52$; $p = 0.001$). Modulation of gut microbiota may have preventive and therapeutic effects in women with IRM.

Keywords: idiopathic recurrent miscarriage, gut microbiota, cortisol, melatonin, TNF α , IL17

Author contribution: Gumenyuk LN — study idea and design; Bordyugov MD, Sarchuk EV — data collection, analysis and interpretation; Knyazeva SV, Zastavsky VA — statistical data processing; Kritskaya DV, Saytibragimova SE, Kurtvelieva AI — article authoring.

Compliance with ethical standards: the study was approved by the Ethics Committee of the Medical Academy named after S. I. Georgievsky of Vernadsky Crimean Federal University (Minutes № 10 of October 16, 2021); it was planned and conducted in compliance with the Declaration of Helsinki. All participants of the study signed the voluntary informed consent form.

 **Correspondence should be addressed:** Lesya N. Gumenyuk
Bul'var Lenina, 5/7, 295006, Simferopol, Republic of Crimea; lesya_gumenyuk@mail.ru

Received: 04.01.2024 **Accepted:** 02.02.2024 **Published online:** 21.02.2024

DOI: 10.24075/brsmu.2024.004

ОСОБЕННОСТИ МИКРОБИОТЫ КИШЕЧНИКА У ЖЕНЩИН С ИДИОПАТИЧЕСКИМ ПРИВЫЧНЫМ ВЫКИДЫШЕМ

Л. Н. Гуменюк , М. Д. Бордюгов, Е. В. Сарчук, С. В. Князева, В. А. Заставский, Д. В. Крицкая, Ш. Э. Сайтибрагимова, А. И. Куртвелиева

Медицинский институт имени С. И. Георгиевского (структурное подразделение Крымского федерального университета имени В. И. Вернадского), Симферополь, Россия

В настоящее время существенный интерес у исследователей вызывает сопряженность микробиоты кишечника и идиопатического привычного выкидыша (ИПВ). Целью работы было проанализировать изменения таксономического состава микробиоты кишечника и оценить на уровне родов их взаимосвязь с показателями в плазме крови кортизола, мелатонина, TNF α и IL17 у женщин с ИПВ. У 55 женщин с ИПВ и 60 женщин с физиологически протекающей беременностью изучали таксономический состав микробиоты кишечника, концентрацию в сыворотке крови кортизола, мелатонина, TNF α и IL17. Установлено, что у женщин с ИПВ изменения таксономического состава микробиоты кишечника характеризуются статистически значимым снижением α -разнообразия бактериального сообщества (индекс Chao1, $p = 0,014$), представленности *Bifidobacterium* ($p < 0,001$), *Lachnospira* ($p = 0,032$), *Roseburia* ($p = 0,003$), *Coprococcus* ($p = 0,012$) и увеличением представленности *Ruminococcus* ($p < 0,001$) и *Klebsiella* ($p = 0,002$). Продемонстрировано наличие статистически значимой взаимосвязи между значениями кортизола и представленностью бактерий *Lachnospira* ($r = -0,51$; $p = 0,002$), мелатонина и представленностью бактерий *Coprococcus* ($r = -0,49$; $p = 0,012$). Выявлена также взаимосвязь между концентрацией TNF α и IL17 и индексом Chao1 ($r = -0,51$; $p = 0,002$, $r = -0,54$; $p = 0,001$ соответственно), TNF α и представленностью бактерий *Ruminococcus* ($r = 0,51$; $p = 0,002$), IL17 и представленностью *Bifidobacterium* ($r = -0,52$; $p = 0,001$). Коррекция микробиоты кишечника может иметь потенциальную профилактическую и терапевтическую значимость для женщин с ИПВ.

Ключевые слова: идиопатический привычный выкидыш, микробиота кишечника, кортизол, мелатонин, TNF α , IL17

Вклад авторов: Л. Н. Гуменюк — идея и дизайн исследования; М. Д. Бордюгов, Е. В. Сарчук — сбор, анализ и интерпретация данных; С. В. Князева, В. А. Заставский — статистическая обработка данных; Д. В. Крицкая, Ш. Э. Сайтибрагимова, А. И. Куртвелиева — написание статьи.

Соблюдение этических стандартов: исследование одобрено этическим комитетом Медицинского института имени С. И. Георгиевского ФГАОУ ВО «Крымский федеральный университет имени В. И. Вернадского» (протокол № 10 от 16 октября 2021 г.), спланировано и проведено в соответствии с Хельсинской декларацией. Все лица, включенные в исследование, подписали добровольное информированное согласие.

 **Для корреспонденции:** Леся Николаевна Гуменюк
бул. Ленина, 5/7, 295006, г. Симферополь, Республика Крым; lesya_gumenyuk@mail.ru

Статья получена: 04.01.2024 **Статья принята к печати:** 02.02.2024 **Опубликована онлайн:** 21.02.2024

DOI: 10.24075/vrgmu.2024.004

Recurrent miscarriage (RM) is a heterogeneous condition that implies two or more clinical pregnancy losses before 22nd week of gestation [1]. It is diagnosed in 2–5% of pregnant women [2]. After two miscarriages, the risk of pregnancy termination more than doubles and reaches 36–38% [3].

The discerned etiological factors behind RM are chromosomal abnormalities (2–6%), anatomical changes in the uterus (10–15%), infectious and inflammatory (2–6%), endocrine (17–20%), autoimmune (20%) diseases [4], thrombophilic conditions (10%) [5].

Yet, about 50% of RM cases are idiopathic, i.e., unexplained [6]. Idiopathic recurrent miscarriage (IRM) remains an urgent problem for reproductive medicine worldwide [7].

According to the current concepts, one of the key processes in the pathogenesis of IRM is aberrant production of proinflammatory cytokines accompanied by dysregulation of the immune response [8, 9]. Tumor necrosis factor alpha (TNF α) [10] and interleukin IL17 [11], which offer embryotoxic and antithrophoblastic activity, are of particular interest in this

context [12]. There is evidence that women with IRM have significantly higher peripheral blood level of TNF α (40–70% higher than in control group) [13], which is associated with initiation of apoptosis [14] and inhibition of trophoblast invasion [15], activation of thrombinase [16], deceleration of expression of nucleotide-binding oligomerization domain [17], growth of cytotoxicity of dNK cells [18], all of which, in turn, compromise spiral artery remodeling [16], cause thrombosis, trophoblast infarction and detachment [16], corrupt functions of decidual cells [17], trigger immunological rejection of the fetus [18], and, ultimately, miscarriage. Most researchers believe that women with IRM have elevated serum levels of IL17 [11], so it can be taken as a prognostic factor of the condition [19]. High level of IL17 inversely correlates with the content of T_{reg} cells in peripheral blood and decidual membrane [20], the low level of which potentiates the processes of embryo rejection [21]; it is independently associated with activation of expression of NF- κ B (transcription nuclear factor), decelerated expression of progesterone receptors and weakened functional activity thereof, which leads to decidual dysplasia, insufficiency of embryo nutrition, stimulation of myometrial contractility and, in the end, miscarriage [22].

At the same time, the immune system is closely linked to the neuroendocrine system. Teams of researchers actively discuss how dysregulation of the epiphyseal-pituitary-adrenal axis ups the risk of IRM, pointing to the special importance of changes in the secretion of melatonin and cortisol [23, 24.]. Analysis of the hormonal profile of blood of women with IRM revealed elevated cortisol and decreased melatonin levels [25, 24.]. Moreover, cortisol level fluctuations were associated with important etiological factors of IRM, such as subnormal fibrinolytic activity of the vascular wall, impaired trophoblast invasion and functions [26, 27], induction of apoptosis [28], inhibition of progesterone secretion [29]. In turn, lower blood melatonin level is linked to immunological trophoblast rejection (due to progesterone secretion inhibition) and myometrial contractility stimulation (through reinforced prostaglandin synthesis) [30].

Contemporary research reports confirm that gut microbiota plays a role in the pathophysiology of IRM, since it is crucial to formation and modulation of neuro-immune-endocrine reactions. Convincing data on qualitative changes of microbial makeup in women with IRM have been presented [31]. In general, they tend to have poorer bacterial diversity, depleted useful commensals and abundant pathobionts [32–33]; however, information about their microbiome's generic composition is fragmentary and contradictory. Besides, scientific literature contains only isolated reports on the association between gut microbiota and inflammatory biochemical markers in women with IRM, and there are no studies that investigated the relationship between intestinal bacteria and concentration of cortisol and melatonin in IRM cases.

Thus, exploration of the association between gut microbiota and IRM condition is a relevant problem. In the context of this study, we aimed to analyze taxonomic changes of gut microbiota and assess, at the level of childbearing, its relationship with plasma levels of cortisol, melatonin, TNF α and IL17 in women with IRM.

METHODS

This prospective comparative cross-sectional study was conducted at the gynecological department of the perinatal center of the Semashko State Medical University (Simferopol). It involved 55 women with primary IRM (median age — 31.6

[26.9; 33.9] years), who made up the treatment group (TG), and 60 women with normal pregnancy (NP) (median age — 30.3 [25.9; 33.2] years) who applied for an abortion and made up the control group (CG).

Criteria for inclusion in the TG: confirmed IRM diagnosis; 35 years or age or younger; correct couple karyotype.

Criteria for exclusion from the TG: underweight or overweight; genetic and anatomical causes of RM; chronic infectious, inflammatory, endocrine, autoimmune, thrombophilic, oncological diseases; irritable bowel syndrome; chronic diseases of digestive and hepatobiliary systems; bacterial, viral and fungal infectious diseases; mental pathology; tobacco abuse; stool changes (diarrhea/constipation) and intake of drugs that affect stool within 30 days before the study; vaccination 60 days before the study; intake of antibacterial, probiotic, prebiotic, antiviral, symbiotic, or acid-suppressing drugs within 90 days before the study.

Criteria for inclusion in the CG: 35 years or age or younger; normal pregnancy; uncomplicated gynecological and obstetric anamnesis; one or more successful pregnancies; no chronic extragenital pathology and allergic reactions in the anamnesis; no mental pathology in the anamnesis; no more than 3 respiratory infections a year; no infectious and acute diseases, changes in stool (diarrhea/constipation); no intake of drugs affecting stool within 60 days before the study; no intake of antibacterial, probiotic, prebiotic, antiviral, symbiotic, or acid-suppressing drugs within 90 days before the study.

Criteria for exclusion from the CG: pregravid underweight or overweight; ART pregnancy; high risk of miscarriage; body temperature above 36.9 °C.

Recurrent miscarriage was diagnosed under the codification criteria of the European Society of Human Reproduction and Embryology (ESHRE) [34].

We analyzed taxonomic composition of the gut microbiota of all study participants. Stool samples were collected when the women were admitted to the hospital, in the morning (8.00–11.00); after collection, they were frozen and stored in plastic containers at –80 °C up to the day of metagenomic analysis. Total DNA were extracted with the help of phenols. DNA libraries of 16S rRNA gene fragments were prepared under the standard protocol recommended by the manufacturer of MiSeq SOLiD 5500 Wildfire sequencer (AppliedBiosystems; USA), using primers for V3 and V4 variable regions of the 16S rRNA gene [35]. To filter quality of readings and classify their taxonomy, we used QIIME software (v.1.9.1) [36]. Identification of the taxonomic affiliation of readings was done in two stages: first, we selected a reference set of operational taxonomic units (OTU) of bacteria by comparing our readings of the 16S rRNA gene with data from the GreenGenes database version 13.5 [37]; secondly, we identified taxonomic affiliation of the OTE using the RDP algorithm and referring to HITdb, a specialized database of human gut microbiota [38].

The identified species, genera and phylum of the microorganisms were the basis for assessment of the qualitative and quantitative composition of gut microbiota. To evaluate α -diversity, we calculated the Chao1 index, number of the detected taxa (Sobs), indicator reflecting the real number of taxa (ACE). For this operation, we used Mothur software (v.1.22.0) (<https://www.mothur.org>).

Serum concentrations of cortisol, melatonin, TNF α , and IL17 were established with the help of solid-phase enzyme immunoassay, using test systems from Vector-Best (Russia) and Immuno Biological Laboratories (Germany). Fasting blood samples were taken from cubital vein in the morning (7.00–10.00), after 15 or more minutes of rest.

Table 1. Characteristics of patients with idiopathic primary miscarriage and healthy women

Indicator	Women with IRM (n = 55)	Control group (n = 60)	p
Average age, years, median [25%; 75%]	31.6 [26.9; 33.9]	30.3 [25.9; 33.2]	0.122
Body mass index, kg/m ² (m ± CD)	21.7 ± 0.4	20.6 ± 2.1	0.087
Number of miscarriages			
Two (n,%)	34 (61.8)	–	–
Three or more (n,%)	21 (38.2)	–	–

Note: IPM — idiopathic primary miscarriage.

STATISTICA 8.0 software package (StatSoft Inc.; USA) was used to statistically process the data obtained. For normal distribution cases, quantitative indicators are given as means and standard deviations, in abnormal distribution situations — as medians (Me) and 25th and 75th percentiles. Qualitative attributes were described with the help of the absolute number of values and percentages. Quantitative group-wise comparison of the data relied on the Student *t*-test and Mann–Whitney *U*-test, qualitative comparison — on the chi-squared test. To establish correlation between the values, we calculated the Spearman's rank correlation coefficient. The differences were considered statistically significant at $p < 0.05$.

RESULTS

Table 1 describes the participants. The groups were comparable in age ($p = 0.122$) and body mass index ($p = 0.087$).

Intergroup comparison of gut microbiota revealed a significantly decreased α -diversity in the treatment group

(Chao1 $p = 0.014$), as well as a downward trend of the ACE and Sobs curves ($p = 0.053$ and $p = 0.051$, respectively) (Fig. 1).

Compared to the CG, women of the TG had significantly decreased abundance of *Bifidobacterium* ($p < 0.001$), *Lachnospira* ($p = 0.032$), *Roseburia* ($p = 0.003$), *Coprococcus* ($p = 0.012$) and increased abundance of *Ruminococcus* ($p < 0.001$) and *Klebsiella* ($p = 0.002$) (Fig. 2).

In women with IRM, compared to women with normal pregnancy, levels of plasma cortisol, TNF and IL17 were significantly higher, and melatonin — significantly lower (Table 2).

We have established statistically significant correlations of cortisol levels with abundance of *Lachnospira* ($r = -0.51$, $p = 0.002$), relationship between melatonin level and abundance of *Coprococcus* ($r = -0.49$, $p = 0.012$), correlations between TNF/IL17 concentrations and Chao1 ($r = -0.51$, $p = 0.002$; $r = -0.54$, $p = 0.001$, respectively), found TNF concentration to cross-correlate with abundance of *Ruminococcus* ($r = 0.51$; $p = 0.002$), and IL17 concentration to negatively correlate with *Bifidobacterium* abundance ($r = -0.52$, $p = 0.001$).

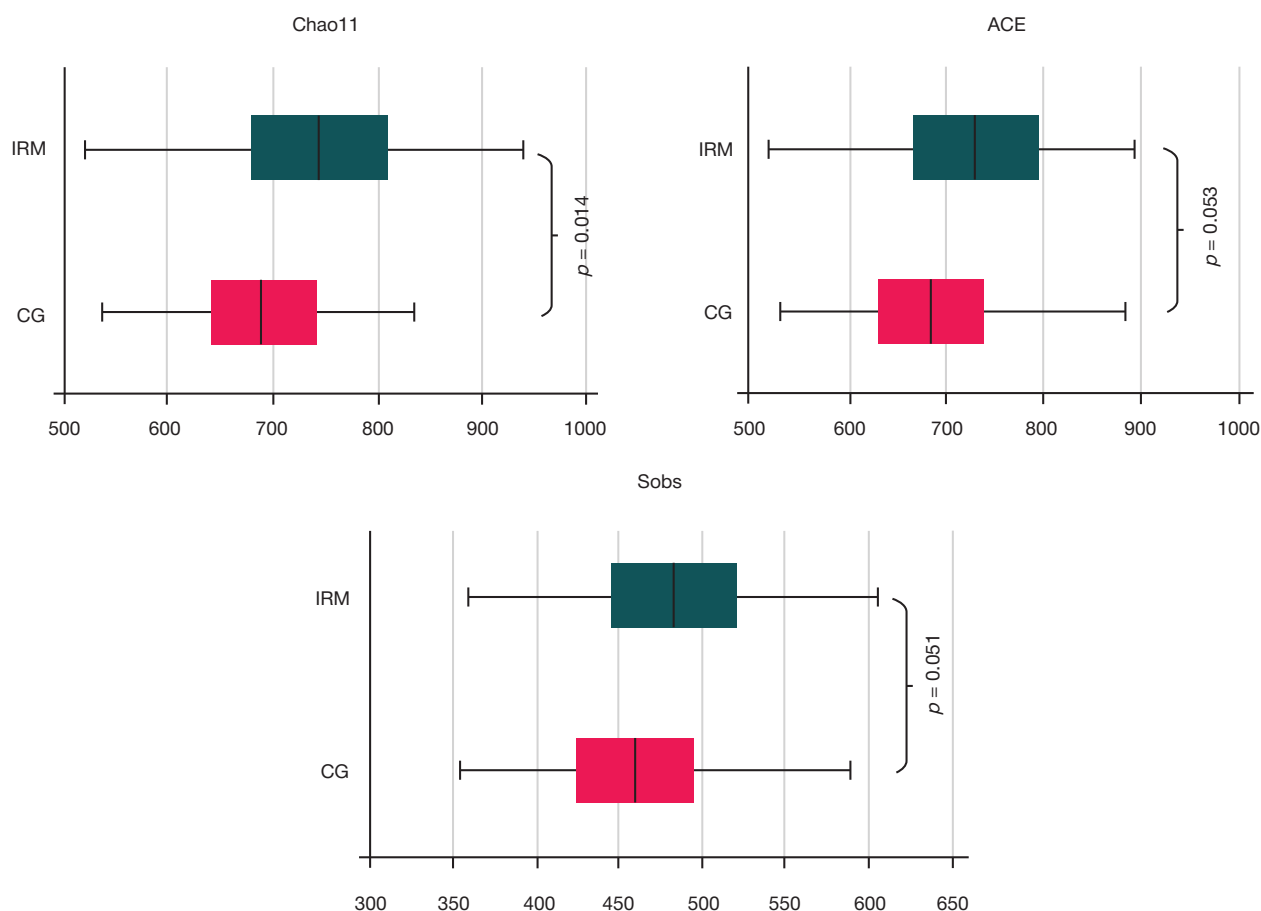


Fig. 1. Phylogenetic composition of gut microbiota in patients with idiopathic primary miscarriage and healthy women. IPM — idiopathic primary miscarriage, CG — control group

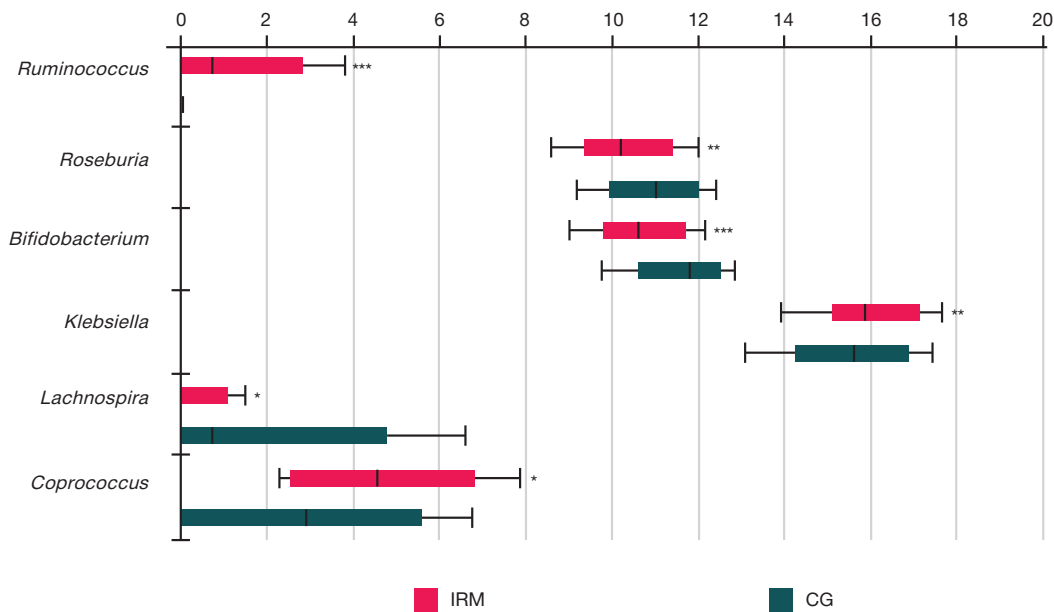


Fig. 2. Comparative analysis of the generic composition of gut microbiota in patients with idiopathic primary miscarriage and healthy women. IPM — idiopathic primary miscarriage, CG — control group

DISCUSSION

In this study, we refined the data on the changes in taxonomic composition of gut microbiota in women with IRM at the level of childbearing, and established the links between the said changes and plasma concentrations of cortisol, melatonin, TNF and IL17.

A number of previous studies reported gut microbiota alterations in women with IRM [31–33], and in this work, we have also shown that to be significantly different from gut microbiota of women with normal pregnancy. According to our data, women with IRM, compared to women with normal pregnancy, have lower bacterial α -diversity, which is confirmed by a significantly lower Chao1 value. These findings are consistent with the results of earlier studies [33, 39]. In addition, dysbiosis in women with IRM decreased the abundance of bacteria capable of immunomodulation, namely, *Bifidobacterium*, *Lachnospira*, *Roseburia*, *Coprococcus*, and *Prevotella*, which are known to produce butyrate and propionate short-chain fatty acids (SCFAs). The respective deficit translated into activation of histone deacetylase and inhibition of G-protein receptors GPR41, GPR43 and GPR109A, and, as a result, development of a chronic inflammation [40]. At the same time, we registered increased abundance of potential pathobionts, namely, bacteria of genera *Ruminococcus* and *Klebsiella*. In this respect, our data is only partially consistent with the findings of other researchers. One study reported women with IRM to have low abundance of *Prevotella*, *Roseburia*, *Lachnospira*, and high abundance of *Ruminococcus* and *Klebsiella* bacteria [32]. Other studies reported diminishing numbers of *Lachnospira*, *Roseburia*, *Prevotella* [33], and decreasing

abundance of *Prevotella* [31]. These inconsistencies may largely be explained by differences in geographical locations and participant inclusion methodologies. In our study, to prevent distortion of the results, we refrained from enlisting women with a complicated gynecological history and comorbid extragenital pathology, as well as those who took probiotics, prebiotics, and symbiotic drugs within 3 months before the study. Another important factor is the small sample size in the mentioned studies [32, 33].

As already noted, women with IRM had high blood concentrations of cortisol, TNF, IL17, and low concentrations of melatonin; all these hormones and proteins have been confirmed to play a part in the pathogenesis of IRM [13, 11, 23, 24]. Our results are consistent with the findings reported earlier: as a condition, IRM, compared to normal pregnancy, is associated with significantly different plasma concentrations of cortisol, melatonin, TNF, and IL17. A fundamental aspect is that in women with IRM, some gut microbiota species correlate with plasma concentrations of studied biomarkers; this fact may indicate a relationship between composition, abundance of the microbiota, and IRM. Plasma concentration of cortisol was shown to negatively correlate with the number of *Lachnospira* bacteria, which points to their possible role in the disruption of operation of hypothalamic-pituitary-adrenal axis (HPAA) in IRM cases. We failed to find studies investigating the relationship between gut microbiota and cortisol in women with IRM. One paper reported patients with Cushing's syndrome to have *Lachnospira* negatively correlating with cortisol expression [41]. A similar pattern was shown in another study: decreasing abundance of *Lachnospira* was closely associated with higher cortisol concentrations in healthy children aged 8–16 years

Table 2. Comparative analysis of serum levels of cortisol, melatonin, TNF α and IL17 in patients with idiopathic primary miscarriage and healthy women

Indicator	Women with IRM (n = 55)	Control group (n = 60)	p
Cortisol, nmol/l	627.1 \pm 15.4	321.4 \pm 33.2	< 0.001
Melatonin, pg/ml	18.1 \pm 5.3	31.6 \pm 8.4	0.002
TNF α , pg/ml	12.3 \pm 2.3	6.1 \pm 1.4	0.001
IL17, pg/ml	5.2 \pm 1.2	2.6 \pm 1.3	0.011

Note: IPM — idiopathic primary miscarriage.

[42]. We have found a probable interpretation of this correlation in the literature. *Lachnospira* is known to be one of the main butyrate-producing species. Since SCFAs can penetrate the blood-brain barrier (through circumventricular organs), it is reasonable to discuss how they act directly on the secretory tone in pituitary neurons of the medial paraventricular nucleus, this modulating activity of HPAA [43]. There are experimental and clinical studies that have shown the ability of SCFAs to affect cortisol expression. In one of such studies, mice were administered SCFAs (67.5 mM acetate + 25 mM propionate + 25 mM butyrate) for seven days, which resulted in inhibition of stress-potentiated corticosterone secretion [44]. Another study reported that seven-day administration of physiological doses of SCFAs directly into the colon of healthy individuals increased their concentration in the systemic bloodstream and attenuated intensity of cortisol response to acute psycho-social stress [45].

There was established a correlation of the level of melatonin with the abundance of *Coprococcus*, which may be mediated by blocked signals in the system of p-CREB-binding protein, arylalkylamine-N-acetyltransferase, due to the inhibition of tryptophan [46], a precursor of serotonin, from which melatonin is subsequently synthesized. Research papers cover similar associations in patients with juvenile idiopathic arthritis [47] and type 2 diabetes mellitus [48], confirmed by direct close correlations of *Coprococcus* abundance with the levels of tryptophan metabolites [48] and plasma melatonin [47, 48].

Discussing our results regarding the relationship between gut microbiota and blood levels of TNF and IL17 in the TG, it is important to note that only some of them are consistent with data found in the previously published study reports. Interconnections of gut microbiota and proinflammatory cytokines have been evaluated in an earlier work [33], which found women with IRM to exhibit lower bacterial diversity in association with increasing blood concentrations of TNF and IL17. Our findings are consistent with these results. This fact may indicate that in the patients with IRM, microbiome's proinflammatory effects are probably caused by a holistic dysbiosis. In addition, we have registered direct relationship between TNF blood levels and abundance of *Ruminococcus*. *Ruminococcus* bacteria are known to synthesize glucoramanan, an inflammatory lipopolysaccharide, which, by activating TLR4-mediated reactions, induces production of proinflammatory

cytokines (including TNF) by bone marrow dendritic cells [49]. Currently, a sufficient number of studies indicate that *Bifidobacterium* can influence the severity of inflammatory reactions [50–54]. Thus, lower abundance of *Bifidobacterium* is associated with development of preeclampsia [51], shorter life of a heart allograft [50], increased risk of autoimmune conditions [52], and inflammatory bowel diseases [53]. Moreover, low numbers of *Bifidobacterium* is known to be linked to activation of histone acetylation and suppression of DNA methylation, which, in turn, leads to boosted activation of NF- κ B-mediated transcription and intensification of the IL17 expression [50]. The negative correlation between blood concentration of IL17 and abundance of *Bifidobacterium* that we have registered is an additional evidence of this association. At the same time, our results conflict with findings of the study [33], which established a negative relationship between blood concentration of IL17 and abundance of *Prevotella* in women with IRM. This inconsistency, as pointed out above, is most likely a consequence of differences in designs of the studies: we did not enlist women with IRM that had gynecological pathologies and metabolic disorders, while the authors of study [33] did not regard polycystic ovary syndrome and insulin resistance as exclusion criteria. This fact could have influenced the differences between TNF and IL17 associations with the gut microbiota species in women with IRM as they are reported in the literature. Nevertheless, the data published in study [33] and the results of our work suggest a significant role played by the gut microbiota in the immunogenesis of IRM. Apparently, the causal relationships between gut microbiota and blood levels of proinflammatory cytokines in IRM cases require further, more scrupulous investigations.

CONCLUSIONS

Women with IRM were found to have pronounced abnormalities in abundance and taxonomic composition of gut microbiota. The statistically significant correlations found between some species in microbiota and hormonal and inflammatory markers confirm the postulate about connections between gut microbiota abundance/diversity and IRM. Modulation of gut microbiota may have preventive and therapeutic effects in women with IRM.

References

- Practice Committee of American Society for Reproductive Medicine. Definitions of infertility and recurrent pregnancy loss: a committee opinion. *Fertil Steril*. 2013; 99 (1): 63.
- El Hachem H, Crepaux V, May-Panloup P, et al. Recurrent pregnancy loss: current perspectives. *Int J Women's Health*. 2017; 9: 31–45.
- Lund M, Kamper-Jørgensen M, Nielsen HS, et al. Prognosis for live birth in women with recurrent miscarriage: what is the best measure of success? *Obstet Gynecol*. 2012; 119 (1): 37–43.
- Jeve YB, Davies W. Evidence-based management of recurrent miscarriages. *J Hum Reprod Sci*. 2014; 7: 159–69.
- Abu-Heijja A. Thrombophilia and Recurrent Pregnancy Loss: Is heparin still the drug of choice? *Sultan Qaboos Univ Med J*. 2014; 14 (1): e26–36.
- Zejnnullahu VA, Zejnnullahu VA, Kosumi E. The role of oxidative stress in patients with recurrent pregnancy loss: a review. *Reprod Health*. 2021; 16; 18 (1): 207.
- Kniotek M, Zych M, Roszczyk A, et al. Decreased Production of TNF α and IL6 Inflammatory Cytokines in Non-Pregnant Idiopathic RPL Women Immunomodulatory Effect of Sildenafil Citrate on the Cellular Response of Idiopathic RPL Women. *J Clin Med*. 2021; 15; 10 (14): 3115.
- Mor G, Aldo P, Alvero AB. The unique immunological and microbial aspects of pregnancy. *Nat Rev Immunol*. 2017; 17 (8): 469–82.
- Yang X, Tian Y, Zheng L, et al. The Update Immune-Regulatory Role of Pro- and Anti-Inflammatory Cytokines in Recurrent Pregnancy Losses. *Int J Mol Sci*. 2023; 21; 24 (1): 132.
- Dai FF, Hu M, Zhang YW, et al. TNF α /anti-TNF α drugs and its effect on pregnancy outcomes. *Expert Rev Mol Med*. 2022; 10: 24–26.
- Saifi B, Rezaee SA, Tajik N, et al. Th17 cells and related cytokines in unexplained recurrent spontaneous miscarriage at the implantation window. *Reprod Biomed Online*. 2014; 29: 481–9.
- Piccinni MP, Raghupathy R, Saito S, Szekeres-Bartho J. Cytokines, Hormones and Cellular Regulatory Mechanisms Favoring Successful Reproduction. *Front Immunol*. 2021; 28; 12: 717808.
- Shaarawy M, Nagui AR. Enhanced expression of cytokines may play a fundamental role in the mechanisms of immunologically mediated recurrent spontaneous abortion. *Acta Obstet Gynecol*

- Scand. 1997; 76: 205–11.
14. Kilani RT, Mackova M, Davidge ST et al. Endogenous tumor necrosis factor — mediates enhanced apoptosis of cultured villous trophoblasts from intrauterine growth-restricted placentae. *Reproduction*. 2007; 133: 257–64.
 15. Salama KM, Alloush MK, Hussini RM. Are the cytokines TNF alpha and IL 1Beta early predictors of embryo implantation? Cross sectional study. *J Reprod Immunol*. 2020; 137: 102618.
 16. Azizieh FY, Raghupathy RG. Tumor necrosis factor- α and pregnancy complications: a prospective study. *Med Princ Pract*. 2015; 24 (2): 165–70.
 17. Zhang Y, Zhang Y, Li H, et al. NOD1 modulates decidual stromal cell function to maintain pregnancy in the early trimester. *Cell Biochemistry and Function* 2019; 37: 464–73.
 18. Yang SL, Tan HX, Niu TT, et al. Kynurenine promotes the cytotoxicity of NK cells through aryl hydrocarbon receptor in early pregnancy. *J Reprod Immunol*. 2021; 143: 103270.
 19. Najafi S, Hadinoushan H, Eslami G, Aflatoonian A. Association of IL17A and IL17 F gene polymorphisms with recurrent pregnancy loss in Iranian women. *J Assist Reprod Genet*. 2014; 31 (11): 1491–6.
 20. Buzzaccarini G, Vitagliano A, Andrisani A, et al. Chronic Endometritis and Altered Embryo Implantation: A Unified Pathophysiological Theory from a Literature Systematic Review. *J Assist Reprod Genet*. 2020; 37: 2897–2911.
 21. Lee SK, Kim JY, Lee M, et al. Th17 and regulatory T cells in women with recurrent pregnancy loss. *Am J Reprod Immunol*. 2012; 67: 311–8.
 22. Sha J, Liu F, Zhai J, et al. Alteration of Th17 and Foxp3+regulatory T cells in patients with unexplained recurrent spontaneous abortion before and after the therapy of hCG combined with immunoglobulin. *Exp Ther Med*. 2017; 14: 1114–8.
 23. McCarthy R, Jungheim ES, Fay JC, et al. Riding the rhythm of melatonin through pregnancy to deliver on time. *Front Endocrinol (Lausanne)*. 2019; 13 (10): 616.
 24. Nepomnaschy PA, Welch KB, McConnell DS, et al. Cortisol levels and very early pregnancy loss in humans. *Proc Natl Acad Sci USA*. 2006; 103: 3938–42.
 25. Palmer KT, Bonzini M, Harris EC, et al. Europe PMC Funders Group Work activities and risk of prematurity, low birthweight and preeclampsia: an updated review with meta-analysis. *Occup Environ Med*. 2013; 70: 213–22.
 26. Kisanga EP, Tang Z, Guller S, Whirlledge S. Glucocorticoid signaling regulates cell invasion and migration in the human first-trimester trophoblast cell line Sw.71. *Am J Reprod Immunol*. 2018; 80: e12974.
 27. Húngaro TGR, Gregnani MF, Alves-Silva T, et al. Cortisol dose-dependently impairs migration and tube-like formation in a trophoblast cell line and modulates inflammatory and angiogenic genes. *Biomedicines*. 2021; 9 (8): 980.
 28. Michael AE, Papageorghiou AT. Potential significance of physiological and pharmacological glucocorticoids in early pregnancy. *Hum Reprod Update*. 2008; 14 (5): 497–517.
 29. Magiakou MA, Mastorakos G, Webster E. The Hypothalamic-pituitary-adrenal axis and the female reproductive system, *annals of the new York Acad Sci*. 1997; 17 (816): 42–56.
 30. Sandyk R, Anastasiadis PG, Anninos PA, Tsagas N. The pineal gland and spontaneous abortions: Implications for therapy with melatonin and magnetic field. *Int J Neurosci*. 1992; 62 (3–4): 243–50.
 31. Jin M, Li D, Ji R, et al. Changes in Gut Microorganism in Patients with Positive Immune Antibody-Associated Recurrent Abortion. *Biomed Res Int*. 2020; 18: 4673250.
 32. Cui Y, Zou L, Ye Q, et al. Gut microbiota composition and functional prediction in recurrent spontaneous abortion. *Research Square*; 2021.
 33. Liu Y, Chen H, Feng L, Zhang J. Interactions between gut microbiota and metabolites modulate cytokine network imbalances in women with unexplained miscarriage. *NPJ Biofilms Microbiomes*. 2021; 17; 7 (1): 24.
 34. ESHRE Guideline Group on RPL. Bender Atik R, Christiansen OB, Elson J, et al. ESHRE guideline: recurrent pregnancy loss: an update in 2022. *Hum Reprod Open*. 2023; 2023 (1): hoad002.
 35. Mitra S, Forster-Fromme K, Damms-Machado A, et al. Analysis of the intestinal microbiota using SOLiD16S rRNA gene sequencing and SOLiD shotgun sequencing. *BMC Genomics*. 2013; 14 (5): 16.
 36. Caporaso JG, Kuczynski J, Stombaugh J, et al. QIIME allows analysis of high-throughput community sequencing data. *Nat Methods*. 2010; 7 (5): 335–6.
 37. DeSantis TZ, Hugenholtz P, Larsen N. Greengenes, a chimerachecked 16S rRNA gene database and workbench compatible with ARB. *Appl Environ Microbiol*. 2006; 72: 5069–72.
 38. Ritari J, Salojärvi J, Lahti L, de Vos WM. Improved taxonomic assignment of human intestinal 16S rRNA sequences by a dedicated reference database. *BMC Genomics*. 2015; 16 (1): 1056.
 39. Guang Y, Shen X, Tan Y, et al. Systematic analysis of microbiota in pregnant Chinese women and its association with miscarriage. *Ann Transl Med*. 2022; 10 (20): 1099.
 40. Vinolo MAR, Rodrigues HG, Nachbar RT, Curi R. Regulation of Inflammation by Short Chain Fatty Acids. *Nutrients*. 2011; 3 (10): 858–76.
 41. Zhang Q, Hu WM, Deng YL, et al. Dysbiosis of gut microbiota and decreased propionic acid associated with metabolic abnormality in Cushing's syndrome. *Front Endocrinol (Lausanne)*. 2023; 13: 1095438.
 42. Michels N, Van de Wiele T, Fouhy F, et al. Gut microbiome patterns depending on children's psychosocial stress: Reports versus biomarkers. *Brain Behav Immun*. 2019; 80: 751–62.
 43. Ziegler DR, Herman JP. Neurocircuitry of stress integration: anatomical pathways regulating the hypothalamo-pituitary-adrenocortical axis of the rat. *Integr Comp Biol*. 2002; 42: 541–51.
 44. Van de Wouw M, Boehme M, Lyte JM, et al. Short-chain fatty acids: microbial metabolites that alleviate stress-induced brain-gut axis alterations. *J Appl Physiol*. 2018; 596: 4923–44.
 45. Dalile B, Vervliet B, Bergonzelli G, et al. Colon-delivered shortchain fatty acids attenuate the cortisol response to psychosocial stress in healthy men: a randomized, placebo-controlled trial. *Neuropsychopharmacol*. 2020; 45: 2257–66.
 46. Song L, He M, Sun Q, et al. Roseburia hominis Increases Intestinal Melatonin Level by Activating p-CREB-AANAT Pathway. *Nutrients*. 2022; 14: 117.
 47. Porosjuk MV, Klementev DD, Hodov NA, i dr. Izmeneniya mikrobioty kishhechnika u bol'nyh juvenil'nym idiopatcheskim artritom. *Vestnik RGMU*. 2022; (6): 13–9. Russian.
 48. Huang X, Qiu Y, Gao Y, et al. Gut microbiota mediate melatonin signalling in association with type 2 diabetes. *Diabetologia*. 2022; 65 (10): 1627–41.
 49. Henke MT, Kenny DJ, Cassilly CD, et al. Ruminococcus gnavus, a member of the human gut microbiome associated with Crohn's disease, produces an inflammatory polysaccharide. *Proc Natl Acad Sci*. 2019; 116: 12672–7.
 50. Bromberg JS, Hittle L, Xiong Y, et al. Gut microbiota-dependent modulation of innate immunity and lymph node remodeling affects cardiac allograft outcomes. *JCI Insight [Internet]*. 2018; 3 (19): e121045.
 51. Miao T, Yu Y, Sun J, et al. Decrease in abundance of bacteria of the genus Bifidobacterium in gut microbiota may be related to pre-eclampsia progression in women from East China. *Food Nutr Res*. 2021; 28: 65.
 52. Vatanen T, Kostic AD, d'Hennezel E, et al. DIABIMMUNE Study Group Variation in microbiome LPS immunogenicity contributes to autoimmunity in humans *Cell*. 2016; 165: 842–53.
 53. Henrick BM, Chew S, Casaburi G, et al. Colonization by B. infantis EVC001 modulates enteric inflammation in exclusively breastfed infants *Pediatr. Res*. 2019; 86: 749–57.
 54. Feng Y, Duan Y, Xu Z, et al. An examination of data from the American Gut Project reveals that the dominance of the genus Bifidobacterium is associated with the diversity and robustness of the gut microbiota. *Microbiologyopen*. 2019; 8 (12): e939.

Литература

- Practice Committee of American Society for Reproductive Medicine. Definitions of infertility and recurrent pregnancy loss: a committee opinion. *Fertil Steril*. 2013; 99 (1): 63.
- El Hachem H, Crepaux V, May-Panloup P, et al. Recurrent pregnancy loss: current perspectives. *Int J Women's Health*. 2017; 9: 31–45.
- Lund M, Kamper-Jørgensen M, Nielsen HS, et al. Prognosis for live birth in women with recurrent miscarriage: what is the best measure of success? *Obstet Gynecol*. 2012; 119 (1): 37–43.
- Jeve YB, Davies W. Evidence-based management of recurrent miscarriages. *J Hum Reprod Sci*. 2014; 7: 159–69.
- Abu-Heija A. Thrombophilia and Recurrent Pregnancy Loss: Is heparin still the drug of choice? *Sultan Qaboos Univ Med J*. 2014; 14 (1): e26–36.
- Zejnullahu VA, Zejnullahu VA, Kosumi E. The role of oxidative stress in patients with recurrent pregnancy loss: a review. *Reprod Health*. 2021; 16; 18 (1): 207.
- Kniotek M, Zych M, Roszczyk A, et al. Decreased Production of TNF α and IL6 Inflammatory Cytokines in Non-Pregnant Idiopathic RPL Women Immunomodulatory Effect of Sildenafil Citrate on the Cellular Response of Idiopathic RPL Women. *J Clin Med*. 2021; 15; 10 (14): 3115.
- Mor G, Aldo P, Alvero AB. The unique immunological and microbial aspects of pregnancy. *Nat Rev Immunol*. 2017; 17 (8): 469–82.
- Yang X, Tian Y, Zheng L, et al. The Update Immune-Regulatory Role of Pro- and Anti-Inflammatory Cytokines in Recurrent Pregnancy Losses. *Int J Mol Sci*. 2023; 21; 24 (1): 132.
- Dai FF, Hu M, Zhang YW, et al. TNF α /anti-TNF α drugs and its effect on pregnancy outcomes. *Expert Rev Mol Med*. 2022; 10: 24–26.
- Saifi B, Rezaee SA, Tajik N, et al. Th17 cells and related cytokines in unexplained recurrent spontaneous miscarriage at the implantation window. *Reprod Biomed Online*. 2014; 29: 481–9.
- Piccinni MP, Raghupathy R, Saito S, Szekeres-Bartho J. Cytokines, Hormones and Cellular Regulatory Mechanisms Favoring Successful Reproduction. *Front Immunol*. 2021; 28; 12: 717808.
- Shaarawy M, Nagui AR. Enhanced expression of cytokines may play a fundamental role in the mechanisms of immunologically mediated recurrent spontaneous abortion. *Acta Obstet Gynecol Scand*. 1997; 76: 205–11.
- Kilani RT, Mackova M, Davidge ST et al. Endogenous tumor necrosis factor — mediates enhanced apoptosis of cultured villous trophoblasts from intrauterine growth-restricted placentae. *Reproduction*. 2007; 133: 257–64.
- Salama KM, Alloush MK, Hussini RM. Are the cytokines TNF alpha and IL 1Beta early predictors of embryo implantation? Cross sectional study. *J Reprod Immunol*. 2020; 137: 102618.
- Azizieh FY, Raghupathy RG. Tumor necrosis factor- α and pregnancy complications: a prospective study. *Med Princ Pract*. 2015; 24 (2): 165–70.
- Zhang Y, Zhang Y, Li H, et al. NOD1 modulates decidual stromal cell function to maintain pregnancy in the early trimester. *Cell Biochemistry and Function* 2019; 37: 464–73.
- Yang SL, Tan HX, Niu TT, et al. Kynurenine promotes the cytotoxicity of NK cells through aryl hydrocarbon receptor in early pregnancy. *J Reprod Immunol*. 2021; 143: 103270.
- Najafi S, Hadinedoushan H, Eslami G, Aflatoonian A. Association of IL17A and IL17 F gene polymorphisms with recurrent pregnancy loss in Iranian women. *J Assist Reprod Genet*. 2014; 31 (11): 1491–6.
- Buzzaccarini G, Vitagliano A, Andrisani A, et al. Chronic Endometritis and Altered Embryo Implantation: A Unified Pathophysiological Theory from a Literature Systematic Review. *J Assist Reprod Genet*. 2020; 37: 2897–2911.
- Lee SK, Kim JY, Lee M, et al. Th17 and regulatory T cells in women with recurrent pregnancy loss. *Am J Reprod Immunol*. 2012; 67: 311–8.
- Sha J, Liu F, Zhai J, et al. Alteration of Th17 and Foxp3+regulatory T cells in patients with unexplained recurrent spontaneous abortion before and after the therapy of hCG combined with immunoglobulin. *Exp Ther Med*. 2017; 14: 1114–8.
- McCarthy R, Jungheim ES, Fay JC, et al. Riding the rhythm of melatonin through pregnancy to deliver on time. *Front Endocrinol (Lausanne)*. 2019; 13 (10): 616.
- Nepomnaschy PA, Welch KB, McConnell DS. et al. Cortisol levels and very early pregnancy loss in humans. *Proc Natl Acad Sci USA*. 2006; 103: 3938–42.
- Palmer KT, Bonzini M, Harris EC, et al. Europe PMC Funders Group Work activities and risk of prematurity, low birthweight and preeclampsia: an updated review with meta-analysis. *Occup Environ Med*. 2013; 70: 213–22.
- Kisanga EP, Tang Z, Guller S, Whirledge S. Glucocorticoid signaling regulates cell invasion and migration in the human first-trimester trophoblast cell line Sw.71. *Am J Reprod Immunol*. 2018; 80: e12974.
- Húngaro TGR, Gregnani MF, Alves-Silva T, et al. Cortisol dose-dependently impairs migration and tube-like formation in a trophoblast cell line and modulates inflammatory and angiogenic genes. *Biomedicines*. 2021; 9 (8): 980.
- Michael AE, Papageorgiou AT. Potential significance of physiological and pharmacological glucocorticoids in early pregnancy. *Hum Reprod Update*. 2008; 14 (5): 497–517.
- Magiakou MA, Mastorakos G, Webster E. The Hypothalamic-pituitary-adrenal axis and the female reproductive system, *annals of the new*. 1997; 17 (816): 42–56.
- Sandyk R, Anastasiadis PG, Anninos PA, Tsagas N. The pineal gland and spontaneous abortions: Implications for therapy with melatonin and magnetic field. *Int J Neurosci*. 1992; 62 (3–4): 243–50.
- Jin M, Li D, Ji R, et al. Changes in Gut Microorganism in Patients with Positive Immune Antibody-Associated Recurrent Abortion. *Biomed Res Int*. 2020; 18: 4673250.
- Cui Y, Zou L, Ye Q, et al. Gut microbiota composition and functional prediction in recurrent spontaneous abortion. *Research Square*; 2021.
- Liu Y, Chen H, Feng L, Zhang J. Interactions between gut microbiota and metabolites modulate cytokine network imbalances in women with unexplained miscarriage. *NPJ Biofilms Microbiomes*. 2021; 17; 7 (1): 24.
- ESHRE Guideline Group on RPL. Bender Atik R, Christiansen OB, Elson J, et al. ESHRE guideline: recurrent pregnancy loss: an update in 2022. *Hum Reprod Open*. 2023; 2023 (1): hoad002.
- Mitra S, Forster-Fromme K, Damms-Machado A, et al. Analysis of the intestinal microbiota using SOLiD16S rRNA gene sequencing and SOLiD shotgun sequencing. *BMC Genomics*. 2013; 14 (5): 16.
- Caporaso JG, Kuczynski J, Stombaugh J, et al. QIIME allows analysis of high-throughput community sequencing data. *Nat Methods*. 2010; 7 (5): 335–6.
- DeSantis TZ, Hugenholtz P, Larsen N. Greengenes, a chimerachecked 16S rRNA gene database and workbench compatible with ARB. *Appl Environ Microbiol*. 2006; 72: 5069–72.
- Ritari J, Salojärvi J, Lahti L, de Vos WM. Improved taxonomic assignment of human intestinal 16S rRNA sequences by a dedicated reference database. *BMC Genomics*. 2015; 16 (1): 1056.
- Guang Y, Shen X, Tan Y, et al. Systematic analysis of microbiota in pregnant Chinese women and its association with miscarriage. *Ann Transl Med*. 2022; 10 (20): 1099.
- Vinolo MAR, Rodrigues HG, Nachbar RT, Curi R. Regulation of Inflammation by Short Chain Fatty Acids. *Nutrients*. 2011; 3 (10): 858–76.
- Zhang Q, Hu WM, Deng YL, et al. Dysbiosis of gut microbiota and decreased propionic acid associated with metabolic abnormality in Cushing's syndrome. *Front Endocrinol (Lausanne)*. 2023; 13: 1095438.
- Michels N, Van de Wiele T, Fouhy F, et al. Gut microbiome patterns depending on children's psychosocial stress: Reports versus biomarkers. *Brain Behav Immun*. 2019; 80: 751–62.
- Ziegler DR, Herman JP. Neurocircuitry of stress integration: anatomical pathways regulating the hypothalamo-pituitary-adrenocortical axis of the rat. *Integr Comp Biol*. 2002; 42: 541–51.

44. Van de Wouw M, Boehme M, Lyte JM, et al. Short-chain fatty acids: microbial metabolites that alleviate stress-induced brain-gut axis alterations. *J Appl Physiol*. 2018; 596: 4923–44.
45. Dalile B, Vervliet B, Bergonzelli G, et al. Colon-delivered shortchain fatty acids attenuate the cortisol response to psychosocial stress in healthy men: a randomized, placebo-controlled trial. *Neuropsychopharmacol*. 2020; 45: 2257–66.
46. Song L, He M, Sun Q, et al. Roseburia hominis Increases Intestinal Melatonin Level by Activating p-CREB-AANAT Pathway. *Nutrients*. 2022; 14: 117.
47. Поросюк М. В., Клементьев Д. Д., Ходов Н. А., и др. Изменения микробиоты кишечника у больных ювенильным идиопатическим артритом. *Вестник РГМУ*. 2022; (6): 13–9.
48. Huang X, Qiu Y, Gao Y, et al. Gut microbiota mediate melatonin signalling in association with type 2 diabetes. *Diabetologia*. 2022; 65 (10): 1627–41.
49. Henke MT, Kenny DJ, Cassilly CD, et al. Ruminococcus gnavus, a member of the human gut microbiome associated with Crohn's disease, produces an inflammatory polysaccharide. *Proc Natl Acad Sci*. 2019; 116: 12672–7.
50. Bromberg JS, Hittle L, Xiong Y, et al. Gut microbiota-dependent modulation of innate immunity and lymph node remodeling affects cardiac allograft outcomes. *JCI Insight [Internet]*. 2018; 3 (19): e121045.
51. Miao T, Yu Y, Sun J, et al. Decrease in abundance of bacteria of the genus Bifidobacterium in gut microbiota may be related to pre-eclampsia progression in women from East China. *Food Nutr Res*. 2021; 28: 65.
52. Vatanen T, Kostic AD, d'Hennezel E, et al. DIABIMMUNE Study Group Variation in microbiome LPS immunogenicity contributes to autoimmunity in humans *Cell*. 2016; 165: 842–53.
53. Henrick BM, Chew S, Casaburi G, et al. Colonization by B. infantis EVC001 modulates enteric inflammation in exclusively breastfed infants *Pediatr. Res*. 2019; 86: 749–57.
54. Feng Y, Duan Y, Xu Z, et al. An examination of data from the American Gut Project reveals that the dominance of the genus Bifidobacterium is associated with the diversity and robustness of the gut microbiota. *Microbiologyopen*. 2019; 8 (12): e939.

ASSESSING CLINICAL EFFICACY OF NEW METHOD FOR ADAPTIVE INFUSION CONTROL IN PHACOEMULSIFICATION

Aznabaev BM^{1,2}, Mukhamadeev TR^{1,2}, Ismagilov TN^{1,2}✉, Dibaev TI^{1,2}

¹ Bashkir State Medical University, Ufa, Russia

² ZAO "Optimeservis", Ufa, Russia

Reduction of the adverse effects of intraoperative intraocular pressure fluctuation referred to as post-occlusion surge on the intraocular structures is an important task for ensuring phacoemulsification safety. In this regard, the method to control infusion during phacoemulsification based on controlling the infusion and aspiration flow rates in combination with monitoring of vacuum parameters was developed. The study was aimed to provide comparative assessment of clinical and functional characteristics of the eye in patients after phacoemulsification using the new and already existing adaptive infusion control methods. A total of 38 patients aged 66.4 ± 7.8 years (15 males and 23 females) in the index group (Optimed Profi system with the use of new method) and 35 patients aged 68.7 ± 7.5 years (16 males and 19 females) in the control group (Centurion Vision System with Active Fluidics) underwent surgery due to cataract. The patients underwent comprehensive eye examination before surgery and on days 1, 7, 30, months 3, 6 after surgery. The smaller loss of corneal endothelial cells on months 3 and 6 after surgery was observed in patients of the index group with grade III and IV cataract ($p < 0.05$). Comparison of macular microcirculation parameters revealed the reduced FAZ area by month 6 of postoperative follow-up in the index group, along with the increased total vascular density of the deep vasculature ($p < 0.001$). A significant decrease in the total density of the superficial and deep vascular plexuses by month 6 of postoperative follow-up was observed in the control group ($p < 0.05$). The use of new adaptive infusion control method contributes to effective phacoemulsification of cataracts of varying density with the lower percentage of the corneal endothelial cells lost in the late postoperative period.

Keywords: phacoemulsification, postocclusion surge, intraocular pressure, corneal endothelium, ocular perfusion pressure, optical coherence tomography

Author contribution: Aznabaev BM — developing the concept, approving final version of the article; Mukhamadeev TR — developing the concept, manuscript editing; Ismagilov TN — research procedure, manuscript writing and editing; Dibaev TI — manuscript writing and editing.

Compliance with ethical standards: the study was approved by the Ethics Committee of the Bashkir State Medical University (protocol № 10 dated 15 December 2021). All patients submitted the informed consent to surgical treatment and personal data processing.

✉ **Correspondence should be addressed:** Timur N. Ismagilov
Lenina, 3, Ufa, 450008, Russia; ismagilov-timur@bk.ru

Received: 19.01.2024 **Accepted:** 10.02.2024 **Published online:** 28.02.2024

DOI: 10.24075/brsmu.2024.009

ОЦЕНКА КЛИНИЧЕСКОЙ ЭФФЕКТИВНОСТИ НОВОГО СПОСОБА АДАПТИВНОГО УПРАВЛЕНИЯ ИНФУЗИЕЙ ПРИ ФАКОЭМУЛЬСИФИКАЦИИ

Б. М. Азнабаев^{1,2}, Т. Р. Мухамадеев^{1,2}, Т. Н. Исмагилов^{1,2}✉, Т. И. Дибеев^{1,2}

¹ Башкирский государственный медицинский университет, Уфа, Россия

² Закрытое акционерное общество «Оптимедсервис», Уфа, Россия

Важной задачей для обеспечения безопасности фактоэмульсификации (ФЭК) является снижение негативных воздействий на внутриглазные структуры интраоперационных колебаний внутриглазного давления — постокклюзионных волн (ПОВ). В связи с этим был разработан новый способ управления инфузией при ФЭК, основанный на контроле скорости инфузионного и аспирационного потоков в совокупности с мониторингом параметров вакуума. Целью исследования было дать сравнительную оценку клинико-функциональных показателей глаз пациентов после ФЭК с применением нового и существующего способов адаптивного управления инфузией. По поводу катаракты были прооперированы 38 пациентов в возрасте 66,4 ± 7,8 года (15 мужчин и 23 женщины) в основной группе (система Оптимед Профи с применением нового способа), 35 пациентов в возрасте 68,7 ± 7,5 года (16 мужчин и 19 женщин) в контрольной группе (система Centurion Vision System с функцией Active Fluidics). До операции, а также на 1-е, 7-е, 30-е сутки, на 3-й и 6-й месяцы после операции пациентам проводили комплексное офтальмологическое обследование. У пациентов основной группы с III и IV степенью плотности катаракты отмечена меньшая потеря эндотелиальных клеток роговицы на 3-й и 6-й месяцы после операции ($p < 0,05$). По результатам сравнения параметров микроциркуляции макулярной области, в основной группе к 6-му месяцу послеоперационного наблюдения отмечено снижение площади ФАЗ, а также увеличение общей плотности сосудов глубокой сосудистой сети ($p < 0,001$). В контрольной группе, к 6-му месяцу послеоперационного наблюдения отмечено статистически значимое снижение общей плотности поверхностного и глубокого сосудистых сплетений ($p < 0,05$). Использование нового способа адаптивного управления инфузией способствует эффективному выполнению фактоэмульсификации катаракт различной плотности с меньшим процентом потери эндотелиальных клеток роговицы в отдаленном послеоперационном периоде.

Ключевые слова: фактоэмульсификация, постокклюзионная волна, внутриглазное давление, эндотелий роговицы, глазное перфузионное давление, оптическая когерентная томография

Вклад авторов: Б. М. Азнабаев — разработка концепции, утверждение окончательного варианта статьи; Т. Р. Мухамадеев — разработка концепции, редактирование текста; Т. Н. Исмагилов — проведение исследования, подготовка и редактирование текста; Т. И. Дибеев — подготовка и редактирование текста.

Соблюдение этических стандартов: исследование одобрено этическим комитетом Башкирского государственного медицинского университета (протокол № 10 от 15 декабря 2021 г.). Все пациенты подписали добровольное информированное согласие на хирургическое лечение и обработку персональных данных.

✉ **Для корреспонденции:** Тимур Наилевич Исмагилов
ул. Ленина, д. 3, г. Уфа, 450008, Россия; ismagilov-timur@bk.ru

Статья получена: 19.01.2024 **Статья принята к печати:** 10.02.2024 **Опубликована онлайн:** 28.02.2024

DOI: 10.24075/vrgmu.2024.009

Phacoemulsification (PE), the surgical procedure during which the lens is broken down and emulsified by ultrasound, and then an intraocular lens (IOL) is implanted, is the cataract surgery method most commonly used all over the world [1–3].

Today, reducing intraoperative trauma and the surgical intervention invasiveness is considered to be the main trend in cataract surgery. Reducing the damaging effects of the intraocular pressure fluctuation, resulting from imbalance between fluid inflow and outflow from the anterior chamber of the eye (post-occlusion surge, POS), on the intraocular structures is the major task for ensuring phacoemulsification safety [4–8].

Control over the surgical system infusion component is one of the leading methods to counter POS. The infusion fluid supply is an essential component of cataract surgery ensuring the anterior chamber stability [9–11]. Effective infusion control is impossible without continuous monitoring of the system hydrodynamic parameters (vacuum level in the aspiration line, peristaltic pump speed, infusion line pressure) [12–17]. In this regard, adaptive infusion flow control methods adjusting the infusion pressure to the changing hydrodynamic conditions of the surgical procedure are implemented in modern surgical systems. Despite the existing methods to ensure PE hydrodynamic stability, the problem of POS emergence arises even during operations conducted using advanced surgical systems, the majority of which involve the use of adaptive infusion flow control methods [18–20].

When controlling infusion, great attention should be paid to quick and reliable assessment of the phaco needle travel in different hydrodynamic states. Timely differentiation of consecutive hydrodynamic states (state of phaco needle occlusion, states of occlusion break and traversable phaco needle) by the surgical system is an important aspect of the problem.

The touchless control of flow rates in the system lines can become a solution to the problem of reliable phaco needle transversability assessment, since flow rate is constant along the entire length of the tube. Furthermore, the joint monitoring of flow rate in the infusion and aspiration lines will make it possible to detect minor flow rate fluctuations that can be precursors of occlusion break.

Staff members of the Optalmology Department of BSMU together with the engineers of the Microsurgery Equipment division of ZAO "Optimeservis" have developed a new method for adaptive infusion control in PE (patent RF № 2788289 dated 17.01.2023) based on the Optimed Profi surgical system (RU № FSR 2011/11396 dated 11.11.2013). The method invented allows one to reduce intraoperative intraocular pressure fluctuation (post-occlusion surge) due to rational infusion flow control depending on the aspiration and infusion flow rate parameters, as well as on the vacuum level in the aspiration line [21, 22]. Comparative assessment of the clinical and functional characteristics of patients with age-related cataract subjected to PE with the use of the new adaptive infusion control method based on the Optimed Profi system and the existing adaptive infusion control method based on the Centurion Vision System (Alcon; USA) is relevant.

The study was aimed to provide comparative assessment of clinical and functional characteristics of the eye in patients after PE performed using the new and already existing adaptive infusion control methods.

METHODS

Inclusion criteria: grade (degree of the lens nucleus density) I–IV age-related cataract with the the number of corneal endothelial cells exceeding 1500 c/mm²; no history of corneal

dystrophy or eye surgery. The patients underwent surgery at the Optalmology Department of BSMU, in the Optimed laser vision restoration center (Ufa). In the index group of patients ($n = 38$), phacoemulsification was performed using the Optimed Profi surgical system and the new adaptive infusion control method. In the control group of patients ($n = 35$), surgery was performed using the Centurion Vision System with the Active Fluidics function.

The fundamental difference of the new method for adaptive infusion control in PE from the existing one is represented by phaco needle transversability assessment and infusion pressure management not based on controlling the infusion pressure that can vary between various line parts, but implemented through complex monitoring of the infusion and aspiration flow rates that are constant along the entire length of the line. Vacuum level in the aspiration line is the third parameter to be controlled.

The algorithm of the method involves identification of at least three hydrodynamic states based on the characteristic changes in the infusion and aspiration flow rate parameters and the vacuum level in the aspiration line: "transversable phaco needle", "phaco needle occlusion", "occlusion break"; furthermore, the post-occlusion surge infusion compensation and identification of the "occlusion break" state occur simultaneously.

The advantage of the method developed is that it ensures adaptive infusion control allowing one to improve accuracy and reliability of identification of the hydrodynamic states associated with the phaco needle transversability during phacoemulsification, as well as to reduce intraoperative IOP fluctuation associated with post-occlusion surge.

When enrolling patients, the clinical groups were carefully formed. This was due to the need to create identical conditions for estimation of the clinical and functional surgical outcomes. To form comparable groups, the following was considered: lens nucleus density (according to the generally accepted Buratto classification), features of comorbidities, and gender and age distribution [23].

Non-inclusion criteria: complications or traumatic cataract; grade V cataract according to Buratto classification; pseudoxfoliation syndrome; concomitant eye disorder, such as high ametropia; diabetic retinopathy and other severe somatic disorders.

Patients of both groups underwent a comprehensive eye examination that included estimation of the decimal best-corrected visual acuity (BCVA), biomicroscopy, enumeration of the lost corneal endothelial cells with the EM-3000 endothelial microscope (Tomey; Japan). To assess vascular density of the superficial and deep vascular plexuses in the parafovea and perifovea, as well as to calculate the foveal avascular zone (FAZ) area, we performed optical coherence tomography angiography (OCTA) with the Avanti XR scanner (Optovue; USA) in 25 patients from each group.

Furthermore, mean ocular perfusion pressure (MOPP) was calculated before surgery and throughout the postoperative period in patients of both groups using the following formula:

$$\text{MOPP} = 2/3 \text{ MAP} - \text{IOP},$$

where MAP (mean arterial pressure) = $1/3 \text{ SBP}$ (systolic blood pressure) + $2/3 \text{ DBP}$ (diastolic blood pressure), IOP — intraocular pressure [24].

All surgical procedures were conducted under local anesthesia in outpatient settings. Settings of surgical systems are provided in Table 1.

The inner diameters of the aspiration and infusion line tubes were the same in both groups: 1.3 and 3.25 mm, respectively.

Table 1. Settings of surgical systems used in the index and control groups

Parameter	Groups	
	Index (<i>n</i> = 38) Optimed Profi	Control (<i>n</i> = 35) Centurion Vision System
Vacuum threshold, mmHg	400	400
Aspiration performance, mL/min	35	35
Aspiration mode	Fixed	Fixed
Target IOP, mmHg	45	45
Ultrasound waveforms	3D	Torsion + longitudinal
Ultrasound power, %	0–80	0–80
Ultrasound mode	Hyperpulse	Hyperpulse
Phaco needle gauge	21G	21G
Inner diameters of aspiration and infusion lines, mm	1.3 / 3.25	1.3 / 3.25

Surgical procedures were performed at the target IOP (45 mmHg), in accordance with the up-to-date literature data and the guidelines of the world's association of cataract surgeons. According to their data, the target IOP range that is optimal in terms of PE efficacy and safety is 45–60 mmHg [25–27].

After making corneal incisions and staining the anterior lens capsule, the circular capsulorhexis technique was applied. After the hydrodissection and hydrodelineation phase was over, the phase of the lens nucleus fracture and fragmentation began. The ultrasound power was set individually depending on the cataract density. In general, the ultrasound power set when removing grade I nuclei did not exceed 20%. When removing grade II nuclei, power of 20–35% was used, grade III — 40–50%, grade IV — 50% or more. The hydrodynamic settings of surgical systems used during the surgical procedure (aspiration pump speed, aspiration mode, vacuum level in the aspiration line, target IOP) were the same for all nuclear density degrees. The Phaco Quick Chop method was used to break up the nucleus. A flexible intraocular lens was implanted in the capsular bag.

The follow-up examinations of patients aimed at assessing clinical and functional characteristics of vision, as well as surgical complications, were performed on days 1, 7 and 30, as well as on months 3 and 6 of postoperative period.

Statistical processing of the results was performed using the SPSS ver. 27 software package (IBM Corporation; USA). After testing the distribution for normality, the parametric Student's *t*-test or the nonparametric Mann–Whitney *U* test were used when there were significant differences between two independent samples ($p < 0.05$). When the distribution was normal, the data were presented as mean and standard deviation ($M \pm Sd$), while in case of non-normal distribution the data were presented as median and interquartile range ($Me (Q_1; Q_3)$). The Friedman test was used to perform analysis of variance for related samples ($p < 0.05$).

Table 2. Clinical and demographic data of patients in the index and control groups

Parameter	Index group (<i>n</i> = 38)	Control group (<i>n</i> = 35)
Age, $M \pm Sd$	66.4 ± 7.8	68.7 ± 7.5
Sex		
male	15 (34.78%)	16 (45.71%)
female	23 (65.22%)	19 (54.29%)
Cataract density grade according to Buratto classification		
I	8 (21.05%)	7 (20.00%)
II	14 (36.84%)	13 (37.14%)
III	10 (26.32%)	9 (25.72%)
IV	6 (15.79%)	6 (17.14%)

RESULTS

The clinical and demographic data of patients are provided in Table 2.

High BCVA values (0.86 ± 0.13 in the index group, 0.83 ± 0.16 in the control group) were reported in both groups by day 30 after surgery. BCVA was 0.87 ± 0.14 in the index group and 0.85 ± 0.15 in the control group by month 6 of postoperative follow-up. There were no significant differences in BCVA between groups ($p > 0.05$).

The clinically significant corneal edema was the most common complication in the early postoperative period: there were three cases in the index group (7.9%) and four cases in the control group (11.4%). The clinically significant corneal edema was associated with the decreased corneal transparency, mainly in the optical zone, stromal thickening, and folds in the Descemet membrane. This complication improved due to treatment by day 7 of postoperative period.

Comparison of the corneal endothelial cell loss was performed during months 3 and 6 of postoperative period in accordance with the literature data, since the majority of ophthalmologists believe that endothelial defect repair occurs three months after surgery [28]. The results of the endothelial cell loss comparison between groups is provided in Table 3.

The following features were reported based on the comparison of endotheliocyte loss percentage between groups in the postoperative period: no significant differences were found in patients with grade I cataract after three ($p = 0.206$) and six ($p = 0.155$) months. Estimation of endotheliocyte loss in patients with grade II cataract also revealed no significant intergroup differences three ($p = 0.135$) and six ($p = 0.087$) months after surgery. The loss of corneal endothelial cells in patients of the index group with grade III cataract was significantly lower on months 3 ($p = 0.012$) and 6 ($p = 0.025$) of postoperative follow-up. Furthermore, significantly lower endotheliocyte loss was

Table 3. Dynamic changes in the corneal endothelium loss observed in the index and control groups 3 and 6 months after surgery, % (Me (Q₁; Q₃))

Cataract density	Index group		Control group	
	Month 3	Month 6	Month 3	Month 6
I	5.29 (4.88; 5.67)	5.49 (4.83; 6.25)	5.77 (5.29; 6.18)	5.86 (5.55; 6.32)
II	7.31 (6.63; 7.91)	7.42 (6.81; 8.03)	7.53 (7.31; 8.23)	7.79 (7.37; 8.49)
III	9.22 (8.16; 10.34)	9.83 (9.16; 10.42)	10.24 (9.69; 10.67)	10.59 (9.93; 11.35)
IV	10.72 (9.95; 11.62)	11.59 (9.86; 12.24)	11.78 (11.13; 12.59)	11.89 (10.42; 12.67)

Table 4. Postoperative dynamic changes in MOPP values in the index and control groups, mmHg (M ± Sd)

Follow-up period	Index group (n = 38)	Control group (n = 35)
Before surgery	52.44 ± 7.95	52.83 ± 8.83
Day 1	52.27 ± 8.80	52.53 ± 9.19
Day 7	52.59 ± 7.68	53.14 ± 8.77
Day 30	52.91 ± 7.48	53.29 ± 7.53
3 months	53.81 ± 6.78	53.70 ± 7.52
6 months	54.54 ± 7.15	54.31 ± 7.66

reported in patients of the index group with grade IV cataract on months 3 ($p = 0.007$) and 6 ($p = 0.038$) after surgery.

The intergroup comparison of MOPP values revealed no significant differences at appropriate time points of the study ($p > 0.05$). The dynamic changes in this parameter are provided in Table 4.

We noted the decrease in MOPP values by month 6 after surgery in both studied groups, however, these were non-

significant based on the Friedman test for related samples ($p > 0.05$).

Comparison of macular microcirculation parameters showed a significant decrease in FAZ area and an increase in the total vascular density of the deep vasculature in the index group by month 6 of postoperative follow-up (Table 5; Fig. 1). A significant decrease in the total density of superficial and deep vascular plexuses was reported in

Table 5. Postoperative dynamic changes in the macular OCTA parameters observed in the index group, $n = 25$; M ± Sd)

Parameter	Day 1	Day 7	Day 30	Month 3	Month 6	p-value
SVP total density, %	48.21 ± 4.39	50.73 ± 4.46	51.32 ± 4.80	51.48 ± 5.13	51.14 ± 5.05	$p = 0.113$
DVP total density, %	46.98 ± 5.42	48.22 ± 5.02	49.63 ± 4.89	50.54 ± 5.58	51.02 ± 4.72	$p < 0.001^*$
FAZ area, mm ²	0.296 ± 0.082	0.271 ± 0.079	0.270 ± 0.091	0.275 ± 0.068	0.274 ± 0.091	$p < 0.001^*$

Note: * — significance based on the Friedman test for related samples.

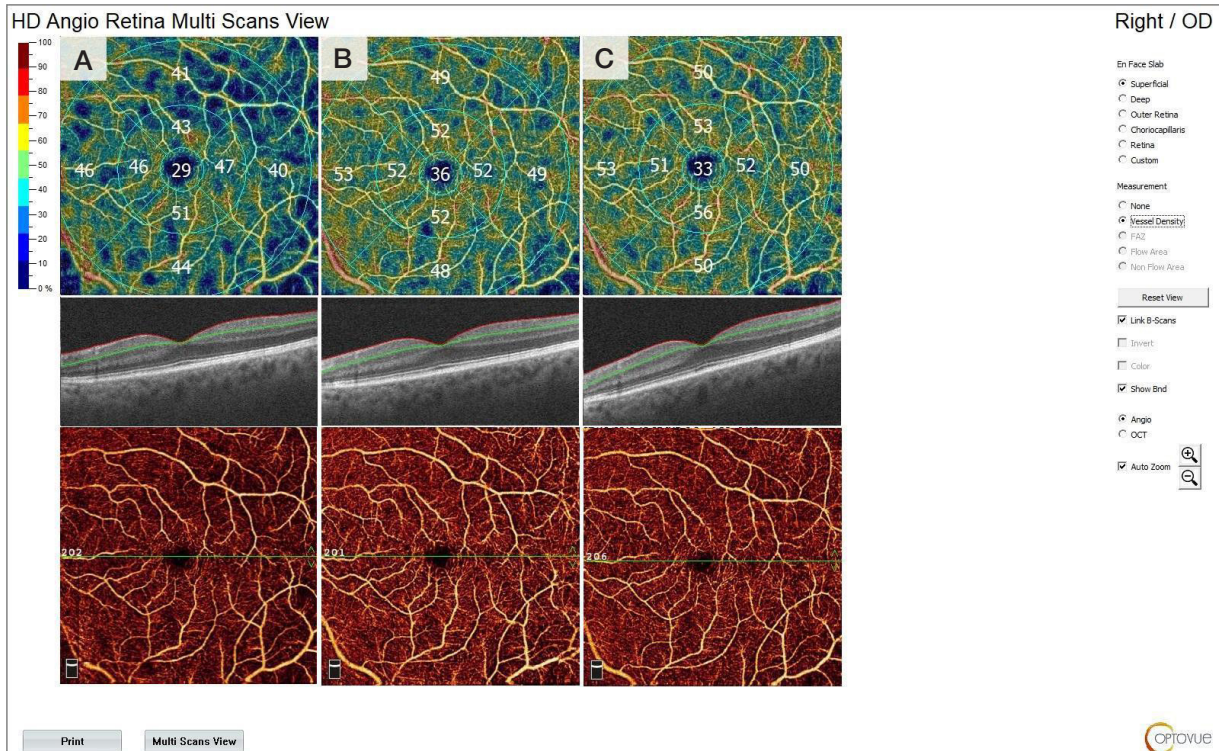


Fig. 1. Increased total vascular density of the macular zone in the index group based on the OCTA data (Multi Scans mode): on day 7 (A), month 3 (B), and month 6 (C) after PE

Table 6. Postoperative dynamic changes in the macular OCTA parameters observed in the control group, ($n = 25$; $M \pm Sd$)

Parameter	Day 1	Day 7	Day 30	Month 3	Month 6	p -value
SVP total density, %	48.62 ± 5.02	50.49 ± 4.73	50.97 ± 5.11	51.09 ± 5.05	50.80 ± 4.69	$p = 0.012^*$
DVP total density, %	47.42 ± 4.89	48.93 ± 5.05	49.52 ± 4.73	50.49 ± 4.22	50.07 ± 4.84	$p < 0.001^*$
FAZ area, mm ²	0.281 ± 0.082	0.275 ± 0.101	0.270 ± 0.121	0.268 ± 0.186	0.269 ± 0.193	$p = 0.206$

Note: * — significance based on the Friedman test for related samples.

the control group by month 6 of postoperative follow-up (Table 6).

No significant intergroup differences in the total vascular density of the superficial and deep vascular plexuses of the macular zone, as well as in the FAZ area were revealed at any time point of the study ($p > 0.05$).

DISCUSSION

Given the results obtained, we can conclude that the dynamics of corneal endotheliocyte loss observed when performing phacoemulsification using the new adaptive infusion control method based on the Optimed Profi surgical system is comparable with that observed when using the existing adaptive infusion control method based on the Centurion Vision System, despite significant differences revealed by certain intergroup comparisons that do not change the overall trend.

The findings are compliant with the literature data reporting lower corneal endothelial loss associated with the use of adaptive infusion control during PE compared to the use of conventional gravity infusion [29, 30]. When assessing endothelial cell loss, it is necessary to consider multifactorial nature of endothelial injury that can be caused by both mechanical and hydrodynamic factors [31]. However, the smaller corneal endothelial cell loss observed on months 3 and 6 of postoperative period when using the new adaptive infusion control method can be associated with the smaller intraoperative amplitude of post-occlusion surge and the reduced time of intraocular pressure improvement to the target levels, as earlier reported [22].

The results of our study focused on BCVA estimation in the control group are compliant with the data of the foreign study, during which BCVA (LogMAR) reached 0.04 by month 1 after surgery involving the use of the existing adaptive infusion control method (Centurion Vision System with Active Fluidics function), which corresponded to decimal visual acuity of 0.84–0.85 [32].

The clinically significant corneal edema occurring in patients during their early postoperative period was a non-specific complication that was equally frequent in both studied groups and found mostly in patients with the IV nuclear density degree. In our opinion, this complication was not associated with performance of the surgical system hydrodynamic component. It could be caused by high cataract density.

References

1. Avetisov SJe, Jusef JuN, Jusef SN, Avetisov KS, Ivanov MN, Fokina ND, i dr. Sovremennye vozmozhnosti hirurgii starcheskoj katarakty. Klinicheskaja gerontologija. 2017; (11–12): 84–96. Russian.
2. Kulikov AN, Churashov SV, Danilenko EV, Shamrej DV. Sravnitel'naja ocenka variantov hirurgicheskogo lechenija katarakty, oslozhnennoj slabost'ju svjazochnogo apparata hrustalika. Oftal'mologija. 2020; 17 (3): 577–84. Russian.
3. Bourne R, Steinmetz J, Saylan M, Mersha A, Weldemariam A,

The MOPP values obtained in both groups are compliant with the world's literature data, according to which the value of this parameter should be 45–60 mmHg after the non-complicated PE [33]. Despite the fact that MOPP depends on BP and IOP, higher MOPP in the postoperative period can be indirect evidence of functional hyperemia of the macular zone [34].

Assessment of the OCTA data revealed the signs of functional hyperemia of the macular zone in the form of the increased area occupied by blood vessels and reduced FAZ area in both groups by month 6 after PE, as previously reported in the literature [34]. The specifics of changes in vascular density of the macular zone following PE are usually associated with the decrease in IOP and the factors of intraocular inflammation, as well as with the better preserved retinal perfusion [32].

The use of different surgical systems in each group of patients preventing achieving complete identity of the phaco machine ultrasound parameters, specifically the type of ultrasonic waves, is a limitation of our study. However, the earlier studies confirmed consistency of surgical systems using 3D and the combination of torsion and longitudinal ultrasonic waves in terms of cutting capacity, retained lens fragments, and endothelial cell loss in the postoperative period [35, 36]. We determined consistency of hydrodynamic settings of both surgical systems in the pre-clinical phase of this study within the framework of medical engineering experiments on modeling post-occlusion surge under similar condition *in vitro* (in the test chamber) and *ex vivo* (in the separated porcine eyes), as well as *in vivo* when subjecting the eyes of laboratory animals (rabbits, chinchillas) to PE [22].

Despite the limitations, we selected settings of both surgical systems to be most close to identical, which could be considered optimal for both phaco machines in accordance with the manufacturers' guidelines and the literature data.

CONCLUSIONS

Thus, the findings make it possible to conclude that the use of the new adaptive infusion control method contributes to effective phacoemulsification of cataracts of varying density with the lower percentage of corneal endothelial cells lost during the late postoperative period ensuring achieving high visual acuity and low rate of surgical complications. The increase in mean ocular perfusion pressure and vascular density of the macular zone are reported when using the new and already existing adaptive infusion control methods in phacoemulsification.

4. Wondmeneh T, et al. Causes of blindness and vision impairment in 2020 and trends over 30 years, and prevalence of avoidable blindness in relation to VISION 2020: The Right to Sight: An analysis for the Global Burden of Disease Study. Lancet Glob. Heal. 2021; 9 (2): e144–e160.
4. Shuhaev SV, Bojko JeV. Sravnenie plotnosti jendotelial'nyh kletok rogovicy posle fakojemul'sifikacii plotnoj katarakty s ispol'zovaniem kombinirovannogo ul'trazvuka i torsionnogo

- ul'trazvuka s Intelligent Phaco. Oftal'mologija. 2018; 2 (15): 145–52. Russian.
5. Loskutov IA, Fedorova AI. Fakožemul'sifikacija s implantaciej IOL pri kritičeskom urovne jendotelial'nyh kletok rogovicy. Oftal'mologičeskie vedomosti. 2023; 3 (16): 63–69. Russian.
 6. Anwar N, Qasim MS. Effect of phacoemulsification surgery on central Macular thickness. Ann Med Health Sci Res. 2021; 11: 1536–9.
 7. Bissen-Miyajima H, Weikert MP, Koch DD. Cataract surgery: Maximizing outcomes through research. Cataract Surgery: Maximizing Outcomes Through Research. Springer, 2014; 211 p.
 8. Benjamin L. Fluidics and rheology in phaco surgery: What matters and what is the hype? Eye. Nature Publishing Group. 2018; 32 (2): 204–9.
 9. Agarwal A, Agarwal A, Agarwal S. Air pump to prevent Surge. In: Agarwal S. Advances in Ophthalmology. Jaypee Brothers Medical Publishers, 2002; 3000 p. DOI: 10.5005/jp/books/10033_13.
 10. Pérez-Arteaga A. Anterior vented gas forced infusion system of the Accurus surgical system in phakonit. Journal of cataract and refractive surgery. 2004; 30 (4): 933–35.
 11. Jensen D, Jensen B, Boulter B, Nathan G, Lambert B, Zaugg B, et al. Intraocular pressure study using monitored forced-infusion system phacoemulsification technology. J Cataract Refract Surg. 2016; 42 (5): 768–71.
 12. Hopkins MA, inventor., Novartis AG inc. Aspiration control via flow or impedance: United States patent 8246580 B2. 2012; p. 1–5.
 13. Hajishah A, inventor, Abbott Medical Optics inc. Advanced occlusion management methods for a phaco system: United States patent US 2019/0099526 A1. 2019; (1): 1–24.
 14. Mehta D, inventor, Johnson & Johnson Surgical Vision inc. System, apparatus and method for monitoring anterior chamber intraoperative intraocular pressure: United States patent US 11071816. 2021; p. 6.
 15. Gordon R, inventor, Alcon Research Ltd. Pressure control in phacoemulsification: United States patent US 9119701 B2. 2015; p. 13.
 16. Peterson J, Cooper C, Ungricht E. Measurement of phacoemulsification vacuum pressure in the Oertli CataRhex3. Clinical Ophthalmology. 2022; 16 (April): 1731–7.
 17. Miller KM, Dyk D, Yalamanchili S. Experimental study of occlusion break surge volume in 3 different phacoemulsification systems. Journal of cataract and refractive surgery. 2021; 47 (11): 1466–72.
 18. Kim YJ, Park SH, Choi KS. Fluctuation of infusion pressure during microincision vitrectomy using the constellation vision system. Retina. 2015; 35 (12): 2529–36.
 19. Thorne A, Dyk A, Fanney D, Miller D, Kevin M. Phacoemulsifier occlusion break surge volume reduction. J Cataract Refract Surg. United States. 2018; 44 (12): 1491–6.
 20. Zhou J, Han D. Post-occlusion surge and anterior chamber stability in a new phacoemulsification machine with small-bore, dual-durometer aspiration tubing. Invest Ophthalmol Vis Sci. 2021; 62: 574.
 21. Aznabaev BM, Muhamadeev TR, Dibaev TI, Ismagilov TN, avtory; ZAO «Optimedservis», patentoobladatel'. Sposob adaptivnogo upravlenija infuziej vo vremja fakožemul'sifikacii. Patent RF # 2788289 S1. 17.01.2023. Russian.
 22. Ismagilov TN, Aznabaev BM, Muhamadeev TR, Dibaev TI. Kolichestvennaja ocenka postokkjuzionnoj volny pri fakožemul'sifikacii s novym sposobom adaptivnogo upravlenija infuziej. Sovremennye problemy nauki i obrazovanija. 2023; 2: 73. Russian.
 23. Buratto L. Phacoemulsification/ SLACK. 1998; 544 pp.
 24. Rossi T, Querzoli G, Gelso A, Angelini G, Rossi A, Corazza P. Ocular perfusion pressure control during pars plana vitrectomy: testing a novel device. Graefes Arch Clin Exp Ophthalmol. 2017; 255 (12): 2325–30.
 25. Zhao Z, Yu X, Yang X, Zhang J, Zhang D, Sun N. Elevated intraocular pressure causes cellular and molecular retinal injuries, advocating a more moderate intraocular pressure setting during phacoemulsification surgery. Int Ophthalmol Springer Netherlands. 2020; 40 (12): 3323–36.
 26. Malik PK, Dewan T, Patidar A, Kr Sain E. Effect of IOP based infusion system with and without balanced phaco tip on cumulative dissipated energy and estimated fluid usage in comparison to gravity fed infusion in torsional phacoemulsification. Eye Vis. London. 2017; 4: 22.
 27. Boukhny M, Mackool RJ, Lindstrom RL. Cataract & Refractive surgery today. The Centurion Vision System: the next step in cataract surgery. 2014; pp. 1–8.
 28. Maljugin BJe. Mediko-tehnologičeskaja sistema hirurgičeskoj reabilitacii pacientov s kataraktoj na osnove ul'trazvukovoj fakožemul'sifikacii s implantaciej intraokuljarnoj linzy [dissertacija]. M., 2002. Russian.
 29. Chaudhry P, Prakash G, Jacob S. Safety and efficacy of gas-forced infusion (air pump) in coaxial phacoemulsification. Journal of Cataract and Refractive Surgery. 2010; 36 (12): 2139–45.
 30. Sorrentino FS, Matteini S, Imburgia A. Torsional phacoemulsification: a pilot study to revise the "harm scale" evaluating the endothelial damage and the visual acuity after cataract surgery. PloS One. 2017; 12 (10): e0186975.
 31. Nayak BK, Shukla RO. Effect on corneal endothelial cell loss during phacoemulsification: fortified balanced salt solution versus Ringer lactate. Journal of cataract and refractive surgery. 2012; 38 (9): 1552–8.
 32. Luo Y, Li H, Chen W. Active-fluidics versus gravity-fluidics system in phacoemulsification for age-related cataract (AGSPC): study protocol for a prospective, randomised, double-blind, controlled clinical trial. BMJ open. 2022; 12 (1): e059062.
 33. Kim M, Kim S, Kwon H, Koh H, Lee S. Association between choroidal thickness and ocular perfusion pressure in young, healthy subjects: Enhanced depth imaging optical coherence tomography study. Invest Ophthalmol Vis Sci. 2012; 53 (12): 7710–7.
 34. Križanović A, Bjeloš M, Bušić M, Elabjer, Kuzmanović B, Rak B. Macular perfusion analysed by optical coherence tomography angiography after uncomplicated phacoemulsification: benefits beyond restoring vision. BMC Ophthalmol. 2021; 21 (1): 1–11.
 35. Dibaev TI, Ramazanov VN, Rahimov AF. Ocenka rezhushhej sposobnosti otechestvennogo ul'trazvukovogo instrumenta dlja fakožemul'sifikacii, osnovannogo na neprodol'nyh kolebanijah. Sovremennye tehnologii v oftal'mologii. 2015; 3: 61–63. Russian.
 36. Aznabaev BM, Muhamadeev TR, Dibaev TI. Kliničeskie rezul'taty ul'trazvukovoj fakožemul'sifikacii na osnove trehmernyh kolebanij. Sovremennye tehnologii v oftal'mologii. 2015; 4: 11–14. Russian.

Литература

1. Аветисов С. Э., Юсеф Ю. Н., Юсеф С. Н., Аветисов К. С., Иванов М. Н., Фокина Н. Д. и др. Современные возможности хирургии старческой катаракты. Клиническая геронтология. 2017; (11–12): 84–96.
2. Куликов А. Н., Чурашов С. В., Даниленко Е. В., Шамрей Д. В. Сравнительная оценка вариантов хирургического лечения катаракты, осложненной слабостью связочного аппарата хрусталика. Офтальмология. 2020; 17 (3): 577–84.
3. Bourne R, Steinmetz J, Saylan M, Mersha A, Weldemariam A, Wondmeneh T, et al. Causes of blindness and vision impairment in 2020 and trends over 30 years, and prevalence of avoidable blindness in relation to VISION 2020: The Right to Sight: An analysis for the Global Burden of Disease Study. Lancet Glob. Heal. 2021; 9 (2): e144–e160.
4. Шухаев С. В., Бойко Э. В. Сравнение плотности эндотелиальных клеток роговицы после факоемульсификации плотной катаракты с использованием комбинированного ультразвука и торсионного ультразвука с Intelligent Phaco. Офтальмология. 2018; 2 (15): 145–52.
5. Лоскутов И. А., Федорова А. И. Факоемульсификация с имплантацией ИОЛ при критическом уровне эндотелиальных клеток роговицы. Офтальмологические ведомости. 2023; 3 (16): 63–69.
6. Anwar N, Qasim MS. Effect of phacoemulsification surgery on central Macular thickness. Ann Med Health Sci Res. 2021; 11: 1536–9.

7. Bissen-Miyajima H, Weikert MP, Koch DD. Cataract surgery: Maximizing Outcomes Through Research. *Cataract Surgery: Maximizing Outcomes Through Research*. Springer, 2014; 211 p.
8. Benjamin L. Fluidics and rheology in phaco surgery: What matters and what is the hype? *Eye*. Nature Publishing Group. 2018; 32 (2): 204–9.
9. Agarwal A, Agarwal A, Agarwal S. Air pump to prevent Surge. In: Agarwal S. *Advances in Ophthalmology*. Jaypee Brothers Medical Publishers, 2002; 3000 p. DOI: 10.5005/jp/books/10033_13.
10. Pérez-Arteaga A. Anterior vented gas forced infusion system of the Accurus surgical system in phakonit. *Journal of cataract and refractive surgery*. 2004; 30 (4): 933–35.
11. Jensen D, Jensen B, Boulter B, Nathan G, Lambert B, Zaugg B, et al. Intraocular pressure study using monitored forced-infusion system phacoemulsification technology. *J Cataract Refract Surg*. 2016; 42 (5): 768–71.
12. Hopkins MA, inventor., Novartis AG inc. Aspiration control via flow or impedance: United States patent 8246580 B2. 2012; p. 1–5.
13. Hajishah A, inventor, Abbott Medical Optics inc. Advanced occlusion management methods for a phaco system: United States patent US 2019/0099526 A1. 2019; (1): 1–24.
14. Mehta D, inventor, Johnson & Johnson Surgical Vision inc. System, apparatus and method for monitoring anterior chamber intraoperative intraocular pressure: United States patent US 11071816. 2021; p. 6.
15. Gordon R, inventor, Alcon Research Ltd. Pressure control in phacoemulsification: United States patent US 9119701 B2. 2015; p. 13.
16. Peterson J, Cooper C, Ungricht E. Measurement of phacoemulsification vacuum pressure in the Oertli CataRhex3. *Clinical Ophthalmology*. 2022; 16 (April): 1731–7.
17. Miller KM, Dyk D, Yalamanchili S. Experimental study of occlusion break surge volume in 3 different phacoemulsification systems. *Journal of cataract and refractive surgery*. 2021; 47 (11): 1466–72.
18. Kim YJ, Park SH, Choi KS. Fluctuation of infusion pressure during microincision vitrectomy using the constellation vision system. *Retina*. 2015; 35 (12): 2529–36.
19. Thorne A, Dyk A, Fanney D, Miller D, Kevin M. Phacoemulsifier occlusion break surge volume reduction. *J Cataract Refract Surg*. United States. 2018; 44 (12): 1491–6.
20. Zhou J, Han D. Post-occlusion surge and anterior chamber stability in a new phacoemulsification machine with small-bore, dual-durometer aspiration tubing. *Invest Ophthalmol Vis Sci*. 2021; 62: 574.
21. Азнабаев Б. М., Мухамадеев Т. Р., Дибаяев Т. И. Исмагилов Т. Н., авторы; ЗАО «Оптимедсервис», патентообладатель. Способ адаптивного управления инфузией во время факоемульсификации. Патент РФ № 2788289 С1. 17.01.2023.
22. Исмагилов Т. Н., Азнабаев Б. М., Мухамадеев Т. Р., Дибаяев Т. И. Количественная оценка постокклюзионной волны при факоемульсификации с новым способом адаптивного управления инфузией. *Современные проблемы науки и образования*. 2023; 2: 73.
23. Buratto L. *Phacoemulsification/ SLACK*. 1998; 544 pp.
24. Rossi T, Querzoli G, Gelso A, Angelini G, Rossi A, Corazza P. Ocular perfusion pressure control during pars plana vitrectomy: testing a novel device. *Graefes Arch Clin Exp Ophthalmol*. 2017; 255 (12): 2325–30.
25. Zhao Z, Yu X, Yang X, Zhang J, Zhang D, Sun N. Elevated intraocular pressure causes cellular and molecular retinal injuries, advocating a more moderate intraocular pressure setting during phacoemulsification surgery. *Int Ophthalmol Springer Netherlands*. 2020; 40 (12): 3323–36.
26. Malik PK, Dewan T, Patidar A, Kr Sain E. Effect of IOP based infusion system with and without balanced phaco tip on cumulative dissipated energy and estimated fluid usage in comparison to gravity fed infusion in torsional phacoemulsification. *Eye Vis*. London. 2017; 4: 22.
27. Boukhny M, Mackool RJ, Lindstrom RL. *Cataract & Refractive surgery today. The Centurion Vision System: the next step in cataract surgery*. 2014; pp. 1–8.
28. Малугин Б. Э. Медико-технологическая система хирургической реабилитации пациентов с катарактой на основе ультразвуковой факоемульсификации с имплантацией интраокулярной линзы [диссертация]. М., 2002.
29. Chaudhry P, Prakash G, Jacob S. Safety and efficacy of gas-forced infusion (air pump) in coaxial phacoemulsification. *Journal of Cataract and Refractive Surgery*. 2010; 36 (12): 2139–45.
30. Sorrentino FS, Matteini S, Imburgia A. Torsional phacoemulsification: a pilot study to revise the “harm scale” evaluating the endothelial damage and the visual acuity after cataract surgery. *PloS One*. 2017; 12 (10): e0186975.
31. Nayak BK, Shukla RO. Effect on corneal endothelial cell loss during phacoemulsification: fortified balanced salt solution versus Ringer lactate. *Journal of cataract and refractive surgery*. 2012; 38 (9): 1552–8.
32. Luo Y, Li H, Chen W. Active-fluidics versus gravity-fluidics system in phacoemulsification for age-related cataract (AGSPC): study protocol for a prospective, randomised, double-blind, controlled clinical trial. *BMJ open*. 2022; 12 (1): e059062.
33. Kim M, Kim S, Kwon H, Koh H, Lee S. Association between choroidal thickness and ocular perfusion pressure in young, healthy subjects: Enhanced depth imaging optical coherence tomography study. *Investig Ophthalmol Vis Sci*. 2012; 53 (12): 7710–7.
34. Križanović A, Bjeloš M, Bušić M, Elabjer, Kuzmanović B, Rak B. Macular perfusion analysed by optical coherence tomography angiography after uncomplicated phacoemulsification: benefits beyond restoring vision. *BMC Ophthalmol*. 2021; 21 (1): 1–11.
35. Дибаяев Т. И., Рамазанов В. Н., Рахимов А. Ф. Оценка режущей способности отечественного ультразвукового инструмента для факоемульсификации, основанного на непродольных колебаниях. *Современные технологии в офтальмологии*. 2015; 3: 61–63.
36. Азнабаев Б. М., Мухамадеев Т. Р., Дибаяев Т. И. Клинические результаты ультразвуковой факоемульсификации на основе трехмерных колебаний. *Современные технологии в офтальмологии*. 2015; 4: 11–14.